5

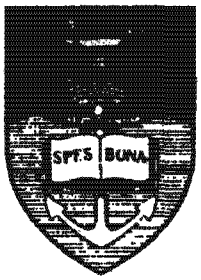

A STUDY OF THE DIAMONDS, DIAMOND INCLUSION MINERALS AND OTHER MANTLE MINERALS FROM THE SWARTRUGGENS KIMBERLITE, SOUTH AFRICA

NEIL Mc KENNA

BSc. (Hons) (University of the Witwatersrand)

Thesis Presented for the Degree of

MASTER OF SCIENCE

in the Department of Geological Sciences

Faculty of Science

University of Cape Town

NOVEMBER 2001

ACKNOWLEDGEMENTS

I am particularly grateful to John Gurney for providing me with the opportunity to undertake this study, as well as for his supervision over the duration of the project. John Gurney always expressed a keen interest in the project and was always willing to offer advice and support. It was a privilege to have John Gurney as my Supervisor. Thanks too, to my co-supervisor, Steve Richardson who always made himself available to offer assistance. His broad knowledge of mantle geology made light of many of the problems I encountered during my work.

Thanks to Jim Davidson and Helam Diamond Mine (Pty) Ltd for providing the diamonds and kimberlite samples so freely, as well as for accommodating me on the mine during my visits. Howard Bell (Zlotowski's Diamond Cutting Works (Pty) Ltd) is thanked for cutting and polishing some of the Helam diamonds into plates.

Technical support was contributed by numerous people: Particular thanks to Craig Smith and the staff of the De Beers Geoscience Centre (GSC), Johannesburg for allowing me the use of the electron microprobe facility at short notice. Thanks to Rene Dobbe and his team for their patient training of me on the instrument, and technical support during its operation. I am grateful to Fanus Viljoen and Ingrid Chinn for their advice and technical support, particularly with regards to the infrared analysis of the diamonds. I am grateful to Graeme Hill (Debtech) for offering to run EPR on some of the Helam diamonds. The staff of the GSC have always welcomed my visits over the years, and their collective enthusiasm for mantle and diamond studies is responsible for my own fanaticism of the subject. At the University of Cape Town, Dane Gerneke and Miranda Waldon at the Electron Microscope Unit assisted in obtaining SEM and cathodoluminescence images of the diamonds. Thanks also to Eva Anckar of the Kimberlite Research Group for all her help in accessing data from the Kimberlite Research Group Database. Special thanks too to Kalle Westerlund, for his advice and the initial technical training that formed the basis of my work. In addition Kalle is thanked for the time spent at the Carnegie Institute of Washington analysing Re-Os isotopes of some of the Helam sulphide inclusions. Special thanks to Judith Milledge at University College, London who was always ready to answer a query, and for her input with regards to FTIR analysis of the Helam diamonds.

Finally to my family and friends: Thank you for your love, support and encouragement.

TABLE OF CONTENTS

1 INTRODUCTION

While a clear and unequivocal model for the formation of diamonds is still lacking, the past few decades have seen a 'revolution' in the scientist's perception of mantle processes, particularly that regarding diamond formation. Kramers (1977) first clearly recognised the ancient origin of diamonds from his studies of composited sulphide inclusions. However, it was not until mid-Archean ages were obtained from syngenetic garnet inclusions in diamond by Richardson *et al.* (1984), that it became generally accepted that most diamonds were in fact very much older than their kimberlitic hosts, and could therefore not have been precipitated from the kimberlite magma.

Subsequently, numerous other studies have provided evidence that diamonds are xenocrysts rather phenocrysts within the kimberlite and may have an ancient origin. Some workers (e.g.: Kramers, 1977; Richardson 1986; Pearson *et. al*, 1998) however, also present quantitative information suggesting *younger* diamond formation events, possibly even concurrent with the emplacement of the host kimberlites themselves. Such studies have shown that while certain diamonds are associated with ancient ages, additional diamond formation events have evidently occurred episodically over time. Of similar significance, such studies have demonstrated that the inert nature of diamond is capable of preserving a *pristine* mantle sample at the time of diamond formation, within a *closed* system, providing a unique opportunity to study mantle conditions and processes as far back as the Archean. These findings have enhanced the potential significance of diamond inclusion studies.

1.1 Diamond Source Regions

From detailed studies of syngenetic mineral inclusions in diamond, together with mantle xenoliths entrained within kimberlite, researchers have been able to constrain the environments within which diamonds crystallise. From such studies it has emerged that there are two principal diamond parageneses within the cratonic lithosphere (eg: Meyer, 1985). Peridotitic diamonds are associated with rock types consisting primarily of olivine, chromite, orthopyroxene, pyrope garnet and diopsidic clinopyroxene. Eclogitic diamonds however, are associated with source regions

comprising principally pyrope-almandine garnet and clinopyroxene (Meyer, 1987). Detailed studies of southern African localities indicate a probable overall peridotite/eclogite source abundance ratio of approximately 3/1, however there exist highly diversified paragenetic proportions for individual localities (Gurney, 1990).

Very rare occurrences of certain diamonds are suggestive of an asthenospheric origin, and are consequently associated with very high pressure-temperature phases such as ferro-periclase (e.g.: Stachel *et al.*, 1998) and majoritic garnet (e.g.: Moore & Gurney, 1985; Wilding *et al.*, 1989 and Gurney *et al.*, 1991). Rare occurrences of mineral inclusions with wehrlitic, websteritic (Gurney *et al.*, 1984b) and calc-silicate (Sobolev *et al.*, 1984) compositions have also been recovered, suggesting that mantle regions of considerably dissimilar mineralogies may play host to the processes of diamond formation.

1.1.1 Diamonds within the Lithosphere

Detailed thermobarometric studies have demonstrated that peridotitic diamonds crystallise within the diamond stability field (Meyer, 1987), and that they are only stable at pressures in excess of 50 kbars (Kennedy & Kennedy, 1976) at reasonable estimates of geothermal conditions (35-45 mW/m^2). Along such geotherms, most peridotitic mineral inclusions within diamond record ambient temperatures between 900 - 1200 °C, and provide evidence that diamonds have crystallised and were immobilised in a lithospheric keel that extended to depths of 150-200 km (Boyd *et al.*, 1985). While no barometer is currently available for eclogitic diamonds, most eclogitic mineral inclusions within diamond record comparable or slightly higher temperatures of formation, suggesting a similar or slightly deeper environment of formation (Navon, 1999).

1.1.2 Diamonds within the Asthenosphere

Geothermobarometry on mantle xenoliths, together with certain geophysical evidence, indicate a major thermal boundary between the lithosphere and the asthenosphere at a depth of between 170 – 190 km (Boyd & Gurney, 1986). This boundary is manifested by a significant change in the textural and mineralogical nature of the mantle. Rare

high temperature-pressure mineral inclusions in diamond such as ferro-periclase (Stachel *et al.*, 1998) and majoritic garnet (Moore & Gurney, 1985; Wilding *et al.*, 1989 and Gurney *et al.*, 1991) are indicative of an asthenospheric source region with pressures up to 15 Gpa. Other examples of high-pressure phases (e.g.: Scott-Smith *et al.*, 1984; Moore *et al.*, 1986, Harte & Harris, 1994; Stachel & Harris, 1997) all support such an asthenospheric paragenesis.

1.2 Other Mantle Minerals

In order to portray a more holistic view of the mantle profile, it is important to briefly consider other mantle minerals, which are sampled by kimberlite. Harte & Gurney (1981) suggest that megacryst minerals such as those described at Monastery Mine (Gurney *et al.*, 1979) and Jagersfontein Mine (Hops *et al.*, 1989), precipitated from melts that experienced thermal death near the lithosphere-asthenosphere boundary. It has been suggested that deformed, high temperature peridotites (Boyd, 1973) are associated with the megacryst suite, having been derived from similar mantle depths (Gurney & Harte, 1980). These rocks, like the megacryst minerals, are characterised by depleted radiogenic isotope signatures, which are suggestive of asthenospheric origins.

The minerals within deformed peridotites are sometimes zoned (e.g.: Smith & Boyd, 1987; Griffin *et al.*, 1989; Hops *et al.*, 1989). Gurney & Harte (1980) have suggested that the observed zoning may have been produced from the metasomatic fluids that precipitated the megacrysts. This association is made from observations of their similar pressure and temperature conditions, geochemistry and regional distribution. More recent Re-Os isotope studies of deformed peridotites (e.g.: Irvine *et al.*, 2001) demonstrate that the minerals associated with these rocks exhibit ancient (Archean) ages, suggesting that they do not represent asthenosphere, but are in fact lithospheric rocks, with an asthenospheric overprint.

1.3 Theories of Diamond Formation

The nature of the source region of diamond formation and the mechanism by which diamond formation occurs, remain contentious. Below is a brief summary of the various environments and mechanisms proposed for diamond formation.

1.3.1 Peridotitic Diamond Formation

The relative abundance of mineral inclusions in diamond suggests that peridotitic diamonds are more abundant than eclogitic diamonds (Gurney, 1989). Peridotitic diamonds may be divided into lherzolitic and harzburgitic sub-parageneses based on the presence or absence of clinopyroxene respectively, of which harzburgitic inclusions are far more common (Meyer, 1987). With regard to major element compositions, the constituent minerals of these rocks are extremely refractory, the harzburgites being more so than the lherzolites (Meyer, 1987).

There is conflicting evidence regarding whether peridotitic diamonds are metasomatic, metamorphic or igneous in origin. In general, peridotitic diamonds appear to be Archean in age, and have formed in a chemically depleted peridotite near the base of the lithosphere (Gurney, 1989). Richardson *et al.* (1984), have shown that despite this initial depletion, subsequent enrichment in elements such as potassium, rubidium and LREE has occurred through a process of metasomatism. This metasomatic overprint is particularly evident within the 'G10' peridotitic garnet inclusions, and is quite different from commonly described mantle metasomatic events, which commonly result in enrichment of titanium (e.g.: Kramers *et. al.*, 1983; Harte & Hawkesworth, 1986; Menzies & Hawkesworth, 1987; Dawson, 1999). Boyd & Finnerty (1980) suggest either a sub-solidus metamorphic or metasomatic origin for harzburgitic diamonds. This suggestion is made in the light of the observations that many peridotitic diamond inclusion equilibration temperatures are lower than the C-H-O solidus of ultramafic rocks.

There is increasing evidence indicating that the formation of some diamonds are closely associated with the subduction of oceanic lithosphere. Compositions and thermobarometry of mineral inclusions within diamond support this suggestion (Kesson & Ringwood, 1989). Despite consensus on the general subduction mechanisms, there still exist contrasting views regarding the nature of the protolith, and the nature of the process following subduction, that may result in diamond genesis.

Schulze (1986) suggests that subducted meta-serpentinite (which is sufficiently depleted in calcium) may have been a protolith for harzburgitic diamonds, and that this process may explain the extreme calcium depletion associated with harzburgitic mineral inclusions found within diamond. It is argued that with

subduction and prograde metamorphism, serpentinites would re-equilibrate as harzburgites and dunites, with diamond being produced or introduced during the process of metamorphism. Haggerty (1986) too proposes metamorphic growth of peridotitic diamonds by sulphur reduction of CO_2, and suggests that solid-state metamorphic growth of diamonds within a closed environment, is a suitable mechanism for diamond genesis.

Kesson & Ringwood (1989) invoke an igneous origin for harzburgitic diamonds, suggesting that a refractory harzburgite is more suited as a protolith, and propose a mechanism by which hydrous partial melts from subducted oceanic crust interact with overlying peridotite in the mantle wedge (slab-melt interaction), to produce peridotitic diamonds. This model invokes an exceptionally refractory harzburgite or dunite, formed after the extraction of komatiitic magmas from mantle peridotite in the Archean. Griffin *et al.* (1992) also support an igneous origin, on the basis of the higher equilibration temperatures obtained from peridotitic mineral inclusions in diamond, compared with the experimentally derived C-H-O solidus.

Evidence of a metasomatic event in ancient times (Richardson *et al.*, 1984) can not be adequately explained by any of the above mentioned subduction models. The assumption therefore that all peridotitic diamonds can be related to a subduction event remains questionable.

The carbon isotope composition of diamonds has important implications regarding models of diamond genesis (e.g.: Deines *et al.*, 1984; Kirkley *et al.*, 1991b). The overall range in $\delta^{13}C$ for combined peridotitic and eclogitic diamonds is between +5 per mil and –34.4 per mil (Harris, 1987). While it has been shown that the carbon isotope composition of diamonds is complex and heterogeneous, diamonds of the peridotitic paragenesis are generally confined to $\delta^{13}C$ values between –2 per mil and –9 per mil (Sobolev *et al.*, 1979; Deines *et al.*, 1984). From such isotopic studies it is suggested (eg: Kirkley, 1991a), that peridotitic diamonds have a primary carbon source that is derived from the homogenized convecting asthenosphere.

1.3.2 Eclogitic Diamond Formation

While it is still not possible to unequivocally determine the equilibrium temperatures and pressures from minerals of the eclogitic suite, estimated equilibration

temperatures for non-touching eclogitic mineral inclusions within diamond appear to be generally higher than those of the peridotitic suite, ranging up to 1400 – 1500 °C (eg: Griffin *et al.*, 1988). Diamond-bearing eclogites are distinctive in that their garnets have detectable Na_2O (>0.06 wt%), and the pyroxenes have trace levels of K_2O (>0.04 wt%). Eclogitic garnet inclusions in diamond are also associated with HREE enrichment, which is in contrast to the patterns associated with peridotitic garnets. These features are suggestive of a high-pressure origin, yielding diamonds formed by processes quite distinct from those that produced peridotitic diamonds (McCandless & Gurney, 1989).

The nature and formation of eclogitic diamonds within the Earth's mantle, remains a highly contentious issue. A favored model, suggests that eclogitic diamonds are formed in the mantle from an input of subducted crustal material (e.g.: Kirkley, 1991a). There are two lines of evidence in support of this; Firstly, the spread of ages for eclogitic diamonds span a large range, from 2.9 billion years (e.g.: Kimberley diamonds, South Africa (Richardson *et al.*, 2001)), to ages that closely approach kimberlite emplacement (eg: Premier mine, South Africa (Richardson, 1986)). Such a range in ages suggests that eclogitic diamonds are the result of some repeated, episodic process, rather than a unique event that occurred 3 billion years ago (Kirkley, 1998). Secondly, isotopic evidence shows that eclogitic diamonds span the full range of carbon isotope compositions from +5 per mil to –34.4 per mil (Harris, 1987). The depletion in ^{13}C of many of the eclogitic diamonds has been suggested to be the result of an input of organic carbon, by the subduction of crustal material into the mantle (Kirkley *et al.*, 1991b). Additional support for an organic source of carbon is given by Boyd & Pillinger (1994), who show both depletion in ^{13}C and enrichment in ^{15}N within eclogitic diamonds.

Various models have been proposed for the formation of eclogite by underplating and subduction. Some workers have suggested that eclogites represent metamorphic fragments of crustal material (e.g.: Helmstaedt & Doig, 1975 and Jacob *et al.*, 1994). Ringwood (1982) however, suggests that the subducted crustal material becomes remelted before being underplated onto the base of the lithosphere.

The crystallisation of diamond within such eclogite, too is a contentious issue. Kesson & Ringwood (1989) suggest that diamond crystallises from partial melts in a closed-system crystal-fluid fractionation process. However, Griffin *et al.* (1988) and

Gurney *et al.* (1984) argue that diamonds crystallise during an open-system fluid-flux process through the eclogite protolith.

The above models conflict with that of Haggerty (1986) who suggests that eclogitic diamonds are melt-derived, with crystal growth proceeding by solid-state diffusion, dependent on sulphide liquid immiscibility. Earlier workers (e.g.: Hatton, 1978; MacGregor & Carter, 1970) invoke a magmatic origin for eclogites as mantle cumulates or melts.

As discussed previously, a very deep origin (> 300 km) for a small proportion of eclogitic diamonds is evident. This assertion was made after the discovery of pyroxene solid solution in garnet inclusions in diamond from the Monastery Mine (Moore & Gurney, 1985). Similar garnets have subsequently been discovered from Jagersfontein Mine (Hops *et al.*, 1989; Rickard *et al.*, 1991) and in Sao Luiz, Brazil (Wilding *et al.*, 1998), providing further evidence for a deep, and significantly different mantle environment in which some eclogitic diamonds may crystallise.

1.4 Fibrous Diamonds

While the majority of diamonds studied have been associated with ancient ages, some diamonds appear to have crystallised in relatively recent times. For example, studies of the nitrogen content within fibrous diamonds, reveal exceedingly low levels of nitrogen aggregation, often suggestive of very short mantle residence times (Navon, 1999).

Fibrous diamonds differ from other diamonds in that they do not display the well-defined crystallographic surfaces of the more common octahedra. These diamonds consist of radiating diamond fibers, with growth proceeding through the development of cubic faces (Navon, 1999). In most cases therefore, the growth of fibrous diamond results in cubic morphologies. In cases where this younger generation of fibrous, cubic diamond grows upon a pre-existing octahedral diamond, a coated diamond results (Kamiya & Lang, 1965).

The fibrous diamond commonly traps inclusions between the diamond fibers. As with other diamonds, inclusions from different *fibrous* diamonds have proven to be of both eclogitic and peridotitic affinity, and these fibrous diamonds have also been observed within mantle xenoliths (Talnikova, 1995). Analyses of fluid inclusions trapped within these diamonds suggest that they grew from penetrating melts/fluids

which interacted with the host rocks in more recent times (Navon, 1999). The fluid inclusions suggest that the fibrous diamonds grew in the presence of fluids enriched in potassium, CO_2 and H_2O (Navon *et al.*, 1988). Coated diamonds are thus the result of fluid penetration of a host rock that had previously been successful in crystallising diamond. Such overgrowth phenomena attest to a mantle capable of multiple, episodic diamond forming events over considerable periods of geological time. Such episodic diamond growth will be a recurrent theme within this report.

1.5 Summary

Studies of mantle xenoliths and mineral inclusions in diamond provide evidence for the stabilisation of a thick (150-200 km), cool, predominantly peridotitic cratonic keel beneath southern Africa as early as the Archean. The initial peridotite keel may be the residue from komatiitic melt extraction events in the asthenosphere. Following the initial peridotitic keel development, subordinate amounts of eclogite have been added to the lithosphere via some episodic process that began in the Archean. Favoured models invoke subduction of oceanic crust as the most likely mechanism of introducing eclogite to the cratonic keel. Processes of melt formation, metasomatism, crustal recycling and deformation have subsequently modified the mantle lithosphere, resulting in a highly heterogeneous lithospheric profile.

The majority of African diamonds are derived from the Archean peridotites and Archean-Proterozoic eclogites, which have subsequently been sampled from their host environment by asthenospherically derived melts, and brought to the surface by kimberlite. Having been derived from great depths, kimberlites are also capable of sampling sub-lithospheric mantle minerals. Younger, deformed and metasomatised peridotite as well as megacryst minerals may represent a mantle sample from depths in excess of 200 km, close to the asthenosphere-lithosphere boundary. More strikingly, some kimberlites sample diamonds which contain mineral inclusions of asthenospheric affinity (e.g.: majorite; ferro-periclase), attesting to the existence of a diamond bearing source, well beyond the confines of the lithosphere.

It is clear that studies of mantle minerals provide a unique opportunity to study mantle conditions and processes, and are crucial to the understanding of both mantle *and* crustal evolution. While greatly contested, figure 1.1 (Haggerty, 1986 Model) has been included in the report as it is successful in illustrating the various domains that

are understood to represent the mantle beneath an idealised craton, and are consequently involved in the processes of diamond formation, preservation and transportation. This model too, forms the basis of discussion regarding the results obtained from this study.

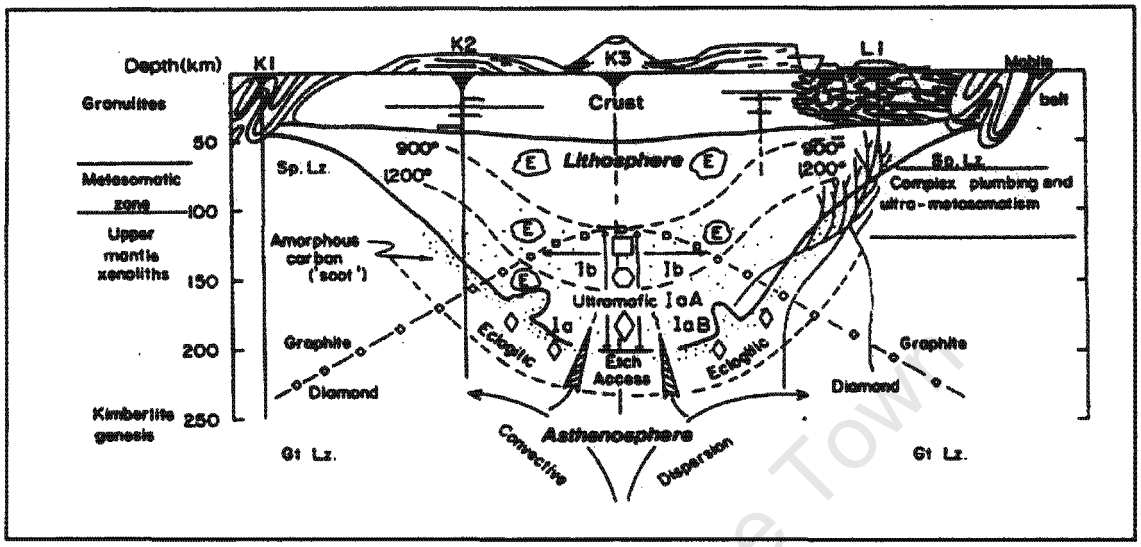

Figure 1.1 Schematic representation of an idealised craton, and its subcratonic lithosphere (from Haggerty, 1986). The asthenosphere is characterised by spinel lherzolite (Sp.Lz) and garnet lherzolite (Gt.Lz), spinel lherzolite being restricted to the lithospheric margins at shallow asthenosphere depths. The asthenosphere has a higher oxygen fugacity, density and temperature, and is geochemically more fertile, and rheologically more ductile than the overlying lithosphere. The lithosphere by contrast is characterised by a dominance of harzburgite with subordinate amounts of dunite. The cooler lithosphere results in concave isotherms, and the diamond-graphite curve is therefore convex. The symbols along the diamond-graphite curve depict high-temperature octahedral crystal forms (diamond symbol), intermediate-temperature cubo-octahedrons (hexagon symbol) and low-temperature cubes (cubic symbol). Diamond nucleation is unlikely in the asthenosphere due to the elevated oxygen fugacities. Irregular pods of eclogite (E) are shown to be sinking through the lithosphere, and accumulating at the lithosphere-asthenosphere contact. Diamond types (I) are nitrogen bearing and are either aggregated (a) into A or B aggregates at low and high temperatures respectively, or unaggregated (b) in the cooler interior of the lithosphere. K1, K2 and K3 represent typical kimberlite sampling profiles, L1, representing the complex plumbing suggested to be the cause of Australian lamproites.

1.6 Framework and Objectives of the Study

Recent seismic data over the southern African region, demonstrates that the sub-Bushveld lithospheric mantle is characterised by lower seismic velocities than is

observed in regions of undisturbed cratonic mantle (James *et al.*, 2001). These low mantle velocities may indicate chemical modification of the mantle during the magmatic emplacement of the complex (ca. 2.05 Ga). Being on the southwestern edge of the Bushveld Complex, the Swartruggens Dyke system is an interesting locality to study, as its mantle sample may provide additional information with regards to this 'anomaly'.

Samples of kimberlite and run-of-mine diamond production have been made available to the author, courtesy of Helam Diamond Mine (Pty) Ltd, in order to conduct an integrated, multidisciplinary study of the diamonds, the diamond mineral inclusions, and other mantle minerals from this previously poorly studied location. It is anticipated that integration of data from independent studies will realise a better understanding of the mantle within the region.

Compositions of mantle macrocryst minerals, derived from the Swartruggens Kimberlite, were measured by electron microprobe in order to identify the various lithologies that comprise the mantle beneath this locality. These minerals were assessed in terms of their paragenetic suitability for diamond crystallisation. In addition a comparison was made between mineralogical assemblages characteristic of high and low diamond grades, within petrographically distinct kimberlite dykes. From such a study it becomes possible to speculate as to the sources of the diamonds and to comment on the relative importance of these sources in establishing diamond grade.

Infrared absorption characteristics of the 'Helam Diamonds' were determined in order to differentiate between different diamond sub-populations as well as to elucidate the nature of the environments of crystallisation from the nitrogen concentrations and aggregation states of the respective diamonds. This study also allowed for estimates of time-averaged temperatures for mantle residence to be made. An integrated study of cathodoluminescence images of polished diamond plates with traverses of their respective infrared absorption characteristics was also undertaken. This 'high-resolution' study was conducted in order to reveal subtle chemical variations within the diamonds, and to better understand the mechanisms involved in diamond crystallisation.

Chemical compositions of syngenetic silicate, oxide and sulphide mineral inclusions in diamond were investigated with the aid of an electron microprobe, in order to confirm the various protoliths in which the diamonds have crystallised. The

study of 'pristine' mantle minerals has allowed for an accurate documentation of the mantle environment within the region, at the time of diamond crystallisation.

All diamonds analysed for their infrared absorption characteristics and mineral inclusion compositions were described in terms of their physical characteristics, with the objective to integrate these observations with measured chemical characteristics. In addition, this study attempts to document the geological processes that have affected the various diamonds subsequent to their crystallisation.

The study of the diamonds, mineral inclusions in diamond, and other mantle minerals sampled by the Swartruggens Kimberlite, therefore provide integrated information regarding the nature of the anomalous mantle below region of the Kaapvaal Craton. The study aims to provide a more complete understanding of the environment and nature of the diamond forming processes that characterise the mantle below the Kaapvaal Craton, particularly within the vicinity of the Bushveld anomaly. Further, this study reviews the theories and models of the day with respect to this unique and previously poorly studied mantle sample, that are the *gems* of the Swartruggens Kimberlite.

2 GEOLOGICAL SETTING

2.1 Introduction

Occurences of diamondiferous kimberlites in South Africa are concentrated within the boundaries of the Kaapvaal craton, where the ages of basement crustal rocks can exceed 3,5 Ga (e.g.: Hamilton *et al.*, 1979; de Wit *et al.*, 1992). The Swartruggens Kimberlite Dyke Swarm is one such kimberlite occurrence, situated approximately 60 km west of the town of Rustenburg, North-West Province, South Africa. The Elands River flows through the north of the region. The dyke swarm comprises numerous east-west trending, near vertical, kimberlite dykes (Harris *et al.*, 1979). This dyke system is commonly referred to as the 'Swartruggens Kimberlite', and is the highest grade kimberlite occurrence in South Africa. The Helam Diamond Mine (figure 2.1) currently exploits the dyke system for its diamonds. The western sections of the dyke are reported to carry 150 – 200 ct/100 tonnes, with grades as high as 500 ct/100 tonnes having been recorded. Toward the eastern sections of the dyke however, the grades and diamond quality decrease considerably with a maximum of only 80 ct/100 tonnes being reported (Gurney & Kirkley, 1996).

2.2 Historical

Alluvial diamonds were first discovered on the banks of the Elands River in 1933. By the late 1930's however, most of the alluvial gravels had been worked out, and some of the underlying kimberlite dykes had been discovered. New discoveries continued to be made into the 1950's, resulting in a combined kimberlite strike length of approximately 7 km. At this time the various holdings had developed into 16 separate operations, which made use of vertical shafts to access the kimberlite dykes at depth. By 1963 however, Helam Mining (Pty) Ltd owned virtually the entire kimberlite strike length (Davidson, 1998).

For the initial 11 year period 1964-1974 after the consolidation, Helam Mine produced an average of 157 270 carats per annum. However, between 1975 and 1983 the mine suffered a significant decline in production, only averaging 80 000 carrats per annum. The drop in yield was, in part, attributed to mining of the lower grade eastern extensions of the mine. In 1989 the present owners purchased the mine and by

1990 the operators (CJ Dippenaar and JM Davidson) had turned the mine to profit, and re-opened the western sections of the mine (Davidson, 1998).

The mine is still operating after more than 60 years of production and is believed to have produced a similar amount of diamonds to the famous Kimberley Mine on which De Beers initially created its wealth (Gurney & Kirkley, 1996). The mine currently exploits the kimberlite to depths in excess of 800 m.

2.3 Regional Geology

The Swartruggens Dyke intrudes the rocks of the Proterozoic Transvaal Sequence. At surface the kimberlite is observed to have intruded the andesitic lavas of the Pretoria Group, and with depth the kimberlite intrudes the shales and carbonates of the Chuniespoort Group (Skinner & Scott, 1979). In addition to the kimberlite, the shales are intruded by an older dolerite sill. The rocks of the Transvaal Sequence dip gently to the north, under the Bushveld Complex (which outcrops $\pm$ 30 km to the north and east of the dyke system).

The dyke system intrudes the central regions of the Kaapvaal Craton (figure 2.1). Its proximity to the Bushveld Complex adds interest to this kimberlite occurrence, as it should reflect the nature of the underlying mantle in the vicinity of the Bushveld Complex. The diamonds and diamond inclusion minerals should record the mantle environment at the time of diamond formation, while other mantle minerals will reflect mantle conditions at the time of kimberlite emplacement.

2.4 The Kimberlite

The major kimberlite mines of the world all exploit diatremes, however kimberlite is frequently emplaced in the form of dyke swarms. Where kimberlite dykes are rich enough, they have been exploited from the surface in several parts of the world. However it is only in South Africa that kimberlite dykes have been successfully mined underground. Moreover, only Group II kimberlite dykes have been mined economically in South Africa. The Swartruggens Dyke is one such Group II kimberlite dyke that is mined to depths in excess of 800 m, at the Helam Mine.

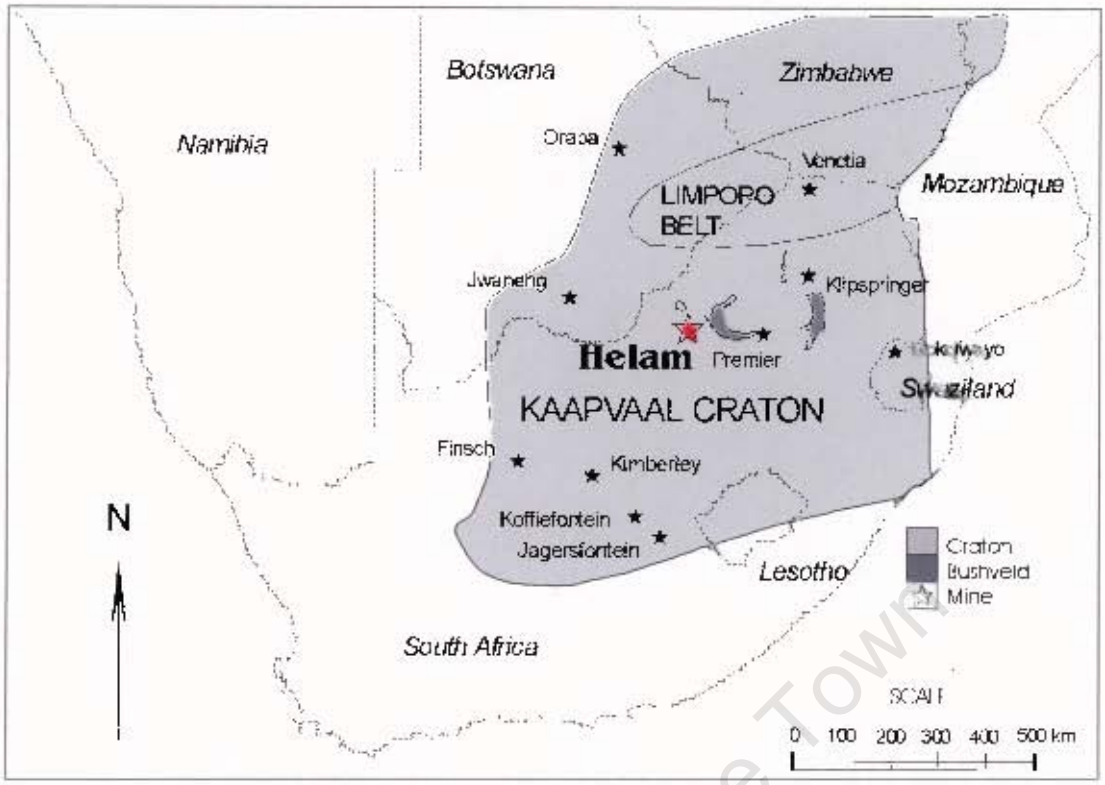

Figure 2.1 Locality map illustrating the positions of various diamondiferous kimberlites (Adapted from Westerlund, 2000). Helam Diamond Mine exploits the Swartruggens kimberlite. Notice the proximity of the mine to the Bushveld Complex, and its spatial relationship to other well studied kimberlite occurrences: Klipspringer and Premier mines.

2.4.1 Group I and Group II Kimberlites

Isotopic studies have been instrumental in developing models for the formation of, and differentiating between, Group I and II kimberlites. Smith's (1983) model, invokes separate origins for Group I and Group II kimberlites. Group I kimberlites have Sr, Nd and Pb isotopic signatures similar to those commonly associated with ocean island basalts and have been interpreted as being derived from the asthenosphere. Group II kimberlites however, exhibit higher $^{87}Sr/^{86}Sr$ ratios and somewhat lower $^{143}Nd/^{144}Nd$ ratios than Group I kimberlites. Consequently the Group II kimberlites have been interpreted as being derived from a source within the sub-continental lithosphere. It is interesting to note that megacrysts and hot, deformed peridotites are predominately found within Group I kimberlites (Gurney, 1990).

More recent Hf isotope data (Nowell *et al.*, 1999) challenge this conventional model for kimberlite genesis. These authors present data that show striking isotopic

similarities between Group I and Group II kimberlites (both display linear arrays, which are noticeably oblique to the main terrestrial magmatic array), which do not reconcile with the Smith (1983) model. The new data suggest a common sub-lithospheric source for both magma types.

Nowell *et al.* (1999) suggest that the isotopic signatures of both Group I and Group II kimberlites are most consistent with a model that invokes a source located at sub-lithospheric mantle depths, where ancient subducted oceanic crust is residing at depths of perhaps the 650 km discontinuity, or even the D'' layer. This model is consistent with the presence of diamonds that contain ultra-deep, possibly lower mantle, inclusions in some kimberlites (e.g.: Gurney & Moore, 1985). This model is also in agreement with le Roex (1986) who demonstrates that both groups of kimberlite can be generated within the asthenosphere by hot-spot activity, Group II kimberlites involving some component of recycled lithospheric material. If such hypotheses are to hold, then they must explain why the isotopically enriched Group II kimberlites do not sample the full megacryst suite nor the high temperature, deformed peridotites.

The classification of the Swartruggens Kimberlite as a Group II kimberlite has significance for the study of its entrained mantle sample. If Smith's (1983) model is correct (i.e.: that Group II kimberlites have a lithospheric source), then one would not expect any asthenospheric samples to be entrained within the Swartruggens Kimberlite. However, if suggestions made by Le Roex (1986) and Nowell *et al.* (1999) prove to be correct, then it *would* be possible to preserve an asthenospheric component among the mantle sample within the kimberlite.

2.5 Nature and Structure of the Swartruggens Kimberlite Dykes

The Swartruggens Kimberlite occurs as a dyke system of *en echelon* to anastomosing, interwoven kimberlitic lenses that pinch and swell along strike. The emplacement of the dykes (termed 'fissures' on the mine) is controlled by the fractures within the country rocks, commonly exploiting an E-W jointing pattern. The individual dykes are commonly offset from each other by several meters (Gurney & Kirkley, 1996). The dykes display variable dips, strikes and thicknesses that can be attributed to the relatively low competency of the wall rock shales. A thrust fault, located within the

lubricated carbonaceous shales on level 16 of Edward shaft, has had a strong influence on the geometry and emplacement of the kimberlite (Davidson, 1998).

The dykes are characterised by delicate flow banding, and show evidence for multiple intrusive events at the margins of the main body of kimberlite. This banding can only be observed locally as the kimberlite curves around irregular host rock protrusions. Such geometries, together with sharp wall rock contacts, are in support of a relatively slow rate of kimberlite emplacement (Gurney & Kirkley, 1996).

As many as six kimberlite dykes have been identified (Main, Changehouse, Muil, John, North and South fissures), each of which can be distinguished petrographically. Klump (1995) argues however, that the dykes are all genetically linked to a common magma source.

The diamond grades within the different dykes vary considerably, and consequently it has become essential to mine the dykes selectively. The 'Main' and 'Changehouse' fissures, which commonly strike parallel to one another, are the only phases exploited by the mine.

2.5.1 The Main Fissure

The Main Fissure is economically exploitable, and is the thickest dyke in the dyke system, averaging 60 cm. This dyke is highly variable in its dimensions and is characterised by a fine phlogopite groundmass, coarse-grained olivine and phlogopite macrocrysts, as well as orange and purple garnet macrocrysts.

2.5.2 Changehouse Fissure

The Changehouse Fissure is subeconomic and contains coarser phlogopite in its groundmass and more numerous phlogopite macrocrysts than the Main Fissure. This dyke typically reaches a thickness of between 20-40 cm, but also shows great variability along strike (Gurney & Kirkley, 1996). The kimberlite is characterised by olivine macrocrysts (less than Main Fissure), as well as purple, orange and red garnet macrocrysts. Klump (1995) suggests that the appearance of the red garnets in the Changehouse Fissure signifies a drop in the diamond grade, due to secondary processes that occurred within the kimberlite magma. It is estimated that the grade of the Changehouse Fissure is as much as 90% lower than within the Main Dyke.

2.5.3 Muil Fissure

This kimberlite (also referred to as the 'Mail' Fissure) is barren, and has been described as a lamprophyre (Skinner & Scott, 1979), or an extreme end-member of the Group II kimberlites (Allan, 1990). This dyke only occurs in the western sections of the mine, and is characterised by nepheline, sanidine and altered leucite (Skinner & Scott, 1979). The Muil Fissure carries no mantle sample at all, and from various field relations, has been interpreted as representing the youngest of the intrusions (Klump, 1995).

2.6 Age Relationships

Radiometric dating based on the Rb-Sr mica isochrons has reported ages of 147 $\pm$ 4 Ma (Allsopp & Barrett, 1975) and 156 $\pm$ 13 Ma (Smith *et al.*, 1985). Field relationships suggest that the Main Fissure is the oldest phase. It can also be shown that the Changehouse Fissure is younger than the Main Fissure, but older than the Muil Fissure (Klump, 1995). It follows therefore that there appears to be a drop in grade with each successive intrusion of kimberlite. An analysis and explanation of this grade variability is discussed in Chapter 3.

The age of the Swartruggens Dyke is within error of the 147.7 $\pm$ 3.8 Ma age obtained for the Klipspringer kimberlites (Westerlund, 2000), located adjacent to the Eastern Limb of the Bushveld Complex (figure 2.1). The similarity in ages between the Klipspringer and Swartruggens occurrences suggests a widespread Group II kimberlite emplacement event at around 150 Ma (Westerlund, 2000). More importantly though, the similarity in age suggests that the Swartruggens and Klipspringer kimberlites contain mantle material sampled approximately contemporaneously, on *opposite* sides of the Bushveld Complex, from the anomalous mantle which characterises the central regions of the Kaapvaal craton. A comparison of the mantle sample from these two localities, together with that of the older (1250 Ma) Premier kimberlite (Barrett & Allsopp, 1973), which intrudes the Bushveld Complex, will therefore frequently be called upon, in order to better understand this anomalous mantle on a more regional basis.

3 UPPER MANTLE MACROCRYSTS OF GARNET AND CHROMITE

3.1 Introduction

Regular sampling of the Swartruggens Kimberlite dykes encountered underground at the Helam Diamond Mine, has shown that the various kimberlitic phases, comprising the dyke system, can be distinguished petrographically (Allan, 1990). It will be demonstrated that in addition, the macrocryst assemblages among these various phases, can be distinguished compositionally. The principal differentiating factor is the relative abundance of the various types of garnet macrocrysts found within the various kimberlites (or 'Fissures' as termed on the mine). Davidson (Helam Geologist and Director) has made an empirical correlation between the garnet macrocryst populations of the various kimberlite dykes, and diamond grade. This technique has proven to be highly effective in discriminating between high grade kimberlites and those with lower grades. Knowledge of the diamond grade of the various kimberlite dykes is essential for maintaining mine profitability, yet this cannot be provided by bulk sampling in narrow ore shoots of limited tonnage.

Klump (1995), in a pilot study of the Swartruggens Kimberlite dyke swarm, undertook a statistical study of the mantle macrocrysts from the various kimberlite dykes intersected underground at the Helam Mine. Klump (1995) recognized 7 colour categories corresponding to chemically distinct groupings of garnet. Two distinctive chromite populations were defined on the basis of surface characterisation. While thorough in his statistical analysis of the macrocrysts, Klump (1995) did not convincingly explain the association between the mineral compositions and diamond grade.

Gurney & Zweistra (1995) emphasize the importance of the interpretation of the major element compositions of mantle minerals in differentiating diamond grades between various kimberlites. In an attempt therefore to make an association between macrocryst mineralogy and diamond grade, as well as to provide a foundation of comparison between the macrocryst compositions and that of the diamond inclusions, an independent study of the mantle macrocrysts was conducted in this study.

The results are broadly similar to those of Klump (1995), but the data set acquired is more successful in categorising the chemical nature and variability of the mantle macrocrysts. In particular, this study provides valuable insight concerning the

nature of the underlying mantle in the area, and the associations between the diamond grade and other mantle minerals sampled by the kimberlite.

The diamond grade of any kimberlite is dependent on factors such as: (i) the amount of diamond-bearing peridotite and eclogite sampled by the kimberlite; (ii) the diamond grade of the source rocks; (iii) the degree of preservation of the diamonds during their transportation to shallower levels within the crust (Fipke *et al.*, 1995).

Sampling of mantle xenoliths within a kimberlite would be one way of assessing diamond grade of mantle rocks. However these are often very uncommon, and are never available in adequate amounts to permit a quantitative study. It therefore becomes important to study the disaggregated mantle minerals found in the kimberlite. The greater the abundance of macrocrysts from disaggregated, potentially diamondiferous source rocks within a kimberlite, the higher the grade that kimberlite may be (Fipke *et al.,* 1995). This study attempts to analyse the relative contributions from various potentially diamondiferous source rocks, from disaggregated mantle material, in order to explain grade variation among the various kimberlite phases.

3.2 Nature of the Sample

Samples of kimberlite were taken from the Main Fissure (high grade, >1 carat/tonne) and Changehouse Fissure (lower grade, <0.5 carat/tonne) in order to provide a useful comparison between those macrocryst compositions associated with kimberlite of high diamond grade and that associated with low grade. Moreover, these are the two major kimberlites encountered in the mine, consequently the diamonds produced from the mine have originated within them, making a comparison between the macrocrysts and the diamond inclusions particularly significant. The macrocrysts were released from the kimberlite by mechanical crushing and a heavy mineral settling process at the mine. In total, 68 and 88 garnet macrocrysts were sampled from the Main and Changehouse Fissures respectively. While Klump (1995) identified seven garnet colour types, the current study focused on *three* principal colors of the garnet population. Firstly because this is the system employed at the Helam Diamond Mine, and secondly because differentiation by shade of colour is highly subjective, and it was suspected that some apparent colour categories were an artifact of grain thickness.

The Main Fissure (high grade) shows a dominance of purple garnets, with a subsidiary population of orange garnets, and minor red garnet macrocrysts. In contrast, the Changehouse Fissure (sub-economic) is characterised by almost equal abundances of red, purple and orange garnet macrocrysts. This, is the criterion employed by Davidson to distinguish between the higher grade Main Fissure and the lower grade Changehouse Fissure. All three garnet types were sampled from both kimberlites, in proportion to their abundance. In addition, 30 chromites from each kimberlite were sampled, without reference to the classification of Klump (1995).

3.3 Chemical Compositions of the Garnet Macrocrysts

Peridotitic (Cr-rich) garnet macrocrysts are the single most important discriminating mineralogy, in terms of diamond grade potential (Gurney & Zweistra, 1995). In addition, analysis of the compositions of the various garnet macrocrysts, provide useful insight concerning the nature and/or variability of the underlying mantle.

The compositions of the garnet macrocrysts were analysed using an electron microprobe, as described in Appendix 1. The chemical compositions of the garnet macrocrysts are presented in Appendix 1.1 & 1.2, having been presented as oxides rather than cations, simply to allow for comparison with other published data in the same format. The chemical data have been plotted on various bivariant plots as illustrated in figure 3.

Figures 3.1a and 3.1b illustrate that there is a large population of orange, Cr-poor (<1 wt.% Cr_2O_3) garnets associated with both the Main and Changehouse fissures. In addition both kimberlites contain Cr-rich (or peridotitic) garnets with as much as 10 wt.% and 7 wt.% Cr_2O_3 in the Main and Changehouse fissures respectively. These peridotitic garnets correspond to the purple and red macrocryst populations sampled from the kimberlites.

In order to differentiate between diamond-bearing and non-diamondiferous kimberlites on the basis of the composition of peridotitic chrome-bearing pyrope garnets, Gurney (1984) statistically derived a line separating a high and low calcium field in a CaO versus Cr_2O_3 diagram. This line has been illustrated in figures 3.1, and corresponds to the division which is widely used to separate peridotitic garnets into lherzolitic and harzburgitic parageneses respectively (Sobolev *et al.*, 1973; Harris, 1992). The peridotitic garnets (high-Cr) generally plot along and to the low calcium

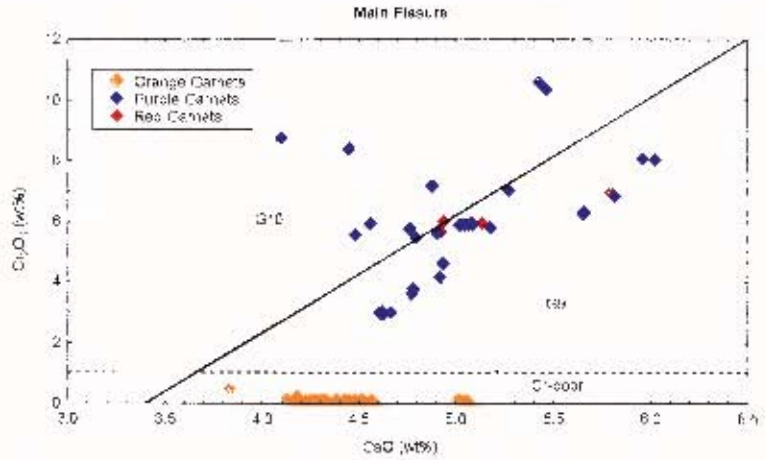

Figure 3.1a Chrome vs. calcium for garnet macrocrysts from the Main Fissure. Dashed line defines the low chromium garnets, and solid line (85% line) defines a lherzolitic trend at 50 kbars pressure (Gurney & Zweistra, 1995)

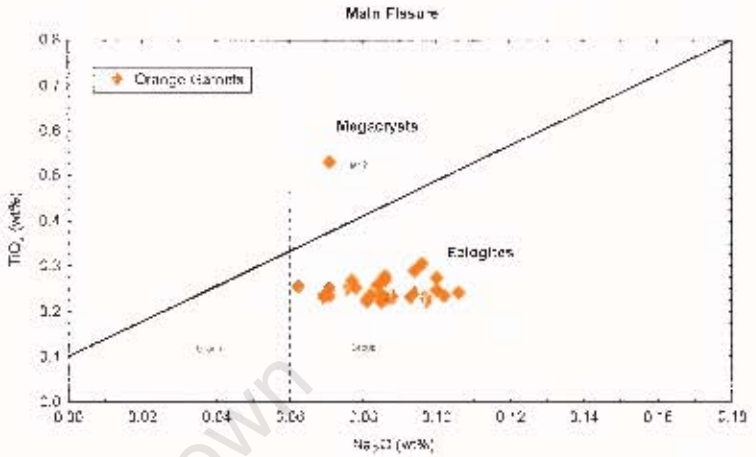

Figure 3.2a Titanium vs. sodium for Cr-poor garnet macrocrysts from the Main Fissure. Dashed line separates between Group I and Group II eclogites (McCandless & Gurney, 1979). Solid line separates Cr-poor megacrysts and eclogitic garnets (Kimberlite Research Group data base, University of Cape Town)

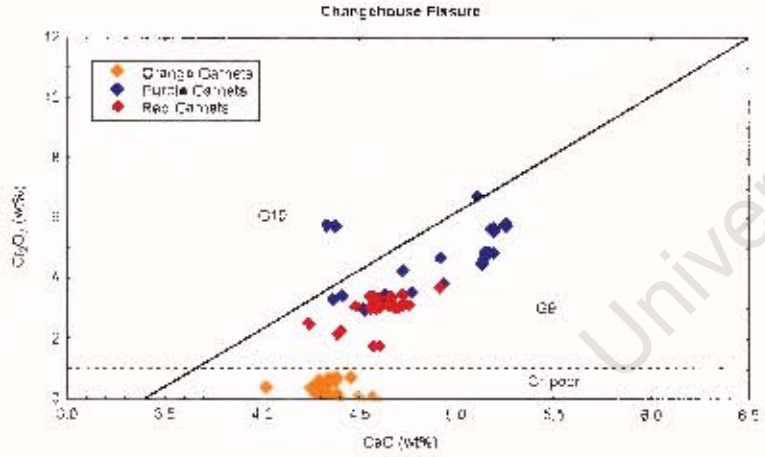

Figure 3.1b Chrome vs. calcium for garnet macrocrysts from the Changehouse Fissure. Dashed line defines the low chromium garnets, and solid line (85% line) defines a lherzolitic trend at 50 kbars pressure (Gurney & Zweistra, 1995)

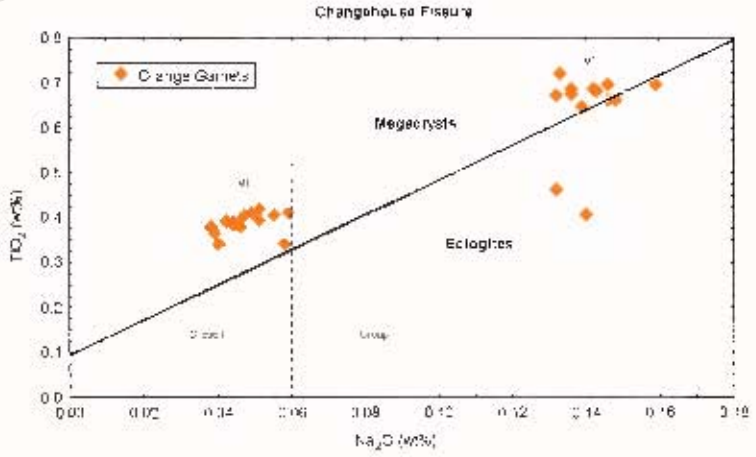

Figure 3.2b Titanium vs. sodium for Cr-poor garnet macrocrysts from the Changehouse Fissure. Dashed line separates between Group I and Group II eclogites (McCandless & Gurney, 1979). Solid line separates Cr-poor megacrysts and eclogitic garnets (Kimberlite Research Group data base, University of Cape Town)

side of the trend commonly observed for lherzolitic garnets (lherzolite trend or 85% line), some however exhibiting significantly elevated Cr_2O_3 values. Gurney & Zweistra (1995) have reported that garnets that plot along this trend have equilibrated at pressures of approximately 50 kbars. The significance of this line is that known diamondiferous kimberlites are commonly associated with garnet mineralogies that plot within the low calcium field as defined by the lherzolite trend line (G10 garnets). The lowest calcium values within garnets from lherzolites are associated with the highest equilibration pressures (Fipke *et al.*, 1995). In addition, kimberlites with higher diamond concentrations tend to have a higher proportion of garnet mineralogies scattered within the low-CaO (or subcalcic) field. Higher chromium garnets (at a given CaO value) too, are generally associated with higher diamond concentrations (Gurney & Zweistra, 1995).

The red garnets of the Main Fissure have compositions that consistently plot among the values associated with the purple garnets. Within the Changehouse Fissure however, the purple garnets are more tightly clustered, and the red garnets appear to define a chemically distinct group, typically exhibiting lower Cr_2O_3 values than the purple garnets. The peridotitic garnets of the Main Fissure show a relatively large range of CaO concentrations, a substantial proportion of which plot within the subcalcic region, as defined by the lherzolite trend. These subcalcic, high-Cr, purple garnets extend into compositions associated with harzburgitic xenoliths, and can be considered diamond indicators. The peridotitic garnets of the Changehouse Fissure however, are differentiated by their comparatively lower Cr contents, and restricted range in CaO concentrations. The vast majority of the Changehouse high-Cr garnets are thus classified as lherzolitic. In addition, the Changehouse Fissure is characterised by a comparatively smaller proportion of garnets plotting within the sub-calcic field. Those garnets that *do* plot within the sub-calcic field are purple in colour, and have relatively low Cr_2O_3 concentrations.

The occurrence of two distinctive types of *low*-Cr, eclogitic garnet was first reported by MacGregor & Carter (1970). The authors termed the two types Group I and Group II eclogites based principally on the differences in their textural characteristics. In general, it has been demonstrated that garnets from the Group I eclogites are enriched in Na_2O compared with the Group II eclogites (McCandless & Gurney, 1989). Further, the mineral compositions associated with Group I eclogites can be correlated with the equilibration conditions understood to be required for the

processes of diamond formation. Diamonds are only found in association with Group I eclogites. It is clear then, that in terms of diamond exploration and diamond grade prediction, it is important to differentiate between eclogitic garnets belonging to these two groups (Gurney, 1984).

Figures 3.2a and 3.2b show the relationships between TiO_2 and Na_2O for the low-Cr, orange garnets from both kimberlites. The majority of the low-Cr garnets within the Main Fissure show an enrichment in Na_2O (>0.06 wt.% Na_2O), and plot within the field ascribed to Group I eclogites. The Changehouse Fissure, by contrast, shows some striking differences from the Main Fissure. While also displaying a large population of low-Cr, orange garnets, the majority of these exhibit highly elevated titanium concentrations. Comparison of these mineralogies with that of the Kimberlite Research Group database (University of Cape Town), shows that they occupy a field assigned to megacryst populations worldwide (see figure 3.2b). The inferred sub-division between eclogitic and Cr-poor megacrystic garnets is represented by the solid division line in figures 3.2a and 3.2b.

It has been shown that megacrysts may be pertrogenetically related to their host kimberlite, having been crystallised from a differentiating magma (e.g.: Moore & Gurney, 1991; Bell *et al.*, 1995). Megacrysts have been found in both Group I and Group II kimberlites but display certain compositional differences. Megacrysts from Group II kimberlites generally display higher Cr_2O_3 contents (up to ~ 5 wt%), higher Mg# (up to ~ 91) and lower TiO_2 (as low as ~ 0.4 wt.%) (Moore & Gurney, 1991; Bell et al., 1995) than megacrysts from group I kimberlites.

It is suggested, based on the compositional similarity with magacrysts from worldwide Group II kimberlites, that the vast majority of the low-Cr garnets of the Changehouse Fissure are in fact megacrystic. Only two low-Cr garnets from the Changehouse Fissure plot within the field ascribed to Group I eclogites. These garnets appear relatively enriched in titanium compared to the Group I eclogites of the Main Fissure.

The megacrystic garnets from the Changehouse Fissure separate into two distinct groups; a low-Na, Low-Ti group (called M1), and a High-Na, High-Ti group (called M2). It can be argued, based on compositional similarity, that the single low-Cr, megacrystic garnet of the Main Fissure is more closely associated with M1.

Figures 3.3a and 3.3b show that the low-Cr, orange garnets of the Main Fissure are associated with a large range in Mg#, typically exhibiting relatively low

values (as low as 60). Data from the Kimberlite Research Group database (University of Cape Town) show that worldwide eclogitic garnets exhibit relatively low Mg#'s (below 75). The assignation of the low-Cr, orange garnets of the Main Fissure to the eclogitic paragenesis is therefore justified. By contrast, the majority of the low-Cr garnets of the Changehouse Fissure show relatively elevated Mg#'s (greater than 70). The high-Cr harzburgitic and lherzolitic garnets from both the Main and Changehouse Fissures, show a restricted range of Mg#'s, which are ubiquitously high (above 85).

Figures 3.4a and 3.4b illustrate some further compositional differences between the garnet macrocrysts from the two kimberlites. The peridotitic (high-Cr) garnets from the Main Fissure show a restricted Ti-content range (typically less than 0.15 wt.% TiO_2). Within the Changehouse Fissure however, it can be observed that a much larger proportion of the high-Cr garnets plot towards high TiO_2 values (up to 0.5 wt % TiO_2). Again, a clear division between the compositions of M1 and M2 can be observed. The high-Ti, low-Cr orange garnet within the Main Fissure, once more appears to be closer in composition to that of the M1 megacryst suite observed within the Changehouse Fissure.

3.4 Chemical Compositions of the Chromite Macrocrysts

A second important peridotitic mineral to consider regarding diamond potential is chromite (Gurney & Zweistra, 1995), the composition of which is not readily affected by metamorphic or metasomatic processes. The composition of chromite is analysed in order to provide an indication of the amount of material in kimberlites derived from disaggregated chromite harzburgite (Fipke *et al.*, 1995). Chromite is useful as a diamond indicator because the chromium content of the mineral is pressure dependent (Daniels, 1991). Fipke *et al.* (1995) have recognised three chromite sub-populations, the most important of which are those associated with the diamond inclusion chromite field (figures 3.5a and 3.5b). This field is characterised by high Cr_2O_3 (60-70 wt.%), and moderate to high levels of MgO (12-16 wt.%). These are further characterised by very low contents of titanium, usually less than 0.6 wt.% TiO_2 (Fipke *et al.*, 1995). It follows therefore that the chromites that fall within this field provide the most useful information regarding diamond grade potential (Gurney & Zweistra, 1995).

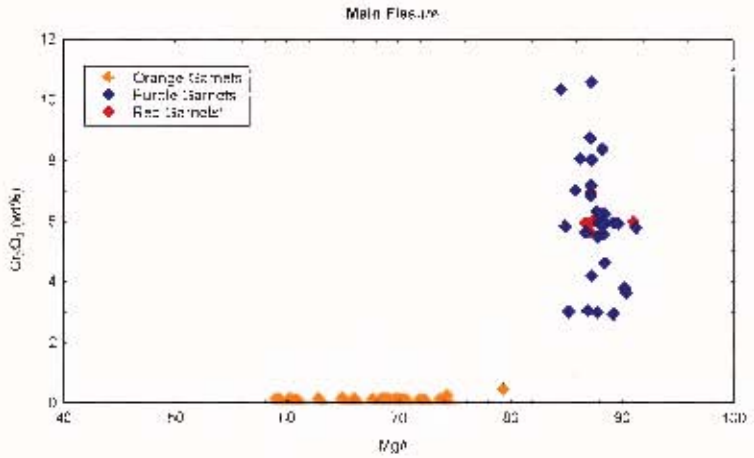

Figure 3.3a Chrome vs. Mg# for the Main Fissure macrocrysts garnets

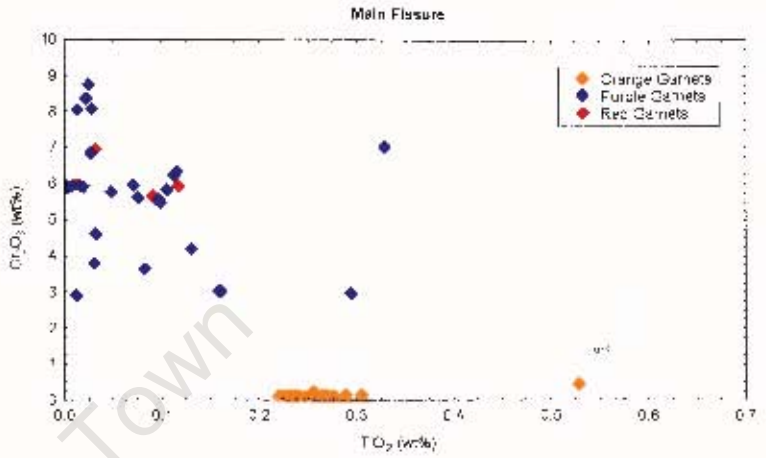

Figure 3.4a Chrome vs. titanium for Main Fissure macrocryst garnets

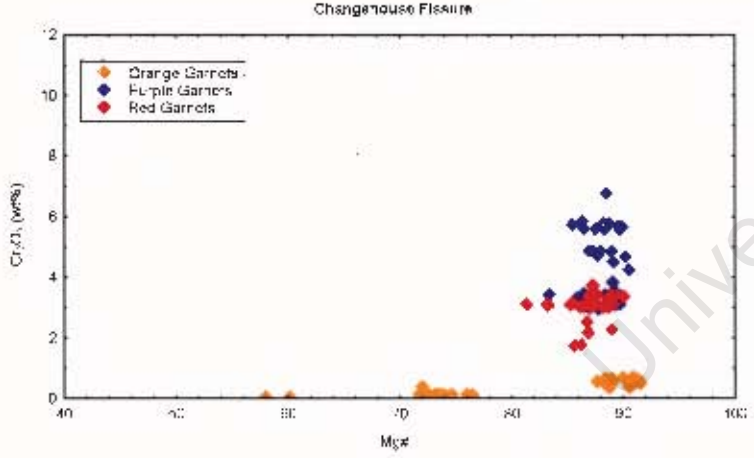

Figure 3.3b Chrome vs. Mg# for the Changehouse Fissure macrocrysts garnets

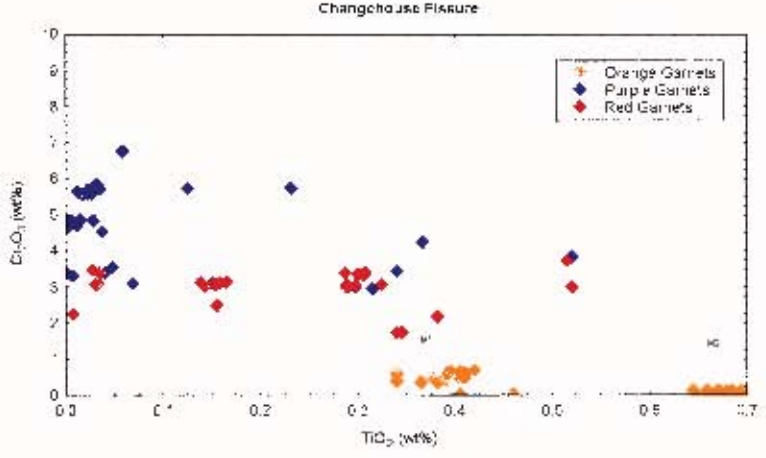

Figure 3.4b Chrome vs. titanium for Changehouse Fissure macrocryst garnets

Chromite macrocrysts from the Main and Changehouse Fissures were analysed using an electron microprobe, as described in Appendix 1. The chemical compositions of these chromite macrocrysts are presented in Appendices 1.3 & 1.4.

Figures 3.5a and 3.5b illustrate the Cr_2O_3-MgO relationships of the various chromite macrocrysts. The chromites from both the Main and Changehouse kimberlites tend to cluster in and around the diamond inclusion field, exhibiting limited variation in both Cr_2O_3 and MgO. Approximately 80% of the chromites within the Main and Changehouse Fissures plot within the field associated with diamond inclusions, according to this plot. The inference, from *this* plot therefore, is that the vast majority of chromites have been derived from disaggregated, potentially diamondiferous chromite-harzburgite. It can be observed perhaps, that the chromites within the Main Fissure cluster more closely within the diamond inclusion field than those within the Changehouse Fissure.

It can be demonstrated however, that mantle-derived chromites exhibit substantial variation in major and minor element concentrations, and it has been shown that several sub-populations of chromites may be present within a kimberlite (Fipke *et al.*, 1995):

(i) macrocrysts sampled from the upper mantle, from both within the diamond stability field and from shallower depths.

(ii) magmatic (phenocryst) chromites

(iii) xenocrysts which have reacted with the host kimberlite.

It is imperative therefore, that a recognition of the various chromite types present in a kimberlite is made, before proceeding with an assessment of diamond potential.

Figures 3.6a and 3.6b illustrate the relationship between Cr_2O_3 and TiO_2. The fields associated with diamond inclusions, chromite phenocrysts and chromite xenocrysts have been superimposed, in order to make a *better* distinction between various types of chromite populations. Fipke *et al.* (1995) caution that overlap commonly occurs between the composition of the various types of chromites. Nevertheless, it becomes clear that according to this plot, only 30% of the chromites from both the Main and Changehouse Fissures exhibit compositions *uniquely* associated with chromite inclusions in diamond. The majority of the chromites however, plot beyond this field, extending towards compositions associated with chromite phenocrysts. Only a small proportion of the chromites (<10%) plot within the field ascribed to chromite xenocrysts. It is clear then, that this plot is more

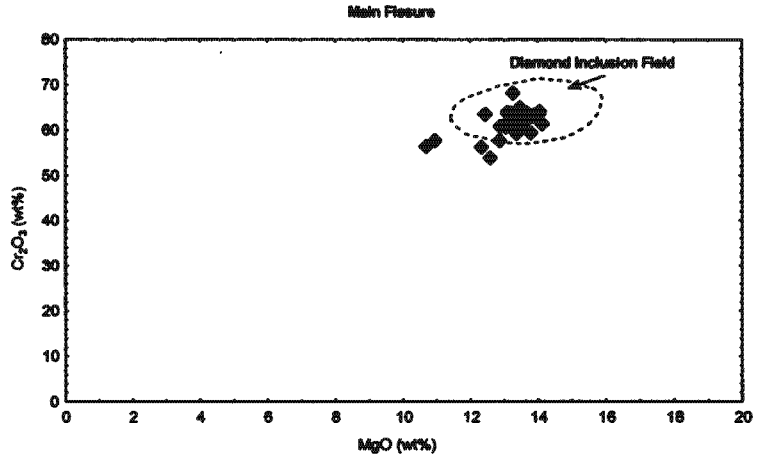

Figure 3.5a Chromium vs. magnesium for Main Fissure macrocryst chromites. Dashed line defines the compositional field associated with chromites found as inclusions within diamond from worldwide localities (Diamond Inclusions Field) (Fipke *et al.*, 1995).

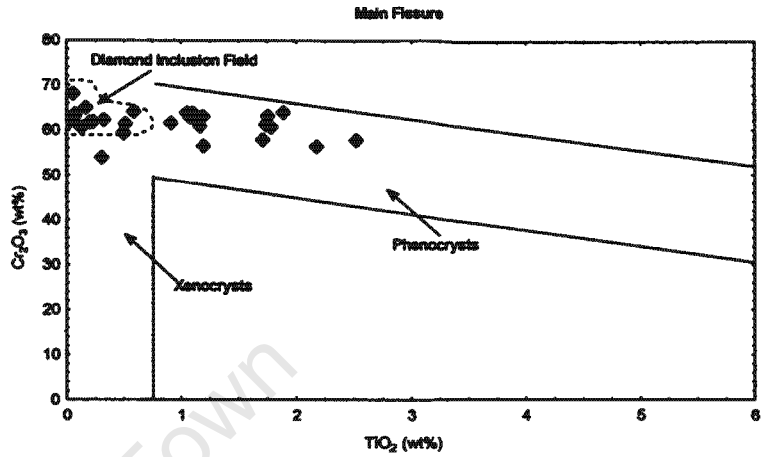

Figure 3.6a Chromium vs. titanium for Main Fissure macrocryst chromites. Dashed line defines the compositional field associated with chromites found as inclusions within diamond from worldwide localities (Diamond Inclusion Field) (Fipke *et al.*, 1995).

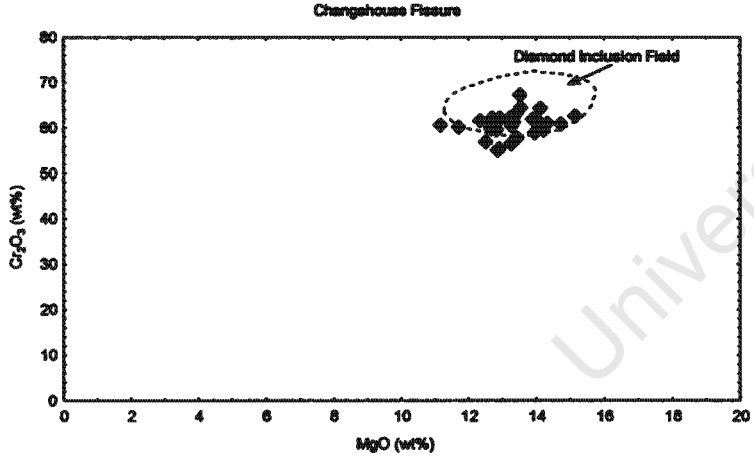

Figure 3.5b Chromium vs. magnesium for Changehouse Fissure macrocryst chromites. Dashed line defines the field of compositions associated with chromites found as inclusions within diamond from worldwide localities (Diamond Inclusions Field) (Fipke *et al.*, 1995).

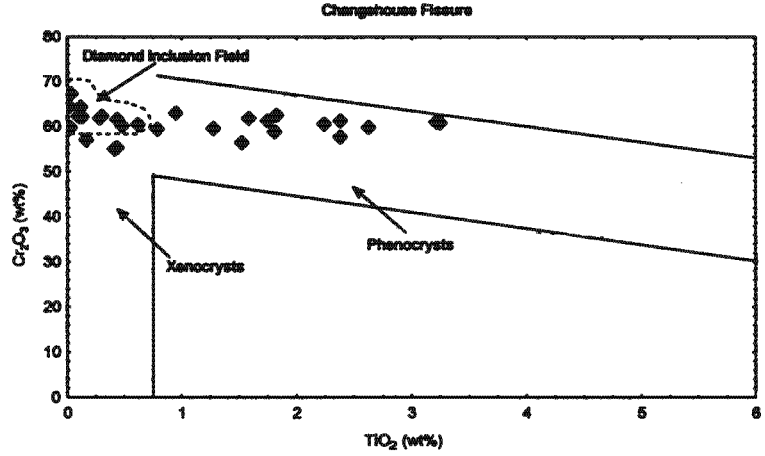

Figure 3.6b Chromium vs. titanium for Main Fissure macrocryst chromites. Dashed line defines the compositional field associated with chromites found as inclusions within diamond from worldwide localities (Diamond Inclusion Field) (Fipke *et al.*, 1995).

successful in discriminating between chromites associated with diamond stability and those that are not. It follows that the plots of figures 3.5, give an overestimation of the amount of disaggregated, potentially diamondiferous chromite-harzburgite.

It is important to note that Klump (1995) found that the chromites within the Changehouse Fissure were often highly resorbed, while within the Main Fissure the chromites appeared more euhedral, with little evidence for resorption. This observation may be significant in considering the relationships between the dykes, as well as their petrogenesis (see below).

3.5 Interpretation and Discussion

It is clear that the mineralogical differences between the Main and Changehouse fissures, correlate well with the empirical observations made on the mine to discriminate between kimberlite associated with high and low diamond grades. Below, the compositional data presented is discussed in terms of mantle stratigraphy, as well as the relationship between the macrocryst compositions and diamond grade.

3.5.1 The Main Fissure

Major element analysis of the garnet macrocrysts from the Main Fissure demonstrate that the underlying mantle sampled by this kimberlite comprises eclogitic, lherzolitic and harzburgitic lithologies. Approximately 30% of the peridotitic (high-Cr) garnets plot within the subcalcic field (all of which are purple, G10 garnets). In addition these garnets display elevated Cr_2O_3 contents, and are good diamond indicators.

The majority of the low-Cr, orange garnets from the Main Fissure plot within the field ascribed to Group I eclogites, with only one point plotting among values associated with megacrysts. The large population of eclogitic macrocrysts attests to an underlying mantle, comprising a volumetrically significant component of eclogite. Moreover, this eclogitic component displays compositions consistent with diamond stability (Group I eclogite). The single megacrystic garnet analysed from the Main Fissure sample, very closely resembles the M1 megacrysts of the Changehouse Fissure.

The chromite compositions in the Main Fissure show that a significant proportion of these macrocrysts (±30%) are similar to those of diamond inclusions,

despite a large phenocryst population. This suggests that the harzburgitic source represented by the harzburgitic garnet macrocrysts, may be a diamond bearing garnet/chromite harzburgite, or that there may be a separate chromite-harzburgite paragenesis.

These characteristics are common to kimberlites with high diamond grade (Gurney, Pers. Comm., 2001). It is clear that the contribution of a potentially diamondiferous harzburgitic source (as manifest by the subcalcic garnets and some of the chromite macrocrysts) and eclogitic source (manifest by the majority of the Cr-poor, orange garnets) has been *additive*, resulting in the overall high grade of the Main Fissure (>1 carat/tonne).

3.5.2 The Changehouse Fissure

The Changehouse Fissure, also exhibits a predominant lherzolitic component, but appears to incorporate a somewhat subordinate quantity of harzburgitic material, and only a very minor contribution from an eclogitic source. The absence of a significant eclogitic mantle component, and the presence of a large megacrystic population, correlates with the relatively lower diamond grade of the kimberlite.

While the red garnets appear to be chemically distinct (lower Cr) from the purple garnets, both peridotitic garnet types appear to be mainly lherzolitic. The greater proportion of Ti-enriched peridotitic garnets within the Changehouse Fissure, in comparison with those of the Main Fissure, is interpreted to be caused by a process of metasomatism that has affected the macrocrysts from the Changehouse Fissure. Enrichment of titanium is frequently a product of metasomatism (e.g.: Kramers *et al.*, 1983; Harte & Hawkesworth, 1986; Menzies & Hawkesworth, 1987; Dawson, 1999). Perhaps, in this case, the relevant metasomatic process has also had a negative effect on the diamond grade of the kimberlite. The absence of such metasomatism among the macrocrysts from the Main Fissure, opens the possibility that this chemical event post-dated the intrusion of the Main Fissure.

While a large proportion of the orange garnets are low-Cr, unlike the Main Fissure, the orange garnets of the Changehouse Fissure are predominantly megacrystic, with only two of the low-Cr garnets showing Group I eclogitic affinity. The Changehouse Fissure exhibits two megacryst populations, a low-Ti group (M1) and a high-Ti (M2) group, indicative of two separate megacryst forming events. It can

be demonstrated that the composition of the single megacryst of the Main Fissure corresponds more closely to the compositions of the low-Ti megacrysts (M1) of the Changehouse Fissure. The M1 megacrysts exhibit relatively lower TiO_2 and Na_2O, and higher Mg#'s, while the M2 megacrysts exhibit relatively higher TiO_2 and Na_2O values, with lower Mg#'s.

The chromite compositions are very similar to those of the Main Fissure with a significant proportion of chromites corresponding to compositions associated with the diamond stability field, but with a predominant phenocryst component. It is suggested therefore that the Changehouse Fissure has most likely sampled the same chromite harzburgite source as the Main Fissure.

The Changehouse Fissure has clearly been far less successful in sampling Group I eclogite. It is reasonable to assume then, that chromite harzburgite has been the only major contributor of potentially diamondiferous material within this kimberlite. This may well explain the significantly lower grade associated with this kimberlite compared to that of the Main Fissure, which exhibits additive contributions from both eclogitic and harzburgitic sources.

3.6 Petrogenetic Model

The geochemical analysis of the macrocryst populations from the Main and Changehouse fissures, has shown that their respective macrocryst populations are distinguishable, and that the diamond grade at the Helam Mine is reflected by the additive contribution of harzburgitic and eclogitic mantle material sampled by the kimberlites. The empirical technique employed on the Helam Mine to assess kimberlite grade is supported by these findings.

The observations made from this data, together with that of Klump (1995) can be used to establish a petrogenetic model for the formation of the Swartruggens Kimberlite dyke system. However, such a petrogenetic model must explain certain key interpretations and observations:

1) The Main, Changehouse and Muil fissures were all derived from a common source (Klump, 1995).
2) Macrocrysts and mineral inclusion data suggest multiple sources of diamond.

3) The Main Fissure (1st intrusive phase) has a higher diamond grade than the Changehouse Fissure (intermediate intrusive phase), and the Muil Fissure (final intrusive phase) is completely barren of all mantle minerals.
4) The dykes show an evolutionary trend from Group II kimberlite (Main Fissure) to a magma transitional in composition between kimberlites and lamproites (Muil Fissure) (Klump, 1995).
5) The Changehouse Fissure exhibits two megacryst populations.
6) The Changehouse Fissure exhibits highly resorbed chromites (Klump, 1995)
7) There is evidence for a metasomatic overprint associated with the garnets from the Changehouse Fissure

Figure 3.7 illustrates the proposed petrogenetic model, which attempts to explain all the above mentioned observations.

It is suggested that a kimberlite, or protokimberlite, originated at depth within the Earth's mantle. Evidence, suggests that this source may have been within the asthenosphere (Chapter 6). The magma migrated into the lithosphere, randomly sampling both diamondiferous eclogite and harzburgite material, as well as other non-diamondiferous lithologies. Chemical interaction between the magma and the surrounding lithosphere may have imparted a lithospheric signature to that magma. It is suggested that this first pulse of magma may have sampled some of the M1 megacrysts, before the M2 megacryst forming event was initiated. The first kimberlite to intrude the crust (Main Fissure) would consequently have had a lithospheric component (i.e.: chemical and petrological characteristics of a Group II kimberlite). Moreover, the Main Fissure would have had a high concentration of both peridotitic and eclogitic diamonds, as well as a small proportion of M1 megacrysts.

At some later time (T=2), a second pulse of magma resulted in the intrusion of another kimberlite dyke (Changehouse Fissure). It is suggested that this occurred at some time subsequent to the M2 crystallisation event (i.e.: that the intrusion of the Changehouse Fissure was delayed sufficiently to allow the crystallisation of the M2 megacrysts). In addition, it is argued that this second thermal pulse occurred at some time subsequent to a metasomatic event within the lithosphere. The observations that the Changehouse Fissure is associated with highly resorbed chromites (Klump, 1995) and contains Ti-enriched garnets, are in agreement with this suggestion. The absence of significant quantities of eclogitic material is perhaps best explained by random

Petrogenetic Model for the Formation of the Swartruggens Kimberlite Dyke System

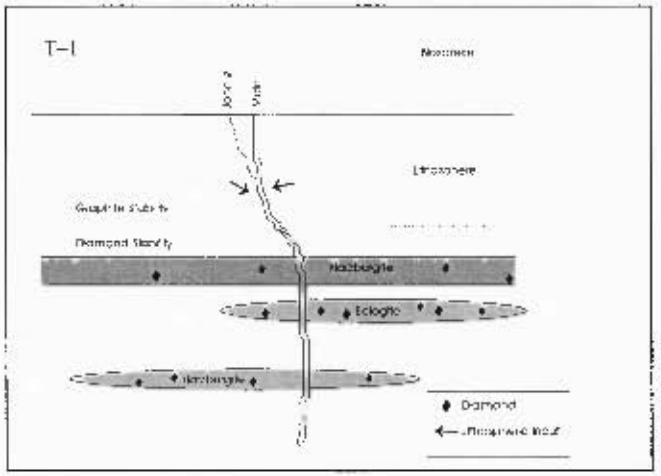

Figure 3.7a The lithosphere in the area is characterised by unmetasomatised, non-diamondiferous peridotite (unshaded), interbedded with mineralised (shaded) harzburgite and eclogite within the diamond stability field. The Main Fissure is derived from a kimberlitic melt, laden with both diamondiferous eclogite and harzburgitic, as well as minor megacrysts. There is limited lithospheric input, and diamond grades within the dyke are high (up to 500 carats/100 tonne). John# Fissure is derived from a melt associated with the Main Fissure.

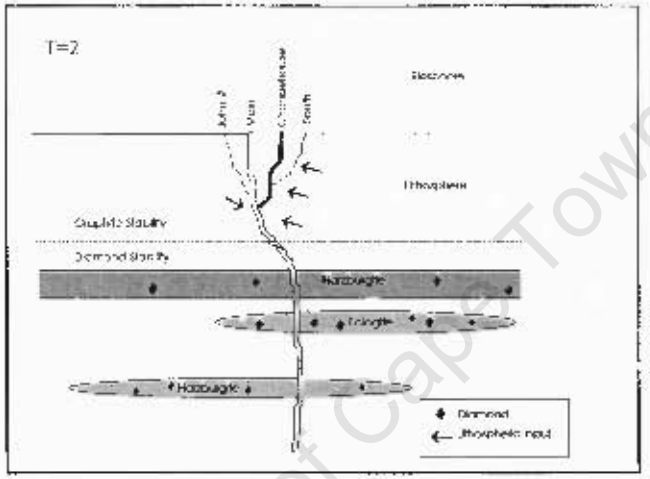

Figure 3.7b After some metasomatic event, a second thermal pulse results in the intrusion of the Changehouse Fissure. Due to random sampling of the mantle by the kimberlite, very little eclogitic material is entrained within the kimberlite. Consequently the kimberlite is dominated by harzburgitic material. In addition this kimberlite samples both M1 and M2 megacrysts. There is increased lithospheric interaction with the kimberlite. The South Fissure is derived from a melt associated with the Changehouse Fissure.

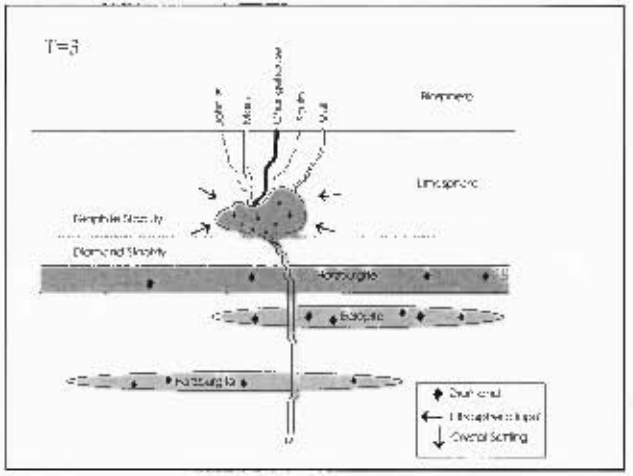

Figure 3.7c Magma is 'pooled' within the lithosphere, outside of the diamond stability field, resulting in increased lithospheric interaction and crystal settling. The changing melt composition, together with the diamonds residence outside diamond stability results in resorption of the crystals. In addition, mantle minerals will settle, resulting in dilution of diamond grade. A final thermal pulse results in the intrusion of the Muil Fissure, which is characterised by a complete absence of mantle minerals.

sampling of the mantle, whereby predominantly harzburgitic lithologies were sampled. The metasomatic event, mentioned above, may also have resulted in resorption of many of the Helam diamonds within the mantle, diluting the potential grade of the kimberlite even further.

It is suggested that after the intrusion of the Changchouse Fissure, the remainder of the melt pooled within the lithosphere (outside of the diamond stability field) in the form of a magma chamber. Increased interaction of the surrounding mantle with the magma chamber, would have imparted a highly lithospheric component to the melt. The changing melt composition, together with residence outside of the diamond stability field, would have resulted in extensive resorption of any diamonds remaining within the magma chamber. It is suggested that the processes of crystal settling *and* chemical resorption, resulted in the complete loss of mantle component before the emplacement of the Muil Fissure.

Klump (1995) suggests that the other petrographically identifiable dykes in the system have been derived from residual melts related to progressive kimberlite emplacement. It is suggested, based on petrographic and mineralogical evidence that the John# fissure was derived from some residual melt during the emplacement of the Main Fissure. In addition it is suggested that the South Fissure was derived from a residual melt during the emplacement of the Changehouse Fissure (Klump, 1995).

3.7 Conclusions

Detailed analysis of the macrocryst population from the Swartruggens Kimberlite has demonstrated that the underlying mantle comprises harzburgitic, lherzolitic and eclogitic lithologies. It has been shown that harzburgitic and eclogitic lithologies have compositions that are consistent with that associated with diamond formation, and it is reasonable to assume that these lithologies hosted the diamonds that were sampled by the kimberlite. A megacrystic component has also been observed within the kimberlite.

It has been successfully demonstrated that the greater the abundance of macrocrysts derived from disaggregated, potentially diamondiferous source rocks in a kimberlite, the better the grade associated with that kimberlite. The additive contribution to the overall diamond population from harzburgitic and eclogitic parageneses has been analysed by establishing the abundance of the garnets and

chromites derived from disaggregated, potentially diamondiferous mantle host-rocks. At this locality it is clear that the eclogitic component found in abundance within the Main Fissure has been fundamental in contributing to the high diamond grade associated with the kimberlite. This has two important implications; Firstly that the eclogitic diamonds must account for a significant proportion of the diamond budget at this locality. Secondly this study emphasizes the importance of an eclogitic component in contributing to the overall diamond grade of a kimberlite.

Finally the study of the mantle minerals sampled by the Swartruggens Kimberlite has contributed to the understanding of the kimberlite's petrogenesis. It is clear that the diamond grade of the various kimberlitic phases is not only controlled by the successful sampling of diamondiferous mantle material, but perhaps also by secondary processes that occur within the lithosphere over time, prior to kimberlitic eruption.

4 PHYSICAL CHARACTERISTICS OF THE HELAM DIAMONDS

4.1 Introduction

The environment in which a diamond resides, be it within the mantle or during and after its transport in the kimberlite, controls and modifies the physical characteristics of the crystal over time. It follows therefore, that a detailed study of the physical characteristics of a diamond population, contributes to the understanding of the environment in which diamonds form, as well as giving clues to any environmental changes that have occurred during mantle residence and subsequent transport by the kimberlite. This study adopts an integrated approach to elucidating the processes involved in diamond formation, preservation, transportation and oxidation. To this end, the documentation of the physical characteristics of the diamond population will used in conjunction with other independent studies in order to interpret such mantle processes.

Studies of diamond suites from numerous individual localities worldwide, have demonstrated the existence of multiple diamond sub-populations, each commonly exhibiting unique and characteristic growth and mantle residence histories. Such diamond sub-populations may be present in different proportions within discrete kimberlite phases of a particular locality, and also vary on an intra-cratonic scale (e.g.: Gurney, 1989, Robinson *et al.*, 1989). The 'Helam' diamond population has been successfully sampled by some of the dykes within the Swartruggens kimberlite dyke system (i.e.: the Main and Changehouse fissures). It will be demonstrated that the Helam diamonds comprise several diamond sub-populations, classified on the basis of both their *physical* and *chemical* differences. Further to this, it will be shown that the characteristics of these sub-populations, reflect distinct differences in their respective growth environments and subsequent geological histories.

Robinson (1979), Robinson *et al.* (1989), and Otter (1990) have conducted detailed studies on the physical characteristics of diamonds, and have proposed a sequence of events that affect diamond morphology and surface characteristics. These events include; crystallisation, residence within the upper mantle, plastic deformation, resorption and etching, crystal breakage and further etching (in order of sequence). It is proposed that the environment of crystallisation controls the primary crystal form, and in some cases dictates the crystal's body colour. Following crystallisation, the

primary diamond physical properties may become modified by the characteristics related to the latter four processes, within the mantle and the kimberlite during their transport to surface. Analyses of *both* the 'primary' and 'secondary' characteristics therefore, provide important information regarding the processes associated with diamond formation, mantle residence and subsequent transport within the kimberlite.

4.2 Nature of the Sample

Physical characteristics of the Helam diamonds have been described for all diamonds on which mineral inclusion and/or FTIR studies were performed. Such descriptions attempt to more fully document the characteristics of the Helam diamond suite, which to date has not been studied in any great detail. To the author's knowledge, the only other published studies of the characteristics of these diamonds were those by Harris *et al.* (1979) and Robinson (1979), who only provide brief overviews of the diamond suite characteristics. In addition, the current study has been conducted in order to establish relationships (if any) between the different physical and chemical characteristics of the diamond sub-populations.

As a consequence of the diamonds having been selected principally on the basis of their mineral inclusion content and/or their suitability for FTIR analyses (flat faces or evenly fractured stones), a bias in the sample may inadvertently have been induced. Nevertheless some distinctive features can be recognised, which appear to apply to the entire diamond population, and which are largely in agreement with initial observations made by Harris *et al.* (1979) and Robinson (1979).

4.3 Physical Characteristics

As mentioned previously, the morphology of diamonds is a direct result of their growth and/or dissolution and thus reflects the mechanisms and conditions of growth and dissolution, as well as the geological history that the diamond has experienced (Sunagawa, 1984a).

Detailed descriptions of the physical characteristics of over 350 Helam diamonds are presented in Appendix 2. The characteristics discussed below reflect the detailed descriptions of the selected diamonds listed in Appendix 2.1, as well as general (brief) observations made from thousands of other Helam diamonds within

the sample, in an attempt to limit any bias created by the selected stones. The description of the physical characteristics of the Helam diamonds broadly follows that of Otter (1990).

The Helam diamond population is unusual in comparison to other Southern African diamond suites. The presence of cuboid (± 5%) and yellow (or amber) diamonds (+ 5%), and the scarcity of macles (<1%) are all notable characteristics of this diamond population (Harris *et al.*, 1979; Robinson, 1979). Figure 4.1 illustrates a typical sample of the Helam diamond population, and is useful in illustrating the variability in morphology and body colour associated with this diamond population. The variability and uniqueness of this diamond suite warrants a full and detailed study of their physical characteristics.

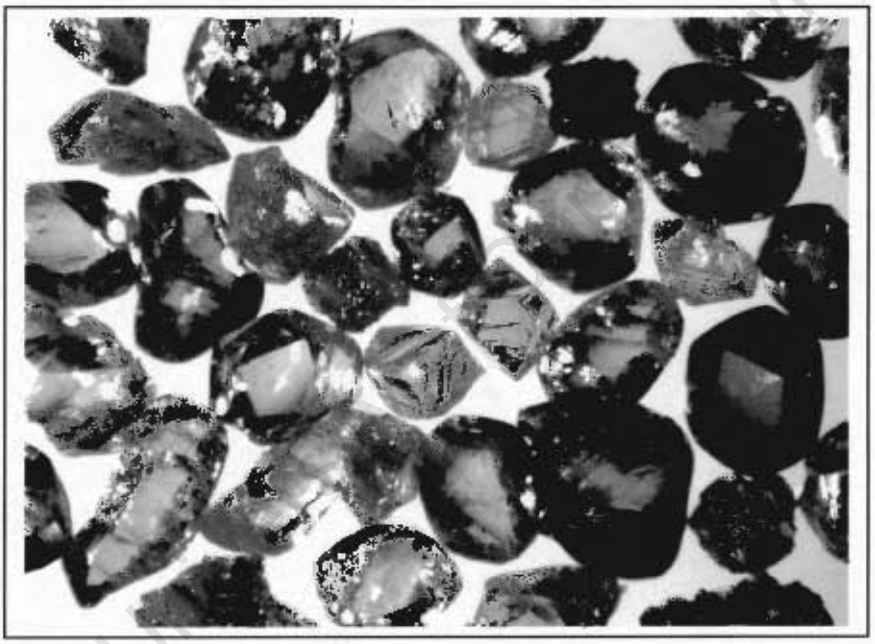

Figure 4.1 Typical sample of the Helam diamond population (FOV = 20 mm), displaying a variety of crystal morphologies and crystal body coloration.

4.3.1 Size

The diamonds studied vary in size from less than 1mm in diameter (small), to 5 mm in diameter (large). The small-size fraction (<3 mm) made up the majority of the sample (450 carats), while the larger fraction (>3 mm) accounted for only 11 carats. Consequently little can be said of the changes in characteristics between the different size fractions. The small size fraction was used for the majority of the descriptions of

the diamonds, FTIR analysis and inclusion studies, while the larger size fraction was used primarily for integrated diamond plate studies.

4.3.2 Colour

The property of diamond coloration primarily distinguishes the various diamond sub-populations. The sample (± 460 carats) is broadly characterised by colourless (65%), brown (20%), green (10%), and yellow (5%) diamonds. These values are similar to those reported by Harris *et al.* (1979) and Robinson (1979), suggesting that sampling bias has been limited. It will be demonstrated that the property of diamond body colour can be strongly correlated with other physical and chemical properties. Because diamond coloration forms the basis for the sub-division of the Helam diamond suite, it is instructive to briefly consider the nature and causes of colour within diamonds.

The causes of diamond body colour are a result of a complex interplay between numerous physical and chemical processes. For a diamond to manifest colour, some impurity or lattice defect that induces energy differences within the visible spectrum, must exist (Harris, 1987). Pure diamond does not create any such energy difference within the visible spectrum and thus appears colourless to the observer. Structural defects within the diamond lattice may act as 'pseudoatoms' and are termed 'colour centres', imparting colour to a diamond. Many such colour centres incorporate nitrogen, which is the most common impurity in diamond (Fritsch, 1998). In addition to nitrogen, boron impurity too, is responsible for some of the colouration observed in diamond (Harris, 1987).

4.3.2.1 Yellow Coloration

Intense yellow colouration of diamonds is commonly related to the presence of dispersed nitrogen within the diamonds (Collins, 1982). Isolated nitrogen atoms within the diamond lattice, are associated with strong absorption of violet and blue light, which results in the observed yellow colouration. Collins (1982) proposes that the colouring power of this substitution is strong, even at very low concentrations of nitrogen. Consequently, diamonds containing this isolated nitrogen display intense or vivid yellow/amber colouration, and are commonly referred to as 'canary' diamonds

(Fritsch, 1998). Diamonds containing such dispersed nitrogen are classified as Type Ib diamonds (Chapter 5) and are very rare in nature (Evans, 1992). These diamonds carry dispersed nitrogen atoms at concentrations of about 50 to 300 ppm (Evans, 1992)

More commonly however, yellow colouration is observed among diamonds containing much higher nitrogen concentrations. Such diamonds are commonly referred to as 'Cape' diamonds. The yellow colouration associated with these diamonds has been attributed to the presence of the so called 'N3 centres', which are believed to be aggregates of three nitrogen atoms occurring within the diamond lattice (Loubser & Wright, 1973). These diamonds commonly exhibit a more subdued yellow colouration than do the Type Ib diamonds.

Yellow crystals are relatively common among the Helam diamonds (comprising approximately 5% of the population). These commonly exhibit vivid yellow colouration, having been described as 'amber' in colour by Harris *et al.* (1979). The inference therefore is that these diamonds (now referred to as 'canary-yellow' diamonds) are akin to Type Ib diamonds. FTIR and EPR analysis of these diamonds (Chapter 5) have indeed confirmed this hypothesis. Such a large component of Ib diamonds among the Helam diamond population is certainly noteworthy, as these are not commonly documented in nature.

In addition however, some Helam diamonds display a subtler yellow colouration, and it is suggested that these are more characteristic of the so-called 'Cape' diamonds. This suggestion is consistent with the higher nitrogen concentrations and aggregation states measured among these diamonds (Chapter 5). These 'Cape' diamonds only account for approximately ¼ of the yellow diamond population (i.e.: approximately 1% of the entire diamond population).

4.3.2.2 Brown Coloration

Brown diamonds worldwide have traditionally been associated with plastic deformation (Harris, 1992). Such diamonds commonly exhibit lamination lines, on resorbed surfaces, caused by plastic slip during the deformation of the crystal. The brown colouration is attributed to graphitisation of the diamond along {111} diamond lattice planes, outside of the diamond stability field (Urusovskaya & Orlov, 1964). The large proportion of brown crystals among the Helam diamonds (~ 20%) suggests

a period of extensive plastic deformation within the upper mantle from which the Helam diamonds were sampled.

4.3.2.3 Green Coloration

Diamonds with a green body colour are rare in nature, however diamonds exhibiting transparent green coats are far more common (Vance *et al.*, 1973), and it can be demonstrated that it is this *external* defect that characterises the 'green' diamonds of the Helam population.

The green Helam diamonds commonly exhibit a homogeneous surface colouration, however in a few of the diamonds, isolated, transparent green spots are observed on the crystal surfaces (figure 4.2). On such diamonds it is clear that the colouration of such diamonds is confined to the crystal surfaces. On cracking of the green diamonds it can be observed that the green colouration of the more homogeneously coloured crystals, is also non-penetrative. It is suggested that such green colouration only penetrates approximately 20 μm of the diamond surface, being attributed to α-particle irradiation after kimberlitic injection and subsequent cooling, by the decay of uranium atoms (Vance *et al.*, 1973). The damage to the crystal is manifest by increased diamond lattice parameters (Meyer *et al.*, 1965) which impart the colour to the diamond.

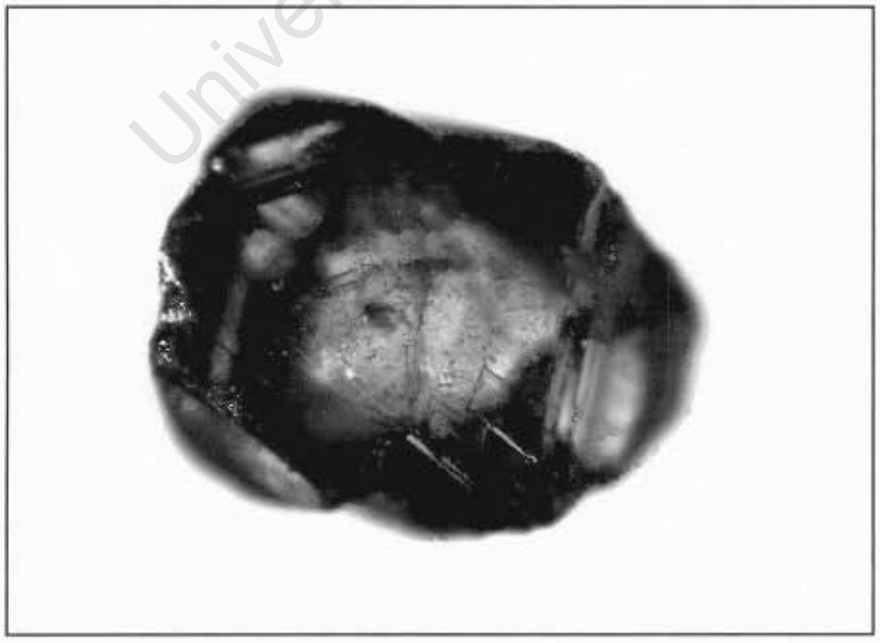

Figure 4.2 HM-A01 – Octahedral diamond exhibiting isolated green spots on the crystal surface. (FOV = 1.2 mm)

Green diamonds can be modified to brown in colour if the temperatures exceed 600 °C (Vance *et al.*, 1973), confirming that radiation damage must have occurred subsequent to kimberlite eruption. It is suggested that contact with radioactive minerals such as perovskite may result in the discreet green haloes or spots (Vance *et al.*, 1973), while the overall green staining is the result of bombardment from uranium and thorium atoms derived from the kimberlite, and circulated by percolating groundwaters. Harris (1987) reports that such green coloured diamonds are commonly only recovered from the oxidised upper parts of kimberlite pipes and dykes. The Helam diamond sample was recovered from depths in excess of 800 m below surface, implying that the processes of irradiation are active to these depths at the Helam Diamond Mine.

4.3.2.4 Blue Coloration

Blue diamonds are not associated with any substitutional nitrogen, and consequently all such diamonds are classified as Type II diamonds (Chapter 5). Not all Type II diamonds are blue in colour, those that are however, all contain low concentrations of boron (Collins, 1982). The inference therefore is that boron imparts the blue colour to these diamonds. Diamonds, deficient in nitrogen but containing trace amounts of boron are classified as Type IIb diamonds. Diamonds exhibiting an absence of both nitrogen and boron are classified as Type IIa diamonds.

Harris *et al.* (1979) report the presence of approximately 0.5% blue diamonds from the Swartruggens Kimberlite among certain (unspecified) diamond size ranges. A comparable proportion of blue diamonds have also been noted from the Premier kimberlite (Harris *et al.*, 1979). In this study, over the size range 1-5mm however, no such diamonds were observed and consequently discussion of the nature of blue colouration will not be pursued further.

4.3.3 Crystal State

The crystal state of a diamond refers simply to whether the diamond is broken or not (Otter, 1990). The crystal states of the Helam diamonds were described according to the percentage of the original volume lost due to cleavage or fracture, following Chinn (1995). The diamonds were classified as whole (no volume loss), chipped

(<10% volume loss), broken (10 – 50% volume loss) or fragmented (> 50% volume loss) according to the classification scheme.

The crystal state data obtained on the Helam diamonds are represented in Appendix 2. Approximately 46.6% of the diamonds within the representative sample were broken, chipped or fragmented in some way (24.5% broken, 9.7% chipped and 12.4% fragments), whereas about 53.4% could be described as whole crystals.

The cleavage and fracture surfaces are commonly unetched and unresorbed, indicating that the majority are the result of brittle deformation that occurred subsequent to the etching and resorption events. The amount of breakage that may be attributed to the crushing processes on the mine has not been established. However, etching and resorption on some breakage surfaces suggest that a period of transient oxidation occurred at some time after the brittle deformation event, and that at least *some* of the diamonds were fractured by natural processes within the kimberlite. The existence of inclusion cavities on such fracture surfaces is in support of Sutton's (1928) suggestion, that diamond breakage can often be attributed to stresses that result from differential expansion between the diamond and the encapsulated mineral inclusions during depressurisation within the mantle and/or kimberlite conduit.

4.3.4 Crystal Regularity

Crystal regularity refers to a deviation (if any) from the regular or equidimensional crystal form (Otter, 1990). This deviation in crystal form is *not* related to crystal deformation per say, but rather to inequalities in facial development during the diamond growth. Robinson (1979) divides diamonds according to whether they are predominantly equidimensional, slightly distorted, flat, elongate or irregular. Flat diamonds are considered to have one dimension less than a third of the other two, and elongate diamonds are considered to have two similar dimensions, both of which are less than a third of the other dimension. Irregular diamonds are considered to be of barely determinate form.

From figure 4.1, and other observations made by the author (Appendix 2.1), it becomes clear that very few of the Helam diamonds display perfect crystal symmetry. The Helam population is characterised by approximately 44% equidimensional crystals, 16% elongate crystals, 16% flattened crystals, and 24 % irregular crystals. Consequently, 56% of the Helam diamonds appear to have experienced either

irregular growth or resorption, or both. This suggests that for the majority of the Helam diamonds, the crystallisation environment deviated somewhat from the ideal diamond forming conditions.

4.3.5 Primary Morphology

Diamond morphology, among other things, is *primarily* controlled by the level of supersaturation between the liquid and solid phases during crystallisation (Sunagawa, 1984a). It is suggested that conditions of relatively low carbon supersaturation promote the crystallisation of single crystals, aggregates and twinned diamond crystals. Under conditions of higher degrees of supersaturation however, polycrystalline aggregates, fibrous cubes and fibrous diamond coats may result. These morphologies are associated with faster growth on multiple nucleation sites at higher degrees of carbon supersaturation (Sunagawa, 1984a).

Diamond morphology is also dependant on the temperature and pressure of formation, as well as the catalyst involved (Sunagawa, 1984a). It has been suggested from experimental work that cubic diamonds are formed at lower temperatures and higher pressures than that required to form octahedral crystals. However, Sunagawa (1984a) cautions that such application to natural diamonds is questionable as the growth of diamonds is affected by *numerous*, poorly understood, chemical and physical systematics.

Haggerty (1986) suggests a relationship between the different diamond morphologies with his proposed mantle stratigraphy (Figure 1.1). It is suggested that annealed high-temperature octahedral diamonds of Type Ia affinity would dominate the basal and contact zones of the lithosphere. Cubo-octahedral diamonds would be expected to develop towards the interior of the lithosphere, while cuboid diamonds would be associated with progressively shallower depths. Haggerty (1986) states that the growth morphologies, diamond type and annealing characteristics of diamonds should be similar for both the eclogitic and peridotitic suite diamonds.

The Helam diamond population is characterised by three principal morphologies; octahedra (figures 4.3 and 4.4), cubo-octahedra (figures 4.5), and cubes (figures 4.6). Minor fibrous diamonds have been observed. Sunagawa (1984b) includes macles, aggregates and coalesced crystals as primary morphologies, however these are exceedingly rare (figure 4.7) among the Helam diamond population.

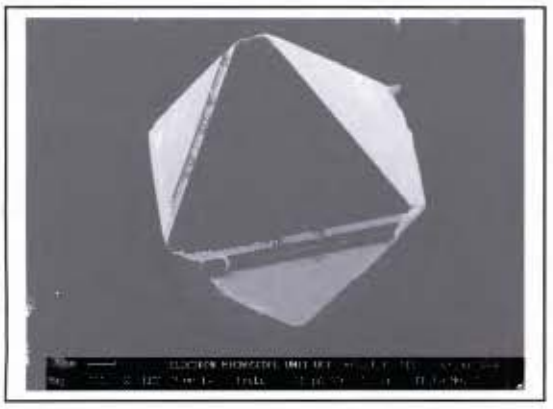

Figure 4.3 SEM photomicrograph of HM-E1. Unresorbed and unetched octahedron with smooth crystal faces and sharp edges.

Figure 4.4 SEM photomicrograph of HM-E3, illustrating a layered octahedral crystal. These crystals are commonly characterised by serrated triangular plates.

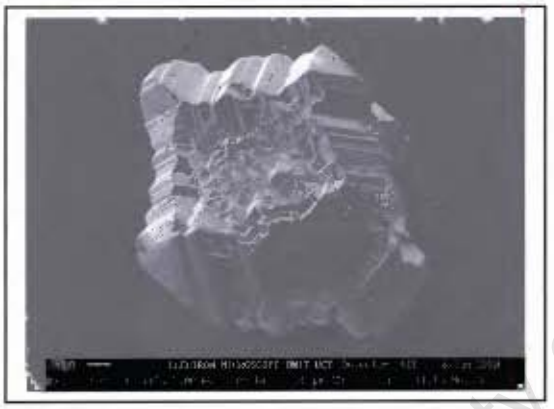

Figure 4.5a SEM photomicrograph of HM-E12. Differentially resorbed, Cubo-octahedron exhibiting smooth faces, triangular plates, sharp edges on its octahedral faces, and tetragonal etch pits on its cubic faces.

Figure 4.5b High magnification SEM photomicrograph of HM-E12. Unetched, serrated triangular plates dominate the octahedral faces (foreground), while tetragonal etch pits dominate the cubic faces (top left).

Figure 4.6a SEM photomicrograph of HM-E11. Highly etched cuboid diamond, characterised by irregular crystal surfaces.

Figure 4.6b High magnification SEM photomicrograph of HM-E11. Cubic faces are dominated by tetragonal etch pits, and ruts (top left). Notice that these ruts are also associated with tetragonal etch pits.

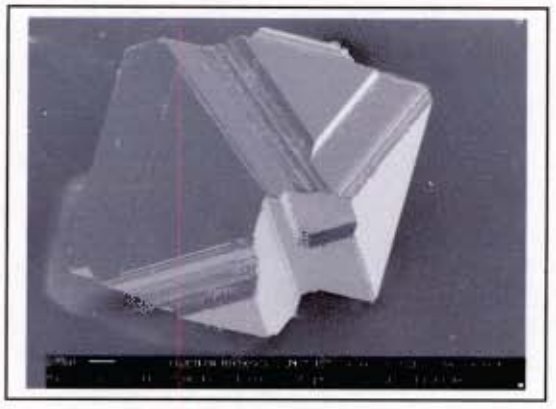

Figure 4.7 SEM photomicrograph of a rare crystal twin (HM-E4). The octahedral faces are characterised by smooth, unresorbed triangular plates with sharp edges.

The variable crystal forms among the Helam diamond population reflect differences in their growth environments, in particular their level of carbon supersaturation. Whether the variable diamond forms record a systematic change in the crystallisation environment over time, or represent multiple disassociated growth environments, remains unclear. Paragenetic differences among the Helam diamonds (Chapter 6) certainly provide the scope for multiple growth environments. However, detailed studies of diamond plates (Chapter 5) show evidence in support of the prior suggestion, documenting continually changing chemical environments within a particular paragenesis. In such diamond plates, it can be demonstrated that an environment associated with an initial period of cubic growth, has over time, been modified to accommodate octahedral growth within individual diamonds (i.e.: systematic decrease in the level of carbon supersaturation).

4.3.6 Resorption

The majority of the Helam diamonds appear to have been extensively resorbed, and commonly occur in the form of tetrahexahedroida (Figures 4.8). It has been demonstrated (Seal, 1965; Moore & Lang, 1974) that such crystal forms are the result of dissolution of the primary diamond crystal forms. Diamond dissolution may not be complete however, and thus various diamonds may preserve a number of stages of resorption between the planar, primary crystal forms, and that of the rounded tetrahexahedroid.

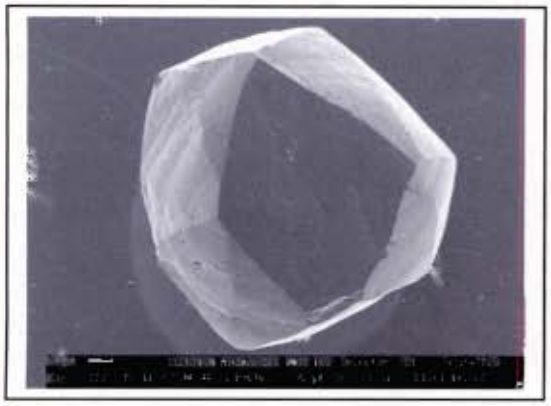

Figure 4.8a SEM photomicrograph of HM-E10. Tetrahexahedoid exhibiting sharp contacts between the resorbed crystal faces, about both four-fold and six-fold crystallographic axes.

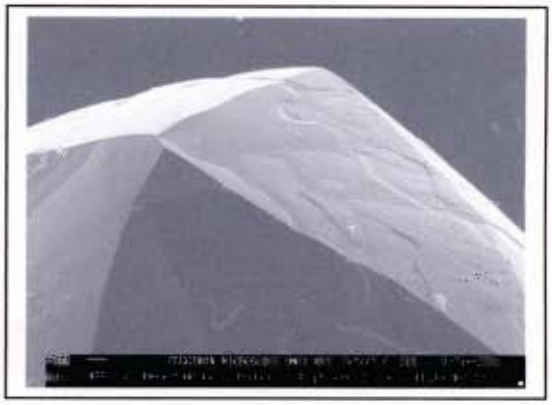

Figure 4.8b High magnification SEM photomicrograph of HM-E10, illustrating a four-fold crystallographic axis. Notice that the surface of the tetrahexahedroid is characterised by corrosion sculptures which circumvent the crystal faces.

McCallum *et al.* (1994) assign six resorption categories as illustrated in Appendix 2.2. Such a classification scheme is a semi-quantitative measure of the volume loss due to diamond resorption. The complete conversion of a regular octahedral diamond crystal to tetrahexahedroidal morphology removes a minimum of 45% of the original mass and volume of the diamond (Robinson, 1979). The dissolution of smooth-faced octahedral diamonds by oxidising agents at elevated temperatures is believed to result in the progressive dissolution of the primary diamond morphology about the four-fold axis of the diamond, as illustrated in Appendix 2.2.

Haggerty (1986) suggests that diamond resorption can occur within the Earth's mantle and therefore pre-dates the entertainment of the diamonds in the kimberlite. Robinson *et al.* (1989), however suggest that the majority of resorption occurs within the kimberlite, and that the liberation of the diamonds from their host xenolith at different depths accounts for the different degrees of resorption between stones.

4.3.7 Surface Features

The description of the surface features of the Helam diamonds follows that of Robinson (1979) and Otter (1990). In order to establish the sequence of events that have affected the diamonds subsequent to their crystallisation, it becomes important to distinguish between features caused by the growth of the diamond, those caused by deformation, and those ascribed to the processes of oxidation and dissolution.

4.3.7.1 Features Associated with Crystal Growth

Sunagawa (1984b) suggests that natural octahedral diamond crystals (single crystalline type) grow by a spiral growth mechanism from a solution phase of low carbon supersaturation, through the progressive incorporation of atomic growth units. Moore & Lang (1974) report that cuboid diamonds exhibit a fibrous growth pattern, with the fibres repeatingly branching to accommodate crystal expansion. Such cubic growth occurs in environments associated with high levels of carbon supersaturation. While these growth structures can not be observed on the crystal faces, numerous other primary features, related to the growth of diamonds can be observed;

Primary growth features include smooth faces, serrate laminae, triangular growth plates and possibly knob-like asperities (Robinson, 1979). Such features are termed xenolithic features by Otter (1990) as these features are associated with diamonds enclosed within xenoliths. Approximately 40% of the diamonds within the Helam diamond population exhibit primary growth (xenolithic) features. Smooth faces, triangular plates and serrate laminae are common (figures 4.3) among Helam diamonds, however knob-like asperities appear to be largely absent.

4.3.7.2 Features Associated with Deformation

Diamond is a brittle solid at room temperature, however experimental studies at pressures and temperatures associated with upper mantle conditions have shown that diamond becomes ductile and may undergo plastic deformation (De Vries, 1975). Robinson *et al* (1989) suggest that plastic deformation is the first process to affect the diamond after its crystallisation, and argues that the processes of deformation may be related to the development of the kimberlite conduit. According to Gurney (1989) deformation occurs during mantle residence, and the deviatoric stress required to impose deformation upon a diamond, implies that the diamonds were present within a sub-solidus environment of less than 23% liquid.

Plastic deformation of diamond results in the development of slip planes which can be seen in the form of lamination lines (figures 4.9 and 4.10) on the resorbed diamond surfaces. Such plastic deformation requires temperatures in excess of 1000°C at 30 kbar (De Vries, 1975). At higher pressures deformation can occur at

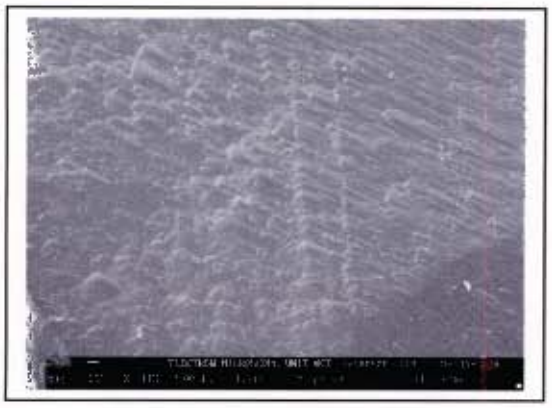

Figure 4.9 SEM photomicrograph of HM-F8, showing the resorbed surface of a tetrahexahedroid. The linear features running from top to bottom of the image are lamination lines associated with deformation. The resorbed surface of the crystal is further characterised by elongate hillocks.

Figure 4.10 SEM photomicrograph of HM-C2, showing a similarly resorbed crystal surface of a tetrahexahedoid with both lamination lines and elongate hillocks.

lower temperatures. These lamination lines represent regions within the diamond that are somewhat harder than the matrix diamond, and delineate the highly strained regions within the diamond (De Vries, 1975). Both parallel wide (>100 μm of separation between lamination lines) and fine (<100 μm of separation between lamination lines) lamination lines are observed among the Helam diamond population. In addition, intersecting lamination lines (Scotch Plaid texture) can commonly be observed. While such lamination lines can be observed among all the diamond sub-populations, lamination lines appear to be more commonly associated with the brown and canary-yellow diamonds. The implications of this will be discussed further in Chapter 5. Suffice it to say that it will be demonstrated that diamonds associated with low nitrogen impurity have been correlated with the most extensive deformation.

These observations are in agreement with suggestions made by Evans (1976), who demonstrates that nitrogen-deficient diamonds have a higher initial density of dislocations and lack of platelets, which impede the movement of dislocations. These diamonds are therefore more susceptible to plastic deformation.

It becomes clear from the proportion of diamond fragments among the Helam diamond population, that brittle fracture has occurred in addition to the plastic deformation. The lack of etching and resorption on many of these fracture surfaces

suggests that the much of the brittle fracture occurred subsequent to the processes of oxidation, as discussed previously.

4.3.7.3 Features Associated with Oxidation and Etching

The etch features observed on many diamonds reflect the temperature and pressure at the time of oxidation, as well as the nature of the oxidising agent and the crystallographic orientation of the etched surface. Trigonal and hexagonal etch pits develop on the octahedral faces and breakage surfaces parallel to octahedral faces (figures 4.11 and 4.12 respectively), while tetragonal etch pits are associated with cubic faces and breakage surfaces parallel to the cubic planes (figures 4.13).

Figure 4.11a SEM photomicrograph of HM-F3. Notice that the smooth octahedral face is characterised by negatively oriented trigons. This etching is terminated at the boundary between the unresorbed octahedral face and the resorbed tetrahexahedroidal face. The resorbed crystal faces are characterised by the presence of elongate hillocks and micro-hillocks.

Figure 4.11b High magnification SEM photomicrograph of diamond HM-F3 showing superimposition of trigons.

Figure 4.12 SEM photomicrograph of HM-C1. Highly resorbed canary-yellow octahedron displaying hexagonal etch pits.

Figure 4.13 High magnification SEM photomicrograph of HM-C9, illustrating the tetragonal etch pits that dominate the cubic faces of diamond

Experimental studies show that negatively orientated etch pits (apex of etch pit orientated in opposite direction to the apex of the octahedral face) are the result of reaction of the diamonds with molten kimberlite. Frank *et al.* (1958) report that such reaction occurs at low pressure and at 1450 °C. Harris & Vance (1974) suggest that such reaction occurs at any temperature exceeding 1300 °C. In addition these authors report that at 1050 °C positive trigonal etch pits (apex of etch pit orientated in the same direction as the apex of the octahedral face) result from kimberlite which predominantly liberates water vapour, and that negative trigonal etch pits are formed when predominantly CO_2 is released. At temperatures of 900 – 1000 °C, hexagonal etch pits can form, possibly as the result of the combined action of CO_2 and O_2 (Phaal, 1965).

The Helam diamonds are not ubiquitously characterised by etching. Where etching is observed however, hexagonal, trigonal and tetragonal etching have been developed. The cuboid and cubo-octahedral diamonds all display marked tetragonal etching (negative) on their cubic surfaces. The colourless, brown and green octahedra exhibit limited negatively orientated trigonal etch pits on their octahedral surfaces, and an absence of positively orientated etch pits. The canary-yellow octahedra are distinctive in that they commonly exhibit intense etching on their crystal faces, with both negatively orientated trigonal etch pits, and hexagonal etch pits having been developed (figure 4.12). It is suggested that the canary-yellow diamonds have been more susceptible to the processes of oxidation within the kimberlite.

Etching is also commonly associated with inclusion cavities (figure 4.14 and 4.15). Such features attest to a time of brittle fracture prior to a process of oxidation, as these pits are associated with trigonal and hexagonal etch features.

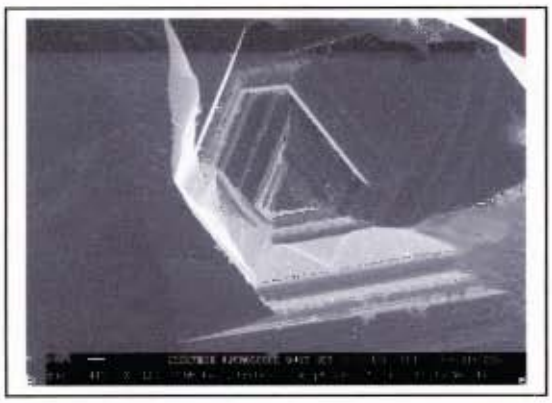

Figure 4.14 High magnification SEM photo-micrograph of HM-C6, showing an inclusion cavity associated with trigonal etch pits

Figure 4.15 High magnification SEM photo-micrograph of HM-C4, showing an inclusion cavity associated with hexagonal etch pits

Ruts are another feature associated with etching, and occur as narrow, elongate depressions which trace octahedral or sub-conchoidal planes on tetrahexahedroidal surfaces. In addition they may be associated with inclusion cavities or may even develop at the contact between interpenetrating twin crystals (Robinson, 1979). Orlov (1973) attributes the development of sinuous ruts to the localised migration of oxidising fluids which penetrate cracks within the host xenolith. Approximately 30% of the Helam diamonds exhibit such ruts (figure 4.6b). These are often associated with inclusion cavities, and typically exhibit a sinuous geometry.

The majority of the Helam diamonds show complete resorption to tetrahexahedroida, and thus the surface features associated with this form dominate. Elongate hillocks and micro-hillocks (figures 4.16) dominate the Helam tetrahexahedroida. The hillock elongation is developed parallel to the strike of the octahedral growth layers, with their morphology determined by the differential resistance of such growth layers to resorption (Robinson, 1979).

Corrosion sculptures are another common feature associated with the resorbed Helam diamonds (Figures 4.8 and 4.17). Robinson (1979) reports that such features develop subsequent to etching events. Gorina (1971) suggests that rapid etching by a gaseous oxidising agent over a short duration is responsible for such features.

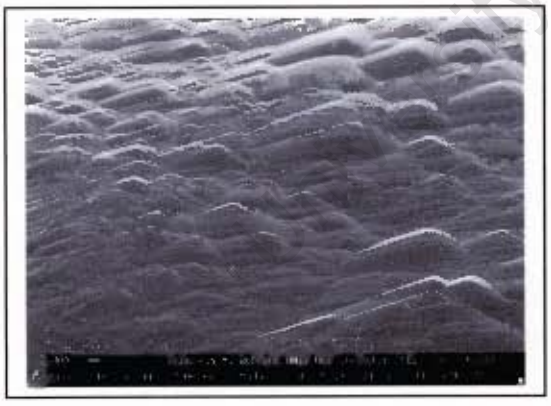

Figure 4.16 High magnification SEM photo-micrograph of HM-C5, illustrating elongate hillocks that commonly characterise the surface of many of the tetrahexahedroida.

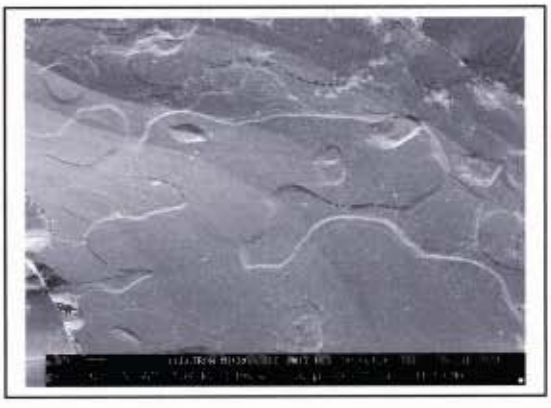

Figure 4.17 High magnification SEM photo-micrograph of HM-C10, illustrating the corrosion sculptures often observed on the surfaces of the tetrahexahedroida.

Wagner (1914) was the first to observe that such features are limited only to diamonds recovered from the deeper sections of kimberlites. This was later supported by Robinson *et al.* (1989) who report such features only amongst diamonds from hypabyssal kimberlite in diatreme root zones. The observations of such features in

association with the diamonds from Swartruggens Kimberlite (which represents a hypabyssal kimberlite dyke) are thus in agreement with these observations of Wagner (1914) and Robinson *et al.* (1989).

The surfaces of the resorbed Helam diamonds are further characterised by the presence of circular micro-disks (Figure 4.18) and pitted hemispherical cavities (Figure 4.19), which further attest to a period of extensive and varied oxidation. These features have also been associated with hypabyssal kimberlite (Wagner, 1914).

Figure 4.18 High magnification SEM photo-micrograph of HM-F5, illustrating circular micro-disc structures on a tetrahexahedroidal surface. Notice that the disks commonly superimpose and/or overlap each other.

Figure 4.19 High magnification SEM photo-micrograph of HM-F6, illustrating an occurrence of pitted hemispherical cavities on a tetrahexahedroidal surface.

4.4 Mineral Inclusion Content

A very small percentage of the Helam diamond population contain visible mineral inclusions. However, because the study of such inclusions is of significant importance in this study, it becomes necessary to briefly discuss their occurrence in qualitative terms. A more detailed quantitative analysis of the inclusion suite will be discussed in Chapter 6.

One of the most common inclusions within the Helam diamonds is that of diamond itself (Figures 4.20 and 4.21). Both brown and colourless diamond have been observed to be included within numerous other diamonds. Of interest however is that; no inclusions of diamond were observed within the brown diamonds, that both brown and colourless diamonds are observed within colourless diamond (brown diamond inclusions being more common), and that canary-yellow diamonds only show inclusions of colourless diamond. Based on such relationships (observed in

several diamonds), it appears therefore that the brown diamonds have crystallised before the colourless diamonds, and that the canary-yellow diamonds appear to represent the youngest generation of diamond. It is clear then, that diamond growth has occurred in several episodes, and that younger generations of diamond tend to nucleate upon existing diamond. This is a theme that will be elaborated upon in Chapters 5 and 6. In addition these observations suggest a spatial relationship between the various diamond sub-populations for at least some of the Helam diamonds.

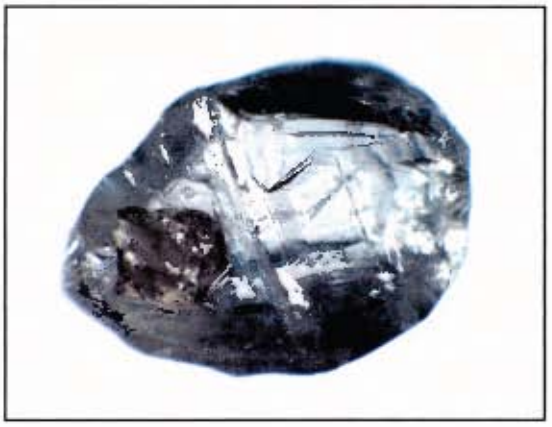

Figure 4.20 Photomicrograph of HM-A1, illustrating a partially exposed inclusion of a brown octahedral diamond within a colourless, resorbed (category 4) octahedral diamond. (FOV – 3 mm)

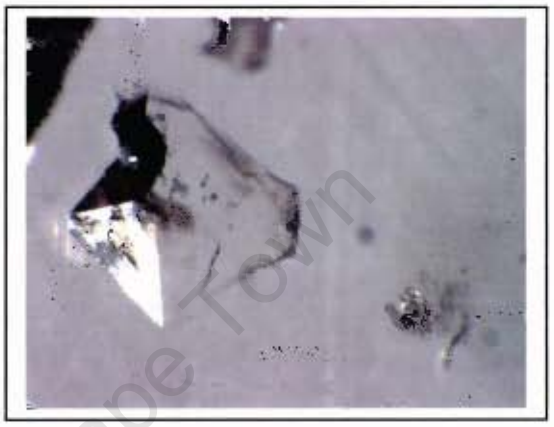

Figure 4.21 Photomicrograph of polished diamond plate HB2D3, illustrating an inclusion of colourless octahedral diamond. It is clear that the included diamond has not been resorbed and displays sharp edged crystal faces. (FOV = 1.5 mm).

Sulphide inclusions predominate, and commonly exist as metallic inclusions set within a rosette structure (figures 4.22a and 4.22b), often near the centre of the diamond. These inclusions are commonly associated with fractures that radiate from the inclusion towards the surface. Where such fractures penetrate the surface, the fractures are commonly filled by secondary minerals and the sulphides usually exhibit reddish-brown colour (figure 4.22c), suggesting that they have been altered. Chromite inclusions also occur in abundance, exhibiting a red or black appearance (figure 4.23), often associated with diamond imposed morphologies. Garnets (figure 4.24) commonly exhibit sub-rounded morphologies, and are exceedingly rare. Other minerals observed within the Helam diamonds include corundum, SiO_2, olivine, clinopyroxene and orthopyroxene, all of which appear largely colourless and will be discussed in greater detail in Chapter 6.

Also deserving of mention are the large number of stones exhibiting spherical clouds, or clusters of opaque mineral inclusions (figure 4.25). The true nature of such

Figure 4.22a Photomicrograph of polished plate HB3C1, illustrating 3 sulphide inclusions, 2 of which occur near the center of the plate, and 1 near the edge. (FOV – 3mm).

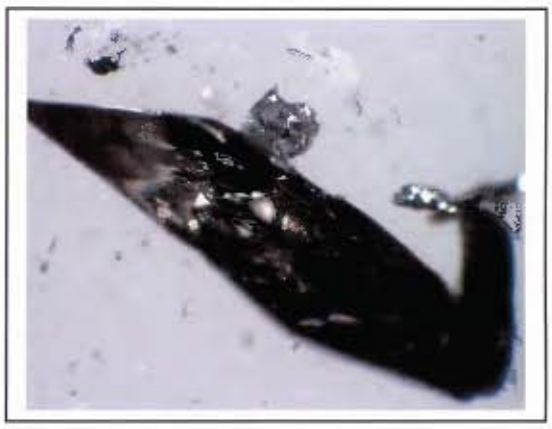

Figure 4.22b High magnification photomicrograph of HB3C1, illustrating the two, unaltered, central sulphide inclusions and their associated rosette structures. Notice their metallic sheen and absence of fractures (FOV = 1.5 mm).

Figure 4.22c High magnification photomicrograph of HB3C1, illustrating the sulphide connected to the surface of the host diamond by a fracture. Notice that the fracture has been filled with secondary (red) minerals, and that the sulphide exhibits a red colour, suggesting that it has been altered. (FOV – 1.5 mm)

Figure 4.23 High magnification photomicrograph of polished plate HB3C3, illustrating two chromite inclusions near the edge of the diamond. Notice their diamond induced morphologies. (FOV = 1.5 mm).

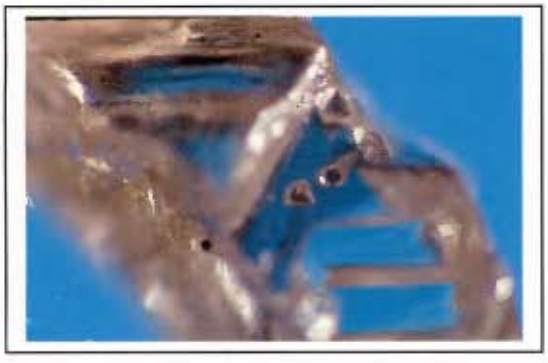

Figure 4.24 Garnet inclusions in diamond HB006. (FOV = 2.5 mm)

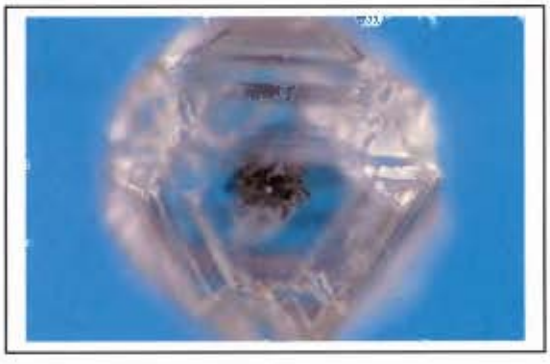

Figure 4.25 Cluster of opaque inclusions at the center of diamond HM-B3. (FOV = 2 mm)

inclusions remains unknown as they have proven too small for sampling, however it is suggested that they may represent clusters of microscopic sulphide inclusions with their associated rosettes. This is consistent with observations made by Viljoen (pers. comm, 2001). It is interesting to note that such clusters always occur at the center of the diamonds, and only occur within the colourless and brown diamonds.

4.5 Cathodoluminescence

Cathodoluminescence (CL) is caused by the excitation of transitions within a crystal, and is a manifestation of defects within a crystal (e.g.: Zezin *et al.*, 1990). Such defects include substitutional chemical impurities, non-stoichiometry, dislocations and α-decay damage. The origin of CL is well beyond the scope of this thesis, but suffice it to say that differences in CL reflect both chemical and physical variations between diamond sub-populations.

The study of the CL characteristics of the Helam diamond population has supplemented the diamond classification, as well as providing new information regarding diamond growth, deformation, dissolution and α-particle damage to the diamonds. In addition CL has been instrumental in interpreting the processes believed to be associated with diamond growth, and will be discussed in greater detail in Chapter 5. Cathodoluminescence has also been conducted on selected whole, rough diamonds, and it is the CL characteristics of these diamonds that are briefly discussed below, in relation to the physical characteristics discussed above.

Figures 4.25 – 4.30 are instructive in illustrating some of the more salient features observed when the whole, rough diamonds are subjected to CL. The first order observation is that the distinctive luminescence characteristics are consistent with the initial classification scheme based solely on diamond colour, as well as interpretations from FTIR analysis (see Chapter 5). The discussion that follows demonstrates the relationship between the CL and physical characteristics of the diamond sub-populations. In addition it lays a foundation for comparison between the characteristics of the whole, rough diamonds, and that of the polished diamond plates discussed in Chapter 5. Discussion of the causes of the various types of luminescence are considered in greater detail in Chapter 5.

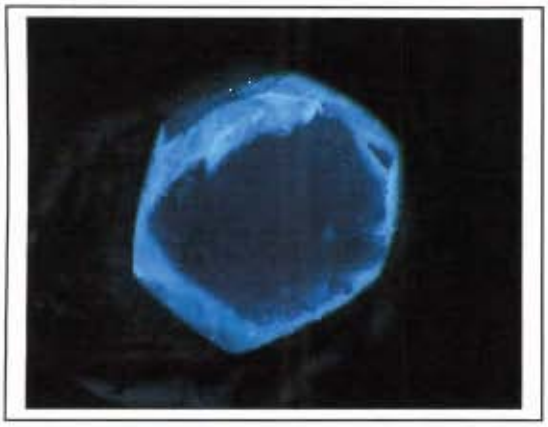

Figure 4.25 CL photomicrograph of HM-C8, illustrating the blue luminescence associated with all of the colourless diamonds of the Helam population. (FOV – 2 mm).

Figure 4.26 CL photomicrograph of HM-C7, illustrating a thin veneer of green luminescence covering a predominantly blue luminescent tetrahexahedroid. (FOV = 2.2 mm)

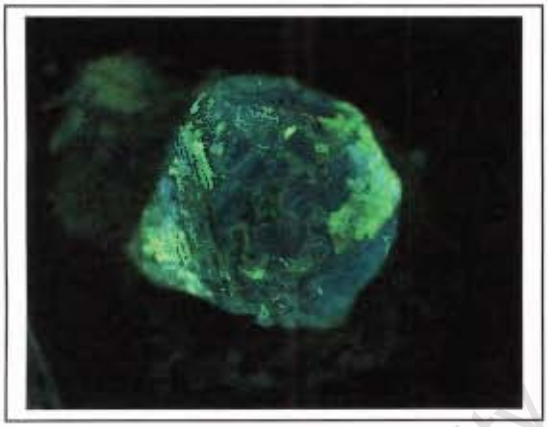

Figure 4.27 CL photomicrograph of HM-C1, illustrating a highly resorbed overgrowth of green luminescent diamond upon a blue luminescent octahedral core. (FOV – 2 mm)

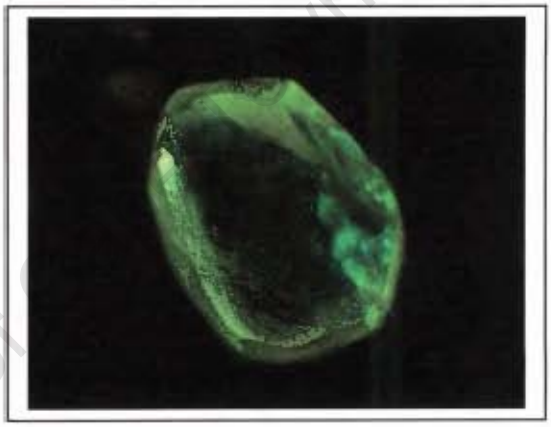

Figure 4.28 CL photomicrograph of HM-F8, illustrating the luminescence associated with some of the canary-yellow diamonds. (FOV – 2.2 mm).

Figure 4.29 CL photomicrograph of HM-C5, illustrating the heterogeneous luminescence associated with some of the canary-yellow diamonds. Such luminescence is always found in association with extensive lamination lines. (FOV = 2.1 mm).

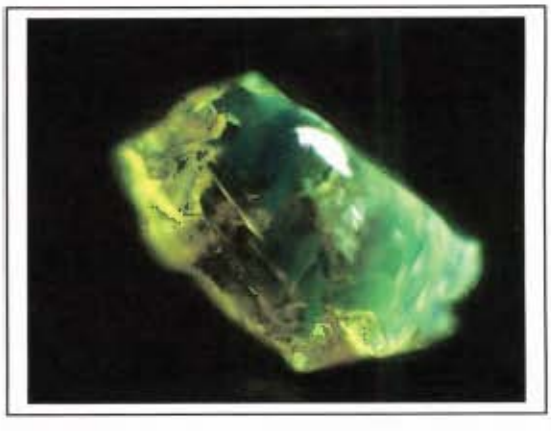

Figure 4.30 CL photomicrograph of diamond fragment HM-F8, illustrating the yellow-green luminescence occasionally associated with brown diamonds from the Helam population. (FOV – 1.9 mm).

The colourless diamonds consistently exhibit relatively homogenous, blue luminescence (figure 4.25). On occasion, the colourless diamonds exhibit a bright-green luminescence in addition to the blue (figures 4.26 & 4.27). This is interpreted as representing an overgrowth of some chemically or structurally different, younger generation of diamond. It is interesting to note that it is commonly upon such overgrowth surfaces, that prominent etching can be observed, the younger overgrowth apparently more susceptible to the processes of oxidation.

In contrast to the colourless diamonds, the canary-yellow diamonds commonly exhibit green or yellow luminescence (figure 4.28). They differ further in that they show a much larger range of luminescence within individual diamonds, and commonly exhibit a 'mottling' effect (figure 4.29). This 'mottling' effect (heterogeneous luminescence) is interpreted to be a manifestation of the low nitrogen contents and crystal deformation that ubiquitously characterise the canary-yellow diamonds.

The green diamonds commonly exhibit a blue luminescence, indistinguishable from that of the colourless diamonds. In cases where the diamonds exhibit isolated green spots, those areas display a complete absence of luminescence.

The brown diamonds, typically exhibit yellow-green luminescence (figure 4.30), but may also appear blue, or even 'mottled' as in the case of most yellow diamonds. This range in luminescence is attributed to the varying degrees of deformation within individual crystals. Those diamonds displaying very subtle brown body colouration are associated with yellow or blue luminescence, while those displaying more intense brown body colouration commonly exhibit the same 'mottling' luminescence as in the yellow diamonds.

4.6 Discussion

A more complete geological history of the Helam diamonds has been established from detailed studies of their physical characteristics. The diamond sub-populations have been defined principally on the basis of their respective crystal colouration. However, their distinction is not restricted solely to their colouration; it appears that the diamond sub-populations can also be characterised by marked differences in other physical properties (e.g.: presence and degree of deformation laminae, etching, α-decay damage). It will be demonstrated that the physical characteristics of the

diamond sub-populations are controlled (either directly or indirectly) by their respective chemical properties. It follows therefore, that the sub-division of the Helam diamond population (by crystal colouration) reflects both physical *and* chemical differences between the diamond sub-populations, and suggests that they each prescribe to somewhat different geological histories.

The brown diamonds attest to a period of ductile deformation that affected some of the diamonds subsequent to their crystallisation. It is suggested that the brown diamonds represent an early deformation event that preceded the crystallisation of many of the other Helam diamonds. The green colouration of some of the Helam diamonds, by contrast reflects a more recent geological event; one of lattice modification, apparently caused by irradiation processes.

The canary-yellow diamonds are unique, not simply due to their colouration. These diamonds are ubiquitously characterised by features associated with deformation and strain, and appear to have been predisposed to the processes of oxidation. It would seem that the deformation associated with the canary-yellow diamonds records a separate, somewhat younger deformation event within the mantle. By contrast however, the Cape-yellow diamonds do not display the characteristics associated with the canary-yellow diamonds, and barring their subtle colouration, appear to exhibit physical properties more akin to the colourless diamonds. It will be demonstrated, based on infrared absorption characteristics, and in terms of nitrogen concentration and aggregation states, that the Cape-yellow diamonds are indistinguishable from the colourless diamonds.

The range in primary morphologies of the various diamonds, may provide further evidence of different crystallisation environments and mantle residence. The dominance of octahedral diamonds, and lack of aggregates in the population suggest that the predominating conditions were of low carbon supersaturation. The cubic diamonds, characterised by fibrous growth, are indicative of an environment associated with high carbon supersaturation, and possibly of crystal growth at lower temperatures, while perhaps the cubo-octahedral diamonds attest to an environment of intermediate conditions. Whether these morphological variations represent disparate chemical and thermal environments (Haggerty Model, 1986), or are suggestive of a mantle having undergone systematic modification over time, remains uncertain. Evidence that will be revealed in subsequent discussions however, suggests that for at least some of the diamonds, systematic change from cubic growth to octahedral

growth within individual diamonds *can* be observed. Where this has been observed the interpretation has been in support of the mantle having undergone systematic chemical modification; from an environment initially ideal for cubic growth to an environment more suited to octahedral growth.

The relative lack of etch features on most of the octahedral and cubic Helam diamonds suggest a somewhat limited exposure to oxidising C-O-H fluids within the kimberlite, or a relative resistance to the processes of oxidation. The canary-yellow diamonds, associated with more intense etching, appear to have been *more* susceptible to the processes of oxidation. The size, depth and abundance of the various etch features is variable between diamonds, and even between the different surfaces of individual diamonds. Sunagawa (1984b) argues that the differences in the degree of dissolution is a manifestation of the differences in the perfection of the various crystals and crystal faces. The presence of negative and positive trigonal etch pits, together with the occurrence of hexagonal etch pits, attest to the reaction of the diamonds with volatiles (CO_2, H_2O and O_2) released by the cooling and decompressing kimberlite. Based on experimental studies discussed previously, the range of etching styles among the Helam diamonds record temperatures of oxidation from in excess of 1300 °C to less than 900 °C. The inference is that the kimberlite released sufficient volatiles to sustain oxidation reactions over a large range of temperatures, as the kimberlite cooled.

Contemporaneous with the oxidation event/s, diamonds entrained within the kimberlite were exposed to stresses associated with depressurisation. This process evidently resulted in the fracturing of some of the diamonds. Resorption of some fracture surfaces suggests that the processes of oxidation remained active within the kimberlite, subsequent to the brittle fracture of the diamonds.

It appears that irradiation of some of the diamonds by circulating, radioactive groundwaters, and touching radioactive minerals was the final natural process to have affected the diamond suite. It is clear however that the effects of this event are non-penetrative, and restricted to a thin veneer on the exterior of some of the diamonds.

CL studies of the Helam diamond suite, confirm the existence of multiple sub-populations of diamond, each having experienced different geological histories. CL provides a useful link between the physical and chemical properties of the diamonds. It has also been useful in demonstrating that diamond formation events have occurred

intermittently through time, with younger generations of diamond nucleating upon existing diamond. This theme of 'episodic growth' will be revisited frequently within this report as it is crucial to the understanding of the mantle processes within the region, and may help explain the overall high grade associated with this kimberlite occurrence.

5 INFRARED ABSORPTION PROPERTIES OF THE HELAM DIAMONDS

5.1 Introduction

Substitutional defects (trace elements) within diamond can be identified due to their characteristic absorption within the mid-infrared region of the electromagnetic spectrum. Developments in infrared (IR) spectroscopy have refined our understanding of trace element distribution patterns and concentrations within diamond, and have advanced our knowledge of the thermal maturation processes that alter such trace elements during residence within the upper mantle. Among other applications, IR microscopes allow the analysis of the envelopes of the one-phonon spectra, in terms of the defect-aggregation sequence for ppm quantities of nitrogen present in diamonds to be determined. Experimentally derived activation energies for the various stages in the sequence of nitrogen aggregation, can be used in conjunction with the concentration of nitrogen defect to estimate the timing or temperature of the diamond formation event within the mantle (Taylor *et al.*, 1990).

The nitrogen aggregation thermometer uses the high temperature sensitivity of the rate of nitrogen aggregation in diamond. The kinetics of nitrogen aggregation is the only method that gives temporal information based on the diamond itself, rather than on its associated mineral inclusions (Navon, 1999).

While Mendelssohn & Milledge (1995) argue that such information is geologically significant, it should be noted that results from this method are subject to large uncertainties. Evans (1992), for example, suggests that deformation of the diamonds may enhance the rate of nitrogen aggregation. The method also assumes that the aggregation proceeds in accordance with second order kinetics. Due to the inherent uncertainties involved with this method, together with the fact that calculated temperatures are time averaged, FTIR data is not considered in isolation in this report, but will serve to supplement information derived from other analyses.

5.2 Infrared Classification of Diamonds and Nitrogen Aggregation

Nitrogen aggregation in diamond is a kinetic phenomenon in which the amount of nitrogen aggregation depends on the nitrogen content, period of mantle residence, and

the diamonds thermal history (Mendelssohn & Milledge, 1995). It follows therefore that by defining one or more of these parameters, much can be learnt about the geological evolution of an individual diamond.

Diamond and its associated substitutional trace elements display absorption within the mid-infrared (IR) range. While all diamonds exhibit intrinsic absorption from 4000 – 1500 cm^{-1}, their perfect symmetry prohibits absorption within the one-phonon region of the IR range. Such intrinsic absorption is the result of two- and three- phonon transitions (Mendelssohn & Milledge, 1995). Robertson *et al.* (1934) found that some diamonds showed both IR and ultraviolet (UV) absorption within the one-phonon range, while others did not, suggesting the existence of two types of diamond. These classes of diamond were assigned as Type I (imperfect), and Type II (perfect) respectively. Since this observation was made, diamonds have been further subdivided into Types IaA, IaB, Ib, IIa and IIb (e.g.: Jones *et al.*, 1992) based on the different lattice arrangements of substitutional defects, all of which can be identified within the IR range.

Type IIa diamond is virtually free of substitutional trace elements, and only displays the intrinsic diamond absorption in the region 4000 – 1500 cm^{-1} due to the inherent two- and three-phonon transitions associated with carbon. Type IIb diamond is rare in nature and contains trace amounts of boron associated with absorption in the two-phonon region at 2460 cm^{-1} (e.g.: Collins, 1982). The boron content of these diamonds commonly imparting a blue colour to the crystal.

Type Ib, IaA and IaB diamond all contain significant amounts of nitrogen (>50 ppm), but are distinguished by their different lattice arrangements. The nitrogen content of the diamonds is believed to be incorporated into the diamond lattice during crystal growth, by the substitution of single nitrogen atoms for carbon atoms. The substitutional nitrogen alters local lattice symmetry, allowing one-phonon transitions to occur and resulting in characteristic IR absorption. The Type Ib diamond carries such dispersed nitrogen atoms (50 – 300 ppm), and is relatively rare in nature (Evans, 1992), displaying predominant absorption at 1130 cm^{-1}. It has been estimated that pure Type Ib diamond will not survive more than 50 years in the mantle, because at the elevated temperatures, the single nitrogen atoms will aggregate into multiples of atoms within the diamond via a series of thermally-controlled diffusion processes (Davies, 1980; Evans & Qi, 1982). It follows from the long mantle residence times

associated with most diamonds (e.g.: Richardson, 1986), that very few natural diamonds are of Type Ib affinity. In general, preservation of diamond with a Type Ib component requires a young crystallisation age, or unusually cool conditions of mantle storage, or both (Taylor *et al.*, 1996).

During extended periods of mantle residence at elevated temperatures, the dispersed nitrogen aggregates to form 'A' aggregates which characterise the Type IaA diamond (Evans & Qi, 1982). Type IaA diamond show prominent absorption at 1282 cm^{-1}, with a subsidiary absorption peak at 1215 cm^{-1}. Davies (1976) suggests that such 'A' aggregates consist of two adjacent nitrogen atoms. With time, further aggregation results in the formation of 'B' aggregates, which are believed to consist of four nitrogen atoms arranged tetrahedrally about a vacancy in the diamond structure (Loubser & van Wyk, 1981). This is characteristic of the Type IaB diamond which shows prominent absorption at 1174 cm^{-1} and a subsidiary peak at 1282 cm^{-1}. Type IaAB diamond contains A and B aggregates in differing proportions, with highly variable nitrogen concentrations of up to several thousand ppm (Woods, 1986). As the complete aggregation series from Type IaA to IaB requires extended periods of geological time at mantle pressures and temperatures, most diamonds display nitrogen aggregation transitional between the two end-members, and consequently most diamonds are of Type IaAB (i.e.: belong to the Type IaA-IaB series).

It is believed that annealing during mantle residence, at elevated mantle temperatures promotes the progressive aggregation of nitrogen atoms (Evans & Qi, 1982). Davies *et al.* (1978) suggest that a very small amount of nitrogen aggregates during such annealing to form clusters of 3 nitrogen atoms (N3 defects) on the (111) planes. This 'N3' defect shows no absorption in the one-phonon region of the IR spectrum, but does show a distinctive absorption in the visible and UV ranges (Davies, 1978). It is believed that the presence of such N3 defects in diamond may impart yellow coloration, due to absorption of light in the visible and UV ranges.

Nitrogen aggregation is also believed to give rise to the development of planar structures (platelets) on the cubic planes of diamond. Such structures have been observed to cause anomalous spikes in X-ray diffraction patterns (Raman, 1944), as well as IR absorption at 1359 – 1378 cm^{-1} (Sobolev *et al.*, 1968). The position of the so called 'platelet peak' varies with the size of the platelets, the larger platelets being associated with lower wavenumbers (Sobolev *et al.*, 1968). The IR absorption caused

by such platelets is referred to as the B' peak. Platelets are visible in Transmission Electron Microscopy (TEM) and Cathodoluminescence (CL), and vary in size from only a few nm, to several μm (Evans & Phaal, 1962).

The intensity of the platelet peak (Sobolev *et al.*, 1968) or more correctly, the integrated platelet area (Woods, 1986), can be directly correlated to the X-ray spike intensity. The correlation therefore suggests that the platelet peak intensity is a measure of the platelet concentration.

The composition of the platelets is the subject of debate. One model invokes nitrogen as the major constituent (e.g.: Lang, 1964), while the other favours carbon (e.g.: Woods, 1986). Nitrogen can be detected within such platelets, but at concentrations too low to support the Lang (1964) model (Berger & Pennycook, 1982). The Woods (1986) model, suggesting that platelets are composed predominantly of carbon (with only minor nitrogen) is thus favoured, with B aggregation providing the mechanism for their formation (Loubser & van Wyk, 1981).

On formation of B aggregates, a single carbon atom is released into the diamond lattice and a vacancy is created. It is suggested (Woods, 1986) that these interstitial carbon atoms aggregate themselves to form the platelets, and occasionally on formation of such platelets, nitrogen may also be incorporated into the structure. This is supported by the positive proportionality between B and B' absorption peaks in the so termed 'regular' diamonds, as it is consistent with nucleation and growth of platelets both concurrent with, and as a result of, the aggregation of A defects to B defects. For 'irregular' diamonds this proportionality does not hold. They show lower B' absorption than would be expected on the basis of their B defect absorption. The deficient B' peak associated with such 'irregular' diamonds is ascribed to catastrophic degradation of the platelets (Woods, 1986). Woods *et al.* (1990) suggest that the B' peak is produced by the remnant platelets following such degradation, and that the process is contemporaneous with the formation of new defects known as voidites. These voidites are reported to be precipitates of a nitrogen-bearing phase which nucleate and grow at the platelet/matrix interfaces, and on dislocations that bound the platelets. It becomes clear therefore that platelets constitute a necessary, if incidental, product of the nitrogen aggregation sequence within diamond (Woods *et al.*, 1990). Figure 5.1 illustrates the progression from pure Type IaA diamond to Type IaB

diamonds as well as the associated evolution and catastrophic degradation of the platelet peak.

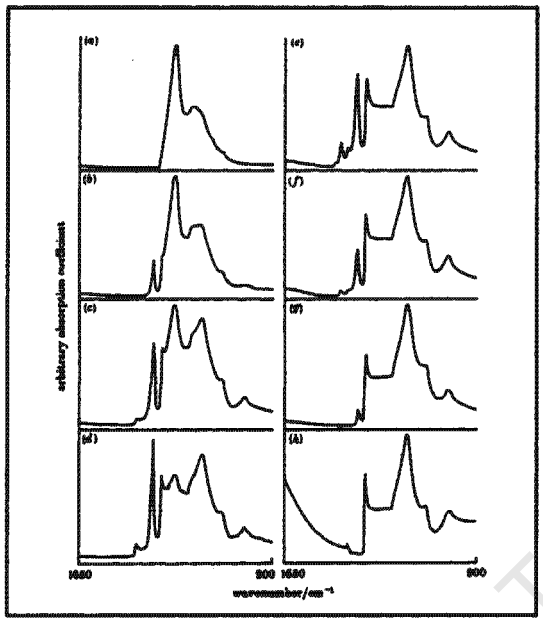

Figure 5.1 IR absorption spectra, illustrating the progression from pure Type IaA diamond (a) through (b-d) to the case of a regular diamond with only B and D lattice absorptions (e), followed by a departure from regularity (f, g) towards a pure Type IaB diamond (h). From Woods (1986)

Haggerty (1986) makes an association between the various types of diamond (based on their nitrogen content) with their lithospheric environment (Figure 1.1). This 'Haggerty-Model' suggests that annealed high temperature octahedral diamonds of Type Ia affinity are expected to dominate the basal and contact zones of the lithosphere. Type Ib diamonds would be expected to dominate the uppermost interior portions of the lithosphere. B-aggregated nitrogen centres would be expected to form near the base of the lithosphere, while A-aggregates should be prevalent in the cooler regions. It is further suggested that Type II diamonds are restricted to isolated regions enriched in boron and depleted in nitrogen.

5.3 Other Chemical Defects within Diamond

The effects of hydrogen substitution within the Helam diamonds are also evident within some diamonds, and should therefore also be discussed briefly. IR absorption due to the presence of hydrogen is correlated to peaks at 3107 cm^{-1} and 1407 cm^{-1}

(Chrenko *et al.*, 1967). The absorption is believed to be the result of vibrations of the sp^2 bonds within the vinylidene group (>C=CH_2), situated at the inclusion-matrix interfaces (Woods & Collins, 1983).

Another defect that has been observed within diamond is that of carbon dioxide, which results in IR absorption at 650 cm^{-1} and 2376 cm^{-1} (e.g.: Schrauder & Navon, 1993; Chinn, 1995). No such absorption has been observed within the Helam diamonds, and as such the effects and causes of carbon dioxide in diamond will not be considered further.

5.4 Qualitative Infrared Classification of the Helam Diamonds

From inspection of the Infrared (IR) data obtained from the Helam diamonds (Appendix 3) it becomes clear that the colourless, brown and green diamonds belong to the Type IaA-IaB aggregation series. Consequently these diamonds have all been classified as Type IaAB diamonds. They typically display a prominent absorption peak at 1282 cm^{-1}, a subsidiary peak at approximately 1215 cm^{-1}, and may or may not display a platelet peak at 1344 cm^{-1}. Figure 5.2a illustrates a typical IR spectrum associated with a colourless Helam diamond.

The canary-yellow diamonds however, display IR spectra that are generally quite distinct from the Type IaAB diamonds, displaying a prominent absorption peak at 1282 cm^{-1}, a subsidiary peak at 1152 cm^{-1}, an occasional Raman Edge at 1330 cm^{-1}, and a complete absence of a platelet peak (figure 5.2c). In addition, these spectra differ from those associated with synthetic Type Ib diamond, which display a prominent absorption peak at 1130 cm^{-1}, and a subsidiary peak at 1344 cm^{-1} (Figure 5.2b).

Figure 5.3 superimposes the IR spectra within the one-phonon region, of pure IaA diamond, pure Ib diamond, and a typical canary-yellow Helam diamond. It is clear that while the main absorption peak of the canary-yellow diamond corresponds with that of a Type IaA diamond, the subsidiary peak occurs at a significantly lower wavenumber than is associated with Type IaA diamond. The subsidiary absorption peak at 1152 cm^{-1} is interpreted to be the result of the presence of a Type Ib diamond component in addition to Type IaA diamond within these crystals, and these diamonds have consequently been classified as belonging to the Type Ib-IaA

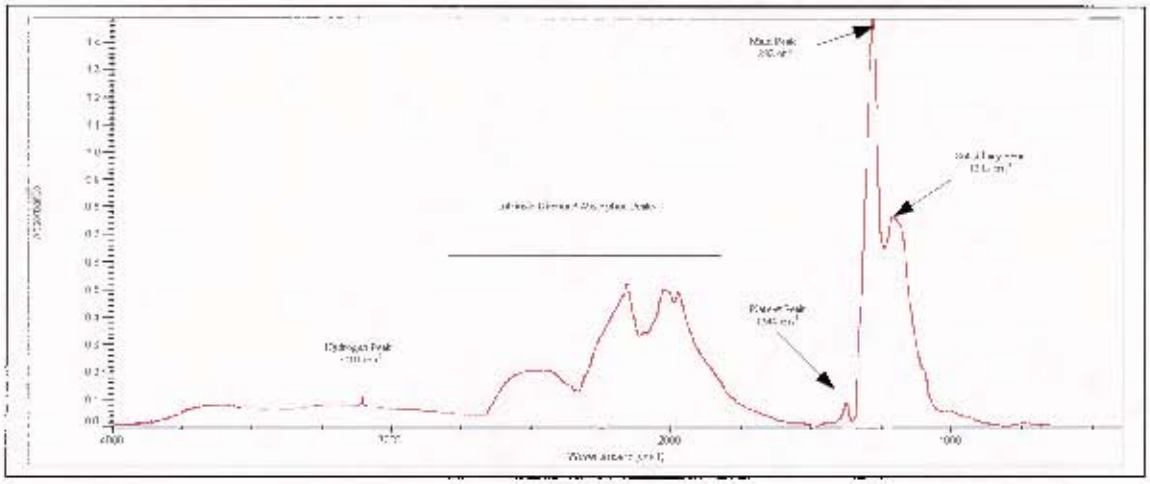

Figure 5.2a IR absorption spectrum of a typical Type IaA-IaB, colourless Helam diamond.

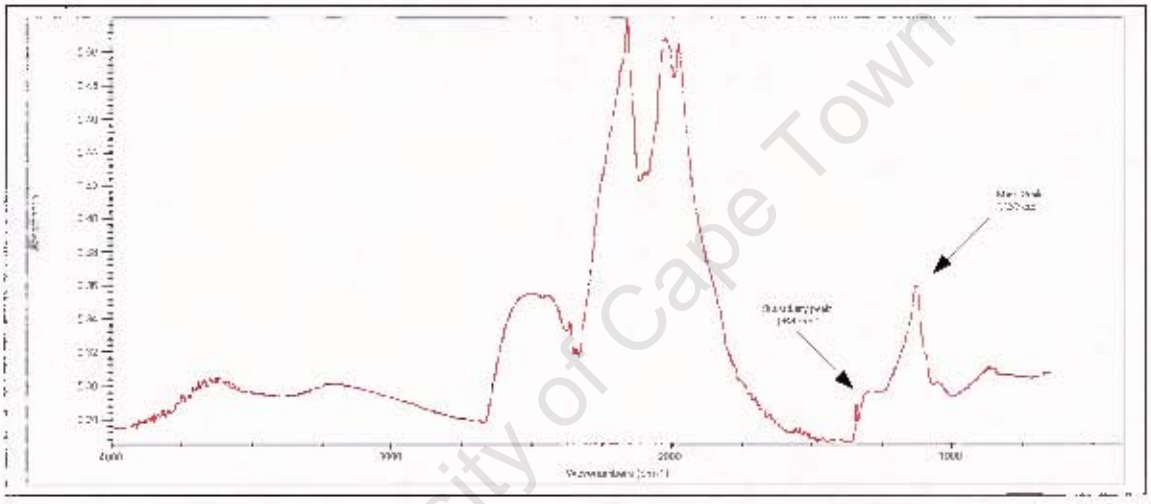

Figure 5.2b IR absorption spectrum of a synthetic Type Ib diamond. Compliments of De Beers Geoscience Centre, Johannesburg.

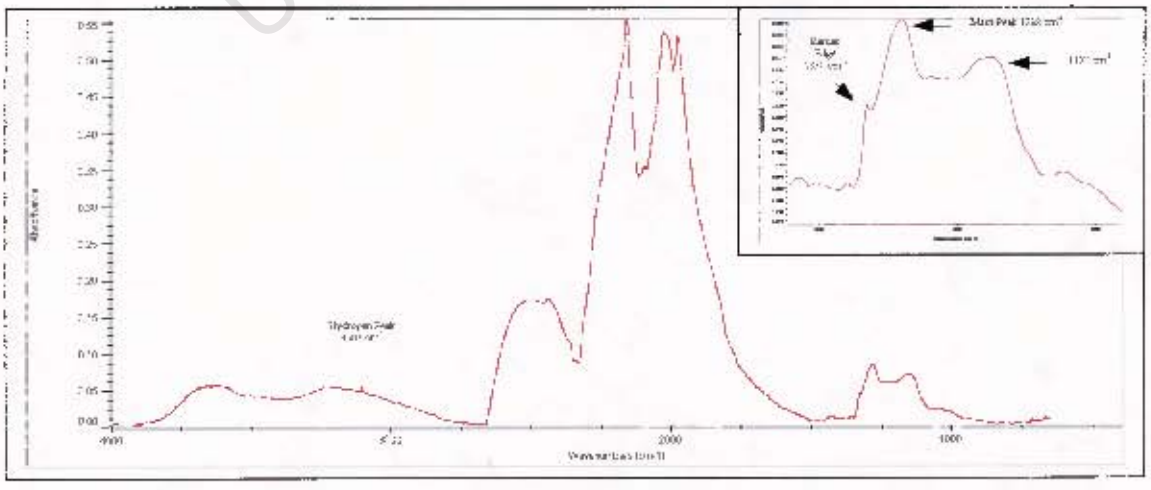

Figure 5.2c IR absorption spectrum of a canary-yellow Helam diamond. Insert illustrates the IR absorption spectrum in the one phonon region, for clarity.

aggregation series. These observations are consistent with those made by Collins (1980) who observed that a natural mixture of Type Ib and IaA diamond results in a broader, and more rounded 1130 cm-1 peak than is associated with synthetic Ib diamonds. This interpretation is also consistent with the observed body coloration of these diamonds, as discussed in Chapter 4.

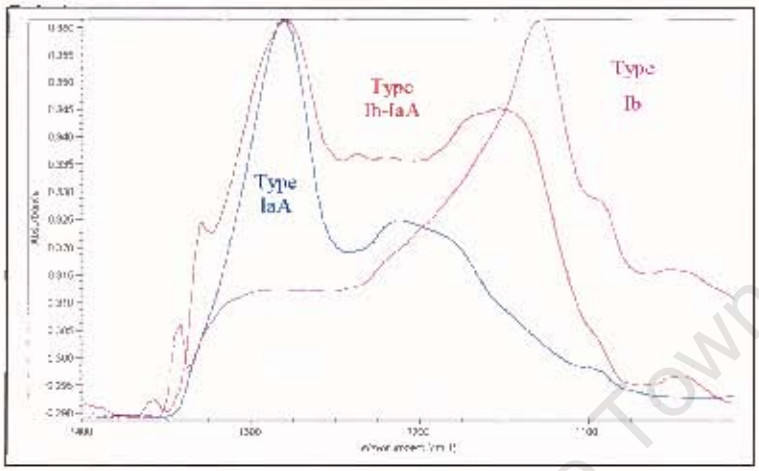

Figure 5.3 Superimposed IR absorption spectra in the one-phonon region for: a natural Type IaA diamond (from Helam population) in which virtually all the nitrogen occurs in the A-aggregate form; a synthetic Type Ib diamond (compliments of De Beers Geoscience Centre, Johannesburg); and a natural Type Ib diamond (canary-yellow Helam diamond), which is a natural mixture of Type IaA and Type Ib material, about 45% of the nitrogen occurs as A-aggregate.

Electron Paramagnetic Resonance (EPR) studies (conducted by Graeme Hill at the De Beers Geoscience Centre, Johannesburg) of some of the canary-yellow Helam diamonds has confirmed the presence of unaggregated substitutional nitrogen. The EPR spectra are typical of samples usually referred to as natural Type Ib diamond (Hill, 2001, pers. comm.). Large concentrations of the EPR centres OK1 and N3 are observed within these diamonds (Note that *EPR* N3 should not be confused with the *optical* centre labelled N3 which has been shown to correlate with the P2 EPR (Hill, 2001, pers. comm)). No P2 centres were observed within these diamonds. The canary-yellow diamonds also contain observable (by EPR) amounts of single, unperturbed, substitutional nitrogen, but far less than the concentrations found in synthetic Type Ib diamond (Hill, 2001, pers. comm).

The currently accepted models for EPR N3 and OK1 are that each contains a single substitutional nitrogen atom with an oxygen atom in the nearest (van *Wyk et al.*, 1992) and second nearest (Newton & Baker, 1989) neighbour site respectively. The

conclusions therefore are that the canary-yellow diamonds contain significant concentrations of unaggregated nitrogen, and that these diamonds may be associated with large amounts of substitutional oxygen.

The presence of a 'Raman Edge' in association with some of IR spectra of canary-yellow diamonds, may be suggestive of an accessory component of IaB diamond, as this feature is commonly associated with B aggregation. While this feature does not ubiquitously characterise the canary-yellow diamonds, it can be argued that at least some of these diamonds are complexly zoned. Perhaps then, the variation in IR properties observed between diamonds is simply the result of differential sampling through distinct zones within the diamond. Nevertheless it is clear that the vivid coloration of these diamonds is the result of an unaggregated nitrogen component within their diamond lattice, and that these diamonds belong to the Ib-IaA aggregation series.

5.5 Quantitative Analysis of IR Absorption Spectra

The various absorption peaks within the IR spectra (figure 5.4) can be used to determine the amount of nitrogen aggregation as well as the nitrogen concentration within a particular diamond sample. The amount of nitrogen aggregation in a diamond is dependent on the amount of nitrogen present as well as on the mantle residence time and temperature. Experimentally derived absorption coefficients can be used together with nitrogen aggregation estimates to determine the nitrogen concentration within a diamond.

Temperature is the more sensitive parameter, and even if mantle residence time can only be estimated in the order of hundreds of millions to billions of years, the residence temperature of the diamonds can still be fairly well constrained. Conversely, in order to constrain the residence time of diamonds, the storage temperature of the diamonds must be precisely defined (Mendelssohn & Milledge, 1995).

A spreadsheet developed by Mendelssohn & Milledge (1995) has been used to make such determinations in the case of the Helam diamonds belonging to the Type IaA-IaB series. The reader is referred to Mendelssohn & Milledge (1995) for a

comprehensive overview of the technique and the operation of the spreadsheet. A brief overview of the technique is considered below.

The spreadsheet analyses the intensities of the Platelet peak ~ 1365 cm^{-1} (T), Raman edge ~1328 cm^{-1} (E), IaAmax ~1282 cm^{-1} (P), Dip ~ 1242 cm^{-1} (D), IaBmax ~1174 cm^{-1} (Q), as well as the subsidiary peaks at 1174 cm^{-1} (R) and 1010 cm^{-1} (S). Quantitative information is derived from analyses of the various IR absorption peak intensities as well as various peak ratios. The positions of the various peaks can vary depending on the amount of aggregation, and each spectrum should therefore be analysed separately. Figure 5.4 demonstrates how these peaks shift in their positions with varying aggregation.

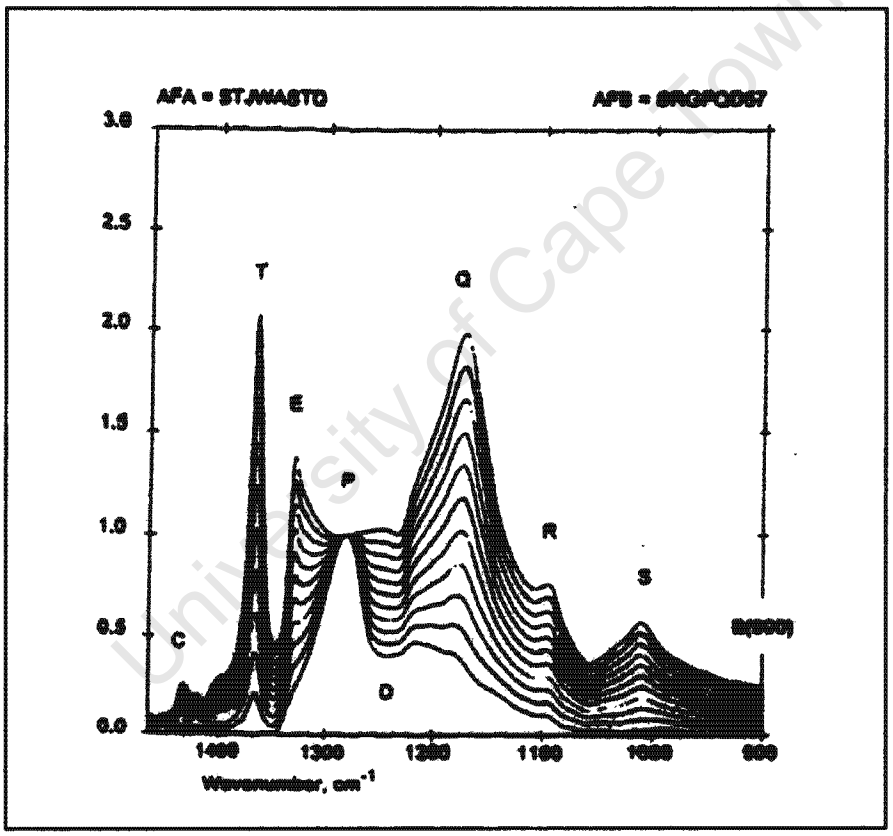

Figure 5.4 Simulated IR absorption spectra illustrating the locations at which data are extracted within the IaA-IaB aggregation series, also indicating where positions and intensities vary with progressive aggregation (From Mendelssohn & Milledge, 1995)

Assuming that diamonds evolve from pure Type IaA to Type IaB as described earlier, and that this evolution is linear, then any Type IaAB diamond is a linear combination of the two end members (Mendelssohn & Milledge, 1995). Comparison of any given

spectrum, to simulated intermediate spectra between these two end members (figure 5.4), can therefore be used to estimate the amount of aggregation in that sample.
The concentration of nitrogen is also assessed (Mendelssohn & Milledge, 1995), and is derived from:

$$N(ppm) = \mu(1282\ cm^{-1}) \times [N/mm(IaA) + N/\%B \times (\%B_{used})]$$

Where:

$N/\%B = \{[N(B) - N(A)]/100\}$

N(A) and N(B) = experimentally derived absorption coefficients per millimetre of diamond at 1282 cm^{-1} for the A and B aggregates respectively.

The Mendelssohn & Milledge (1995) method assumes absorption coefficients $\mu^{A}[1282]$=1/mm for 150 ppm and $\mu^{B}[1282]$=1/mm for 650 ppm. The thickness of the sample is taken into account by normalising the absorption values to a constant pathlength of 1mm, using the ratio of absorption at 1992 cm^{-1} to 1.23, the known absorption value due to the lattice vibrations within a 1mm diamond slab at the same wavenumber.

Time-averaged mantle residence temperatures can be estimated too, assuming that the nitrogen aggregation series obeys second order kinetics by:

$$T_{NA}(°C) = -E_A/R \times \{\ln(([N_{tot}/N_{(A)}]-1)/[t_{MR} \times N_{tot} \times A])\}^{-1} - 273.15$$

Where:

N_{tot} = Concentration of nitrogen (atomic ppm)

E_A/R = activation energy for A to B aggregation divided by the gas constant

E_A = 7.03 eV (Taylor *et al.*, 1990)

$N_{(A)}$ = Nitrogen occurring as A aggregates (atomic ppm)

A = Arrhenius constant = $2.94181 \times 10^{5} s^{-1} ppm^{-1}$

T_{MR} = assumed mantle residence time (years)

A deconvolution programme (written by Dr. David Fisher of the DTC Research Laboratory, Maidenhead) utilised at the De Beers Geoscience Centre to calculate concentrations and aggregation states of nitrogen for diamonds containing a Type Ib

component, was applied to make such calculations from IR spectra derived from diamonds belonging to the Ib-IaA series. Since the method represents in-house intellectual property, the details of this programme can not be discussed or published. Suffice it to say, that the approach is similar to that discussed above, in accordance with the principles of second order kinetics for the aggregation of single nitrogen atoms into pairs of atoms, and encompassing an experimentally derived Type Ib absorption coefficient. Kiflawi *et al.* (1984) report a Type Ib absorption coefficient of $\mu(1134\ cm^{-1}) = 1/mm$ for 250 ppm of nitrogen.

5.6 Quantitative FTIR Measurements of the Helam Diamonds

The majority of the Helam diamonds have been analysed as whole, rough diamonds, or as fragments of diamond after mineral inclusions have been mechanically cracked out. It is the analysis of these whole, rough diamonds that form the basis for the diamond classification, as they provide a more complete data set regarding the Helam diamond population. Where possible, these rough diamonds and fragments were analysed in multiple locations, in order to document variation in the IR characteristics across the diamonds.

In addition some of the larger, inclusion bearing diamonds were selected to be cut into plates, in order to study the growth history of the diamonds, as well as the relationship of the inclusions with respect to the diamond growth. Because these diamonds were selected due to suitability for diamond plate analysis (i.e.: large and inclusion bearing), a sampling bias may have been introduced, and consequently the plates may not be representative of the population as a whole. Regardless, analysis of these plates has revealed some interesting aspects concerning diamond growth, and has aided the understanding of the geological history of some of the Helam diamonds.

5.6.1 Rough Diamonds

The Helam diamond population can be subdivided based on differences in the IR properties of the various diamonds. It will be demonstrated that the IR properties reflect chemical differences between diamonds, which are strongly correlated to the differences in the diamonds' physical appearance. Over 200 diamonds have been

analysed using the FTIR spectrometer at the University of Cape Town, as described in Appendix 3. Most of the diamonds exhibiting mineral inclusions, as well as other selected diamonds have been analysed using this technique. IR data, including calculated time-averaged mantle residence temperatures for the rough diamonds of the IaA-IaB series are recorded in Appendix 3.2. Appendix 3.3 documents the IR data for the diamond of the Ib-IaA series.

5.6.1.1 Nitrogen Content

Helam diamonds exhibit nitrogen concentrations ranging from less than 50 ppm to as much as 2500 ppm. The colourless and brown diamonds together display a very similar range in nitrogen concentrations, typically between 200-1300 ppm (figure 5.5). The green diamonds are commonly characterised by significantly higher nitrogen concentrations, with as much as 2500 ppm nitrogen being recorded. The canary-yellow diamonds are characterised by unusually low nitrogen concentrations, typically between >50-150 ppm (figure 5.7).

The nitrogen concentration within individual diamonds of the IaA-IaB series can be shown to be highly variable (figure 5.6), with a range of as much as 1250 ppm being observed within some diamonds. It can be shown in figure 5.6, that among those whole, rough diamonds exhibiting the most nitrogen content variation, there appear to be increased nitrogen concentrations towards their centres. The colourless and brown diamonds exhibit similar variations in nitrogen, with as much as 300 ppm variation being recorded between the centre and edges of the crystals. The green diamonds are associated with the largest ranges in nitrogen concentrations, with over 1000 ppm nitrogen difference recorded between the centre and edges of these crystals. The canary-yellow diamonds are associated with a comparatively small range in nitrogen concentration, typically less than 20 ppm across the crystals. Whether this reflects a decrease in nitrogen towards the edges of the crystals remains unclear, as a discrepancy of less than 20 ppm falls within the error of measurement.

It is important to note that measurements could not be taken precisely at the edge of each diamond, and consequently measurements described as 'edge' simply refer to some position more distal from the diamond centre. It follows that the above observations only reflect variations within the more central regions of the whole

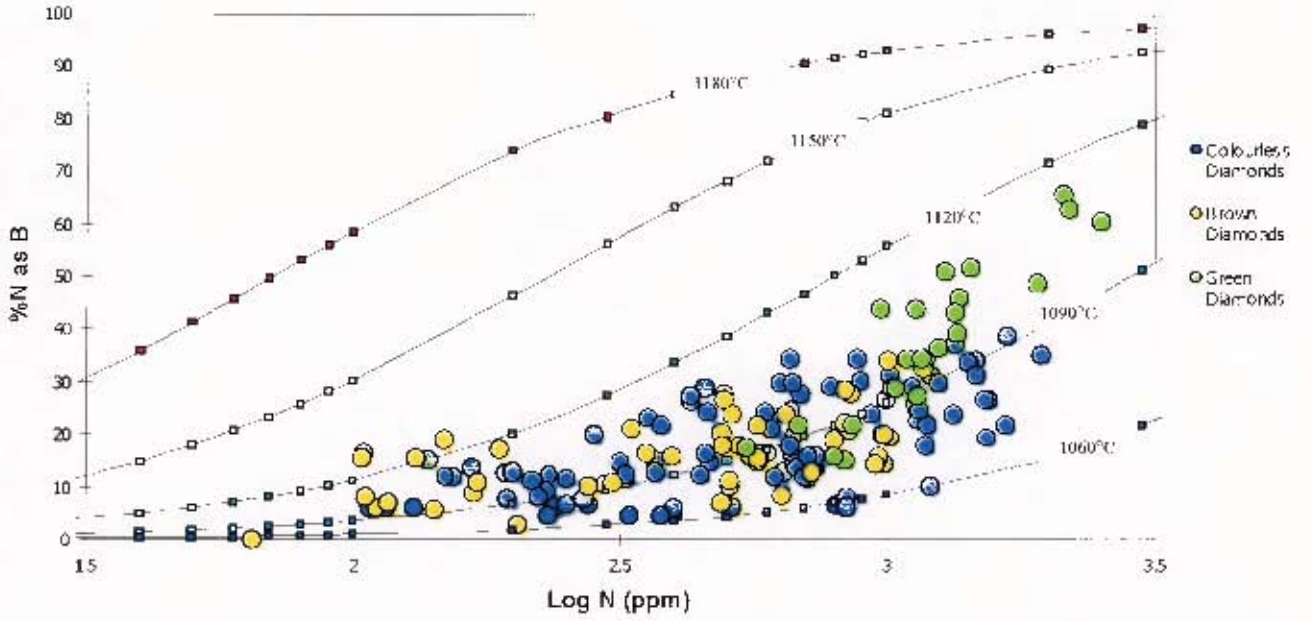

Figure 5.5 Nitrogen concentration versus the percentage of nitrogen occurring as B aggregate (%N as B) for Helam IaAB rough diamonds. Isotherms have been calculated for a mantle residence time of 2.75 Ga.

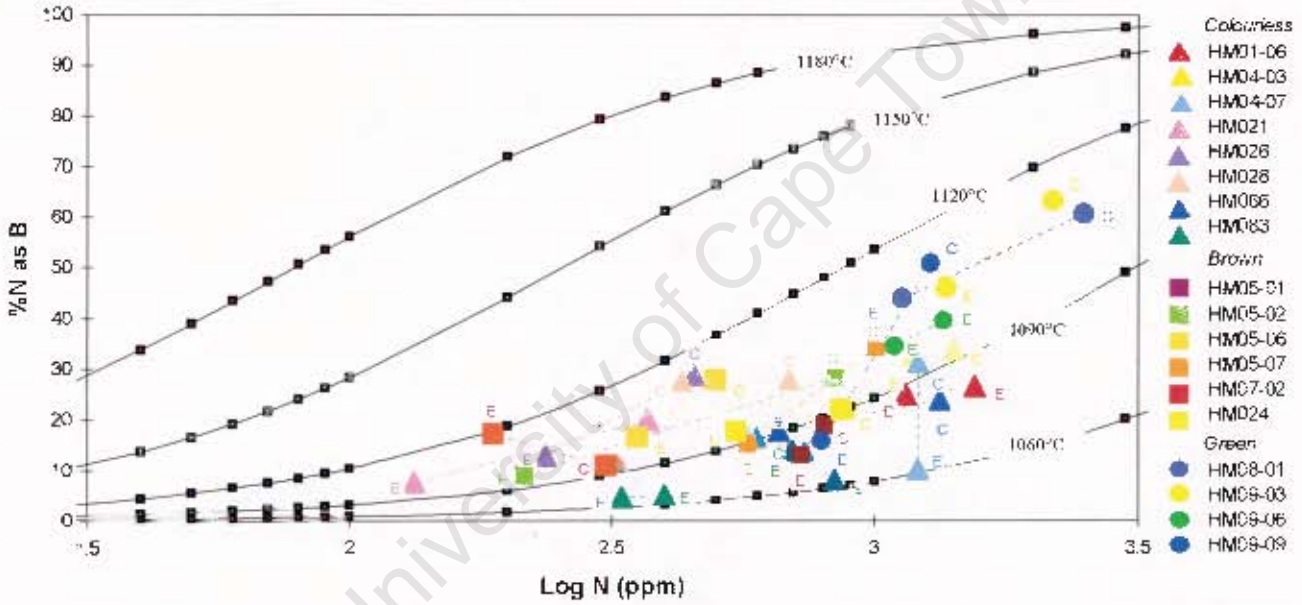

Figure 5.6 Variation in nitrogen concentration and aggregation state for individual IaAB Helam diamonds. C and E indicate analyses near the centre and edge of the crystals respectively. Isotherms are calculated for a mantle residence time of 2.75 Ga.

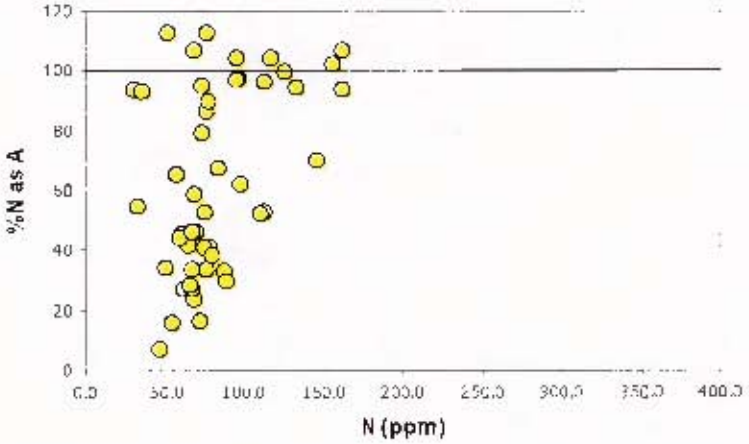

Figure 5.7 Nitrogen concentration versus nitrogen aggregation for the canary-yellow, Ib-IaA, Helam rough diamonds.

crystals, sometimes revealing a marked disturbance in the trends discussed in this section.

5.6.1.2 Nitrogen Aggregation

It has been demonstrated that the colourless, brown and green diamonds belong to the IaA-IaB series. The colourless and brown diamonds appear to exhibit a similar range in aggregation state within the IaA-IaB series, with values of between 10% - 35% of the nitrogen occurring as B aggregate (now referred to as %N as B). The Green diamonds also belong to the IaA-IaB series, but exhibit ubiquitously high aggregation states with as much as 60% N as B.

Nitrogen aggregation too, is observed to vary significantly within individual diamonds (figure 5.6). It can be demonstrated that there is a general decrease in the degree of aggregation towards the edge of the diamonds in accordance with a decrease in nitrogen concentration. The colourless and brown diamonds show similar variation, typically exhibiting a 10% difference in the degree of aggregation between the centre and edges of the crystals. The green diamonds are associated with the largest ranges in aggregation states, with as much as a 35% difference in the aggregation state being recorded. This chemical variation within the Helam diamonds, in part explains the scatter of data in figure 5.6. It is clear, that had only analyses from the central regions of the diamonds been plotted, the points would have been more tightly clustered. In addition this demonstrates the importance of multiple analyses on individual diamonds in order to more accurately document the nitrogen systematics within a diamond population.

Again the reader is cautioned that the above observations only reflect trends associated with the more central regions of the whole diamonds. A more detailed analysis of the variation in nitrogen aggregation will be discussed in Section 5.6.2.

The canary-yellow diamonds have been interpreted as belonging to the Ib-IaA series, and consequently their aggregation states are reported in terms of the percentage of nitrogen occurring as A aggregate (now referred to as %N as A). These diamonds are associated with highly variable aggregation states, with values extending across the range of 7% - 100% N as A (figure 5.7). Some canary-yellow diamonds record values in excess of 100% N as A. When the IR data from these

diamonds were processed using the deconvolution spreadsheet for the IaA-IaB series, negative values of %N as B were recorded. Consequently, these analyses are interpreted as representing diamond at the transition between the Ib-IaA and IaA-IaB series, and demonstrate the limitations that deconvolution programmes have in processing data from such 'transitional' diamonds.

Despite the predominant IaA component associated with these 'transitional' diamonds, Ib diamond must be present, even if at very low concentrations, as these diamonds still display intense yellow coloration. The yellow coloration can not be explained by the existence of optical N3 centres, as low-nitrogen diamonds such as these would require as much as 70% N as B (pers. comm. Hill, 2001), for such defects to occur in the concentrations required to manifest colour. Even then, the coloration would only be very subtle. Hill (2001, pers. comm) reports that no optical N3 centres can be observed (by EPR) within these canary-yellow diamonds. Perhaps the diamonds exhibiting erroneous values are in support of the suggestion that some of the canary-yellow diamonds may be complexly zoned. Perhaps these analyses are the result of sampling only some of the Type Ib diamond that has imparted the coloration to these diamonds.

5.6.1.3 Platelet Development

In consideration of platelet development, the canary-yellow diamonds are ubiquitously characterised by an absence of platelet peaks. As a result these diamonds will not be considered in the following discussion. However, small platelet peaks *are* visible in the majority of the spectra for the colourless, brown and green diamond sub-populations. It should be noted that while such platelets can be detected, they exhibit relatively low peak intensities (mu(1365) < 0.8). However, some diamonds (approximately 30% of the diamond population) with equivalent nitrogen concentration and aggregation states, show *no* evidence for platelet development in the IR spectra. It will be shown in Section 5.6.2, that absence of such platelets can be attributed to the catastrophic degradation of platelets as a result of deformation.

The position of the platelet peak varies considerably within the Helam diamonds, ranging from 1362-1382 cm^{-1} (figure 5.8a), which is similar if somewhat displaced from the range of 1359-1379 cm^{-1} reported by Hanley *et al.* (1977). As

discussed previously, the position of the platelet peak is correlated to platelet size, the biggest platelets corresponding to the lowest wavenumbers. Among the Helam diamonds, it can generally be seen that the highest wavenumbers correspond to those diamonds exhibiting the highest nitrogen contents.

It can also be demonstrated (figure 5.8a) that it is impossible to discriminate between the different diamond sub-populations on the basis of the estimated time-averaged mantle residence temperatures and platelet peak positions. This is supported by the positive relationship between platelet peak intensity and the concentration of B aggregates (figure 5.8b), showing coincidental platelet evolution for all Type IaA-IaB diamonds within the Helam population. It is clear therefore, that while the various sub-populations of the Helam diamonds can be readily distinguished by their differences in nitrogen concentrations and aggregation states, platelet peak development within the diamonds is ineffective in resolving paragenetic differences between the diamonds of the IaA-IaB series.

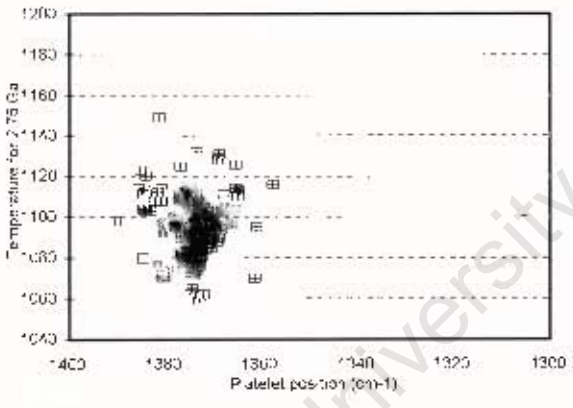

Figure 5.8a Estimated mantle residence temperature versus platelet peak position for Helam IaAB diamonds. Temperatures have been estimated for an assumed mantle residence time of 2.75 Ga.

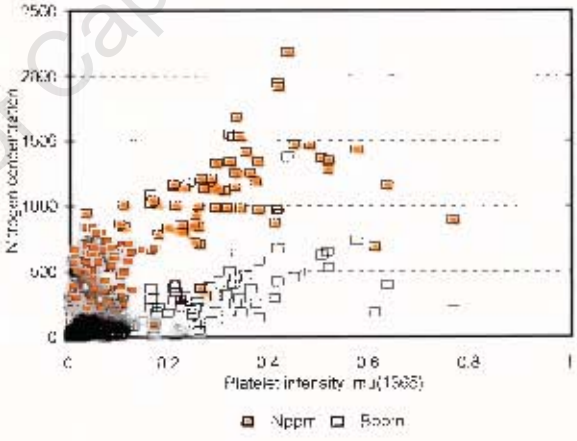

Figure 5.8b Total amount of nitrogen (Nppm) and amount of nitrogen occurring as B aggregate (Bppm) versus the platelet peak intensity for the Helam IaAB diamonds.

5.6.1.4 Hydrogen Content

Many of the Helam diamonds show traces of hydrogen, represented by a weak 'hydrogen peak' at 3107 cm^{-1} in the 3 phonon region of the IR spectrum (figure 5.2a). The absorption is sufficiently low not to display the subsidiary peak (at 1405 cm^{-1}) commonly associated with larger concentrations of hydrogen. All the Helam diamond

sub-populations, exhibit small amounts of hydrogen in some of the stones. While all the diamonds associated with hydrogen defects, have platelet peaks, the converse is not true. It has been demonstrated that platelet peak development can be correlated to hydrogen content (e.g.:Westerlund, 2000), however, in the case of the Helam diamonds, no such relationship can be defined due to the exceedingly low levels of hydrogen incorporated into the diamond lattice, together with the ubiquitously weak platelet peak development within the diamonds.

5.6.1.5 Time-Averaged Temperature Estimations

As discussed previously, experimentally derived activation energies can be used to obtain mantle residence times for a given temperature, or temperatures for a given residence time. Because temperature is the more sensitive parameter, mantle residence temperature for a suite of diamonds can be fairly well constrained even with only very rough estimates of mantle residence time.

The vast majority of African diamonds have been dated as being Archean or middle Proterozoic in age (e.g.: Richardson, 1986). Re-Os data from single eclogitic sulphide inclusions (see Chapter 6) from Helam diamonds, are in support of an ancient age of diamond formation. It is suggested that these inclusions may have recorded a 2.9 Ga diamond formation event, as has been established from some eclogitic sulphide inclusions from Kimberley (Richardson *et al.*, 2001). Taking into account the 150 Ma age of the Swartruggens Kimberlite (Allsopp & Barrett, 1975; Smith *et al.*, 1985), it is reasonable to assume that some of the diamonds resided at mantle conditions for approximately 2.75 Ga. Consequently, a mantle residence time of 2.75 Ga has been used in the derivation of all time-averaged temperatures discussed.

The amount of nitrogen present as B aggregate is plotted versus the nitrogen concentration (Figure 5.5) for all rough diamonds belonging to the IaA-IaB series. In comparing the plots of the different sub-populations it becomes increasingly clear that in general, the diamond sub-populations are distinguishable both in terms of their nitrogen concentration and maturity of aggregation. Despite the range of values, the colourless and brown diamonds plot about the 1090 °C geotherm. The green diamonds overlap somewhat with the field defined by the colourless and brown

crystals, but do show an increased nitrogen content (up to 2500 ppm), and increased B aggregation (up to 68% N as B) in some crystals. The green diamonds plot between 1090 °C and 1120 °C, suggesting exposure to somewhat elevated temperatures. It should be noted that accuracy of this geothermometer is associated with an error of up to 50 °C (Chinn, pers. comm., 2001), and thus the assumption that the green diamonds represent slightly elevated ambient temperatures remains questionable. Figure 5.8a illustrates the range of estimated mantle residence temperatures for the IaAB diamonds, and it can be demonstrated that these values fall well within error of one another.

The canary-yellow diamonds, while displaying a limited range in nitrogen concentration (between 36 – 162 ppm), are characterised by highly variable calculated aggregation states (figure 5.7). There appears to be a positive correlation between the concentration of nitrogen and %N as A. However, in the absence of independent age constraints for these diamonds, it is impossible to estimate their residence temperatures (and visa versa), as has been done for the diamonds of the IaA-IaB series.

Studies of natural Type Ib diamond commonly report young ages of crystallisation, often concomitant with, or just preceding kimberlite emplacement (e.g.: Taylor *et al.*, 1996). These 'young' diamonds are commonly characterised by high nitrogen concentrations (1000 ppm) and variable aggregation states (between 20-80% N as A). However, the observation that many of the canary-yellow Helam diamonds are highly aggregated *despite* their very low concentrations of nitrogen, preclude the suggestion of a young formation age for these diamonds. It is suggested therefore that the canary yellow diamonds are related to a separate diamond formation event that occurred at some time subsequent to the crystallisation of the other Helam diamonds, but well before the intrusion of the Swartruggens Kimberlite. For these diamonds, an age of approximately 2 Ga would require mantle residence temperatures in the range of 1000 °C – 1100 °C. It follows therefore that an ancient age does not necessitate unusually hot mantle conditions. If however these diamonds were 1 Ga old or younger, mantle residence temperatures in excess of 1200 °C would be required to account for the observed aggregation states. In the absence of any information suggesting that these diamonds have been exposed to unusually high mantle

temperatures, it is reasonable to assume that these diamonds are old (> 1 Ga), having resided in a mantle thermal regime indistinguishable from the rest of the Helam diamonds.

Westerlund (2000) demonstrates that spurious temperature estimates can be attributed to the sampling of different layers within a diamond, and it is suggested that the variability in estimated temperatures among the unpolished, whole diamonds may be a result of such an effect. Analysis of the rough diamonds, precludes the analysis of individual growth layers within a particular diamond as spectra are generated from sampling through the entire thickness of the diamond, and consequently sampling of multiple growth layers is inevitable if the diamonds are zoned. Spurious temperature estimates (as indicated by the scatter of temperature data in figure 5.5) associated with rough diamonds are thus not surprising. It follows therefore, that temperature can only be more tightly constrained if samples can be taken from within particular growth layers of the diamond, and it is to *this* end that detailed analyses of diamond plates are warranted (see Section 5.6.2).

5.6.1.6 Implications

It is clear that the different diamond sub-populations, classified empirically on the basis of coloration, can also be distinguished in terms of their characteristic nitrogen contents and aggregation states. Among the Helam diamonds, the development of platelets however, has proven to be a poor discriminant between the sub-populations, other than distinguishing between the canary-yellow diamonds that show an absence in platelet development, and the remainder of the diamond population which show variable platelet development.

Nitrogen concentration and aggregation states within the individual diamonds have been demonstrated to be highly variable, with a general decrease in nitrogen concentration and aggregation state recorded towards the edges of the crystals. This may suggest that the diamonds have grown in an environment that has become progressively depleted in nitrogen with successive diamond growth. This observation will be reviewed and elaborated upon, in the discussion of the IR characteristics of the diamond plates.

The chemical and thermal similarities between the colourless and the brown diamonds, suggest a similar environment of formation. The brown coloration of diamonds is commonly ascribed to graphitisation along the (111) lattice planes as a result of diamond deformation out of the diamond stability field (Urusovskaya & Orlov, 1964). The inclusion of brown diamond within colourless diamond, confirms the spatial relationship between the two sub-populations, and suggests that the crystallisation of the brown diamond preceded that of the colourless crystals. In addition this relationship suggests that a significant deformation event occurred before the crystallisation of the colourless diamonds.

The green diamonds show many similarities with the colourless and brown diamonds, but exhibit relatively higher nitrogen concentrations and aggregation states, suggesting that they may have formed at somewhat elevated mantle temperatures. As was discussed previously, the green coloration is attributed to radiation damage to the surface lattice structure of the crystals after emplacement within the kimberlite. High residence temperatures can not be *directly* related to the green coloration. Perhaps then, the green diamonds present a case that the nitrogen content and/or aggregation state of a diamond, facilitates the development of the lattice disorder associated with radiation. This suggests that diamonds with specific IR characteristics may propitiate the production of vacancies in the diamond lattice.

The canary-yellow diamonds are clearly distinguishable from the other crystals, due to their ubiquitously low nitrogen concentrations, variable aggregation states and absence of platelet development. The difference in physical appearance, together with their characteristics IR and EPR properties (Type Ib diamond) suggests that the canary-yellow diamonds are associated with a separate diamond formation event, and consequently ascribe to a different geological history. It has been demonstrated that while these diamonds appear to have crystallised subsequent to that of the other Helam diamonds, these diamonds must be significantly older than the emplacement age of the Swartruggens Kimberlite. This assertion, does not necessitate unusually hot mantle residence temperatures to explain the aggregation states associated with these diamonds.

5.6.2 Diamond Plates

It is clear from the discussion above, that the nitrogen content and aggregation state of the diamonds, correlate well with the sub-division of the diamond population based

on their physical characteristics. The study of whole, rough diamonds has also demonstrated that significant chemical variability exists within individual diamonds. In an attempt therefore to study such internal chemical variation in more detail, as well as to comment on the processes of diamond growth, deformation and resorption, nine diamond plates have been cut from the larger Helam diamonds. These plates have been analysed using the FTIR spectrometer in traverses across the plates, and the results have been interpreted in association with the CL images of the diamond plates. The IR data, together with calculated time-averaged mantle residence times for the diamond plates are reported in Appendix 3.4. The positions of the analyses are indicated on the CL images (figures 5.11 – 5.21). CL imagery provides a spatial context for interpreting the distributions of nitrogen content, nitrogen aggregation and other defects (e.g.: Bulanova, 1999). Figure 5.9 illustrates the chemical variations observed across the diamond plates with respect to variations in CL imagery.

Colour variations on a CL image are believed to be mainly the result of variations in nitrogen content between different parts of a diamond, and to a lesser extent, to the presence of other trace elements (Davies *et al.*, 1999b). As discussed previously (Chapter 3) the presence of nitrogen commonly results in blue luminescence, bright luminescence corresponding to high nitrogen concentrations. Regions with very low amounts of nitrogen (Type II) correspond to the darker, or non-luminescent regions (e.g.: Daniels *et al.*, 1999; Westerlund, 2000). Yellow and green luminescence, while uncommon, does not appear to reflect substitutional elements, but rather reflect stressed or defect zones with low nitrogen concentrations (Daniels & Gurney, 1999).

It will be demonstrated that the growth layers of the Helam diamonds, are often associated with significant differences in nitrogen concentration and aggregation states. It has been shown (Mendelssohn & Milledge, 1995), that growth layers are commonly inclined to the cut of the diamond plates, rather than normal to it. It follows therefore that, as was the case for the whole diamonds, individual IR measurements from diamond plates may sample more than one type of growth zone. This phenomenon has two important implications which require discussion before the analyses of the diamond plates are considered. Firstly, the existence of multiple growth layers can often suggest a gradual change in nitrogen concentration and/or aggregation state. However because diamond growth is usually episodic

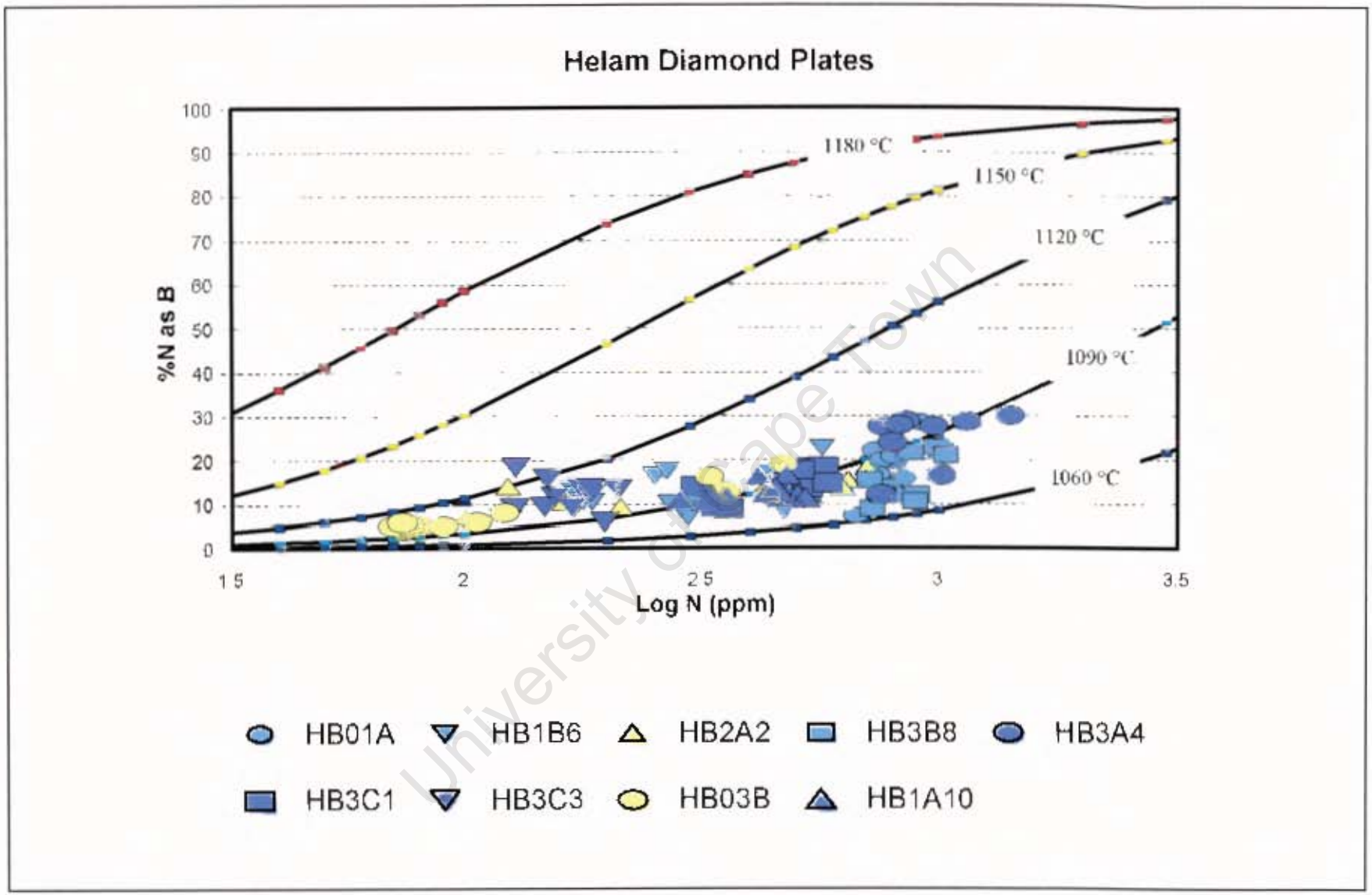

Figure 5.9 Nitrogen concentration versus nitrogen present as B aggregates for the Helam diamond plates. Isotherms have been calculated for a mantle residence time of 2.75 Ga.

(Medelssohn & Milledge, 1995), the changes are more likely to be abrupt rather than gradual. Secondly, the sampling of different growth layers, may result in spurious estimates of residence temperatures, as is illustrated in figure 5.10, and discussed below.

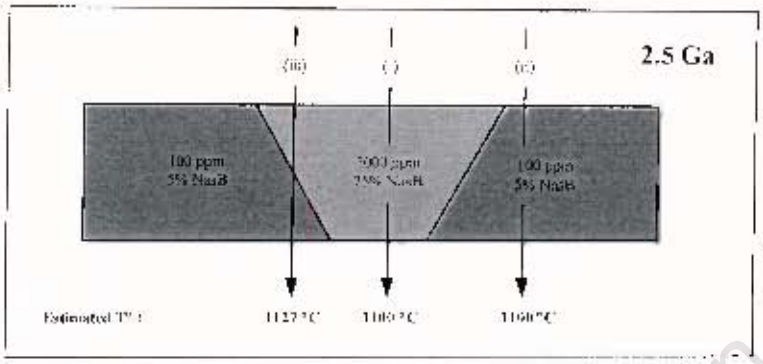

Figure 5.10 A schematic diagram illustrating a hypothetical diamond plate, demonstrating the effect that sampling multiple growth layers of a diamond has on calculated mantle residence temperatures.

Consider a hypothetical case of IR analysis through a diamond plate comprising two distinct growth layers (figure 5.10), that are inclined at some angle to the cut of the plate. The central region (core) contains 1000 ppm nitrogen, 25% of which occurs as B aggregate. Surrounding this, is a diamond layer (overgrowth) with only 100 ppm nitrogen and only 5% nitrogen occurring as B aggregate. Analysis (i) only samples the diamond core, resulting in a measured nitrogen concentration of 1000 ppm, and 25% nitrogen occurring as B aggregate. Assuming a mantle residence time of 2.5 Ga, the calculated residence temperature would be 1100 °C. Analysis (ii) would only sample the overgrowth layer, resulting in a measured 100 ppm nitrogen with 5% occurring as B aggregate. Assuming a 2.5 Ga residence time, this analysis too, would result in a calculated residence temperature of 1100 °C. Both these analyses would therefore result in the '*correct*' estimation of residence temperature for the diamond. Should an analysis sample both diamond layers, as is represented by analysis (iii) which samples 50% of each of the growth layers, the 'apparent' nitrogen concentration would be measured as 550 ppm with 37.5% nitrogen occurring as B aggregate. This analysis would consequently result in an overestimation of the mantle residence temperature (1127 °C) for an assumed mantle residence time of 2.5 Ga.

It is imperative, therefore to consider the effects of multiple diamond layers when interpreting IR data from diamond plates. Below are detailed descriptions of each of the nine diamond plates and their geochemical variations associated with diamond growth. It is important to note, that an assumed mantle residence time of 2.75 Ga (as discussed previously) was used in all calculations of mantle residence temperatures discussed below.

5.6.2.1 Plate HB01A

This plate was cut from a colourless octahedral diamond. The diamond is characterised by an inclusion of an older generation of diamond (Figure 5.11i) which can be seen through the host diamond due to the differential reflection off its surfaces. This diamond inclusion also displays octahedral morphology, the crystal faces sub-parallel to that of the host diamond. The central region of the host diamond is characterised by 'rounded' or hummocky growth zones of Type I diamond, reminiscent of cubic growth. It is interesting to note that the diamond inclusion has been enveloped by these hummocky growth zones, and that they terminate along the peripheral crystal faces of the diamond inclusion. It appears therefore that the diamond inclusion acted as a focus for the crystallisation of the cubic growth zones, and together the diamond inclusion and the cubic growth zones comprise a 'core' around which the more peripheral diamond growth zones crystallised. The enclosing diamond growth layers are characterised by uninterrupted octahedral growth of variably luminescent Type I diamond.

Nitrogen concentration across the plate is restricted between 667 – 909 ppm (figure 5.9), and there appears to be no systematic change in concentration with successive growth (figure 5.11ii). The high and relatively uniform nitrogen concentration across the plate is consistent with the blue luminescence associated with the diamond (insert of figure 5.11i) and lack of colour contrast between the different growth layers. Nitrogen aggregation varies between 7.2 % and 28.4 %N as B (figure 5.9), in accordance with changes in nitrogen concentration (figure 5.11iii), and also displays no systematic variation with successive growth. The subtly variable luminescence across the plate may be attributed to these localised variations in nitrogen concentration and aggregation states.

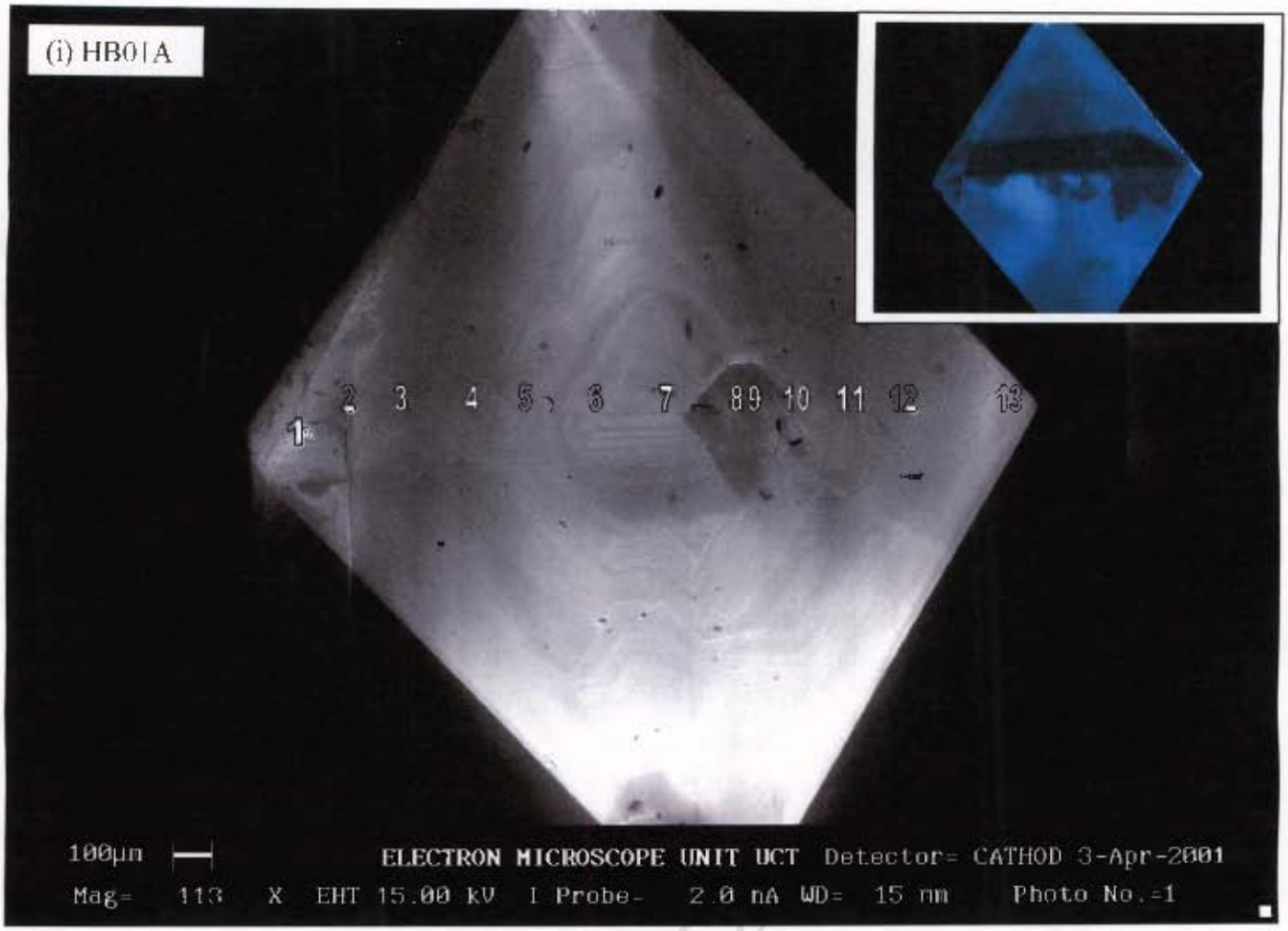

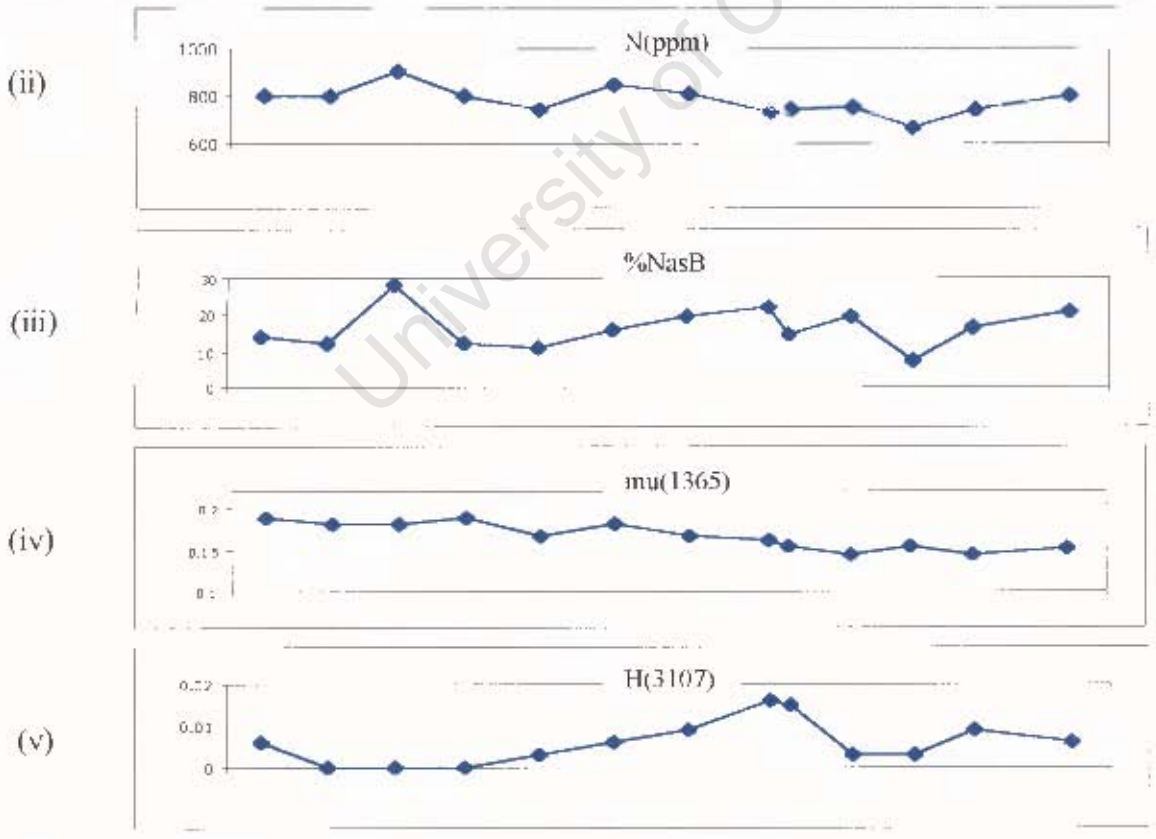

Figure 5.11 (i) CL photomicrograph of HB01A (optical CL insert) The variation in nitrogen concentration (N ppm), the percent of nitrogen occurring as B aggregate (%N as B), platelet peak intensity (mu (1365)) and hydrogen peak intensity (H(3107)) across the plate are illustrated in (ii) – (v) respectively.

Platelet peak intensities [mu(1365)] vary between 0.145 and 0.187 across the plate (figure 5.11iv), however there is no correlation between platelet peak development and the amount of nitrogen aggregation. Perhaps the most striking chemical variation within the plate is that of the hydrogen peak [H(3107)] intensity (figure 5.11v). While ubiquitously low, there appears to be a gradual increase in hydrogen from the periphery to the core. Analysis of the diamond inclusion shows the highest hydrogen peak intensities (up to 0.016), suggesting that the diamond inclusion grew in an environment, somewhat more enriched in hydrogen than the enclosing diamond. The decrease in hydrogen peak intensity from this inclusion towards the rim of diamond host suggests that the diamond host grew in an environment in which the concentration of hydrogen was systematically decreasing. Alternatively, the decrease in hydrogen content may be attributed to a decrease in K_d(diamond/fluid) of hydrogen with successive growth zonation.

Calculated temperatures range from 1067°C to 1098°C, defining a broad isothermal region in figure 5.9. The calculated temperatures from the diamond inclusion do not vary considerably from the remainder of the plate, suggesting that the inclusion, cubic and enclosing octahedral diamond grew within a similar isothermal environment, characterised by a decreasing hydrogen and variable nitrogen content. The sharp boundaries between the diamond inclusion, and the cubic and octahedral growth zones, suggest hiatus in growth and provide evidence for episodic diamond crystallisation associated with this diamond. While nitrogen concentration appears to have remained relatively stable over time, the hiatus in growth between the diamond inclusion and the enclosing diamond, appears to have recorded a significant decrease in hydrogen concentration of the environment in which the diamond grew.

5.6.2.2 Plate HB3C1

This plate was cut from a colourless tetrahexahedroid. The diamond contains two sulphide inclusions near its centre, as can be seen in the optical CL insert in figure 5.12i. These sulphide inclusions are also illustrated in figures 4.22. This diamond does *not* appear to contain a structurally different 'core' and is comprised entirely of uninterrupted octahedral growth zones of varyingly luminescent Type I diamond (figure 5.12i). These octahedral growth zones have been cut by the six

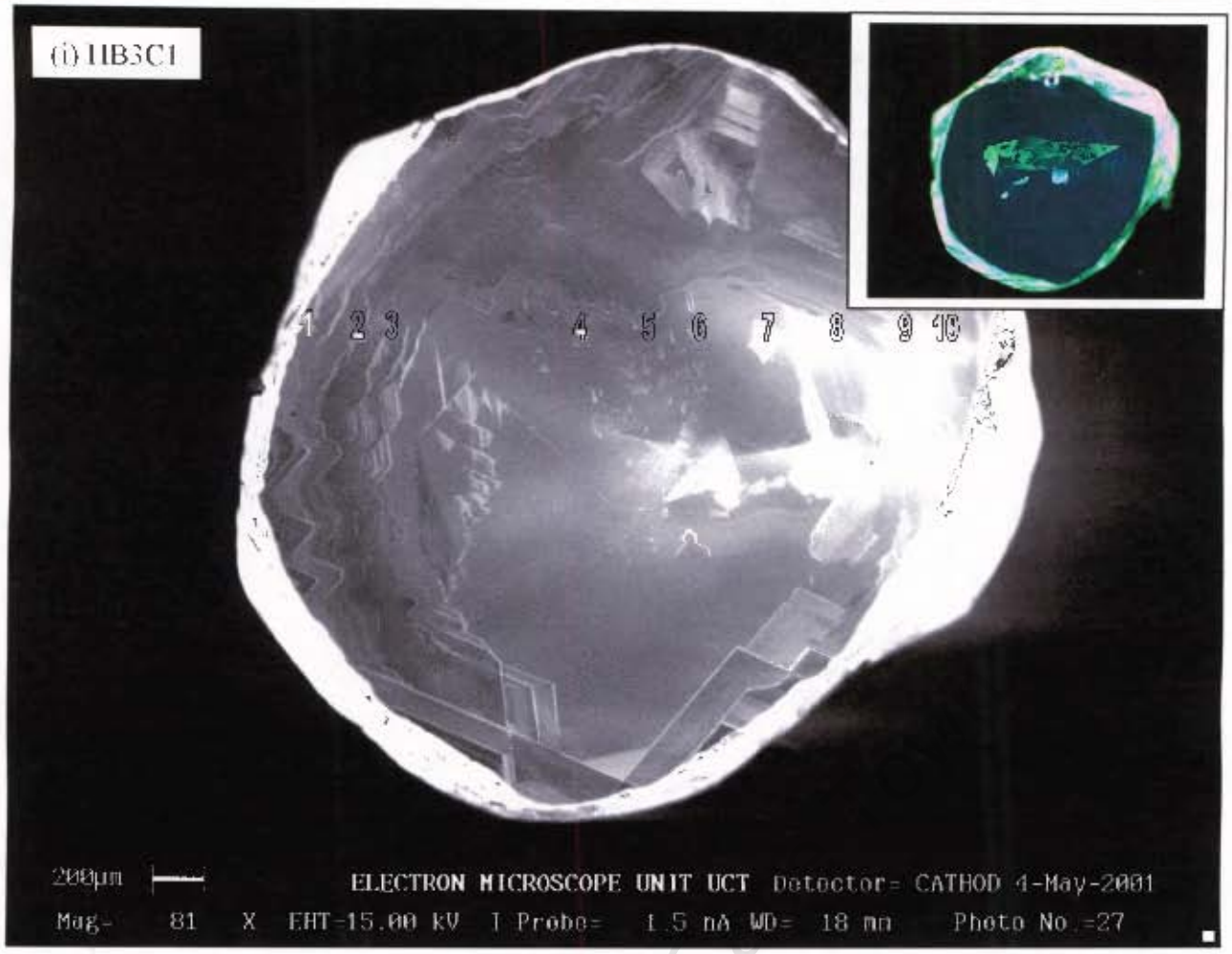

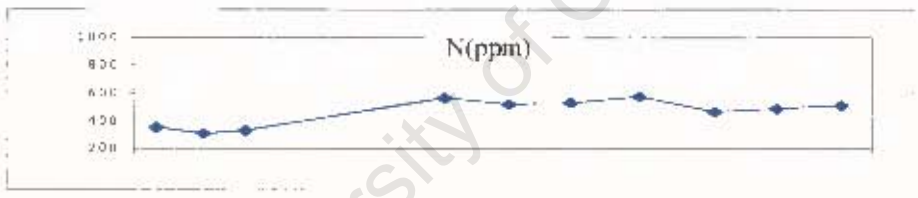

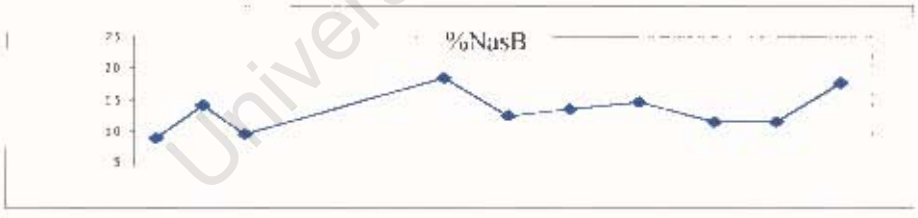

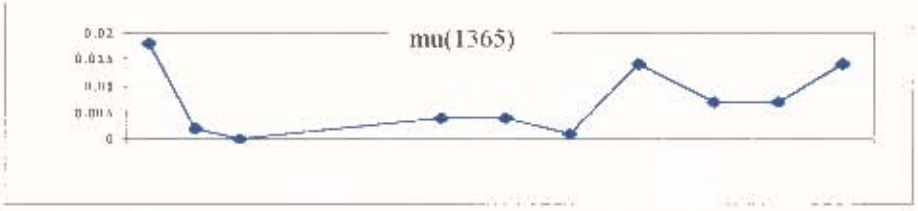

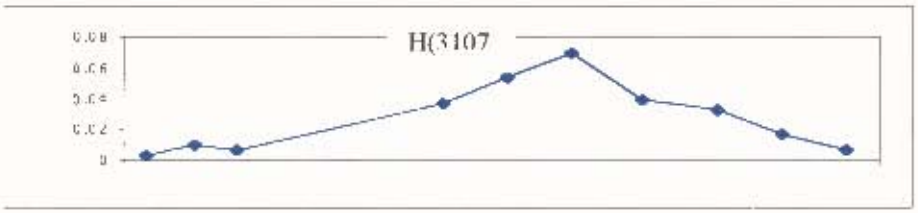

Figure 5.12 (i) CL photomicrograph of HB3C1 (optical CL insert) The variation in nitrogen concentration (N ppm), the percent of nitrogen occurring as B aggregate (%N as B), platelet peak intensity (mu (1365)) and hydrogen peak intensity (H(3107)) across the plate are illustrated in (ii) – (v) respectively.

tetrahexahedroidal faces (which can broadly be made out) at the surface of the diamond. This is clearly a result of extensive resorption of an octahedral diamond, and is useful in illustrating that the tetrahexahedroidal form of diamond is indeed a result of resorption of an octahedral growth form as was demonstrated by Seal (1965) and Moore & Lang, (1974). While no lamination lines can be observed, strain structures (left, centre) not unlike those identified by Davies *et al.* (1999) within Australian diamonds, *do* appear to suggest some limited influence of deformation.

The nitrogen concentration across the plate is relatively low and varies between 307 - 580 ppm (figure 5.9), with the higher concentrations of nitrogen occurring towards the centre of the diamond (figures 5.12ii). The low nitrogen concentration of the diamond together with evidence of deformation, may explain the yellow-green luminescence of the diamond plate (insert of figure 5.12i). Nitrogen aggregation varies between 8.8 and 18.3 %N as B (figure 5.9), which appears to be higher towards the central regions of the plate (figure 5.12iii) in accordance with the higher nitrogen concentrations. These observations are consistent with those made from the whole, rough diamonds (Section 5.6.1).

Conversely, platelet peak [mu(1365)] intensity appears to decrease towards the centre of the plate (figure 5.12iv), from as high as 0.018 at the rim to 0 near the centre, suggesting a negative correlation between nitrogen aggregation and platelet peak development. This observation attests to catastrophic degradation of platelets as a result of the deformation associated with the more central regions of the diamond plate. As a result, this diamond can be termed 'irregular' according to the classification of Woods (1986). Hydrogen appears to be concentrated in the central regions of the plate (figure 5.12v), with peak intensities [H(3107)] of 0.054 near the centre. As in HB01A, therefore, this diamond attests to an initial period of elevated nitrogen and hydrogen concentrations, which have become systematically depleted with successive diamond growth.

Calculated temperatures for the plate show a restricted range (between 1086°C - 1102°C), defining a narrow isothermal region in figure 5.9. Slightly elevated temperatures are associated with the peripheral regions of the diamond. This can be explained by the sampling of multiple layers of diamond, which are *more* apparent towards the periphery of the diamond plate. The estimated temperatures from the peripheral diamond are therefore assumed to be slight overestimates of mantle

residence temperatures. Those temperatures corresponding to the central regions may yield more accurate estimates based on the observations of chemical homogeneity associated with the centre of the diamond. However the range in temperature remains well within error of the technique, and as such is not considered to be significant.

5.6.2.3 Plate HB1A10

This plate was cut from a partially resorbed colourless octahedron. As in plate HB3C1, this plate is primarily characterised by uninterrupted octahedral growth of varyingly luminescent Type I diamond (figure 5.13i). Partial resorption of the diamond has resulted in some of these octahedral growth zones being 'cross-cut' in places (bottom left). Two small colourless inclusions (most likely olivine) reside near the centre of the diamond (insert of figure 5.13i), however these could not be analysed, due to their small size. Unlike plate HB3C1 this diamond is characterised by pervasive lamination lines, which display a brighter luminescence, and attest to a period of deformation. Scotch-plaid lamination lines, visible within the vicinity of analyses 11 and 12 are suggestive of extensive deformation incurred by the diamond.

Chemical variation within the stone is very similar to that of plate HB3C1. Nitrogen concentrations vary between 284 - 522 ppm (figures 5.9 and 5.13ii), while nitrogen aggregation spans a range between 9.2 16.5 %N as B (figures 5.9 and 5.13iii). Both nitrogen concentration and aggregation state appear to increase towards the centre of the diamond. A significant difference in the concentration of nitrogen has been recorded across the boundary between the lightly luminescent central growth zones, and the darker luminescent peripheral zones. Significantly higher hydrogen peak [H(3107)] intensities (figure 5.13v) can also be observed towards the centre of the crystal. It appears therefore that this plate grew in a mantle environment in which nitrogen and hydrogen have become progressively depleted over time.

The absence of platelet peak [mu(1365)] data over much of this plate may be attributed to the observed deformation (i.e.: catastrophic degradation of platelets). The effects of deformation together with the relatively low nitrogen concentration across the diamond plate may also explain the yellow-green luminescence (insert of figure 5.13i) associated with the diamond.

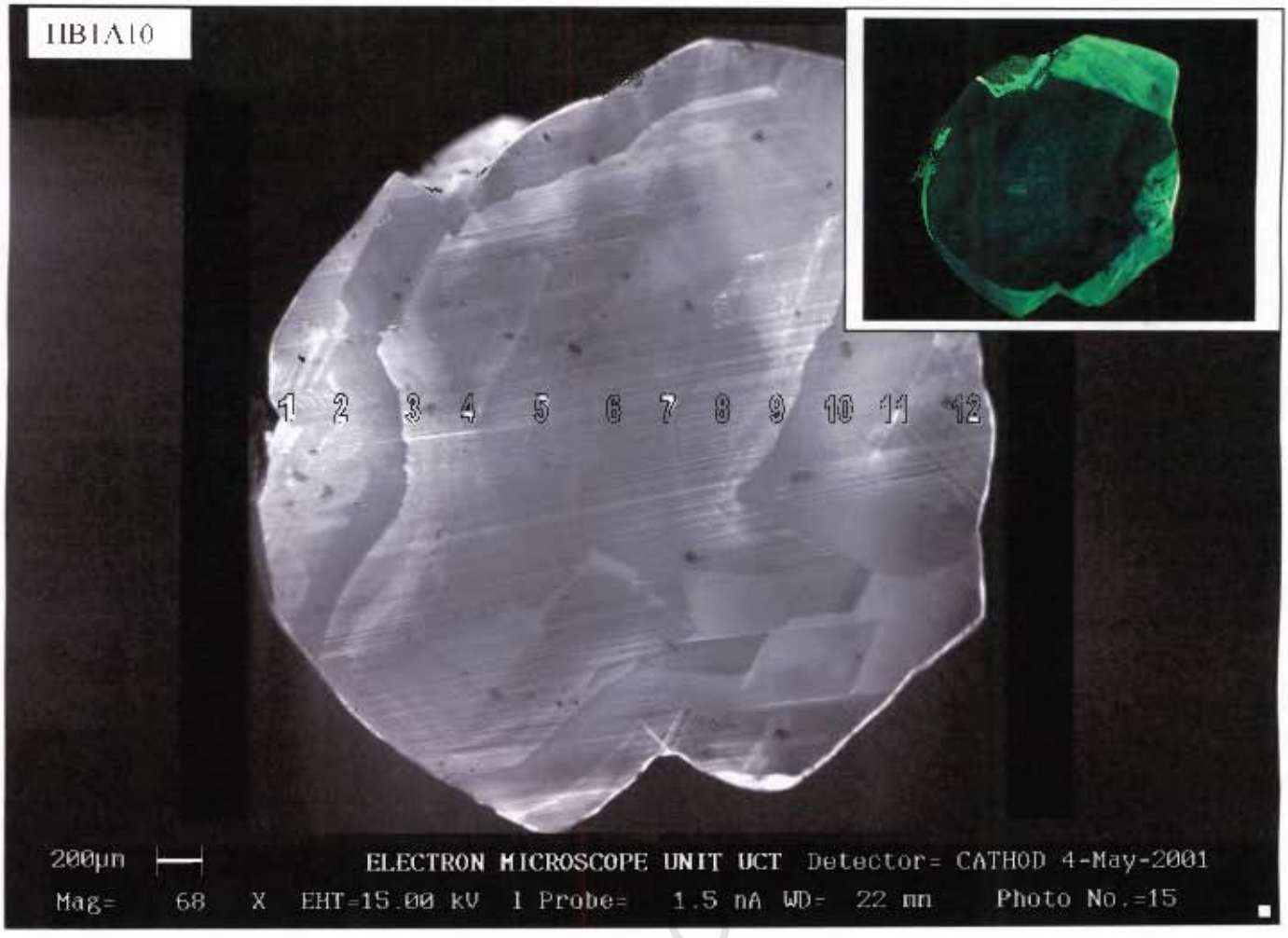

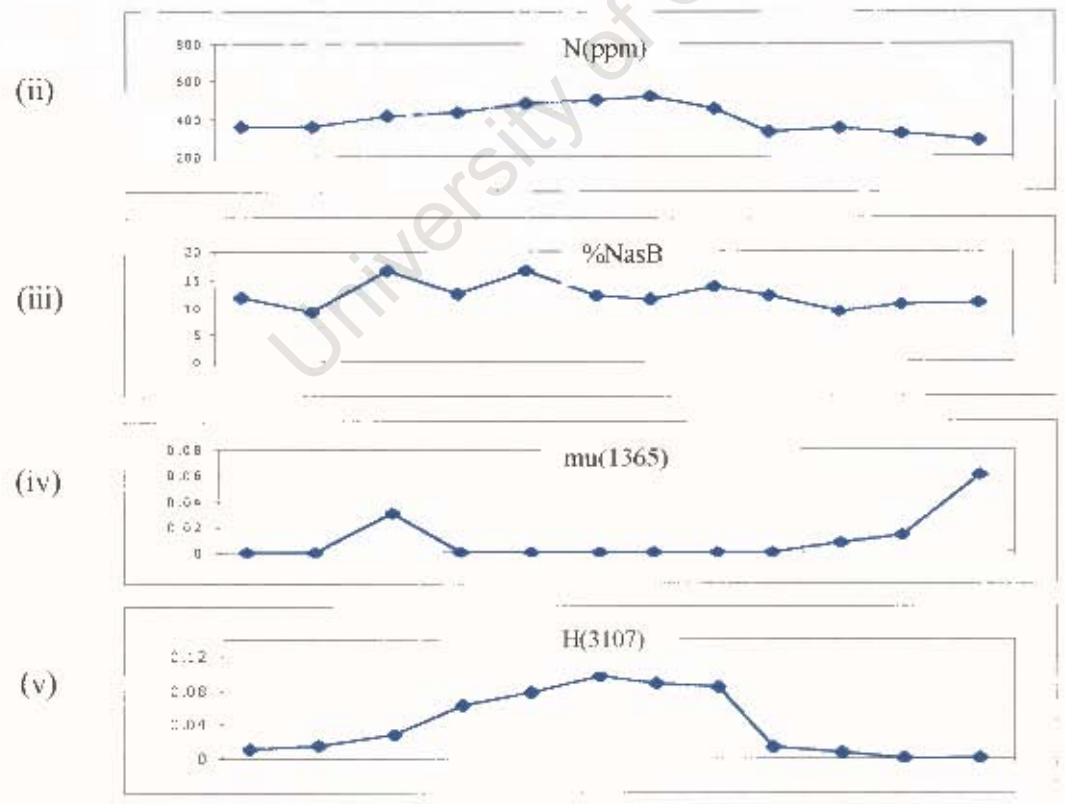

Figure 5.13 (i) CL photomicrograph of HB1A10 (optical CL insert) The variation in nitrogen concentration (N ppm), the percent of nitrogen occurring as B aggregate (%N as B), platelet peak intensity (mu (1365)) and hydrogen peak intensity (H(3107)) across the plate are illustrated in (ii) – (v) respectively

Estimated mantle residence temperatures vary from 1087°C to 1100°C, defining a restricted isothermal range in figure 5.9.

5.6.2.4 Plate HB3C3

This plate was cut from a large, colourless tetrahexahedroidal diamond with numerous chromite inclusions (see Chapter 6 for analyses) and an inclusion of diamond (insert of figure 5.14i). The diamond can consequently be associated with a peridotitic paragenesis (see Section 6.4.2.1). Figure 5.14i shows that this peridotitic diamond is characterised by a central 'core' of variably luminescent Type I diamond, displaying hummocky, cubic growth. This 'core' is surrounded by Type I diamond of low luminescence, and it is only within these growth zones, that the chromite inclusions reside. The diamond is further characterised by scotch-plaid deformation lines of bright luminescence. These deformation lines are so intense, that they mask much of the growth zoning within the diamond.

Nitrogen concentrations are ubiquitously low across the plate, varying between 127 – 210 ppm (figure 5.9), the lowest concentrations occurring towards the periphery of the diamond (figure 5.11ii). Nitrogen aggregation varies between 5.9 and 18.3 %N as B (figure 5.9), becoming systematically higher towards the rims (figure 5.14iii). The 'core' appears to be associated with relatively lower nitrogen concentration and aggregation state in comparison to the enclosing diamond. The low nitrogen concentration, together with the extensive deformation, may account for the green luminescence (insert of figure 5.14i) displayed by this diamond. While there appears to be no systematic variation of the platelet peak [mu(1365)] across the diamond (figure 5.14iv), the hydrogen peak [H(3107)] intensity increases from 0 at the rim to 0.02 near the centre (figure 5.14v). There does not appear to be a relationship between the hydrogen peak intensity and platelet peak intensity. It is suggested that the lack of such a relationship, together with non-systematic platelet peak evolution, is a result of the deformation incurred by the diamond.

Estimated temperatures range between 1090°C and 1130°C, defining a broad isothermal envelope in figure 5.9. The estimated temperatures appear to be higher towards the periphery of the diamond, suggesting that these temperatures are overestimates as a result of the sampling of multiple growth layers within the

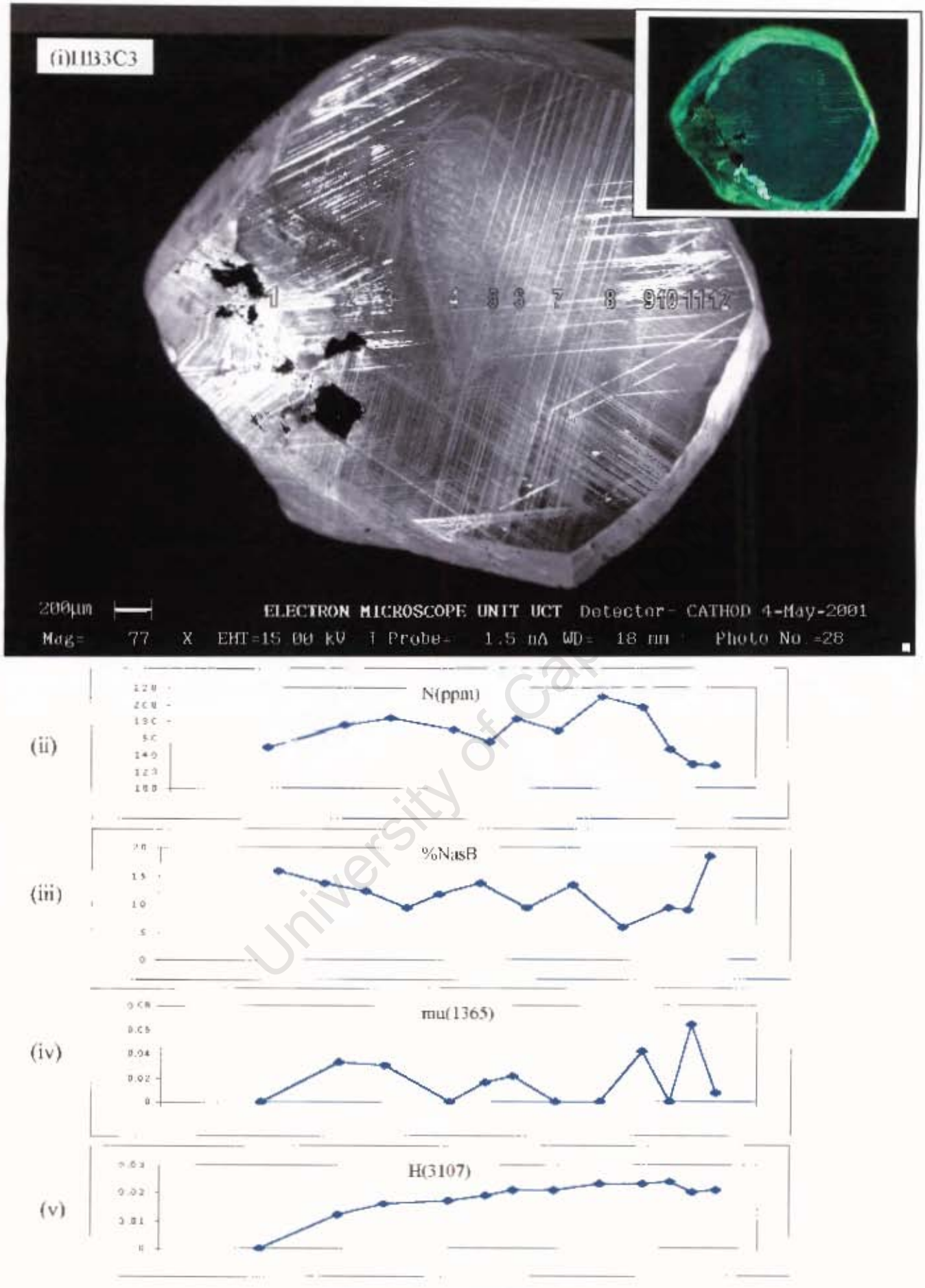

Figure 5.14 (i) CL photomicrograph of IIB3C3 (optical CL insert). The variation in nitrogen concentration (N ppm), the percent of nitrogen occurring as B aggregate (%N as B), platelet peak intensity (mu (1365)) and hydrogen peak intensity (H(3107)) across the plate are illustrated in (ii) (v) respectively.

diamond. The temperatures calculated from the more central regions of the diamond plate are therefore believed to be more accurate.

5.6.2.5 Plate 1IB3B8

This plate was cut from a colourless tetrahexahedroid. The diamond plate is characterised by a dark luminescent core of Type I diamond displaying hummocky or cubic growth zonation (figure 5.15i), and characterised by the presence of multiple, unidentifiable inclusions (insert of figure 5.15i). This 'core' has been overgrown by brighter luminescent growth zones of Type I diamond, displaying growth more akin to octahedral zonation. The lack of numerous variably luminescent growth zones, attests to extended crystallisation in environments of consistent chemical composition. Nevertheless the boundary between the inner 'core' and peripheral octahedral diamond displays significant chemical differences (figures 5.15ii-v), suggesting a hiatus in growth during which significant chemical change occurred.

Nitrogen concentrations are relatively high and vary considerably across the diamond (715 – 1035 ppm), the lowest concentrations associated with the dark luminescent 'core' (figure 5.15ii). The high nitrogen concentrations and absence of deformation may explain the more characteristic blue luminescence associated with the diamond (insert of figure 5.15i). Nitrogen aggregation too, shows considerable variation (8.8 - 22.9 %N as *B*), with the lowest values corresponding to the 'core' (figure 5.15iii) in accordance with the changes in nitrogen concentration. Likewise, there exists a good correlation between nitrogen aggregation and platelet peak [mu(1365)] evolution, higher platelet intensities recorded towards the periphery of the diamond. Conversely hydrogen [H(3107)] appears to be systematically concentrated towards the centre of the diamond (figure 5.15v), with peak intensities of 0.16 being recorded in the core.

Estimated temperatures exhibit a restricted range between 1070°C to 1090°C (figure 5.9), with slightly higher temperatures being estimated from the analyses near the periphery of the diamond. The reverse side of the diamond plate, exhibits only octahedral growth layers, suggesting that analyses through the centre of the diamond plate, will result in a mixed sample from both the core and the enclosing octahedral diamond. In this case therefore, the estimated temperatures from the centre of the

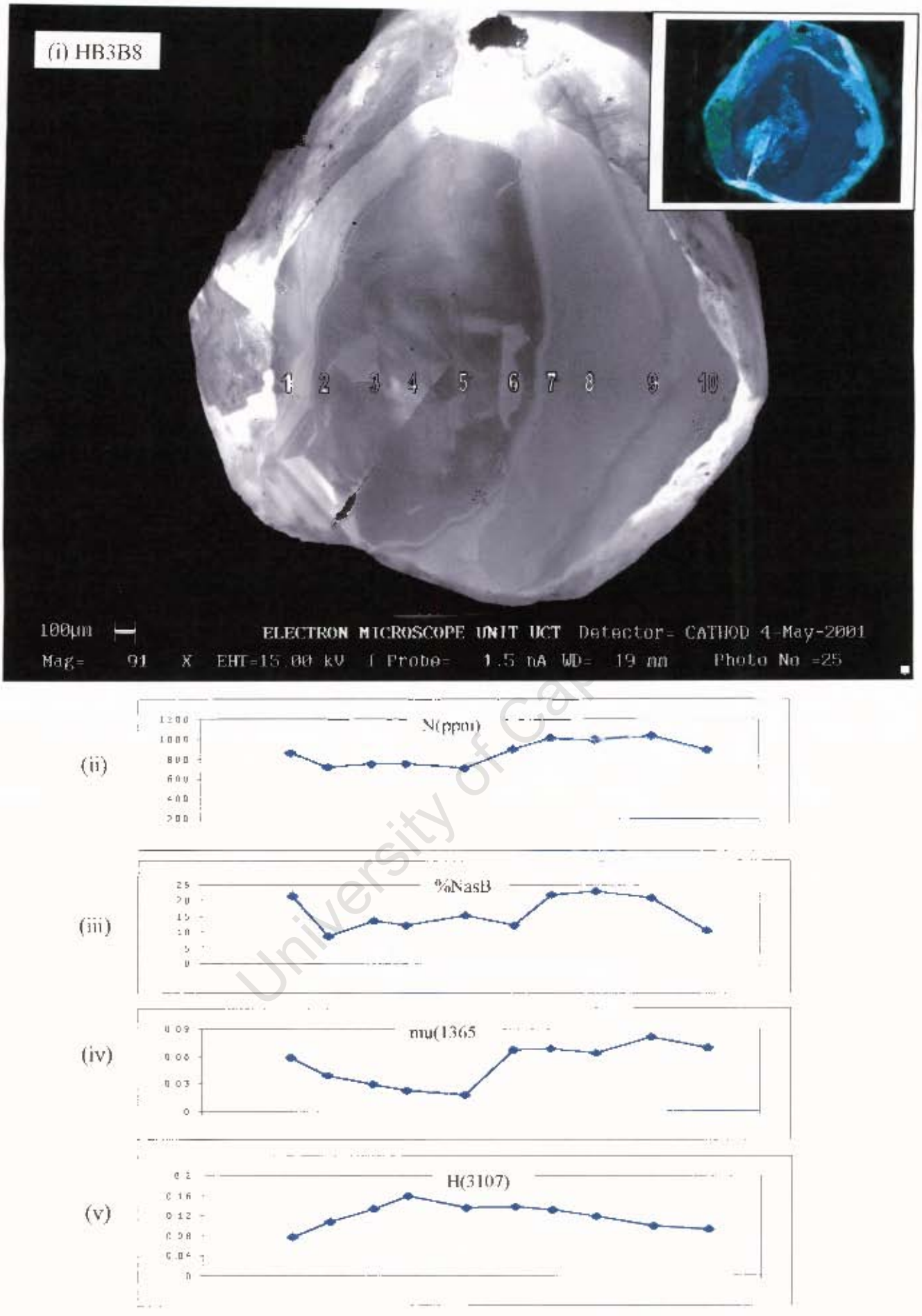

Figure 5.15 (i) CL photomicrograph of HB3B8 (optical CL insert). The variation in nitrogen concentration (N ppm), the percent of nitrogen occurring as B aggregate (%N as B), platelet peak intensity (mu (1365)) and hydrogen peak intensity (H(3107)) across the plate are illustrated in (ii) – (v) respectively.

diamond plate are believed to be underestimates of temperature, as a result of the sampling of the nitrogen rich octahedral layers in addition to the low nitrogen core. Despite this mixed sampling effect on temperature estimates, it can still be demonstrated that the contact between the 'core' and the octahedral diamond layers represents a hiatus, across which significant changes in the crystallisation environment has occurred.

5.6.2.6 Plate HB3A4

This diamond plate was cut from a colourless tetrahexahedroid. The diamond plate is characterised by a growth zonation texture that has not been documented before (figure 5.16i). The diamond appears to comprise several dark luminescent cores of Type I diamond displaying typical octahedral growth geometries. Within these 'cores' octahedral zonation of varyingly luminescent octahedral growth layers are easily discernible. These 'cores' are characterised by brightly luminescent linear features, that terminate at the boundary between the octahedral growth, and the more complex growth associated with the enclosing diamond. These linear features resemble lamination lines observed in many of the other plates, but exhibit some important differences. They are widely spaced (up to 200 μm apart), and, more importantly they lie parallel to some of the octahedral surfaces, suggesting that they are in fact features related to octahedral growth rather than to deformation. The blue luminescence of this diamond (insert of figure 5.16i) adds support to this theory, as the diamonds displaying more typical deformation lines are all associated with a yellow-green luminescence (which has been associated with deformation). If these features were indeed lamination lines then it would be necessary to explain how *only* these inner 'cores' were deformed. It could be argued that they were deformed by an event that preceded the crystallisation of the enclosing diamond, however this is unlikely as these features would be expected to have annealed after such a time. It is more reasonable to assume therefore that these linear features represent octahedral growth features.

Surrounding these 'cores' is a thin (<50μm) layer of non-luminescent diamond. While there are no analyses that may confirm its nature, it is suggested that these layers represent Type II diamond, which characteristically displays no

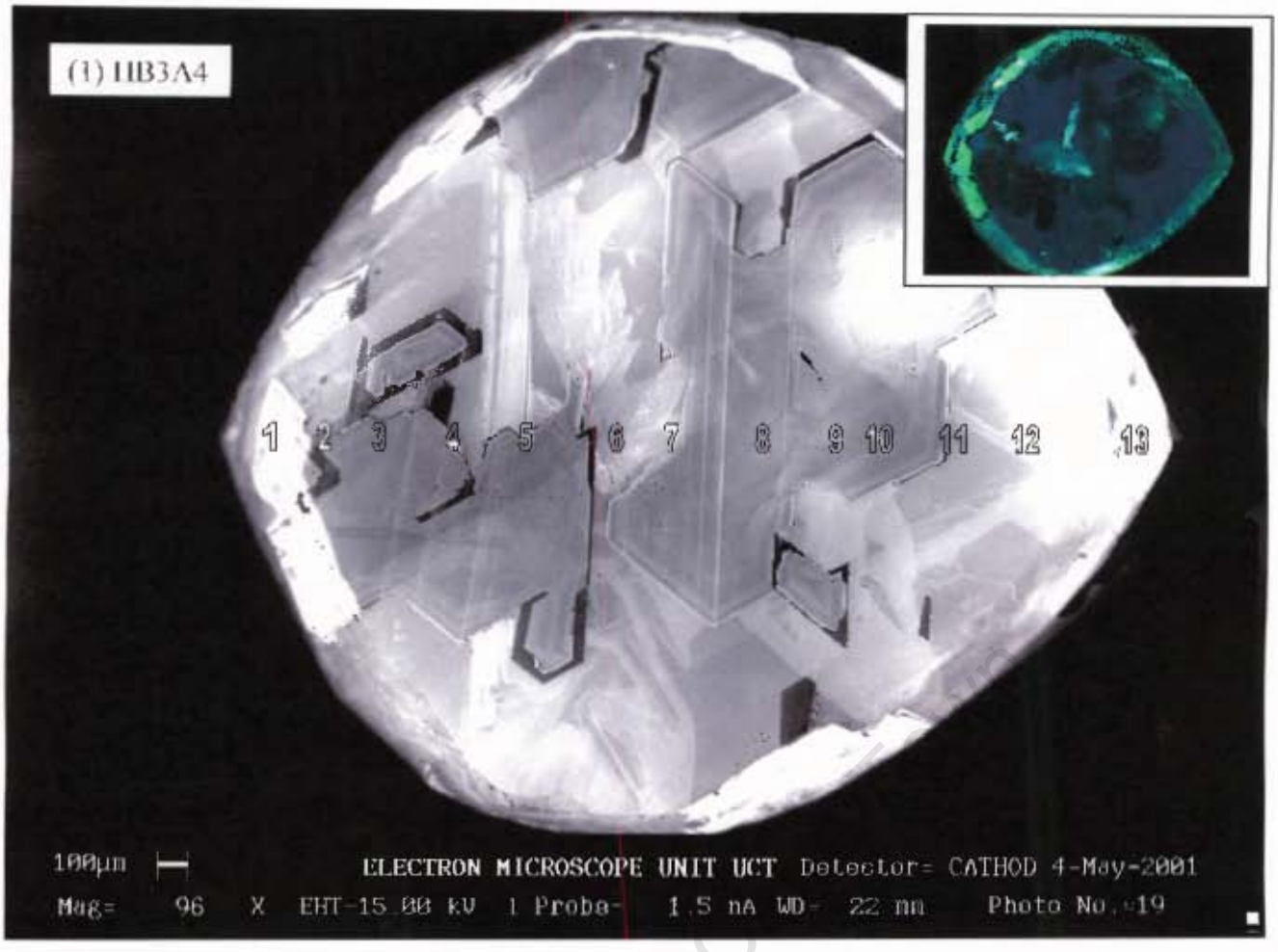

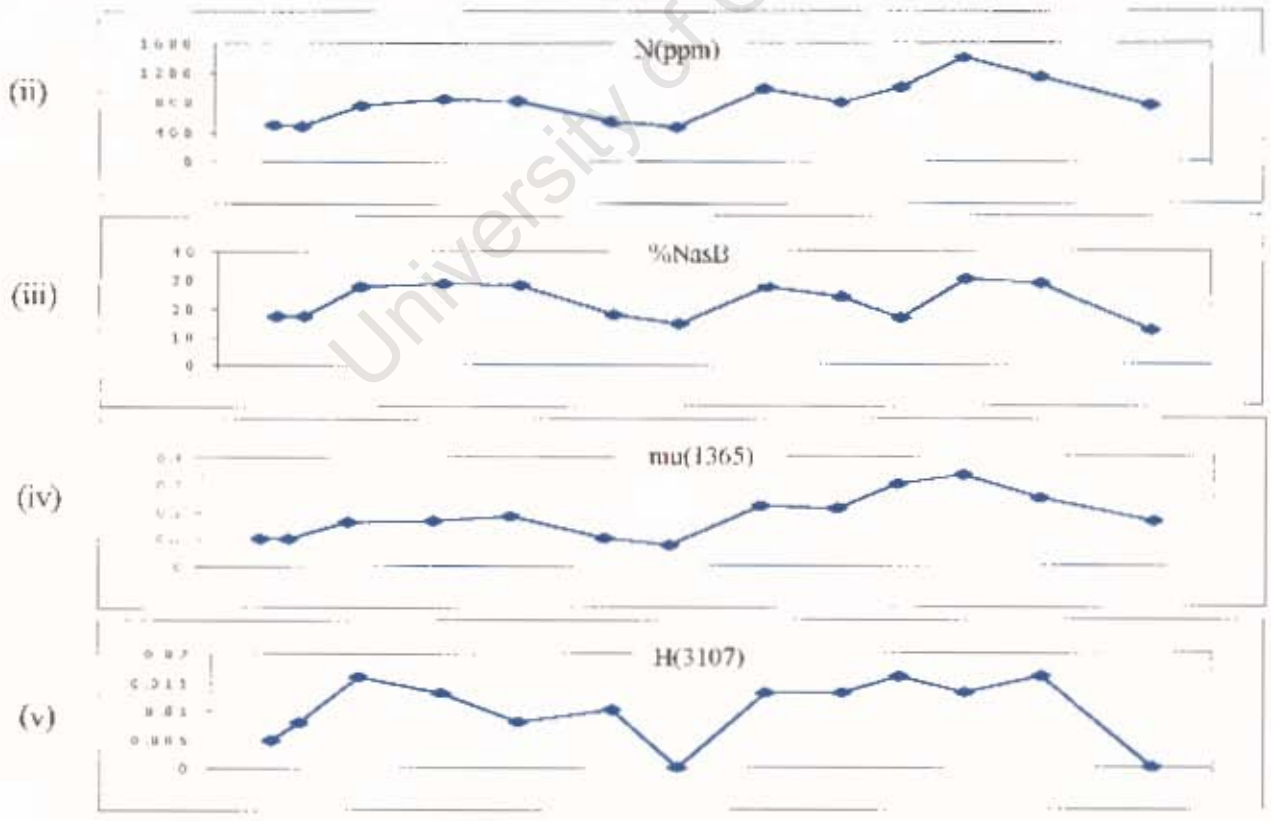

Figure 5.16 (i) CL photomicrograph of HB3A4 (optical CL insert). The variation in nitrogen concentration (N ppm), the percent of nitrogen occurring as B aggregate (%N as B), platelet peak intensity (mu (1365)) and hydrogen peak intensity (H(3107)) across the plate are illustrated in (ii) – (v) respectively.

luminescence due to absence of nitrogen (e.g.: Davies *et al.*, 1999; Westerlund, 2000). This 'Type II' diamond can also be observed to occur along dissolution boundaries (figure 5.17), as has been documented by Bulanova *et al.*, (1999) and Davies *et al.*, (1999) in Siberian and Australian diamonds respectively. This phenomenon, therefore appears to be fairly common, and is certainly not restricted to mantle changes beneath the Swartruggens Kimberlite.

Surrounding these 'cores' diamond growth appears to be far more complex, characterised by highly variable luminescence (and by inference, highly variable nitrogen characteristics), with no obvious geometrical character. It is suggested that this diamond is the result of continually changing growth rates, with variable nitrogen concentrations and aggregation states. Clearly this unstable chemical environment was very different to that in which the octahedral diamond 'cores' crystallised. Figure 5.17 shows that there is evidence for partial resorption of these inner cores. Such resorption must have occurred during a hiatus preceding the crystallisation of the Type II diamond, as this non-luminescent form of diamond occurs along such resorption features rather than having been resorbed as well.

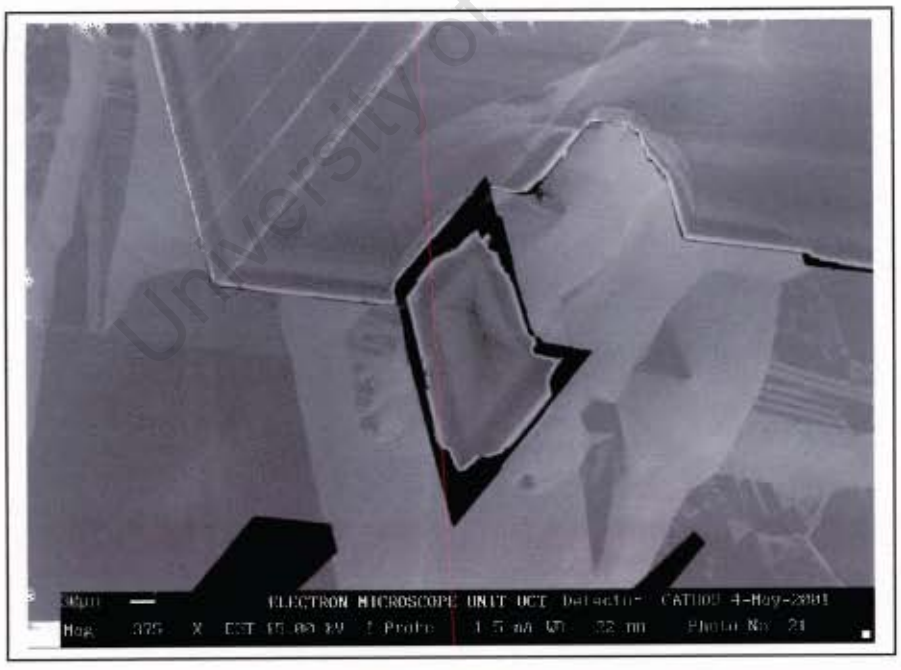

Figure 5.17 High magnification CL photomicrograph of HB3A4, illustrating the growth zonation associated with the diamond 'cores' as well as a sinuous resorption feature (top right) associated with the larger 'core'. The linear octahedral growth features can also be observed as well as the layer of rare Type II diamond (non-luminescent) that surrounds such 'cores'.

Such changes are reflected in the chemical variability across the diamond plate. Nitrogen concentration varies considerably, with values between 452 - 1403 ppm (figure 5.16ii) being measured. If the assumption that the non-luminescent diamond represents Type II diamond is correct, then the actual variability in nitrogen is in fact much greater (between 0 – 1403 ppm) than the measured variability. Nevertheless it is demonstrated that the 'cores' are associated with significantly higher nitrogen concentrations than the enclosing diamond. There is a clear positive correlation between nitrogen concentration and nitrogen aggregation, with the highest degrees of aggregation being associated with the 'cores' (figure 5.16iii). Likewise, platelet and hydrogen peaks appear to be more developed within the 'cores' (figures 5.16iv and 5.16v respectively).

Despite the chemical variability within this diamond, there is surprisingly little apparent temperature variation (figure 5.9) across the diamond (between 1078 °C - 1101 °C). Estimated mantle residence temperatures from measurements taken from the 'cores' and the enclosing diamonds are remarkably similar. Only three analyses resulted in temperature estimates of less than 1090 °C, and it is suggested that these analyses represent underestimates as a result of mixed sampling of both the core and enclosing diamond growth zones. The striking similarities of estimated mantle residence temperatures between the different growth zones suggest, that while a hiatus in crystallisation certainly did occur, the hiatus does not represent a significant time period. Had the hiatus represented significant periods of geological time (billions of years) between diamond crystallisation, the assumed 2.75 Ga residence time for the entire diamond would have resulted in the enclosing diamond recording *gross* underestimates of mantle residence temperatures.

From the above observations it becomes clear that the 'cores' crystallised within a stable chemical environment associated with high nitrogen and hydrogen concentrations. This was followed by a brief period of crystallisation within an environment associated with a complete absence of nitrogen (Type II diamond). After some 'brief' hiatus the enclosing diamond crystallised, incorporating the older 'cores', in a chemically unstable environment associated with significantly lower nitrogen and hydrogen concentrations.

5.6.2.7 Plate HB1B6

This plate was cut from a colourless octahedral diamond, characterised by a low-luminescent 'core' displaying octahedral geometry of Type I diamond (figure 5.18i). This 'core', is characterised by highly-luminescent linear features, which as in the case of Plate HB3A4, it can be argued as to whether these represent octahedral growth features, or deformation lines. Once more it is suggested that these represent growth features for the reasons discussed above. This 'core' is surrounded by alternating layers of non-luminescent 'Type II' diamond and brightly luminescent Type I diamond octahedral growth Zones.

Nitrogen concentration varies considerably across the diamond, with measured concentrations of between 168 – 571 ppm (figures 5.9 and 5.18ii). It is clear that had the non-luminescent Type II diamond been analysed, the measured nitrogen variability would have been much greater (between 0 – 571 ppm). Nevertheless, lower nitrogen concentrations appear to be associated with the 'core' (figure 5.18ii). A difference of up to 400 ppm is recorded across the boundary between this core and the peripheral diamond. Nitrogen aggregation varies between 6.8 and 22.6 %N as B, with the lowest values generally corresponding to the 'core' (figure 5.18iii). Platelet [mu(1365)] and hydrogen [H(3107)] peaks are ubiquitously under-developed, and consequently little can be said of their relationship to one another or to nitrogen concentration, other than that there appears to be a small increase in platelet and hydrogen peak development within the core.

Estimated temperatures vary between 1079°C and 1114°C defining a broad isothermal envelope in figure 5.9, with the peripheral diamond associated with significantly lower temperature estimates than the 'core'. This phenomenon can be explained by the core having crystallised within a somewhat hotter mantle environment than did the younger diamond growth zones. Alternatively the core may represent a *significantly* older generation of diamond. If the high-nitrogen overgrowth diamond did indeed crystallise significantly later than the core, then an assumed mantle residence time of 2.75 Ga for the entire diamond (i.e.: an overestimate of age for the younger diamond), would result in underestimates of mantle residence temperature for the significantly younger generation of diamond.

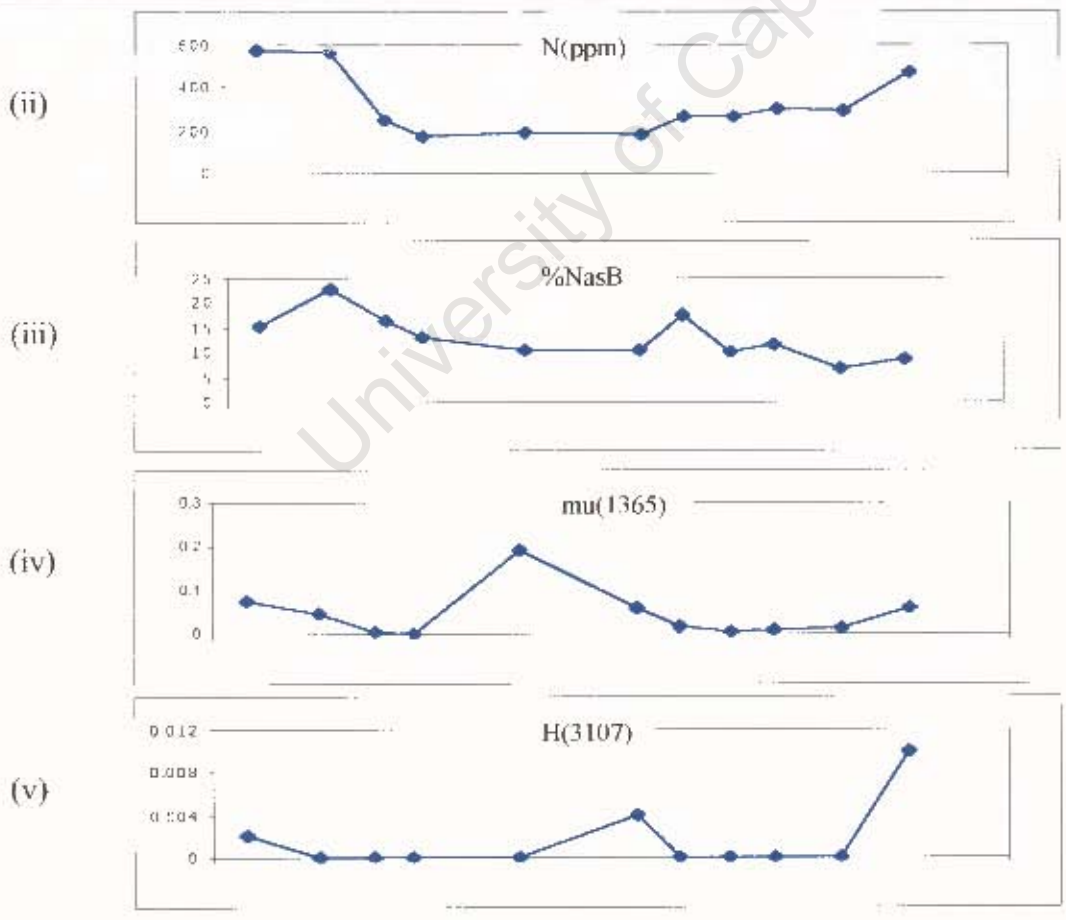

Figure 5.18 (i) CL photomicrograph of HB1B6 (optical CL insert). The variation in nitrogen concentration (N ppm), the percent of nitrogen occurring as B aggregate (%N as B), platelet peak intensity (mu (1365)) and hydrogen peak intensity (H(3107)) across the plate are illustrated in (ii) – (v) respectively.

The latter explanation is favoured by the author, as a hotter crystallisation environment during growth of the core should have been associated with marked difference in the aggregation state of the core. The absence of this therefore suggests that the diamond plate represents a significantly older core of diamond, that crystallised in an environment enriched in hydrogen and relatively depleted in nitrogen. After some *prolonged* hiatus, a second crystallisation event occurred in an environment enriched in nitrogen and depleted in hydrogen.

5.6.2.8 Plate HB2A2

This plate was cut from a most unusual diamond. This diamond exhibits subtle yellow colour, unlike the darker yellow (canary) associated with most of the more common canary-yellow diamonds from Helam. As a result this diamond is believed to represent the small population of 'Cape' diamonds, the yellow coloration being imparted by so-called 'optical N3-centers'. The plate (figure 5.19i) is characterised by mixed-habit, sector growth. The diamond shows complete preservation of the sector growth structures in the two-dimensional plane. Frank (1967) explained that such growth results from epochs of mixed-habit growth in which normal growth on flat octahedral facets is accompanied by non-faceted growth on cubic surfaces approximated to {100}. Figure 5.20 represents a highly simplified model of this structure.

Growth sectoral dependence of unpaired nitrogen defect concentration in synthetic diamonds has been demonstrated (e.g.: Woods & Lang, 1975; Frank *et al.*, 1990). It can commonly be observed that the {111} growth sectors incorporate the highest concentrations of substitutional nitrogen, followed by {113} and {110} sectors, whereas the {100} growth sectors contain highly variable nitrogen contents.

Points 1-13 in figure 5.19i traverse two octahedral growth sectors {111} as well as the central cubic growth sector (001). Linear octahedral growth features can be observed within the octahedral growth sectors, while the central cubic growth sector is characterised by hummocky growth zonation. Points 14-17 in figure 5.19i traverse two cubic growth sectors {100} in order to document any sectoral dependence of nitrogen aggregation within this diamond.

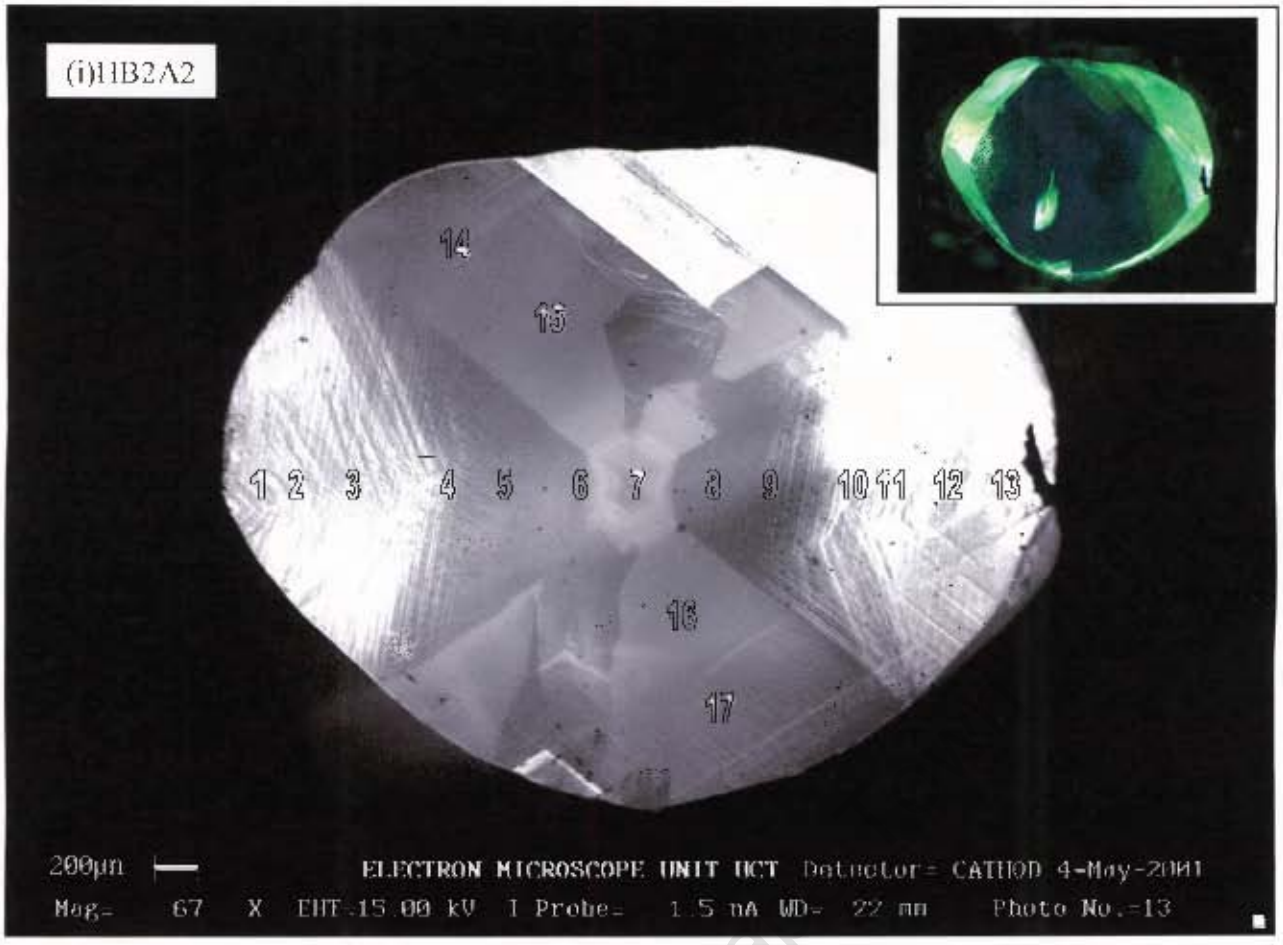

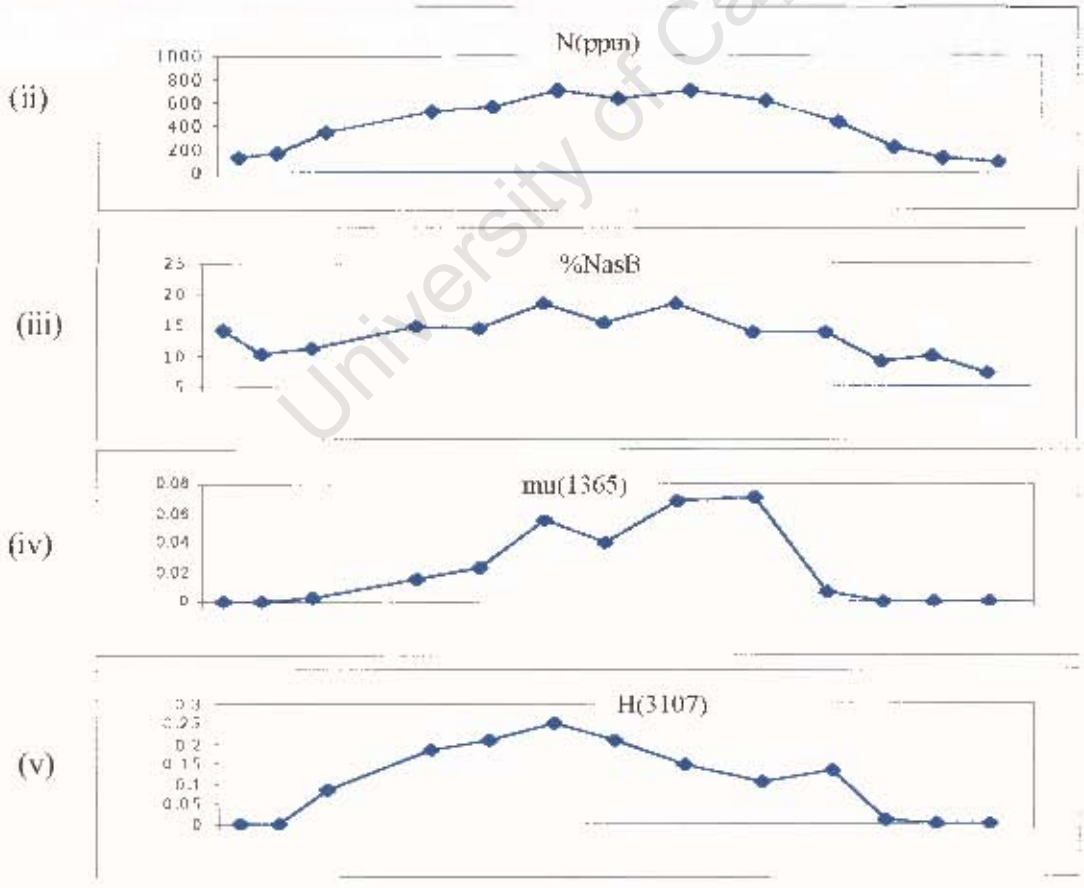

Figure 5.19 (i) CL photomicrograph of 1IB2A2 (optical CL insert). The variation in nitrogen concentration (N ppm), the percent of nitrogen occurring as B aggregate (%N as B), platelet peak intensity (mu (1365)) and hydrogen peak intensity (H(3107)) across the plate are illustrated in (ii) – (v) respectively.

Traverse 1-13 shows a systematic decrease in nitrogen concentration from the centre of the diamond outward (figure 5.19ii). The nitrogen concentration varies from as much as 714 ppm near the centre, to 100 ppm at the rim. The central cubic sector is associated with a slightly lower (642 ppm) nitrogen concentration than the adjacent octahedral sectors. Nitrogen aggregation follows similar trends, in accordance with nitrogen concentration, across the diamond (figure 5.19iii), with as much as 18.3 %N as B near the centre, to 7.2 %N as B at the periphery. Platelet peak [mu(1365)] intensities (figure 5.19iv) and hydrogen peak [H(3107)] intensities (figure 5.19v) also become systematically more depleted towards the rims.

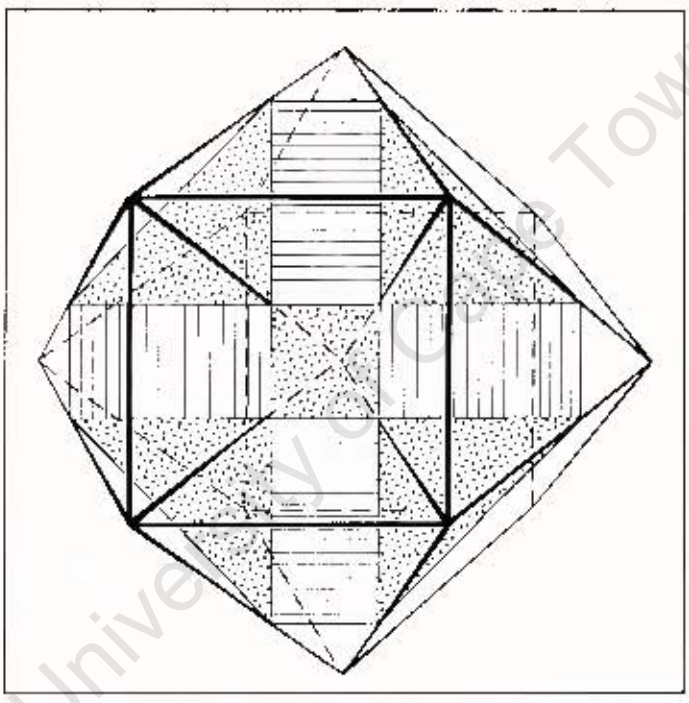

Figure 5.20 Perspective illustration of a cubo-octahedron set with a tetrahexahedroid axis vertical and a cube surface, (001), facing the observer. The shaded section represents a cut parallel to (001) at about one third the distance from the crystal center to the (001) face. The five cube growth sectors intersected by the cut have been stippled. The four octahedral growth sectors are ruled parallel to their respective {111} facets. For clarity, the interior edges of only the (001) growth sector pyramid are shown: as continuos lines on the near side of the cut, and as interrupted lines on the far side (From Lang, 1979).

Traverse 14-17 shows relatively higher nitrogen concentrations (up to 582 ppm) and aggregation states (up to 18.3 %N as B) than at equivalent positions within the octahedral growth sectors. These observations confirm the sectoral dependence of

nitrogen concentration and aggregation, that was assumed from the CL imagery of this diamond.

Estimated temperatures vary between 1085 °C – 1123 °C, defining a broad isothermal envelope in figure 5.9. The estimated mantle residence temperatures appear to become systematically higher towards the periphery of the diamond, and once more this can be attributed to the sampling of multiple growth layers. It follows therefore that the 'elevated' temperature estimates from the periphery of the diamond, can be assumed to be overestimates as a result of this mixed sampling.

The above observations suggest a progressively changing chemical environment, with successive diamond growth. Initially the diamond crystallised in an environment associated with high hydrogen and nitrogen concentrations, as crystallisation proceeded however the environment became systematically depleted in these elements. In addition the observations effectively demonstrate that there is a sectoral dependence of nitrogen concentration and aggregation within this diamond, and that the diamond must have crystallised in an environment intermediate between the environments suitable for only octahedral or cubic growth.

This diamond, despite having been resorbed is believed to represent the large population of cubo-octahedral diamonds associated with the Helam diamond suite. The relatively high nitrogen concentrations and aggregation states confirm this diamond as Type IaAB. It is reasonable to assume therefore that the subtle yellow coloration associated with this diamond, is a result of the of N3-centers within the diamond lattice. This is clearly quite different from the coloration exhibited by the majority of the other, more intensely yellow coloured (canary) diamonds.

5.6.2.9 Plate HB03B

This plate was cut from an octahedral diamond displaying canary-yellow coloration, and hence the assumption was made that this diamond is representative of the natural Type Ib diamonds of the Helam population. EPR studies of the diamond plate confirmed the presence of OK1 and EPR N3 centres as well as other unperturbed singly substitutional nitrogen within the diamond lattice (Hill, 2001, pers. comm.). No optical N3 centres were observed (by EPR), and hence it is reasonable to

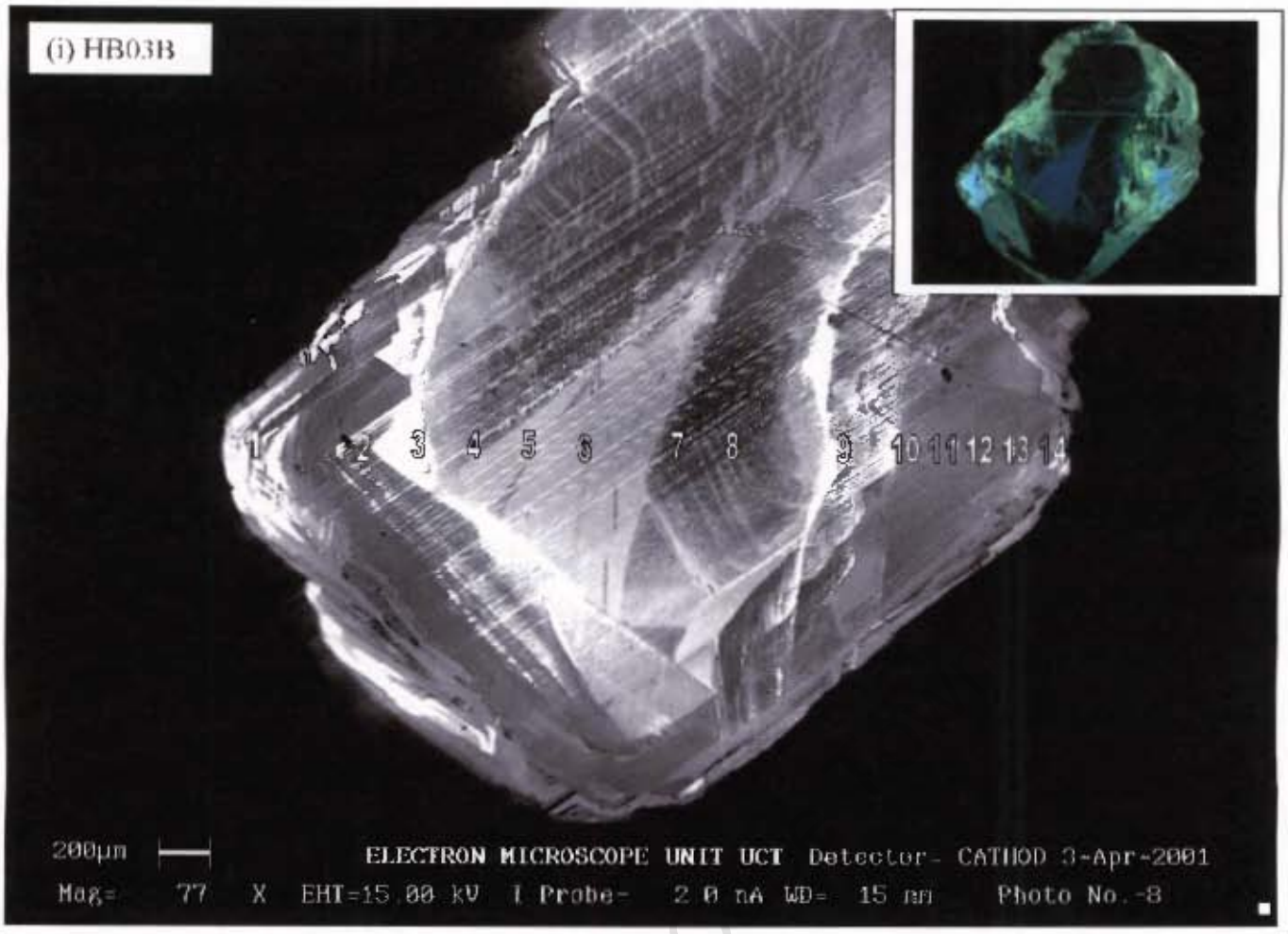

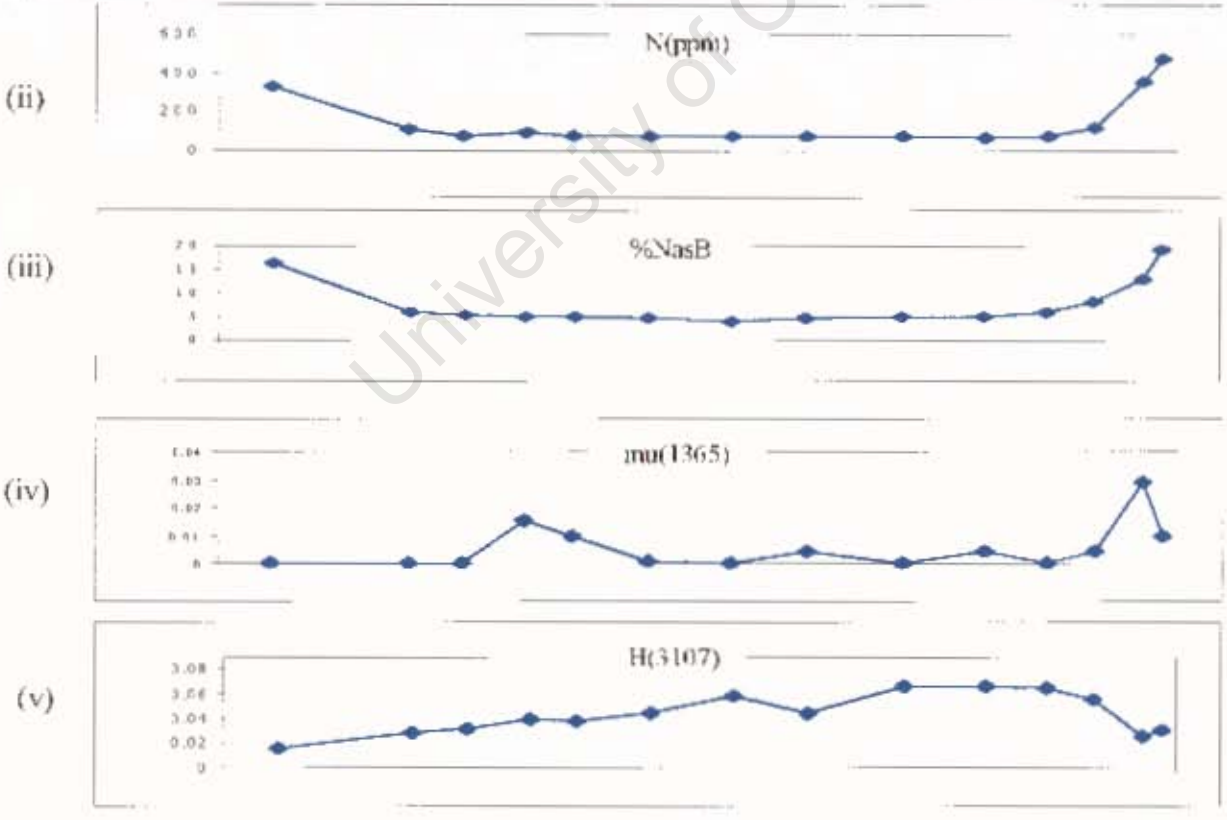

Figure 5.21 (i) CL photomicrograph of HB03B (optical CL insert). The variation in nitrogen concentration (N ppm), the percent of nitrogen occurring as B aggregate (%N as B), platelet peak intensity (mu (1365)) and hydrogen peak intensity (H(3107)) across the plate are illustrated in (ii) (v) respectively.

assume that the coloration of the diamond is a result of singly substitutional nitrogen, and that this plate was indeed cut from a Type Ib diamond, representative of the canary-yellow diamond sub-population.

Figure 5.21i illustrates a CL photomicrograph of the diamond plate. The first order observation is that this diamond is complexly zoned. The plate is characterised predominantly by a 'core' of varyingly luminescent, complexly structured Type I diamond (figure 5.21i). Surrounding this core are alternating layers of low luminescent Type I, and non-luminescent Type II diamond displaying octahedral growth. It becomes clear from figures 5.21ii-v, that there exists significant chemical differences between the core and the peripheral diamond. In addition this plate is characterised by extensive lamination lines (features which ubiquitously characterise the canary-yellow diamond sub-population).

Measured nitrogen concentrations within the core (figure 5.21ii) are ubiquitously low, varying between 73 – 110 ppm (values commonly associated with the canary-yellow diamond sub-population). These low nitrogen concentrations, together with interpreted deformation features may explain the yellow luminescence associated with this diamond (insert of figure 5.21i). However, the periphery of the diamond, exhibits highly elevated nitrogen concentrations (up to 470 ppm), which are uncharacteristic of the canary-yellow diamond sub-population.

Despite the confirmed presence of singly substitutional nitrogen (by EPR) within this diamond plate, no observable IR absorption in the region 1152 cm^{-1} was recorded. This suggests that the singly substitutional nitrogen is only present in very low, undetectable concentrations within the diamond. It is suggested that much of this diamond plate is associated with aggregation states transitional between the Ib-IaA and IaA-IaB series.

Nitrogen aggregation varies in accordance with nitrogen concentration. Figure 5.21iii illustrates that the core is associated with relatively immature aggregation states (only between 4.6 – 8.0 %N as B). The peripheral diamond however, displays significantly higher degrees aggregation (between 12.8 – 19.0 %N as B), which are also uncharacteristic of the canary-yellow diamond sub-population.

It is clear therefore that in terms of the nitrogen concentrations and aggregation states across the plate, that the core and periphery of this diamond are very different. It is suggested that the core of this diamond is comprised of complexly

zoned Type Ib and IaAB diamond, typical of the canary-yellow diamond sub-population. It is suggested that the peripheral diamond represents alternating octahedral overgrowth of Type IaAB and Type II diamond. These observations are in agreement with suggestions made in Section 5.4 that many of these canary-yellow diamonds are complexly zoned. Such zonation may explain the presence of IR absorption features typically associated with diamond of the IaA-IaB series (e.g.: Raman Edge), in the spectra generated from these natural Type Ib, canary-yellow diamonds.

Platelets [mu(1365)] appear to be under-developed throughout the stone (figure 5.21iv), which is explained by the extensive deformation that has clearly affected the diamond. This deformation, together with the low nitrogen concentrations associated with this diamond may explain the yellow luminescence of the diamond when subjected to CL (insert of figure 5.21i). Hydrogen [H(3107)] however, appears to be systematically more concentrated towards the centre of the diamond (figure 5.18v) as is commonly observed among the other Helam diamonds.

Despite the chemical differences observed across the diamond plate, estimated residence temperatures exhibit a very narrow isothermal range in figure 5.9, varying between 1096 °C to 1113°C.

In terms of diamond growth therefore, it would appear that the natural Type Ib diamond (core) grew within a chemically unstable, nitrogen depleted and hydrogen enriched mantle environment. It is suggested that this core is representative of many of the other rough canary-yellow diamonds analysed in Section 5.6.2. Following some hiatus in diamond growth, crystallisation resumed in an environment characterised by alternating nitrogen concentrations, resulting in the alternating layers of Type IaAB and Type II diamond.

5.7 Discussion

Data compiled from the diamond plates are consistent with initial observations made from the rough diamonds, defining similar thermal and chemical regimes. It has been demonstrated that detailed studies of the diamond plates were more successful in defining subtle changes in crystal growth and composition. Analyses of the diamond plates were successful in demonstrating that the Helam diamonds are commonly

associated with episodic growth, with evidence for renewed diamond crystallisation perhaps billions of years subsequent to the initial diamond forming event in some cases. Changes in the crystallisation environment over such periods of time are evident from the dramatically different compositions of the diamond between the older cores and the younger overgrowths. Diamond HB2A2 provides evidence for resorption of diamond during a hiatus, perhaps recording a transient change from a reducing, to an oxidising environment, within the mantle.

A synthesis of the observations made from the various diamond plates, together with that made from the whole, rough diamonds help define the crystallisation and deformation history associated with the Helam diamond population. All diamonds show a predominant trend of decreasing nitrogen and hydrogen concentrations with successive growth, suggesting that the mantle in which the Helam diamonds grew, became progressively depleted in these elements with successive growth. All diamonds exhibiting a clear hiatus in growth, record a significant increase in nitrogen concentration within the younger generation of diamond, suggesting a marked change in the crystallisation environment over time. Such abrupt changes in the concentration of nitrogen may record an influx of an N-enriched fluid. Diamond HB2A2 is the exception of course, being associated with a younger generation of diamond having been crystallised in a rapidly changing, chemically unstable environment and recording somewhat lower nitrogen concentrations.

While many of the Helam diamonds appear to have crystallised in relatively stable mantle environments, some diamonds (e.g.: HB2A2, HB03B) suggest periods of diamond crystallisation within rapidly changing, chemically unstable environments. In addition, it is clear that a large proportion of the Helam diamonds have been affected by deformation. The effects of this deformation have been manifest in the IR characteristics of the diamonds. Diamonds displaying lamination lines, or other stress related features, are ubiquitously associated with low nitrogen (< 400ppm) concentrations. It appears therefore that diamonds with low nitrogen concentrations are predisposed to the effects of deformation, as has been suggested for certain Australian diamonds (Davies *et al.*, 1999b). Such diamonds are characterised by an unusual yellow-green luminescence when subjected to CL. It has also been demonstrated that deformation has resulted in degradation of the platelets

within the diamonds, as indicated by the non-uniform relationship between the platelet peak intensities and aggregation states associated with the deformed diamonds.

The undeformed diamonds are associated with higher nitrogen concentrations (> 400 ppm), and exhibit a more characteristic blue luminescence when subjected to CL. In addition these 'regular' diamonds commonly show a positive correlation between the platelet peak development and aggregation state across the diamond.

Analysis of the diamond plates has been successful in constraining the mantle residence temperatures for some of the Helam diamonds. The effect of sampling multiple growth layers was carefully investigated, and consequently, spurious results could be disregarded. It has been demonstrated that such erroneous estimates of residence temperature were commonly associated with the peripheral regions of the diamonds, where evidently more growth layers had been sampled. It is clear that within the central regions of the diamond there was a much better control on the positions of the various growth layers and less interference by multiple layers, and consequently more accurate estimations of residence temperature could be made. From such measurements it is reasonable to constrain time-averaged mantle residence temperatures for the majority of the Helam diamonds between 1090 °C – 1110 °C, assuming a mantle residence time of 2.75 Ga.

Integrated FTIR and CL studies HB03B has shown that some of the canary-yellow diamonds are complexly zoned, and that components of Ib, IaA and possibly even IaB diamond may be present in a single diamond. From the analysis of the rough canary-yellow diamonds, it appears that these diamonds follow a similar trend of decreasing nitrogen and hydrogen contents towards their peripheries. However, the diamond plate (HB03B) is associated with an overgrowth of Type IaAB diamond with high nitrogen concentrations, and hence the general observation of decreasing nitrogen towards the rim does not hold in this case. It is suggested that the canary-yellow diamonds represent a separate diamond forming event, that occurred subsequent to the crystallisation of the other Helam diamonds, but which preceded kimberlite emplacement by a geologically significant time period (perhaps by billions of years). These diamonds thus further attest to a mantle capable of multiple, episodic diamond formation.

Undoubtedly the Helam diamond population represents a suite of diamonds with a complex and extended geological history. It is clear that the various sub-populations of diamond have grown in different environments, each environment having undergone significant chemical variation over time. Furthermore it is clear that diamond crystallisation has occurred intermittently over time, with periods of hiatus in between, in which the mantle had been allowed to evolve significantly. Subsequent to the diamond growth, many of the diamonds have been deformed, manifested by both physical and chemical modifications within the diamonds.

6 DIAMOND MINERAL INCLUSIONS

6.1 Introduction

Diamond is remarkably unreactive, and generally unless under oxidising conditions, it will remain as a metastable phase for billions of years (Meyer, 1987). This chemical inertness, together with the diamonds inherent physical strength prevents any mineral inclusions completely enclosed within the diamond, from re-equilibrating with the external environment. It follows therefore that if the integrity of the diamond is maintained, the mineral inclusion compositions will reflect the mantle environment at the time of diamond formation, preserving isotopic, trace, minor and major element compositions of their formation. Inclusions in diamonds are the only sources of mineral grains that can have *pristine* compositions from the Earth's mantle (e.g.: Boyd *et al.*, 1985; Meyer, 1987). The study of such mineral inclusions within diamond (now referred to simply as 'inclusions'), has greatly contributed to the understanding of diamond genesis, as well as mantle and craton-forming processes.

Mantle conditions can be estimated from the compositions of the inclusion suites, in a similar manner as is commonly done for mantle xenoliths (e.g.: Finnerty & Boyd, 1984; Carswell & Gibb, 1984). However, the circumstances of equilibration of the inclusions is markedly different from that of the xenoliths. Mineral grains within xenoliths were in contact with each other, and pore fluids until the time of kimberlite eruption, and thus had the potential for chemical exchange at high temperatures. Isolated mineral inclusions however, can have chemical compositions that were fixed at the time of diamond crystallisation, and are therefore effective in preserving compositions associated with mantle conditions at the time of diamond formation (Boyd *et al.*, 1985).

Inclusions occur either as totally enclosed, discrete single crystals or as crystalline material occurring within penetrative fracture systems of the diamond (Harris & Gurney, 1979). It is fair to assume that inclusions associated with penetrative fractures have either been altered by changing chemical environments (figure 4.22c), or have been emplaced at some time after the genesis of diamond. It follows therefore that such inclusions provide suspect information regarding mantle

conditions. It is therefore important to establish the genetic association between the inclusion and its diamond host.

Further to this, three types of inclusions can be observed. *Protogenetic* inclusions grew independently of the diamond into which they have been incorporated, and commonly display irregular morphology, or their own morphology. Such protogenetic inclusions may not be directly related to the environment of diamond genesis (Meyer, 1987). *Syngenetic* inclusions grew at the same time as the diamond host, and commonly exhibit diamond induced morphologies. These inclusions are clearly the most important for the study of diamond genesis as they preserve the mineralogy and chemistry of the diamond growth environment (Harris and Gurney, 1979). *Epigenetic* inclusions postdate diamond formation and commonly represent the alteration products of protogenetic and syngenetic inclusions (Meyer, 1987).

Of all the diamond inclusion minerals observed within diamonds worldwide (Table 6.1), only seven species are common (discussed in detail below). Olivine (forsterite), orthopyroxene, Cr-pyrope garnet, and Cr-rich chromite constitute the most abundant primary inclusions of the peridotitic paragenesis. Cr-poor pyrope-almandine garnet and omphacitic clinopyroxene constitute the more common eclogitic inclusion species. Sulphide minerals are associated with both the peridotitic and eclogitic parageneses, and are the most abundant inclusions found within diamonds (Meyer, 1987).

Only about 0.5% of worldwide diamond production are usefully inclusion bearing for geochemical purposes (Harris & Gurney, 1979). The majority of mineral inclusions within diamond are small (~100 μm), and are commonly monomineralic, however polymineralic and multiple inclusions of more than one phase, do also occur. Such inclusions are important as they permit the calculation of equilibrium temperature and pressure conditions, as is done for upper mantle xenoliths (e.g.: Carswell & Gibb, 1984; Finnerty & Boyd, 1984). Calculations done on such co-existing inclusions from the peridotitic paragenesis reveal equilibration temperatures between 900 °C and 1300 °C, and 45 and 65 kbar (e.g.: Meyer, 1987). These values lie close to the 40 mW/m^2 geotherm, and as expected, are consistent with the region ascribed to diamond stability (Kennedy & Kennedy, 1976).

Table 6.1 Mineral inclusions recovered from diamonds worldwide (modified from Meyer, 1987; Harris, 1992; Chinn, 1995 with additions from Harte and Harris, 1984) (from Westerlund, 2000).

Syngenetic Inclusions				**Epigenetic Inclusions**	**Inclusions of Uncertain Origin**
Peridotitic	***Eclogitic***	***Websteritic***	***Sub-Lithospheric***		
Olivine	Omphacitic cpx	Cpx	Majoritic Garnet	Serpentine	Phlogopite
Enstatite	Pyrope-almandine	Opx	Mg-wustite	Calcite	Muscovite
Cr-pyrope	Kyanite	Garnet	Mg-Si-perovskite	Haematite	Amphibole
Chromite	Sanidine	Phlogopite	Ca-Si perovskite	Graphite	Wollastanite
Cr-diopside	Ilmenite			Kaolinite	Magnetite
Sulphides	Sulphides			Acmite	Titanomagnetite
Mg-ilmenite	Coesite			Richterite	Sphene
Mg-wustite	Quartz			Perovskite	Moissanite
Zircon	Corundum			Mn-ilmenite	Apatite
Cohenite	Ruby			Spinel	Si-Ti-K phase
Native iron	Rutile			Xenotime	Ti-K-Al silicate
Diamond	Diamond			Sellaite	Staurolite
Clouds	Clouds			Goethite	Plagioclase
				Cr-Sr-loparite	Albite
				Cr-chevkinite	

Girnis *et al.* (1998) confirmed that different temperature ranges can be calculated for touching and non-touching peridotitic inclusions. It can be shown that touching inclusions show a more restricted range than is associated with non-touching inclusions. Moreover, touching inclusions appear to record lower temperatures than do the non-touching inclusions. Gurney (1989) suggests that a lack of equilibrium between inclusions encapsulated within diamond at different times may result in the larger range of temperatures obtained for non-touching inclusions. The lower temperatures may also reflect a cooling of the source between diamond formation and eruption of the diamonds. This notion is supported by observations by Gurney *et al.*, (1984b) who report final equilibration temperatures for diamondiferous xenoliths from the Roberts Victor kimberlite that are at least 200 °C cooler than those calculated for inclusion minerals within the diamonds. Work done by Phillips & Harris (1995) on mineral inclusions from diamonds from the De Beers Pool diamonds further supports this model.

It is still not possible to determine equilibration temperatures and pressures for inclusions of the eclogitic paragenesis unequivocally, though estimated temperatures do appear marginally higher, but within in range of that of the peridotitic suite (Gurney, 1984).

6.2 Mineral Parageneses

It becomes clear from detailed studies of mineral inclusions from diamonds worldwide, that diamonds are formed within at least two distinct lithospheric environments, one peridotitic, and the other eclogitic (e.g.: Harris & Gurney, 1979; Meyer, 1987). The composition of the inclusions is generally similar to equivalent mineral types found within mantle xenoliths in kimberlite. A websteritic association (orthopyroxene + clinopyroxene $\pm$ garnet) has also been widely recognised, having initially been interpreted as an intermediate paragenesis between the peridotitic and eclogitic suites (e.g.: Gurney, 1984), has been more recently interpreted to be more closely associated with the eclogitic paragenesis (Gurney, pers. comm. 2001). In addition Sobolev *et al.* (1984) suggest a separate calc-silicate paragenesis based on their observations of Ca-enriched garnet and clinopyroxene inclusions, from an Australian source.

The more recent discoveries of the rare and unusual inclusions of majoritic garnets (e.g.: Moore & Gurney, 1985; Wilding, 1989), Mg-Si-perovskite and Ca-Si-perovskite (e.g.: Harte & Harris, 1994; Harris *et al.*, 1997; Hutchinson, 1997; Davies et al., 1999a) and ferropericlase (e.g.: Scott-Smith *et al.*, 1984, Moore *et al.*, 1986; Wilding, 1989; and Davies *et al.*, 1999a) are suggestive of a much deeper, sub-lithospheric origin for some diamonds.

6.3 Inclusion Mineralogies

The minerals described as 'peridotitic' are similar in mineralogy to those found within ultramafic/peridotitic xenoliths within kimberlites and lamproites. Having been protected from re-equilibration with the surrounding mantle, due to their encapsulation within diamond, peridotitic inclusions are commonly more depleted in most magmaphile elements than those observed within the xenoliths. Olivine (a common mineral associated with this paragenesis) is Mg-rich, but shows a restricted range in Mg#'s, typically between 91 and 95. Most olivine inclusions commonly contain trace Cr_2O_3 contents *twice* that of other terrestrial olivine of comparable forsterite content (Meyer, 1987). Peridotitic orthopyroxene inclusions are also ubiquitously Mg-rich, with Mg#'s between 91 –95.

Spinel inclusions are also commonly observed within peridotitic diamonds, and are mostly picrochromites that are extremely enriched in chromium (up to 65 wt% Cr_2O_3), with compositions close to the $FeCr_2O_4$-$MgCr_2O_4$ join (Meyer, 1987). Chromite inclusions are typically characterised by very low titanium contents, usually less than 0.3 wt% TiO_2, but which can be observed to contain TiO_2 contents approaching 2.0 wt.% (e.g.: Viljoen *et al.*, 1999).

Peridotitic clinopyroxene (diopside) are characterised by prominent Cr_2O_3 concentrations, but relatively low Na_2O and Al_2O_3 (Meyer, 1987). Likewise peridotitic garnets (pyrope) exhibit high Cr_2O_3 (up to 16 wt%) concentrations, but are primarily characterised by high MgO contents (24 wt%) and low calcium contents. Eclogitic garnet inclusions (pyrope-almandines) closely resemble those associated with eclogitic xenoliths. They are characterised by lower MgO contents than their peridotitic counterparts, and higher CaO (3-14 wt%) and FeO (10-23 wt%) contents. Cr_2O_3 contents are typically less than 0.1 wt%. Eclogitic garnets are further

characterised by relatively high Na_2O ($\geq$ 0.06 wt%) contents, and are all classified as Group I eclogites according to the McCandless & Gurney (1989) classification (discussed in section 3.3). Eclogitic clinopyroxene inclusions are distinguished from diopsidic crystals by their higher Na_2O and Al_2O_3 contents, and lower Cr_2O_3 contents. Figures 6.1a and 6.1b illustrate worldwide garnet and clinopyroxene inclusion compositions on Ca-Mg-Fe diagrams as reported by Meyer (1987).

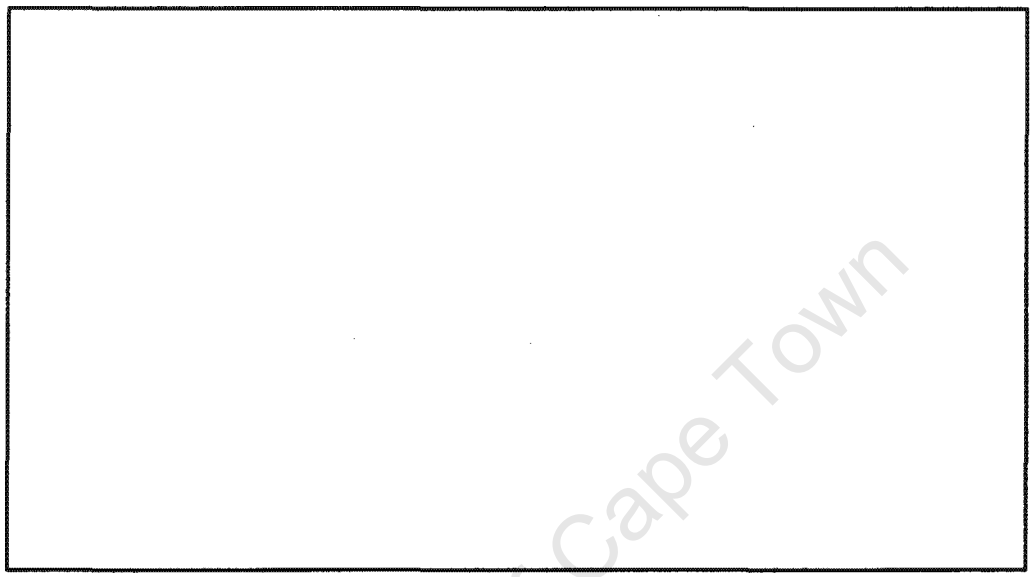

Figure 6.1a Ca-Mg-Fe ternary diagram of both peridotitic (open circles) and eclogitic (filled circles) garnet inclusions from diamonds worldwide. Garnet inclusions from diamonds hosted in lamproite are also illustrated (from Meyer, 1987).

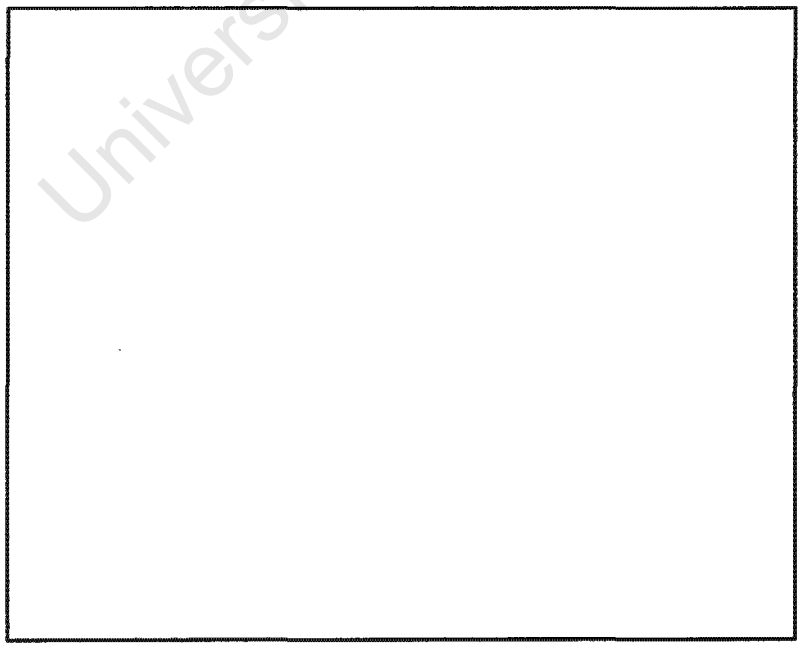

Figure 6.1b Ca-Mg-Fe ternary diagram of both peridotitic (filled circles) and eclogitic (open circles) clinopyroxene inclusions from diamonds worldwide. Also illustrated are the clinopyroxene inclusions associated with the calc-silicate suite (crosses), and those from diamonds hosted by lampoite (from Meyer, 1987).

Sobolev *et al.* (1984) have shown that some garnets and omphacites from southeastern Australia exhibit as much as 32 wt% and 23 wt% CaO respectively, and have suggested that this may indicate the presence of a separate calc-silicate paragenesis. Similar Ca-rich clinopyroxenes have also been observed at Premier (Tsai *et al.*, 1979) and Sloan (Meyer & McCallum, 1986).

Sulphides are relatively common in diamonds from both parageneses, however paragenetic assignation is arduous. Studies conducted on Siberian diamonds (e.g.: Yefimova *et al.*, 1983; Bulanova *et al.*, 1996), have reported sulphide inclusions co-existing with silicate phases, and have therefore been successful in assigning a particular sulphide to a paragenesis, based on the coexisting silicate mineralogies. It can be demonstrated that sulphides from peridotitic and eclogitic parageneses show marked differences in their nickel contents, and consequently it is suggested that this be used as a criterion for the assignation of parageneses for sulphides. Yefimova *et al.* (1983) suggest that all sulphides containing less than 8 wt% Ni are eclogitic, and that those containing more than 8 wt% are peridotitic. Bulanova *et al.* (1996) argues that sulphides with less than 12 wt% should be classified as eclogitic, and that those with over 20 wt% are peridotitic. In addition these workers introduced a 'pyroxenetic' parageneses to account for those sulphides with between 12-20 wt% Ni.

Such a discriminator has proven useful amongst Siberian diamonds, however sulphide inclusions from African diamonds are often quite dissimilar (Deines & Harris, 1995), and perhaps prescribe to somewhat higher 'cut-off' values. This argument will be discussed further in section 6.4.3.

6.4 Mineralogy of the Helam Diamond Mineral Inclusions

Mineral inclusions liberated from the Helam diamonds were analysed using the SX-50 Cameca microprobe at the De Beers Geoscience Centre, Johannesburg. The methodology is described in Appendix 4. A total of 157 inclusion analyses from 60 Helam diamonds (Table 6.2) are considered. Of these 47 inclusions were silicates, 54 were oxides and 56 analyses were from sulphides. Inclusions were recovered from both the small-size (<3 mm) and large-size diamonds (>3 mm). Table 6.4 shows that overall, there appear to be approximately equal numbers of peridotitic (41%) and

Table 6.2: Mineral inclusions recovered from Helam diamonds. (e) eclogitic, (p) peridotitic, (w) websteritic, (cc) calc-silicate mineral, (?) indicates uncertain paragenesis.

	Diamond	corundum	majorite	clinopyroxene	orthopyroxene	coesite	garnet	olivine	chromite	pyrrhotite	monosulphide solution	pentlandite	pentlandite-heazlewoodite	heazlewoodite	Paragenesis
1	HM006						3e								eclogitic
2	HM007			1p											peridotitic
3	HM008			2w				3			1	1		1	peridotitic
4	HM009		2e												peridotitic
5	HM018			1e											eclogitic
6	HM019					1									eclogitic
7	HM031								4						peridotitic
8	HM032								2						peridotitic
9	HM033											1			?
10	HM034					1									eclogitic
11	HM055								2						peridotitic
12	HM059									1					eclogitic
13	HM067								1						peridotitic
14	HM086								1						peridotitic
15	HM108				1w	1									websteritic
16	HM109								3						peridotitic
17	HM111													1	peridotitic
18	HM112	1													eclogitic
19	HM113							1					2		peridotitic
20	HM114	1				3									eclogitic
21	HM115					1				1					eclogitic
22	HM119					1									eclogitic
23	HM123											1			?
24	HM124									1					eclogitic
25	HM126									1					eclogitic
26	HM127											1			?
27	HM203											2			peridotitic
28	HM208							3							peridotitic
29	HM209							1							peridotitic
30	HM210							1							peridotitic
31	HM211					1									eclogitic
32	HM217											1			?
33	HM220											1			?
34	HM221										1	1			peridotitic
35	HM235									1				2	peridotitic
36	HM236					1									eclogitic
37	HM240							3							peridotitic
38	HM1A2									5	2				eclogitic
39	HM1A7									1					eclogitic
40	HM1A9								10						peridotitic
41	HB1A10								1						peridotitic
42	HM1A12						1w								websteritic
43	HM1B2					1	1e								eclogitic
44	HM2A4									1					eclogitic
45	HM2B2	16				1									eclogitic
46	HM2B3	1								3	2				eclogitic
47	HM2B7										2				peridotitic
48	HM2B1	1													eclogitic
49	HM2B11	5													eclogitic
50	HM3A5						1w								websteritic
51	HM3A11									2	1				eclogitic
52	HM3B4							5		1	1				peridotitic
53	HM3B7													4	peridotitic
54	HM3B9								2			2		1	peridotitic
55	HM3B10											1			?
56	HM3B11			1cc			4w								websteritic
57	HB3C3								3						peridotitic
58	HM3C10									1	2				eclogitic
59	HM3D1												1		?
60	HM3D6a									1					eclogitic
															Total:
	TOTAL	25	2	5	1	12	10	17	29	20	12	12	3	9	157

eclogitic (40%) diamonds represented, however it becomes clear that the eclogitic component is significantly more abundant among the larger-sized diamonds. This is consistent with the observation made by Gurney (1989), that there is commonly a general trend for a greater eclogitic component among the larger diamond sizes. An intermediate, websteritic component (which will be shown to be more closely associated with the eclogitic paragenesis) also appears to be more abundant amongst the larger diamonds. Table 6.3 shows the variation in abundance of the various phases with respect to diamond size. The results presented in this table suggest that the larger diamonds are associated with a greater abundance of oxide and sulphide phases. These observations are made tentatively as they may well be a function of a sampling bias.

Table 6.3: Paragenetic assignation of Helam diamond mineral inclusions within both the smaller size fraction (small) and larger size fraction (large) diamonds.

	Eclogitic	Peridotitic	Websteritic	Unknown	Total
Small (< 3 mm)					
Silicates	16	13	3	0	**32**
Oxides	2	13	0	0	**15**
Sulphides	4	13	0	5	**22**
Large (>3 mm)					
Silicates	3	5	7	0	**15**
Oxides	23	16	0	0	**39**
Sulphides	21	11	0	2	**34**
Total	**69**	**71**	**10**	**7**	**157**

Table 6.4: Paragenetic assignation of Helam diamonds based on mineral inclusions, for the entire population studied (all), the smaller size fraction (small), and larger size fraction (large).

	Eclogitic	Peridotitic	Websteritic	Unknown	Total
All	24	25	4	7	**60**
	40%	*41%*	*7%*	*12%*	
Small (<3 mm)	13	18	1	5	**37**
	35%	*49%*	*3%*	*13%*	
Large (> 3 mm)	11	7	3	2	**23**
	48%	*30%*	*13%*	*9%*	

6.4.1 Silicate Inclusions

Silicate inclusions are uncommon among the Helam diamond population. Where they have been found, they tend to be centrally located within the host diamond and are

often very small (typically <50 μm). The mineralogies of the recovered Helam silicate inclusions are considered below. Figure 6.2 illustrates the compositions of the Helam olivine, garnet and pyroxene inclusions with respect to other recorded inclusion compositions, worldwide. Silicate mineralogies are presented in Appendix 4.1.

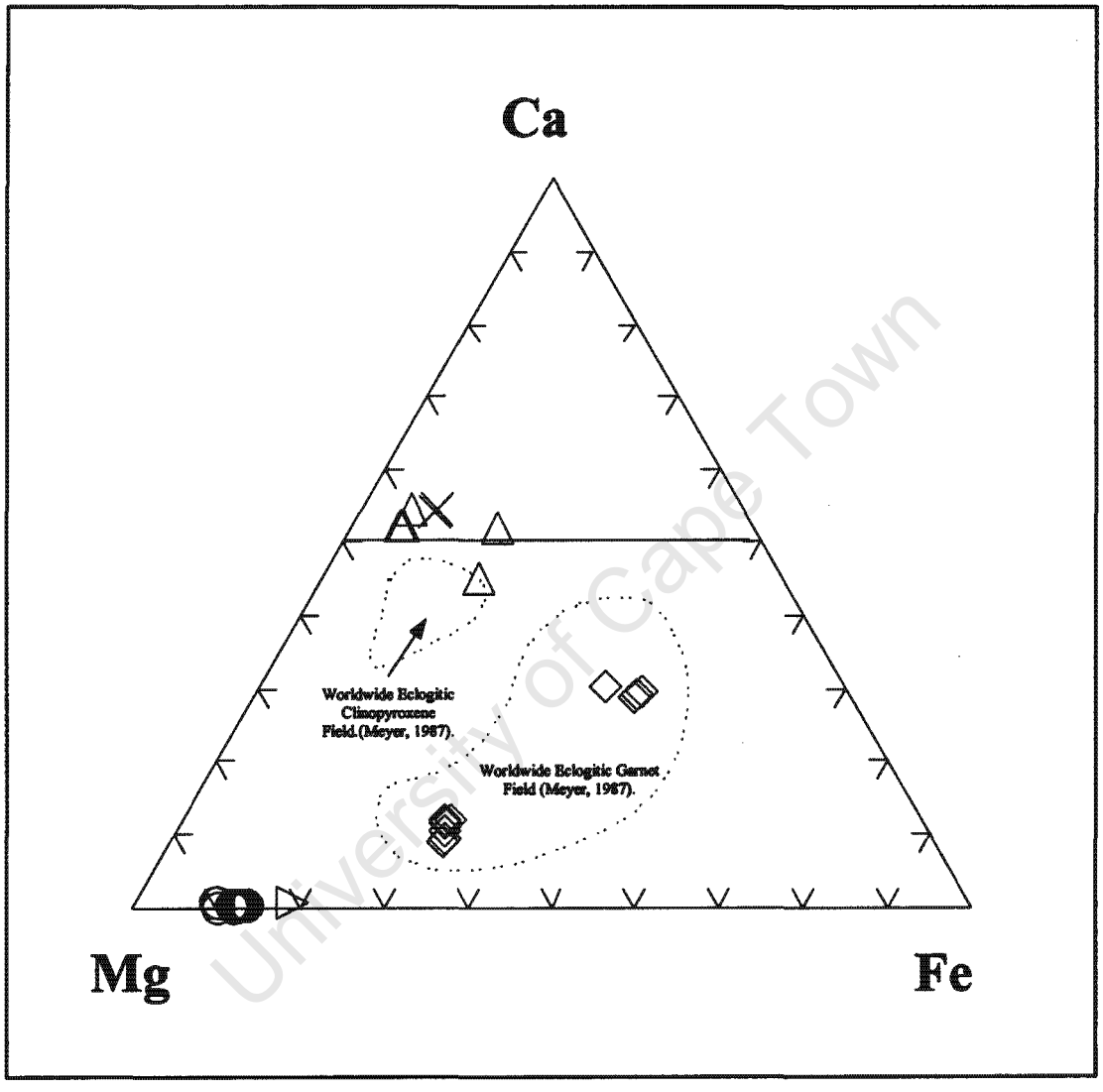

Figure 6.2 Ca-Mg-Fe ternary diagram illustrating the compositions of the Helam silicate inclusions (circles = olivine, diamonds = garnet, upright triangle = pyroxene, titled triangle = orthopyroxene, cross = majorite). Inserted fields reflect worldwide compositions of eclogitic garnet and clinopyroxene inclusions (From Meyer, 1987). Horizontal line joins the pyroxene end-members of diopside and hedenbergite.

6.4.1.1 Olivine

The most abundant silicate mineral among the Helam diamonds is olivine (17 olivine inclusions recovered from 8 diamonds), which typically occur as large (100 μm – 70

μm), colourless inclusions. These inclusions commonly occupy the center of their diamond host and display either cubo-octahedral or sub-rounded morphologies. All olivine inclusions have been interpreted as being syngenetic with respect to diamond growth. The Helam diamonds commonly include multiple inclusions of olivine (up to 5 crystals within one diamond). Some Helam olivine inclusions have been found to coexist with inclusions of clinopyroxene and sulphides (see table 6.2).

The Helam olivines display compositions ranging between $Fo_{91.77}$ and $Fo_{94.25}$ (Appendix 4.1a). These values fall well within the range observed for olivine inclusions worldwide (Meyer, 1987). Cr_2O_3 and NiO have restricted ranges of between 0.02 wt% – 0.07 wt% and 0.32 wt% – 0.42 wt% respectively. Figure 6.3a illustrates the Cr_2O_3 compositions of the olivine inclusions, where it can be seen that there appears to be a predominant bi-modal distribution of Mg#'s for the olivine inclusions. In assessing the relationship between NiO content and Mg# for the Helam olivines (figure 6.3b), *three* groups of olivine (high-, low- and intermediate-Mg olivines) can be identified. The majority of the olivines belong to the intermediate-Mg group. The low- and high-Mg olivines were sampled from single diamonds; HM008 and HM3B4 respectively. Both these diamonds, exhibit olivine coexisting with monosulphide solid solution inclusions. Despite the inhomogeneity associated with the overall olivine population, olivine inclusions from individual diamonds show no significant compositional variability.

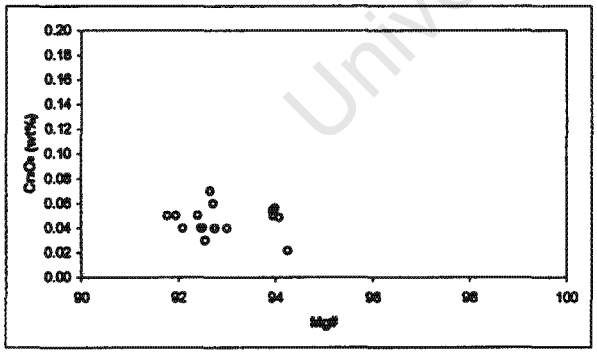

Figure 6.3a Relationship between Cr_2O_3 and Mg# of olivine inclusions from Helam diamonds

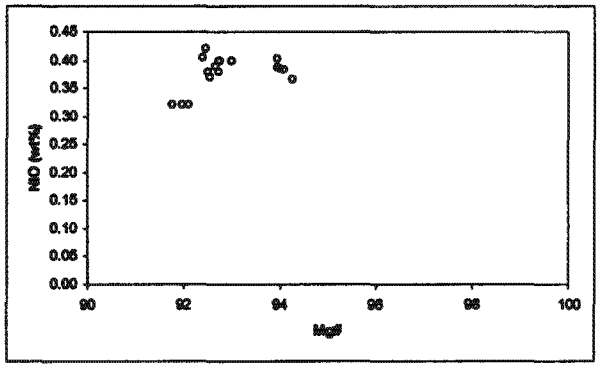

Figure 6.3b Relationship between NiO and Mg# of olivine inclusions from Helam diamonds

The subtle compositional differences between the various olivine crystals may reflect paragenetic differences. Alternatively, the olivines may have recorded a change in the

chemical environment within the same source rock between episodic diamond crystallisation events. Bi-modality among olivine inclusions, has been observed by other workers (e.g.: Moore & Gurney, 1989, Daniels & Gurney, 1999), having been interpreted as representing slightly different parageneses. Harris (1992) reports a mode of Fo_{94} for harzburgitic olivines worldwide. Consequently, those Helam olivines exhibiting the lowest Fo values (< 92) may be reflective of a lherzolitic paragenesis, while those displaying intermediate values (between 92-93) may reflect a harzburgitic paragenesis. Perhaps the *most* refractory olivines are representative of a separate dunitic parageneses. These suggestions can only be made tentatively as while the different parageneses may display different modes, overlap between the different parageneses does exist.

6.4.1.2 Garnet

Garnet inclusions are relatively uncommon among Helam diamonds, despite the abundant sub-calcic and eclogitic garnet macrocryst populations discussed in Chapter 3. The recovered Helam garnet inclusions are generally relatively small in size (<70 μm). The inclusions occur both as cubo-octahedral and sub-rounded crystals (figure 4.24), and have consequently been classified as syngenetic in nature. Two distinctive types of garnet have been identified, both on the basis of their coloration and mineralogy. The two types of garnet have been assigned to the eclogitic and websteritic parageneses respectively. No strictly 'peridotitic' garnet inclusions were observed. The distribution of the Helam garnet inclusions on a ternary Ca:Mg:Fe diagram is illustrated in figure 6.2.

The eclogitic garnets are characteristically orange in colour. Three inclusions were recovered from a canary-yellow diamond (HM006), and one from a colourless diamond (HM1B2). While all broadly similar (Appendix 4.1b), the compositions of the garnets from the different diamonds, show some subtle chemical differences. The eclogitic garnets from HM006 were all recovered from near the rim of the diamond, and all display similar compositions. These garnets are associated with Mg#'s between 51 and 54. They display a limited range in FeO and MgO with between 16.99 wt% - 17.22 wt% and 9.21 wt% - 9.50 wt% respectively. The eclogitic garnet

recovered from HM1B2 however, is characterised by a Mg# of 57 and MgO and FeO contents of 15.43 wt% and 10.60 wt% respectively.

The nitrogen aggregation characteristics of the two diamonds containing eclogitic garnets (Chapter 5), suggest that diamond HM1B2 (colourless diamond) was resident within the mantle for somewhat longer than diamond HM006 (yellow diamond). Diamond HB1B2 being associated with significantly greater nitrogen concentrations, and more mature aggregation states than HM006. It follows therefore, that the garnet of diamond HM1B2, having been encapsulated by diamond first, would have been shielded from environmental changes well before the garnets of HM006.

Figures 6.4a and 6.4b are useful in illustrating the similarities between the compositions of the eclogitic garnet inclusions with that of the eclogitic garnet macrocrysts discussed in Chapter 3. The garnet inclusions appear to be enriched in Ca, but contain Na and Ti concentrations which are indistinguishable from their macrocrystic counterparts. For completion various other bi-minerallic plots have been included (figures 6.4c-f), however in the absence of more abundant data, little can be said of the existence of geochemical trends. Perhaps figure 6.4e alludes to a decrease of Fe with increasing Mg#, which would suggest that the protolith of the source probably formed during an igneous fractionation process.

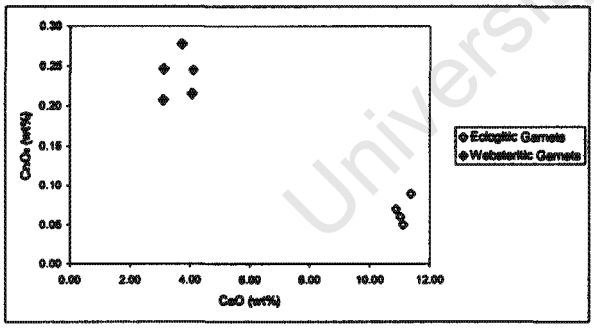

Figure 6.4a Relationship between CaO and Cr_2O_3 of garnets inclusions from Helam diamonds.

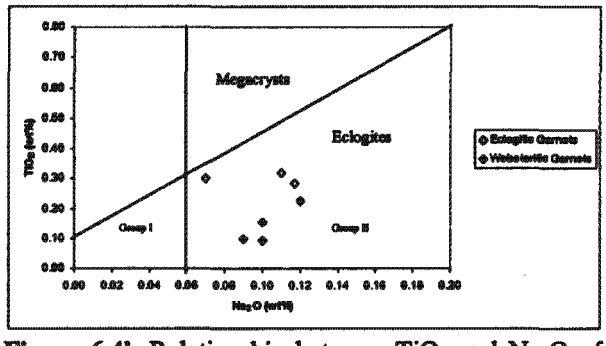

Figure 6.4b Relationship between TiO_2 and Na_2O of garnets inclusions from Helam diamonds. Two eclogitic garnets plot as a single point

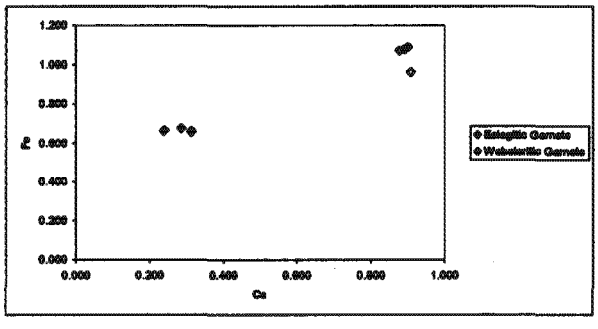

Figure 6.4c Relationship between Fe and Ca for garnet inclusions from Helam diamonds. Units are in cations per garnet formula unit.

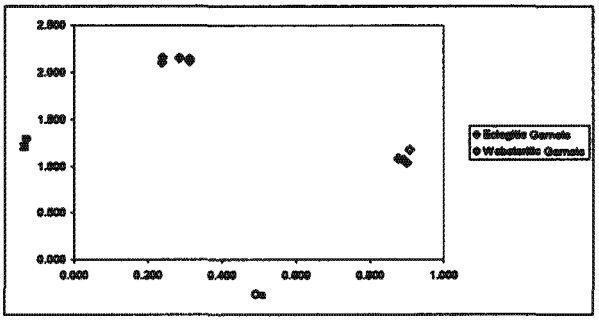

Figure 6.4d Relationship between Mg and Ca for garnet inclusions from Helam diamonds. Units are in cations per garnet formula unit.

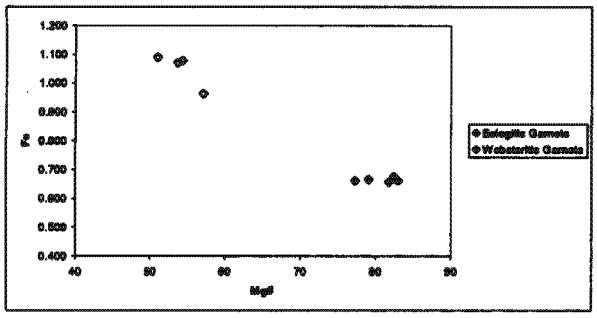

Figure 6.4e Relationship between Fe and Mg# for garnet inclusions from Helam diamonds. For Fe, units are in cations per garnet formula unit.

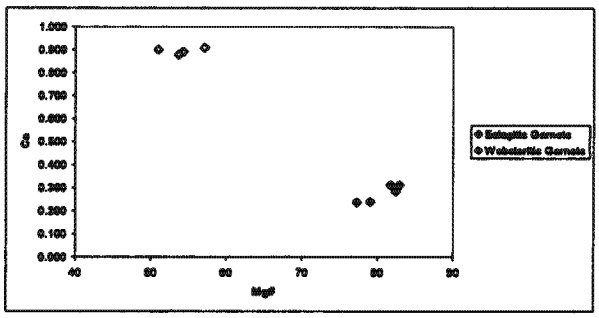

Figure 6.4f Relationship between Mg# and Ca for garnet inclusions from Helam diamonds. For Ca, units are in cations per garnet formula unit.

The second group of garnets are markedly different from the eclogitic garnets (Appendix 4.1b), and have all been recovered from colourless diamonds. These garnets are characterised by Mg#'s between 77 and 83, and relatively high Cr_2O_3 contents (between 0.21 wt% - 0.28 wt%), low FeO contents (between 11.03 wt% - 11.27 wt%) and high MgO contents (between 19.72wt% - 20.13wt%). While the Mg#'s *approach* those associated with peridotitic garnets (Meyer, 1987), the low Cr_2O_3 contents, suggest an intermediate websteritic paragenetic association, more closely associated to the eclogitic suite. These websteritic garnets are similar in composition to those observed by other workers (e.g.: Moore & Gurney, 1989; McDade & Harris, 1999), but exhibit comparative depletion in Ti and Cr.

6.4.1.3 Majorite

Two unusual inclusions were liberated from diamond HM009, the compositions of which are presented in Appendix 4.1b and Table 6.5. On initial inspection, these inclusions display compositions which resemble that of amphibole, however it is suggested here that these mineralogies reflect majorite compositions. Confirmation of a majoritic structure using X-ray diffraction has proved impossible due to the small size of the inclusions (< 40 μm). In the absence of such analyses, the discussion that follows can only be made somewhat speculatively.

The possible majorite association is made principally on the appreciably greater Si content associated with the mineral (+0.508-0.534 above the ideal 3 cations per formula unit of garnet). This necessitates the existence of Si in octahedral coordination, and suggests that these 'garnets' host a component of pyroxene in solid

solution. Akaogi & Akimoto (1979) have shown that pyroxene will become incorporated into the garnet structure at depths of 150 km in the upper mantle. This solid solution manifesting itself in an appreciable increase in the number of Si ions over the ideal 3.0 for 12 oxygens. Moore & Gurney (1985) have demonstrated that such solid solution among garnets found at Monastery Mine is consistent with the pressures and temperatures associated with the asthenospheric mantle and transition zone.

The increased Si is accompanied by increased M values (M = Mg+Fe+Ca+Na) from the ideal 3.0 expected for garnet. These Helam inclusions contain values of M between 3.455-3.468. Moore & Gurney (1985) report that an increase in both M and Si, as observed among these crystals, are required to form solid solution with pyroxene. Ca and Na enrichment is also clearly evident within these inclusions, which further attests to environments associated with exceedingly high pressures (Sobolev & Lavrent'ev, 1971).

There appears to be a negative correlation between Si and Al among these Helam garnets, suggesting that the substitutional scheme of Akaogi and Akimoto (1979) applied by Moore & Gurney (1985) also applies to the Helam diamonds. This scheme involves the substitution of two Al^{3+} ions in the octahedral sites of the garnet structure by both M^{2+} and Si^{4+} ions from the pyroxene structure ($M^{2+} = Mg^{2+} + Fe^{2+} + Ca^{2+}$). Na may be accommodated in the eight-coordinated dodecahedral site as was suggested by Sobolev & Lavrent'yev (1971), and applied by Moore & Gurney (1985).

Table 6.5 presents the compositions of the Helam majorites, together with representative analyses of majorites from Monastery (Moore & Gurney, 1985) and Jagersfontein (Rickard *et al.*, 1991). It is clear that the Helam majorite inclusions exhibit significantly higher chromium contents, possibly suggestive of a peridotitic association. In addition, the Helam majorites show relatively high calcium (between 20.18 - 20.45 wt% CaO) concentrations, and relatively low iron concentrations (between 3.33 – 3.39 wt.% FeO).

A sub-lithospheric component among the Helam diamonds has significance when considering the predicted origin of Group II kimberlites (Section 2.4.1). A majorite occurrence within the Swartruggens Kimberlite would add support to suggestions made by le Roex (1986) and Nowell *et al.* (1999) that Group II

Table 6.5 Chemical compositions for majorites from Helam diamonds, as well as representative analyses of majorite included in diamonds from Monastery (Moore & Gurney, 1985) and Jagersfontein (Rickard *et al.*, 1991) mines respectively. M = (Mg + Fe + Ca + Na)

	Helam		Monastery			Jagersfontein		
Oxides	**HM009e**	**HM009f**	**B9-17**	**A1-20**	**A1-24**	**J25**	**J27a**	**J32a**
SiO_2	47.44	47.98	43.45	45.43	47.43	42.96	44.79	47.29
TiO_2	0.60	0.60	1.15	0.81	0.78	0.19	0.23	0.19
Al_2O_3	10.19	9.71	16.3	14.82	11.29	19.34	16.69	14.09
Cr_2O_3	2.19	2.20	0.06	0.06	0.2	0.2	0.22	0.21
Na_2O	0.99	1.00	0.64	0.58	0.33	0.26	0.29	0.54
FeO	3.33	3.39	12.99	9.77	10.51	13	12.82	11
MnO	0.18	0.20	0.27	0.29	0.19	0.43	0.35	0.29
MgO	13.67	13.70	13.48	18.2	22.05	15.91	18.86	19.35
CaO	20.18	20.45	11.93	9.27	7.11	7.94	6.05	7.03
Total	**98.77**	**99.22**	**100.27**	**99.23**	**99.89**	**100.23**	**100.3**	**99.99**
Cations								
Si	3.508	3.534	3.216	3.316	3.429	3.137	3.246	3.411
Ti	0.033	0.033	0.064	0.044	0.042	0.010	0.013	0.010
Al	0.888	0.843	1.422	1.275	0.962	1.664	1.425	1.198
Cr	0.128	0.128	0.004	0.003	0.011	0.012	0.013	0.012
Na	0.141	0.142	0.092	0.082	0.046	0.037	0.041	0.076
Fe^{2+}	0.142	0.152	0.647	0.474	0.442	0.695	0.649	0.629
Fe^{3+}	0.064	0.057	0.157	0.123	0.194	0.099	0.128	0.035
Mn	0.011	0.012	0.017	0.018	0.012	0.027	0.021	0.018
Mg	1.507	1.504	1.488	1.980	2.376	1.732	2.037	2.081
Ca	1.599	1.613	0.946	0.725	0.551	0.621	0.470	0.543
Total	**8.021**	**8.019**	**8.053**	**8.041**	**8.065**	**8.033**	**8.043**	**8.012**
M	**3.453**	**3.469**	**3.330**	**3.384**	**3.609**	**3.183**	**3.325**	**3.363**

kimberlites may have their origins within the asthenosphere, and not *necessarily* within the lithosphere, as suggested by Smith (1983).

6.4.1.4 Clinopyroxene

Of all the Helam inclusions, clinopyroxene appears to show the greatest diversity in terms of chemical composition between diamonds (Appendix 4.1c). This, despite the fact that only 5 such crystals were recovered. In addition, all clinopyroxenes exhibit significant Ca-enrichment, plotting above the diopside-hedenbergite join in figure 6.2. The clinopyroxenes position on the ternary plot may be caused by their Na- (and thus Fe^{3+}) nature. Alternatively, these clinopyroxenes may indicate a Ca-enriched bulk rock composition. Similar Ca-enrichment has been observed among the clinopyroxene inclusions from Venetia (Viljoen *et al.*, 1999).

Various bi-variant plots of the clinopyroxene compositions are represented in figures 6.5. Due to the lack of data, no trends could be defined, however these figures are useful in illustrating the compositional variability between the different inclusions.

One diopsidic clinopyroxene (HM007a) has been assigned to the peridotitic paragenesis based on its relatively high Cr_2O_3 and MgO contents (3.02 wt% and 15.5 wt% respectively) and its relatively low Na_2O and Al_2O_3 contents (2.74 wt% and 2.11 wt% respectively). According to end-member calculations following Hatton (1978), this diopside comprises 42% enstatite, and 14% jadeite component. This diopside was further characterised by a distinctive pale green coloration.

One colourless omphacitic clinopyroxene (HM018e) is assigned to the eclogitic parageneses based on its relatively high Na_2O and Al_2O_3 contents (5.10 wt% and 5.35 wt% respectively). This omphacitic clinopyroxene is virtually free of Cr_2O_3. The inclusion exhibits a K_2O content of 0.08 wt% which is consistent with the observed enrichment of K in eclogitic clinopyroxene reported by other workers (e.g.: Tsai *et al.*, 1979; Gurney *et al.*, 1984; Moore & Gurney, 1985; McCandless & Gurney, 1989). As is the case for most omphacitic inclusions worldwide, this clinopyroxene appears to be a compositional mixture of jadeite ($NaAlSi_2O_6$) and diopside-hedenbergite ($Ca(Fe, Mg)Si_2O_6$) end-members (Meyer, 1987). This crystal comprises 30% jadeitic and 30% enstatite component, applying end-member calculations according to Hatton (1978).

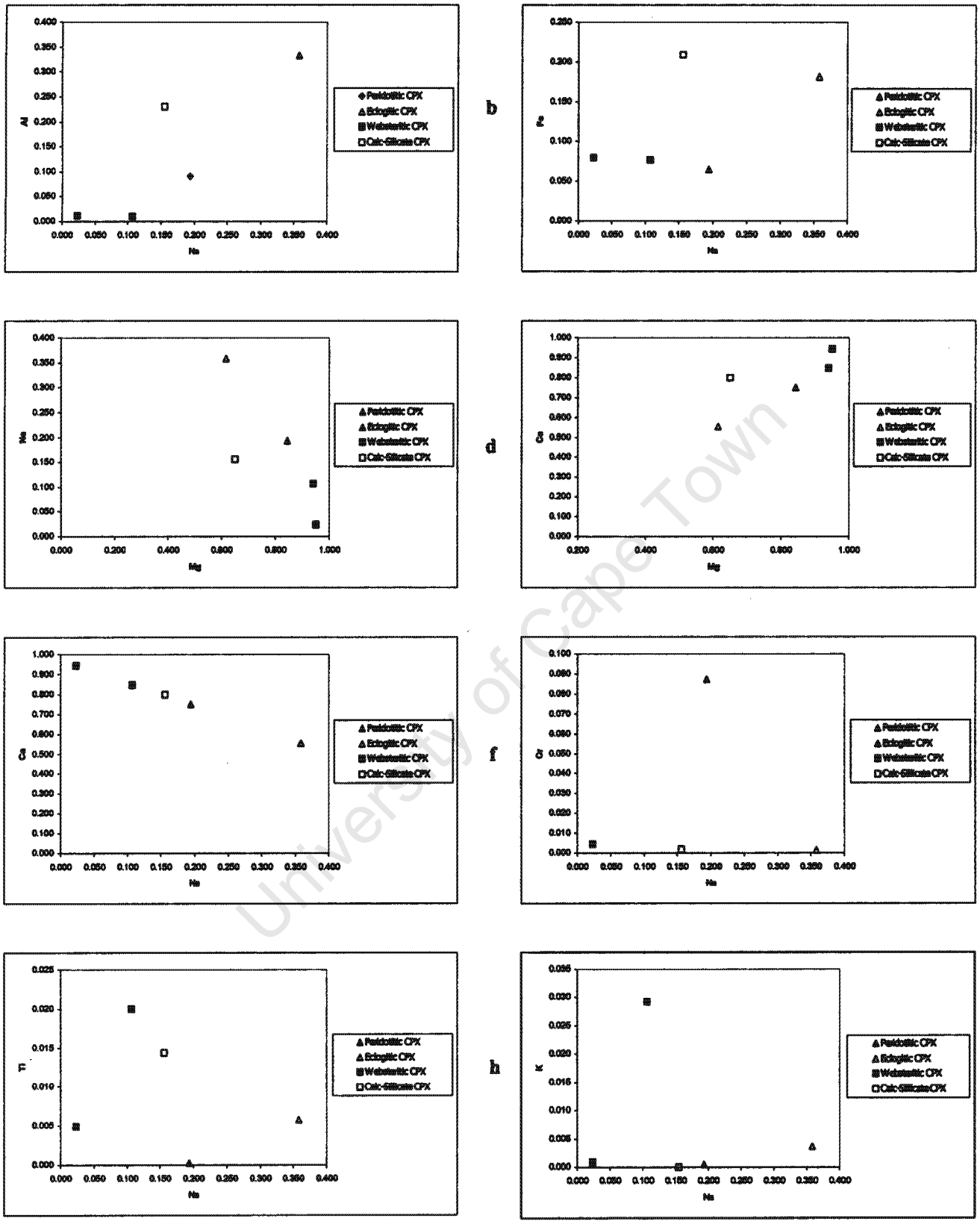

Figure 6.5 Inter-element relationships for clinopyroxene inclusions from Helam diamonds. Units are in cations per clinopyroxene formula unit.

Diamond HM008 yielded two colourless clinopyroxene inclusions with unusual compositions. While occurring within the same diamond, the two inclusions show some remarkable variations. MgO contents are relatively high (approximately 17.50 wt%), and CaO contents of 24.16 wt% and 22.02 wt% have been measured, however the low Cr_2O_3 contents (0.15 wt% and 0.08 wt%) are not consistent with a peridotitic origin. Consequently, these clinopyroxenes have been assigned to a websteritic parageneses.

Another unusual clinopyroxene was recovered from diamond HM3B11. This crystal is characterised by high CaO, Al_2O_3 and Na_2O (20.33 wt%, 5.35 wt% and 2.19 wt% respectively), and relatively low MgO content (11.87 wt%). The inclusion is similar to the Ca-rich pyroxenes from southeastern Australia (Sobolev *et al.*, 1984) and is identical to an inclusion recovered from Premier (Tsai *et al.*, 1979). It appears therefore, that this inclusion is another representative of the relatively uncommon calc-silicate paragenesis (Sobolev *et al.*, 1984). It is interesting to note that the inclusion was found co-existing with four websteritic garnets. This could be explained by episodic diamond crystallisation within two chemically different environments, attesting to a chemically dynamic mantle beneath the Swartruggens Kimberlite. The websteritic garnets together with this clinopyroxene result in unrealistically high mantle temperature calculations, which suggests disequilibrium between the phases.

Cation totals (Appendix 4.1c) suggest close to ideal occupancy of the T, M1 and M2 sites of the pyroxene structures. The eclogitic clinopyroxene appears to be the exception, in its higher than expected Al content and lower Si content, and it is suggested that in order to accommodate this, the pyroxene structure has had to incorporate Al into both the T and M1 sites. Excess Al can be accommodated by both the jadeite and enstatite components.

6.4.1.5 Orthopyroxene

One orthopyroxene crystal was recovered from diamond HM108 (Appendix 4.1c). This crystal is characterised by a Mg# of 88.3, which is lower than the worldwide range of peridotitic orthopyroxene (between 91-95) summarised by Meyer (1987). In addition the Helam orthopyroxene is virtually free of Cr_2O_3, and contains

approximately 0.22 wt% and 0.12 wt% CaO and Na_2O respectively. On this basis the orthopyroxene crystal has been assigned to the websteritic paragenesis.

6.4.1.6 SiO_2

An almost pure SiO_2 phase, while an uncommon inclusion within diamond, is well documented and has been associated with the eclogitic paragenesis (e.g.: Gurney *et. al*, 1984 and Moore & Gurney, 1989). At mantle pressures and temperatures SiO_2 is stable as coesite, and it follows therefore, that all SiO_2 inclusions *should* occur as coesite. The presence of coesite (high-pressure polymorph of SiO_2) as an inclusion within diamond was first identified by Milledge (1961). Subsequently numerous other studies have also positively identified coesite (e.g.: Gurney *et. al*, 1984 and Moore & Gurney, 1989) as the predominant form of SiO_2 in diamond. On this basis, more recent studies (e.g.: Chinn, 1995 and Westerlund, 2000) have identified coesite as an inclusion without confirming the crystal structure (the only reliable way to identify coesite).

Such assumptions should be made tentatively though, as quartz (1 atm. Polymorph of SiO_2), has also been observed within some diamonds (e.g.: Harris, 1968). It is suggested that the presence of quartz within a diamond is the result of polymorphic inversion from coesite (Meyer, 1987).

Twelve SiO_2 inclusions were recovered from ten Helam diamonds, occurring as small, colourless, cubo-octahedral inclusions. None of the inclusions were associated with penetrative fractures, and are all believed to be primary in nature. In one diamond (HM1B2) this mineral has been found to co-exist with an eclogitic garnet, confirming the association to the eclogitic paragenesis. SiO_2 has also been observed to coexist with corundum (HM114 and HM2B2) and eclogitic garnet (HM1B2). These SiO_2 inclusions are all essentially free of any minor element impurities (Appendix 4.1d).

Single crystal X-ray diffractometry was conducted on one such inclusion in order to establish its polymorphic structure. However, due to the small size of the inclusion, ambiguous and inconclusive data was generated. Assignation of the correct SiO_2 polymorph could thus not be made.

6.4.2 Oxide Inclusions

Oxide mineral inclusions are relatively common among the Helam diamond population, and commonly exist as multiple inclusions within a single diamond. Oxide mineralogies are presented in Appendix 4.2. It has been demonstrated that the oxide minerals of chromite and corundum, appear to be more abundant among the larger diamonds.

6.4.2.1 Chromite

Chromite inclusions are common among the Helam diamonds (28 recovered from 10 diamonds), and commonly occur as large (>100 μm), red-black inclusions displaying diamond induced morphologies (figure 4.23). All chromite inclusions have consequently been interpreted as being syngenetic with respect to diamond growth.

The Helam chromite inclusions have a restricted geochemical range (Appendix 4.2a), the majority of which fall within the range of most other chromite inclusions from worldwide localities (Meyer, 1987). The chromites are extremely rich in chromium, varying between 63.69 wt% and 69.39 wt% Cr_2O_3 (figure 6.6a). TiO_2 values are low varying between 0.05 wt% and 0.82 wt% (figure 6.6b). The Cr/(Cr+Al) ratio of the chromites is restricted between 0.91 and 0.97. While numerous inclusions may occur within a single diamond, the compositions of such inclusions are almost identical, despite differences in position within a diamond. Compositional variability can however be noted between mineral inclusions from different diamonds.

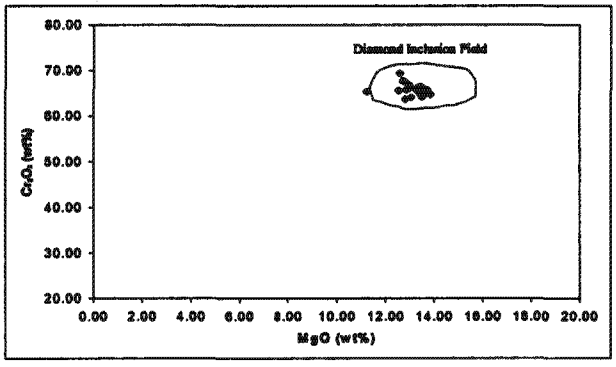

Figure 6.6a Relationship between Cr_2O_3 and MgO for chromite inclusions from Helam diamonds. Worldwide diamond inclusion field is shown.

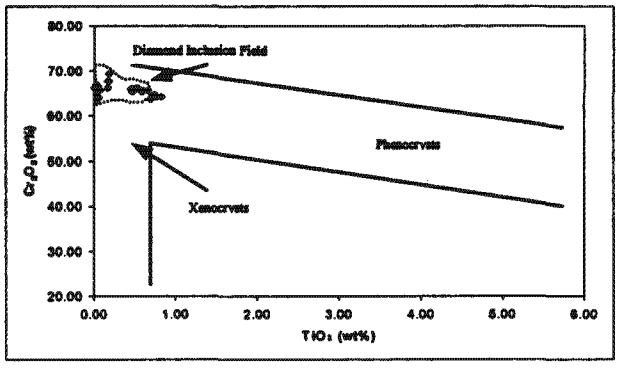

Figure 6.6b Relationship between Cr_2O_3 and TiO_2 for chromite inclusions from Helam diamonds. Worldwide diamond inclusion field is shown.

There appear to be three compositionally different species of chromite (figure 6.6c) among the Helam diamonds. The first group is associated with relatively low TiO_2 contents (between 0.00 wt% and 0.16 wt%), and variable Al_2O_3 contents (between 4.25 wt% and 5.89 wt%). The second group comprises chromites associated with somewhat higher TiO_2 contents (between 0.46 wt% and 0.76 wt%), and less variable Al_2O_3 contents (confined between 4.25 wt% and 4.86 wt%). The high-Ti chromites, while all closely associated with values from other diamond chromites, exhibit TiO_2 values which tend towards values more commonly associated with phenocrystic garnets. These unusually high-Ti chromites are not unlike those from Dokolwayo observed by Daniels (1991). The third group (all obtained from a single diamond) is characterised by very low Al_2O_3 contents (between 2.38 wt% and 2.47 wt%), and highly restricted TiO_2 contents (between 0.17 wt% and 0.18 wt%). The subtle paragenetic differences alluded to in the discussion of the olivine compositions, is thus supported by the compositional differences among the chromite inclusions, and the suggestion is made that together the olivines and chromites represent three compositionally different peridotitic parageneses. It is suggested that the most refractory mineral inclusions may in fact represent a dunitic paragenesis (an extension of the harzburgite facies).

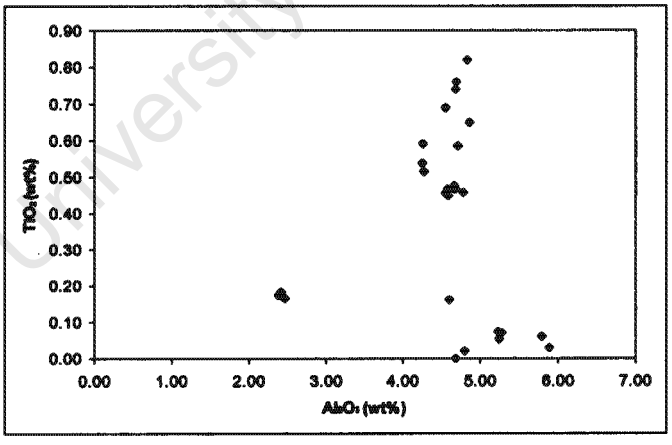

Figure 6.6c Relationship between TiO_2 and Al_2O_3 for chromite inclusions from Helam diamonds.

The solid solution of silicate-spinel component is favored by increasing pressure and temperature (Woodland and O'Neil, 1993). Stachel & Harris (1997) report chromites containing between 0.16 wt% and 0.42 wt% SiO_2, and have interpreted such values to suggest crystallisation unusually great depths. The Helam chromites, while exhibiting

limited solution of silicate-spinel component (between 0.08 wt% - 0.15 wt% SiO_2), are associated with significantly lower SiO_2 values than are reported by Stachel & Harris (1997). The SiO_2 content of the Helam chromite inclusions are more similar to values reported by other workers (e.g.: Tsai et al., 1979; Stachel *et al.*, 1998; Viljoen *et al.* 1999), suggesting that that the Helam chromites have crystallised within 'typical' peridotitic mantle environments.

6.4.2.2 Corundum

Corundum too, is commonly observed within Helam diamonds (25 inclusions recovered from 6 diamonds), and all display cubo-octahedral morphologies. The colourless corundum inclusions commonly occur as clusters of discrete inclusions near the center of diamond host. In two diamonds, corundum is found to co-exist with SiO_2 (HM114 and HM2B2), which both confirms the minerals eclogitic association, and suggests that corundum, SiO_2, and by inference eclogitic garnet are all paragenetically related.

Corundum, while rarely observed as an inclusion within diamond, was first reported by Meyer & Gubelin (1981). The red corundum (ruby) inclusion was recovered from a diamond of unknown origin. Other than Al_2O_3, the only other major component was Cr_2O_3 (1.3 wt%), which most likely imparted the colour to the inclusion. Harris *et al.*, (1994), also document the occurrence of chrome-enriched corundum inclusions, from the Sao Luiz alluvial deposit in Brazil, consisting of 8.58 wt% Cr_2O_3. Another variety of corundum included within diamond, shows enrichment in TiO_2. Moore & Gurney (1989) report the existence of a corundum inclusion from the Monastery mine, with 3.05 wt% TiO_2. In addition Otter & Gurney (1986) document two Ti-enriched corundum inclusions from Sloan, containing 1.1 and 2.0 wt% TiO_2 respectively.

In contrast to the observations made by the above workers, corundum recovered from the Helam diamonds, show an absence of both Cr_2O_3 and TiO_2, and are almost pure Al_2O_3 (Appendix 4.2b). These inclusions are similar to those reported by Viljoen *et al.* (1999), Hill (1989) and Ulansky (pers. comm., 2001) who also report corundum inclusions essentially free of trace element impurities. Analyses conducted on multiple spots on single inclusions have shown that these corundum inclusions are

chemically homogeneous. It appears therefore that the Helam corundum relates more to naturally occurring corundum found within eclogite xenoliths, which also typically contain exceedingly low concentrations of Cr_2O_3, TiO_2 and FeO (Dawson & Carswell 1990).

Corundum is an accessory mineral in eclogite-grospydite mantle xenoliths (Dawson & Carswell, 1990). Within rare corganite and corgaspinite xenoliths, Mazzone & Haggerty (1989) observe as much as 75 modal per cent corundum associated with the rocks. These unusual rock types are related to alkremites. It follows therefore, that the most likely parageneses for the Helam diamonds containing corundum are eclogite-grospydite or corganite-corgaspinite.

Corundum bearing eclogites (peraluminous eclogites) are commonly low in SiO_2, and are very low in iron. The co-existence of SiO_2 with corundum in diamonds HM114 and HM2B2, appear to represent a paradox. Schmidt *et al.* (1997) suggest that coexisting SiO_2 and Corundum would only be stable at exceedingly high pressures (between 14 and 17.5 Gpa at 1000 °C and 2000 °C respectively) as a result of the decomposition of kyanite. Within the Helam diamonds however, these coexisting phases were not found to be touching, and consequently equilibrium between the two phases can not be assumed. It follows therefore that an assumption of a high-pressure paragenesis for these diamonds would be questionable in the absence of independent information. It is perhaps more reasonable to assume that the different oxides were incorporated into the diamonds at different times during diamond growth within somewhat disparate mantle environments.

6.4.3 Sulphide Inclusions

While most other inclusions correspond quite well with mineralogical abundances observed within xenoliths, there is a striking difference in the abundance of sulphide inclusions in diamonds and that associated with xenoliths. Sulphide inclusions are interesting in that they are the most common syngenetic inclusion observed within diamond, and are thus seemingly overrepresented when compared to the abundance of sulphide minerals in mantle xenoliths (Gurney, 1989).

While the relationship between silicate parageneses and sulphide inclusion chemistry is well defined among the Siberian diamonds (e.g.:Yefimova *et al.*, 1983;

Bulanova *et al.*, 1996), this is less clear among the African diamonds. This is principally due to the apparent lack of silicates coexisting with sulphides within African diamonds (Deines & Harris, 1995). As mentioned above, sulphide-bearing diamonds from Siberia can be assigned to a paragenesis based on their Ni content. Peridotitic diamonds have Ni-contents that range between 16.5-29.8 wt%, while the eclogitic sulphides range between 0.5-8.2 wt% (Gurney, 1989).

The major difficulty in working with sulphide inclusions is the fact that they readily re-equilibrate with changing conditions of temperature. Furthermore, the effect of pressure on the stability fields of the various phases remains largely unknown. Kullerud (1962) suggests that under the conditions associated with diamond formation, syngenetic sulphide inclusions in diamond are likely to have formed either by trapping a primary sulphide fluid/melt, or as crystals of monosulphide solid solution (mss) or pyrrhotite during diamond crystallisation. Subsequent subsolidus exsolutions of mss lead to a mineral sequence pyrite, pyrrhotite, chalcopyrite, pentlandite, cubanite and heazlewoodite as the temperature decreases on eruption of the kimberlite (Craig & Kullerund, 1969).

The principal difficulty therefore in any study of sulphide inclusions, is thus interpreting the geological history through which a sulphide inclusion has passed.

56 analyses of 43 sulphides from 28 Helam diamonds have been determined, and have been plotted in figure 6.7 in terms of their S, Fe and Ni contents. Pyrrhotite, monosulphide solution, pentlandite, chalcopyrite and heazlewoodite were all identified as sulphide phases within the Helam diamonds (figure 6.8), the compositions of which are presented in Appendix 4.3. Careful attention was paid to the existence of multiple phases and exsolution features. Where multiple phases were easily distinguished, these phases were analysed individually. It follows therefore that the analyses presented and discussed in this section are a fair reflection of the abundance and variability of sulphide phases within the Helam diamonds. Table 6.6 shows the abundance of sulphide mineral assemblages from the Helam diamonds.

The Helam sulphide inclusions often occur as multiple inclusions within individual diamonds, and commonly occupy the central regions of the diamond host. The sulphide inclusions are ubiquitously characterised by black rosette structures, and vary in size between 40 μm to 150 μm. The sulphide inclusions often exhibit diamond induced morphologies, commonly of rounded cubo-octahedra (figure 6.9), cubo-

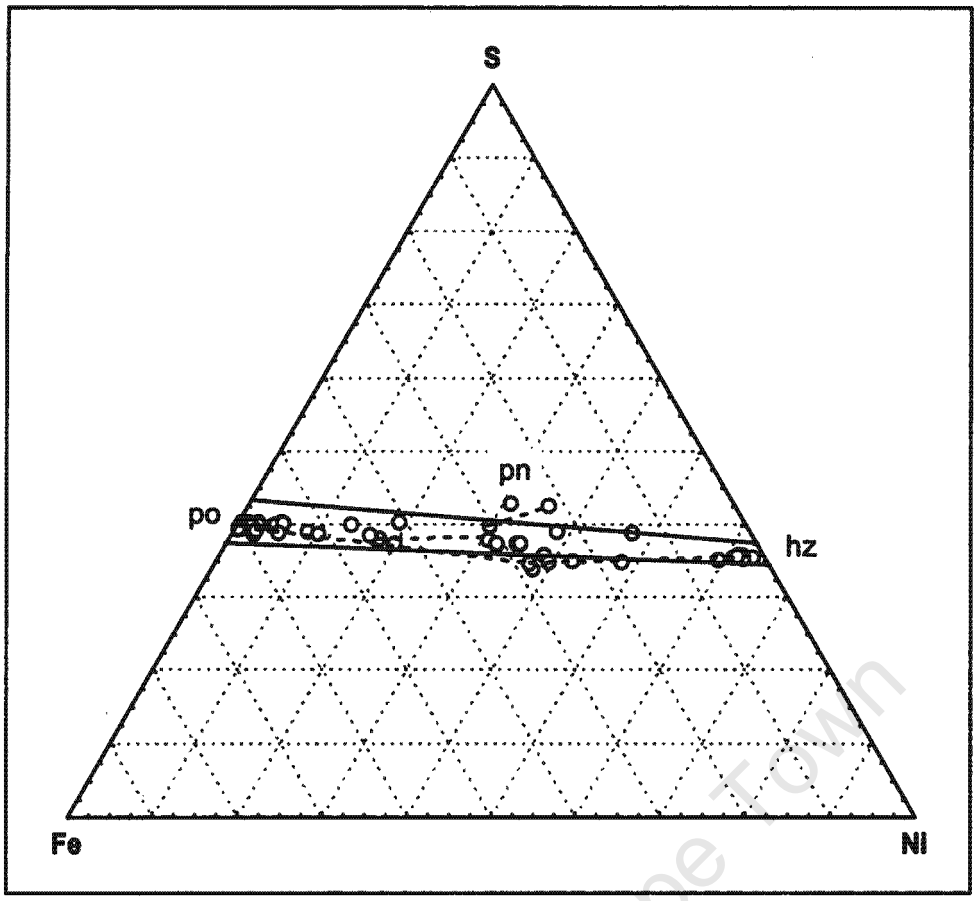

Figure 6.7 S-Fe-Ni ternary diagram showing the compositions of the sulphide phases from Helam diamonds, with respect to mss stability at 650 °C (solid lines). Dashed lines indicate coexisting sulphide phases within individual diamonds. po = pyrrhotite, pn = pentlandite, hz = heazlewoodite.

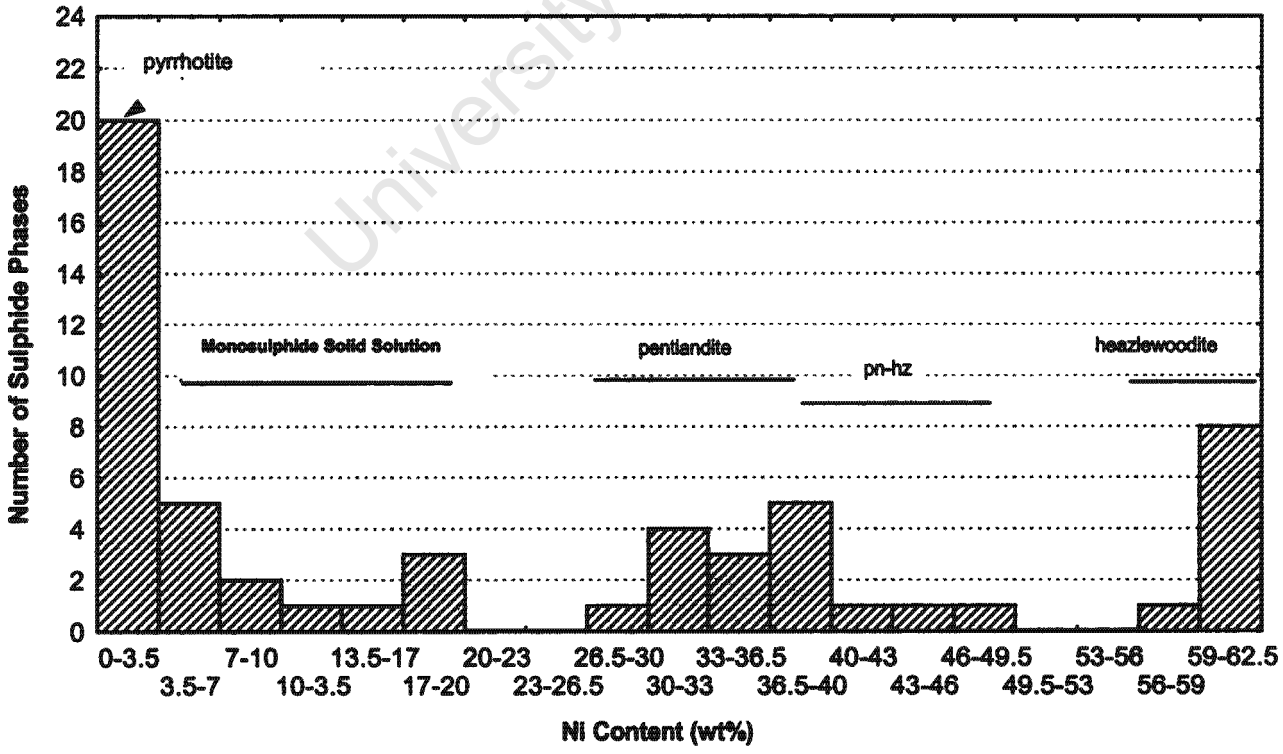

Figure 6.8 Histogram illustrating the number of sulphide phases observed within the Helam diamonds.

octahedra (figure 6.10), and octahedra (figure 6.11), suggesting a syngenetic relationship with their host. While the majority of the sulphides appear to be homogeneous in composition on their exterior surfaces, some sulphides exhibit extensive exsolution lamellae (figures 6.11 & 6.12). Polishing of the inclusions for microprobe analyses have revealed that internally, these sulphides can comprise numerous different sulphide phases.

Table 6.6: The abundance of sulphide minerals (number of observations) from Helam diamonds.

Mineral Assemblage	Number of Observations
mss	3
mss+pn+hz	1
mss+pn	1
mss+po	7
po	12
po+hz	1
pn	9
pn+hz	1
hz	5
pn-hz	3
Total	**43**

mss = monosulphide solid solution, pn = pentlandite, hz = heazlewoodite, po = pyrrhotite.

Many of the sulphides are associated with 'pits' (figures 6.13-16) on their external surfaces (up to 4 μm in size) which are either triangular/prismatic or hexagonal in shape. While the triangular/prismatic pits are easily explained as diamond induced features, the hexagonally shaped pits appear enigmatic. These pits (commonly very shallow) are not associated with ex-solution, as they can be seen to cross-cut ex-solution lamellae (figure 6.16), and are not associated with corresponding topography on the host diamond surfaces. These observations are consistent with those on Klipspringer diamonds, and it has been suggested by Westerlund (2000) that these may represent sites of fluid entrapment.

Figure 6.9a SEM secondary electron photomicrograph of a pyrrhotite inclusion from diamond HM1A11. The inclusion is characterised by a rounded cubo-octahedral morphology and triangular/ prismatic pits.

Figure 6.9b SEM back-scatter photo-micrograph of a pyrrhotite inclusion from diamond HM1A11. Homogeneous surface coloration suggests that pyrrhotite is the only sulphide phase on the inclusions surface

Figure 6.10a SEM secondary electron photomicrograph of a chalcopyrite inclusion from diamond HM1A12. The diamond induced, cubo-octahdral morphology is clearly visible.

Figure 6.10b SEM back-scatter electron photo-micrograph of a chalcopyrite inclusion from diamond HM1A12. Differences in coloration on the crystal surface may indicate subtle chemical variability across the crystal surface

Figure 6.11a SEM secondary electron photomicrograph of a pyrrhotite inclusion from diamond HM3B10. Diamond induced morphologies are apparent, with the inclusion exhibiting octahedral form. The inclusion is characterised by abundant exsolution lamellae.

Figure 6.11b SEM back-scatter photo-micrograph of a pyrrhotite inclusion from diamond HM3B10. Exsolution lamellae are clearly visible

Figure 6.12a High magnification SEM secondary electron photomicrograph of a pyrrhotite inclusion from diamond HM3B10.

Figure 6.12b High magnification back-scatter photo-micrograph of a pyrrhotite inclusion from diamond HM3B10. Exsolution lamellae are clearly visible

Figure 6.13 High magnification SEM secondary electron photomicrograph of a pyrrhotite inclusion from diamond HM1A11, illustrating triangular/ prismatic pits on one of its surfaces.

Figure 6.14 High magnification SEM secondary electron photomicrograph of a pyrrhotite inclusion from diamond HM1A11, illustrating shallow hexagonally-shaped pits on one of its surfaces.

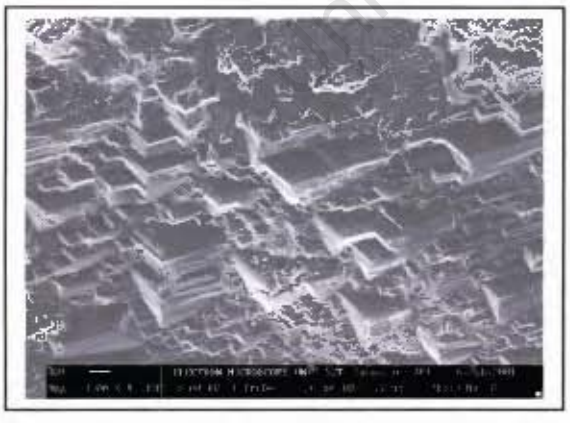

Figure 6.15 High magnification SEM secondary electron photomicrograph of a pyrrhotite inclusion from diamond HM1A6, illustrating numerous triangular/prismatic pits on one of its surfaces.

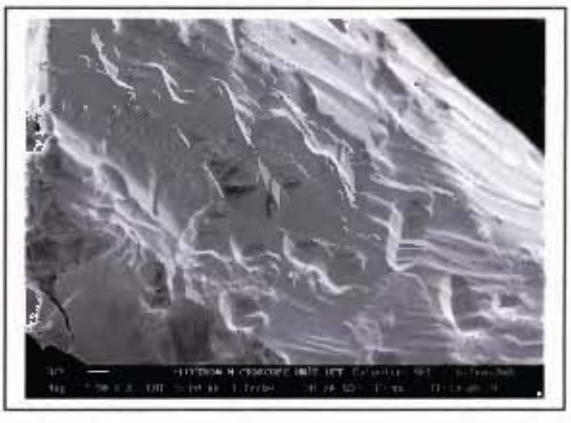

Figure 6.16 High magnification SEM secondary electron photomicrograph of a pyrrhotite inclusion from diamond HM1B2, illustrating both triangular and hexagonal pits on one of its surfaces. The inclusions is further characterised by fine pentlandite exsolution lamellae.

6.4.3.1 Monosulphide Solid Solution

Inclusions of monosulphide solid solution (mss) were identified after careful examination using SEM imagery revealed no exsolution textures, and in addition contained more than 2.5 wt% Ni (Appendix 4.3a). Mss can also be identified as having compositions that do not readily correspond to other common sulphide phases. Figure 6.17 illustrates the composition of the Helam mss inclusions in terms of their Ni content. Of the twelve mss identified among the Helam diamonds, seven correspond to values assigned to Siberian diamonds of the eclogitic paragenesis, and four correspond to those of the peridotitic paragenesis (Yefimova *et al.*, 1983). One mss falls between the two groups, but corresponds with values assigned to the 'pyroxenetic' paragenesis (Bulanova *et al.*, 1996).

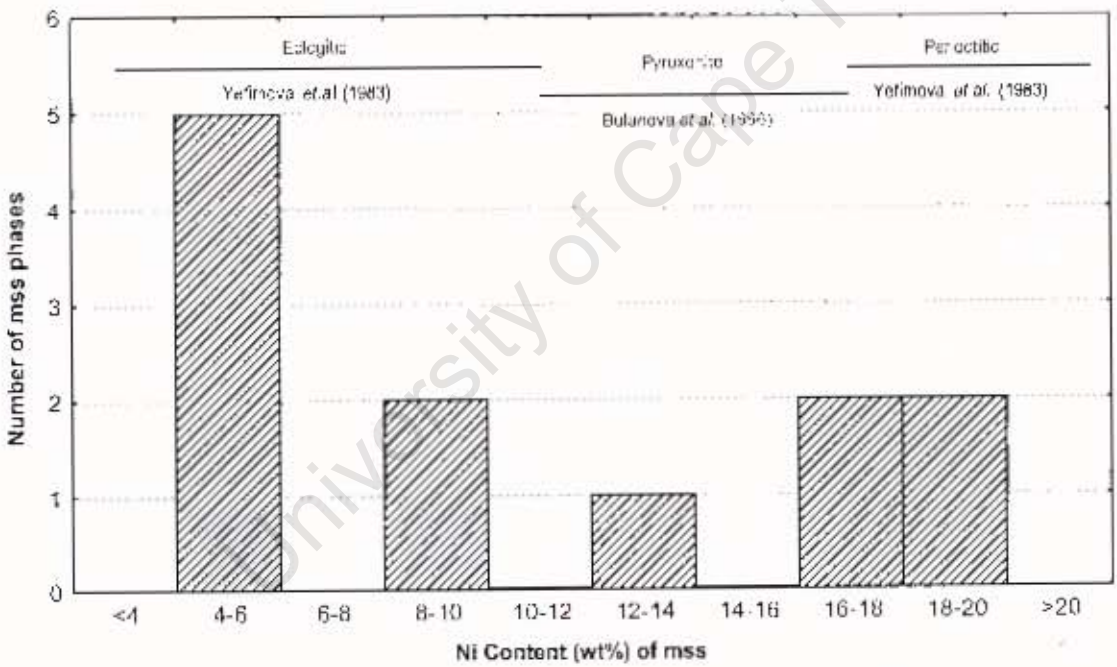

Figure 6.17 Histogram illustrating the number and Ni-content of the mss phases observed within the Helam diamonds with respect to the paragenetic assignation of Siberian diamonds.

These observations are consistent with those of Deines & Harris (1995), who suggest that higher cut-off values should be applied to African diamonds. Perhaps then, the eclogitic field (for African diamonds) should be extended to incorporate the single intermediate mss (ie: up to 16 wt% Ni).

Those Helam diamonds containing mss inclusions were assigned to particular parageneses based on the Ni-content of the mss as discussed above. Two diamonds (HM008 & HM3B4) contained olivine inclusions coexisting with mss inclusions. The Ni-content of the mss from the two diamonds were of 17.3 wt% 19.2 wt% respectively thus complimenting the assignation of a peridotitic paragenesis based on the sulphides co-existence with olivine. Those diamonds without any co-existing silicates or mss were assigned to parageneses based on the estimated bulk Ni-content of their sulphide inclusions, which approximates the Ni-content of the mss from which they must have exsolved. In a few cases, where only one phase was analysed, no estimation of the initial bulk Ni-content could be made, and consequently no paragenetic assignation could be made.

It is interesting to note that the two diamonds (HM008 & HM3B4), that exhibit coexisting olivine and mss, yielded olivine inclusions that were quite distinct from the majority of other olivine inclusions (Section 6.4.1.1). There appears to be a positive correlation between the Ni content of coexisting olivine and mss inclusions among the Helam diamonds.

6.4.3.2 Pyrrhotite

Pyrrhotite represents the first phase to exsolve from an mss (at approximately 1000 °C), as a result of the decrease in temperature associated with the diamonds transport to surface (Craig & Kullerud, 1969).

Individual inclusions from Helam are dominated by pyrrhotite, which commonly constitutes between 90-100% of the inclusion (figure 6.9). The pyrrhotite inclusions exhibit compositions close to pure Fe_7S_8, but all contain some Ni (up to 2.47 wt%), Cu (up to 0.37 wt%) and Co (up to 0.52 wt%) impurity (Appendix 4.3b). The high amounts of Ni present may be the result of Fe substitution within the pyrrhotite structure, or may simply represent sub-microscopic pentlandite exsolution. These minor element concentrations are similar to those observed in association with Klipspringer sulphide inclusions (Westerlund, 2000), suggesting the presence of similar sulphide fluids/melts at the time of diamond formation between the two localities.

6.4.3.3 Pentlandite

Pentlandite can be observed as exsolution lamellae (figures 6.11 & 6.12), or may constitute the major component of the sulphide inclusion. Craig & Kullerud (1969), suggest that exsolution of pentlandite from an mss occurs at 610 °C. The composition of pentlandite among the Helam diamonds is highly variable in terms of its Fe (between 21.4 – 30.4 wt%), Ni (between 28.5 – 38.1 wt%) and Co (between 0.15 – 2.5 wt%) contents (Appendix 4.3c), which is explained simply by varying degrees of Fe and Ni substitution into the $(Fe,Ni)_9S_8$ structure, together with sub-microscopic exsolution which ubiquitously characterise this phase.

6.4.3.4 Heazlewoodite

Heazlewoodite, rarely observed within diamonds (Deines & Harris, 1995), is a relatively common sulphide phase amongst the Helam diamonds. This sulphide represents the lowest temperature exsolution from mss, which occurs below 556 °C (Craig & Kullerud, 1969). These inclusions tend towards the pure Ni_3S_2 structure, however traces of Fe (between 1.47-5.56 wt%), Co (between 0.00-0.35 wt%), and Cu (between 0.00-1.56 wt%) are common (Appendix 4.3d). This can be explained by sub-microscopic pentlandite exsolution. Where such exsolution is prevalent heazlewoodite-pentlandite compositions result (Appendix 4.3d).

6.4.3.5 Chalcopyrite

One chalcopyrite inclusion (HM1A12a) was recovered from the Helam diamonds (figure 6.10), but was not analysed using the electron microprobe, as it was preserved for Re-Os dating. EDS analyses of the surface of the inclusion confirmed the nature of the grain as close to stoichiometric chalcopyrite. It is believed, based on observations made by other authors (e.g.: Westerlund, 2000) that the chalcopyrite mineralisation only represents a thin rim over a pyrrhotite or pentlandite core.

The lack of chalcopyrite within Helam diamonds may be explained by the preferential crystallisation of this phase within the decompression cracks created during the diamonds transport to surface, forming the rosette structures which

characterise the sulphide inclusions. An absence of abundant chalcopyrite, can perhaps also be explained by the ubiquitously low Cu content of the Helam mss.

6.4.3.6 Re-Os Isotope Analysis of Sulphide Inclusions

Re-Os analysis of six Helam eclogitic sulphide inclusions was conducted in an independent study, by K. Westerlund, at the Carnegie Institution of Washington. The Re and Os were analysed using negative thermal ionisation mass spectrometry (NTIMS), employing techniques described in Pearson *et al.* (1998). Despite the generation of reliable Os data, high Re blanks incurred during experimentation have resulted in somewhat spurious Re data, and consequently the integrity of the study is questionable (Westerlund, pers. comm., 2001). Nevertheless, the data has been included and *briefly* discussed as the study provides some important, if somewhat speculative information regarding the age of some of the Helam diamonds.

The morphology of the Helam sulphide inclusions has been described above. The Re and Os contents of the sulphides range between 262 – 1885 ppb and 49 – 222 ppb respectively (Table 6.7). The Os concentrations are consistent with eclogitic sulphide values (Pearson et al., 1998; Richardson *et al.*, 2001). In addition, all $^{187}Os/^{188}Os$ ratios are elevated compared to present day primitive mantle ($^{187}Os/^{188}Os$ = 0.1287), which is also consistent with high $^{187}Re/^{188}Os$ of eclogitic sulphides. The $^{187}Os/^{188}Os$ ratios suggest that the sulphide inclusions crystallised from a source that must have been separated from the primitive mantle at some time in the past to allow for the growth of ^{187}Os to yield $^{187}Os/^{188}Os$ of 0.77-8.55.

Despite the inherent uncertainties associated with this study, due to the spurious Re data, four of the six sulphide inclusions yield *plausible* model ages (1.18 – 3.74 Ga). The other two samples require at least a 2-stage history to explain their unsupported $^{187}Os/^{188}Os$ ratios. Perhaps the most significant conclusion that can be drawn from the data is that there are no hints of a young age, and it is likely that most of the ages are Archean or early Proterozoic, assuming a single stage growth history. Despite the fact that the data is not suitable for detailed petrogenetic discussion, an acceptable constraint on the age of the diamonds can be obtained to be used in conjunction with N-aggregation data, in determining time-averaged temperature estimations for the Helam diamond population (Chapter 5).

Table 6.7 Re-Os abundances, isotopic ratios and model ages for the Helam eclogitic sulphide inclusions. Model ages are calculated assuming a chondritic mantle source. Data and comments courtesy of K. Westerlund.

Sample	Re (ppb)	Os (ppb)	$^{187}Os/^{188}Os$	$^{187}Re/^{188}Os$	Model Age (Ga)	Comments
HM1A12	262	61	2.17	26.1	4.58	Model age = age of the earth, unrealistic
HM1A11	1885	103	8.32	182.2	2.65	Realistic model age, Re content unusually high
HM3A11	642	49	8.55	131.2	3.75	Realistic Re and Os content and model age
HM1A6	349	65	1.92	32.0	3.32	Realistic Re and Os content and model age
HM1B2	329	222	8.39	14.8	27.24	Radiogenic Os unsupported by Re, unrealistic model age
HM3B10	1092	174	0.77	32.9	1.18	High Re content, realistic model age

Figure 6.18 illustrates a Re-Os isochron diagram for the Helam sulphides. Reference lines for a 2.9 Ga and a 1 Ga age have been constructed assuming a chondritic initial isotope composition ($^{187}Os/^{188}Os = 0.1287$; $^{188}Re/^{188}Os = 0.4243$). It is suggested that the sulphides from diamonds HM1A11, HM3A11 and HM1A6 represent a 2.9 Ga diamond forming event, and that this age corresponds to the well constrained 2.9 Ga isochron age reported by Richardson *et al.* (2001) for Kimberley eclogitic sulphide inclusions. It is suggested therefore that these Helam eclogitic sulphide inclusions represent the same regional eclogitic diamond formation event, as a result of Archean subduction of oceanic crust, suggested by Richardson *et al.* (2001).

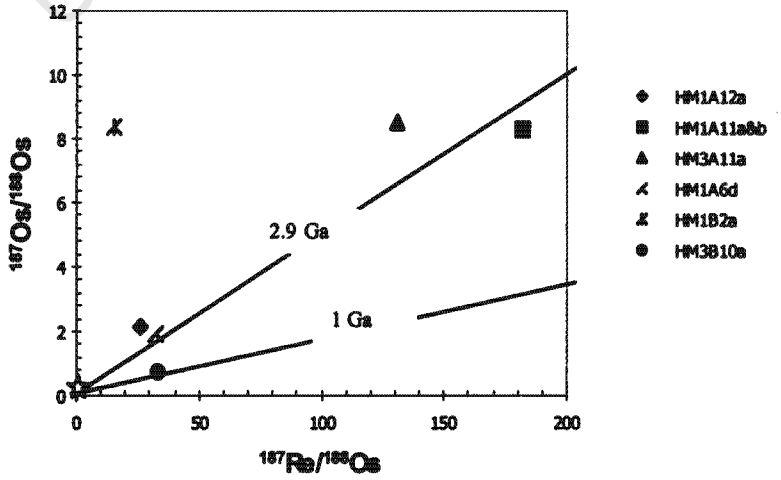

Figure 6.18 Re-Os isochron diagram for Helam eclogitic sulphide inclusions. Solid lines represent reference lines 2.9 Ga and 1 Ga, which have been constructed assuming a chondritic initial isotopic composition. Star marks the position of chondritic mantle.

One sulphide inclusion (HM3B10) yields a model age of 1.18 Ga, possibly suggesting a second, Proterozoic generation of eclogitic diamonds. This Proterozoic age compares favorably with Proterozoic ages from other Kaapvaal eclogitic diamonds (e.g.: Richardson, 1986; Pearson *et al.*, 1998), suggesting episodic diamond formation events.

6.4.4 Inclusions of Diamond

Inclusions of diamond within diamond are common among the Helam diamonds (figures 4.20 & 4.21), attesting to multiple, episodic diamond growth events. They commonly exhibit octahedral morphologies, the crystal faces sub-parallel to that of the host diamond. An inclusion of diamond has been found in association with three chromite inclusions in diamond HB3C3.

6.5 Gethermobarometry

Detailed thermobarometric investigation of the Helam diamond suite has been hampered by the distinct lack of co-existing silicate and oxide minerals. Diamond HM3B11 was the only diamond studied that contained coexisting garnet and clinopyroxene inclusions. Unfortunately, the silicate minerals appear to represent a disequilibrium assemblage indicative of two distinct mineral parageneses; having been incorporated into the diamond during different crystallisation events, associated with different chemical environments. Similar disequilibrium between diamond inclusions has been noted by other workers, and has been as extreme as the coexistence of eclogitic and peridotitic minerals within a single diamond (e.g.: Prinz *et al.*, 1975; Hall & Smith, 1984, Moore & Gurney, 1989, Otter, 1990). Consequently, no reasonable temperature estimates could be made from the mineral inclusion suite.

Assuming a mantle residence time of 2.75 Ga, nitrogen aggregation characteristics of the Helam diamond have been useful in constraining mantle residence temperatures, independently of the mineral inclusions. FTIR analysis of the Helam diamond plates (Chapter 5) suggest mantle residence temperatures in the range of between 1090 °C – 1110 °C for the vast majority of Helam diamonds. No distinctions could be made between the FTIR characteristics of the eclogitic and

peridotitic diamonds (as determined by their inclusion compositions), suggesting that both parageneses were associated with similar temperature environments.

The incorporation of K into the clinopyroxene lattice is pressure dependent (Erlank & Kushiro, 1970), with a minimum of 32 kb required. Harlow (1992) suggests that such K solubility in clinopyroxene exists at temperatures of 1200-1500 °C and pressures of 50-60 kb. The incorporation of 0.08 wt% K_2O in the eclogitic clinopyroxene of diamond HM018 suggests therefore, that such conditions are associated with the eclogitic source. If this assumption is correct, then the eclogitic clinopyroxene records temperatures in excess of 100 °C hotter than the mantle residence temperatures calculated from the FTIR characteristics of the nitrogen impurity within diamond. Perhaps the FTIR data reflects a cooling of the mantle subsequent to the encapsulation of the inclusion.

The existence of a possible majoritic component is suggestive of a deep, possibly asthenospheric source region for some of the Helam diamonds. The co-existence of SiO_2 and corundum within some Helam diamonds may provide yet further evidence for a deep origin for some of the Helam diamonds, but only if these phases were in equilibrium at the time of encapsulation within the diamond. As discussed earlier however, the coexisting oxide phases were non-touching, and thus equilibrium could not be confirmed. Consequently the suggestion that these diamonds represent high pressure diamond parageneses remains questionable.

6.6 Discussion

6.6.1 Diamond Parageneses

From the mineral inclusion studies, it becomes clear that the peridotitic diamonds crystallised within a highly depleted, magnesian substrate/s, which comprised predominantly chromite and olivine. These diamonds prescribe to a substrate that was most likely a chromite-rich harzburgite or chromite-rich dunite (possibly both). Multiple populations of chromite and olivine are suggestive of at least three compositionally different peridotitic parageneses.

Variations in both nitrogen and hydrogen characteristics observed as a function of diamond growth within the Helam diamond plates (Chapter 5), have

provided evidence in support of episodic diamond growth. Mineral inclusions could therefore have been incorporated during *any* of the crystallisation events, which may have been separated by millions of years. It is reasonable then, that the compositional differences observed among the mineral inclusions may have recorded subtle chemical changes that occurred within the mantle between the various crystallisation events. However, the compositional similarities between multiple inclusions from individual stones, *despite* their location within the diamond, suggests that chemical change (in terms of the major elements) within the diamond substrate has been very limited. It is suggested here, therefore, that the multiple populations of silicate and oxide minerals observed among the Helam diamonds, represent disparate mineral parageneses, and attest to a heterogeneous mantle beneath the Swartruggens Kimberlite with several units of diamondiferous source rocks.

A significant contribution of diamond from an eclogitic source is also apparent. It appears that the eclogitic diamonds crystallised in a per-aluminous eclogitic substrate characterised by abundant corundum and/or coesite, two phases not commonly associated with eclogite. It is suggested that subduction of an Al, Ca-rich sediment, may result in the unusual chemistry that characterises the eclogite. It is suggested that the eclogitic diamonds have crystallised within a grospydite-eclogite substrate.

A minor component of the Helam diamond suite is represented by a websteritic paragenesis. Websteritic garnet, clinopyroxene and orthopyroxene have been identified in small amounts. It is suggested that the websteritic component may have manifest itself in the form of veins within the upper mantle. Intrusion of such veins into the chromite harzburgite substrate may explain the co-existence of websteritic inclusions with peridotitic inclusions. Alternatively, episodic diamond growth within two different environments, may explain the co-existence of minerals from different parageneses. A subordinate calc-silicate component may also have been emplaced as veins, imparting the unusual chemistry associated with the calc-silicate clinopyroxene inclusion (HM3B11).

It is suggested that the Helam diamonds crystallised during multiple (at least 3) episodic diamond forming events within a thick, highly depleted, highly magnesian chromite-harzburgite/dunite lithosphere, which enclosed significant per-aluminous eclogite lenses and minor websteritic and calc-silicate veins. This suggestion is

largely consistent with observations made in Chapter 3 based on the kimberlite macrocryst analyses. The absence of sub-calcic garnet inclusions within the Helam diamonds, while somewhat surprising, has been noted by workers from other localities (e.g.: Chinn, 1995; Westerlund, 2000), and demonstrates the importance of both macrocryst *and* inclusion analyses in establishing the paragenetic sources of a diamond population. Clearly a volumetrically significant, peridotitic, potentially diamondiferous, garnet-bearing substrate *has* been sampled by the Swartruggens kimberlite (macrocrysts), however the contribution of diamonds from this source is not large. Instead it is believed that the majority of peridotitic diamonds have sampled from predominantly chromite- and olivine-bearing lithologies (chromite harzburgite/dunite).

Diamonds with mixed parageneses attest to episodic diamond crystallisation within changing chemical environments.

6.6.1.1 Relationship between Paragenetic Assignation and Diamond Body Colour

In general, diamond body colour is not exclusive to any particular paragenesis. The observation that the colourless and brown Helam diamonds play host to both peridotitic and eclogitic mineral inclusions is therefore not surprising. However, it should be noted that only *eclogitic* silicate and oxide inclusions have been found within the low-nitrogen, canary-yellow diamonds. In addition only low-Ni sulphides have been sampled from these canary-yellow diamonds. Consequently it is suggested that all canary-yellow Helam diamonds are eclogitic.

The silicate minerals sampled from these canary-yellow diamonds have been noted to be of subtly different chemical composition than their counterparts found within the colourless diamonds. The inference therefore is that the yellow diamonds crystallised during a distinct eclogitic diamond forming event. While it remains unclear whether these yellow diamonds are spatially related to the other eclogitic diamonds, the broad similarities between the compositions of the various inclusions, suggest that they have formed in a similar environment. It appears that hiatus in diamond growth has been accompanied by subtle chemical evolution of the mantle, resulting in the observed compositional differences between the inclusions from diamonds that have crystallised at different times.

6.6.1.2 Relationship between Paragenetic Assignation and IR Characteristics of the Diamonds

Only eclogitic mineral inclusions have been found within the canary-yellow diamond population, and consequently these diamonds have all been associated with an eclogitic paragenesis. FTIR and EPR analysis of these diamonds (Chapter 5) demonstrate that these diamonds are characterised by ubiquitously low (typically < 150 ppm) nitrogen concentrations, and all contain a Type Ib diamond component.

Despite the considerable overlap in observed IR properties between the diamonds of different parageneses, the range in nitrogen concentrations and aggregation states of the various types of IaA-IaB diamond do appear somewhat distinctive. Apart from diamond HM114 (green diamond), Type IaA-IaB diamonds assigned to the eclogitic paragenesis, are commonly associated with low nitrogen concentrations (104 ppm – 371 ppm), and low aggregation states (> 15 %N as B). It appears therefore that eclogitic diamonds, from both the Ib-IaA series and the IaA-IaB series, are characterised by low nitrogen concentrations and lower aggregation states. This may provide further support for the proposal that the canary-yellow diamonds are associated with a similar crystallisation environment as the other eclogitic diamonds. The similarity in the types and compositions of the eclogitic mineral inclusions found within the different types of diamond, is in agreement with this suggestion. Diamond HM114 displays the elevated nitrogen concentration (1159 ppm), and mature aggregation state (34.5 %N as B) characteristic of the green diamonds. This suggests that the green diamonds may well be associated with a somewhat disparate (eclogitic) mantle environment. Type IaA-IaB diamonds assigned to the peridotitic paragenesis are associated with a larger range in nitrogen concentrations (between 101 – 1331 ppm) and aggregation states (between 4.6 – 34.6 %N as B). The websteritic diamonds contain nitrogen concentrations between 271 – 467 ppm and aggregation states between (7.6 – 20 %N as B).

6.6.1.3 Significance of the Sulphide Component

Analyses of sulphide inclusions have been instrumental in this study. The Helam sulphides have preserved the complete exsolution series from mss to heazlewoodite,

recording a cooling history from mantle temperatures to temperatures of less than 550 °C as the diamonds were transported by the kimberlite. Such a complete cooling history is not commonly preserved in diamonds. More importantly however, the Helam sulphides have proven to be very useful in paragenetic assignation, unlike among many other African diamonds (Deines & Harris, 1995). Further to this, it can be demonstrated (below) that the peridotitic mss can indeed co-exist with the mineralogies associated with the Helam olivine inclusions, and consequently need not prescribe the suggestion of Deines & Harris (1995) who invoke a separate sulphide paragenesis.

Thompson & Barnes (1984) have investigated the distribution of Ni and Fe between cogenetic sulphides and olivine. For a variety of different magmatic sulphide deposits, the mean distribution coefficient for Ni and Fe between the two phases:

$K_D = (X_{Ni}/X_{Fe})_{sulphide} / (X_{Ni}/X_{Fe})_{olivine}$ where X = mole fractions

has a range of between 5 and 20, with a mean of 9.8 (Thompson and Barnes, 1984). Calculated K_D's for diamonds HM008 and HM3B4 (which have coexisting olivine and mss) of 9.7 and 7.2 respectively, are similar to a mean value of 9.8 calculated by Thompson and Barnes (1984). This suggests that the two phases could indeed have been in equilibrium with each other at the time of encapsulation within the diamond. In addition, the relationship of the mss Ni/Fe ratio of these two diamonds with Mg# of their olivine inclusions, is consistent with equilibrium crystallisation associated with a batch melting process within the mantle (figure 6.19).

This implies that both the olivine and peridotitic mss inclusions from these diamonds may have crystallised as a result of a batch melting process of undepleted lherzolite. The remaining two peridotitic mss identified among the Helam diamonds plot among the values associated with HM008 and HM3B4, recording slightly lower Ni/Fe ratios. Nevertheless all peridotitic mss from Helam record Ni/Fe ratios of between 0.29 – 0.46. The eclogitic mss all record significantly lower Ni/Fe ratios (0.08 – 0.20), and as expected do not exhibit any tendency to be in equilibrium with diamond olivines. While the total range in mss composition of the Helam mss is broadly similar to the compositional range of other South African mss (Deines & Harris, 1995), for the Helam diamonds, discriminating easily between peridotitic and

eclogitic mss *is* possible. From the above observations, it is reasonable to assume that the peridotitic mss coexisted with the olivine that may have crystallised from batch melting of a lherzolite. Consequently it is not necessary to draw upon a separate sulphide paragenesis to explain the compositions of the peridotitic sulphides, as has been suggested by other workers (e.g.: Meyer, 1987 and Deines & Harris, 1995).

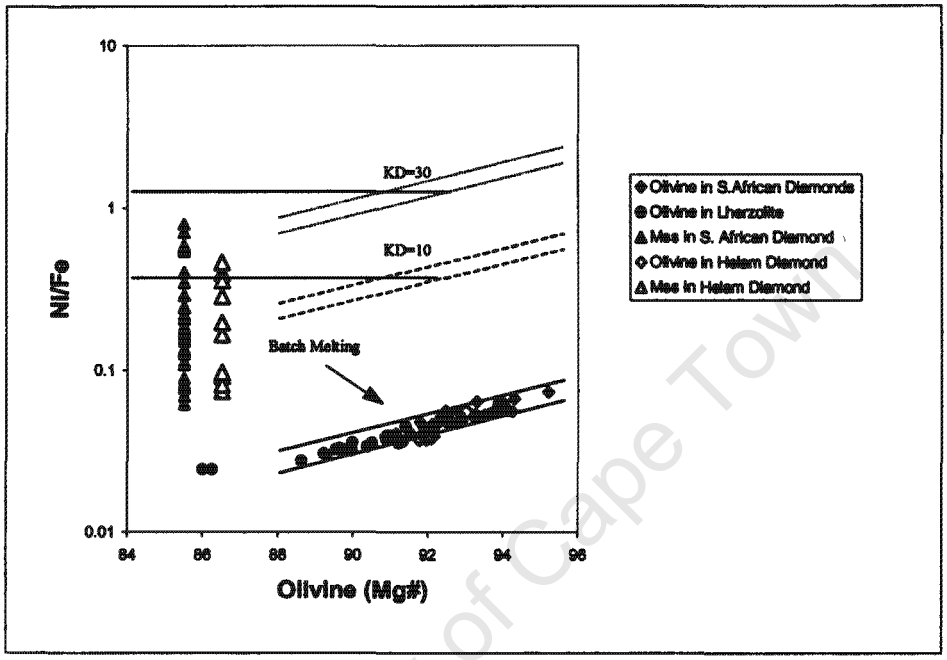

Figure 6.19 The relationship between Ni/Fe ratio and Mg# of olivines from lherzolite (filled circles) (Hervig and Smith, 1982), South African diamonds (filled diamonds) (Hervig *et al.*, 1980), Helam diamonds (open diamonds) and the trend expected during a batch melting process of undepleted lherzolite (solid lines). The dashed lines represent the mss Ni/Fe ratio expected in equilibrium with olivine at any stage of the melting process (Deines & Harris, 1995). Filled triangles, plotted at arbitrary Mg# indicate the mss composition for South African diamonds (Deines & Harris, 1995), while open triangles represent that for the Helam diamonds. (After Deines & Harris, 1995).

6.6.1.4 Relationship between Paragenetic Assignation and Carbon Isotope Data

As discussed in Chapter 1, peridotitic and eclogitic diamonds can be distinguished in terms of their respective variability of $\delta^{13}C$. Figures 6.20a and 6.20b illustrate the range in $\delta^{13}C$ associated with peridotitic and eclogitic diamonds world-wide. It becomes immediately apparent that peridotitic diamonds are associated with a more restricted range of $\delta^{13}C$ values. While eclogitic diamonds exhibit $\delta^{13}C$ values that overlap with the range characterised by peridotitic diamonds, eclogitic diamonds

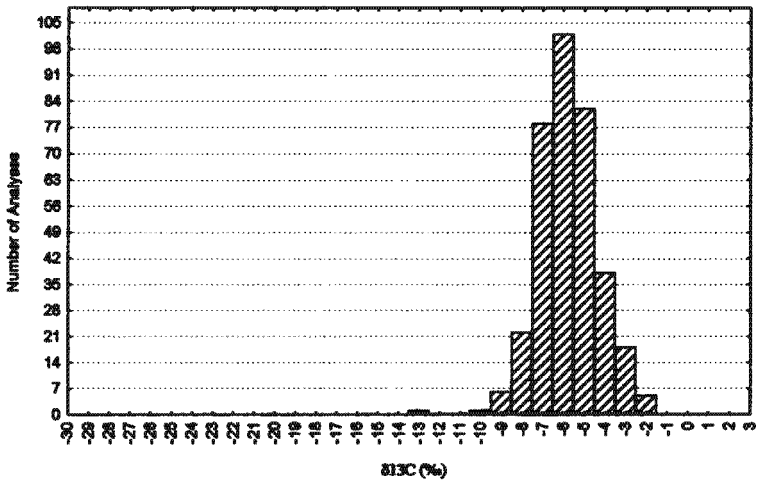

Figure 6.20a The distribution of carbon isotope ratios, $\delta^{13}C$, from peridotitic diamonds worldwide (from Kirkley, 1991).

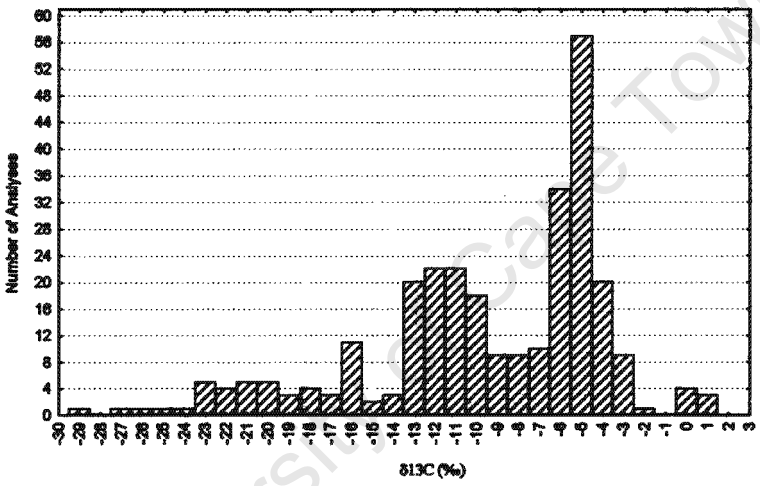

Figure 6.20b The distribution of carbon isotope ratios, $\delta^{13}C$, from eclogitic diamonds worldwide (from Kirkley, 1991).

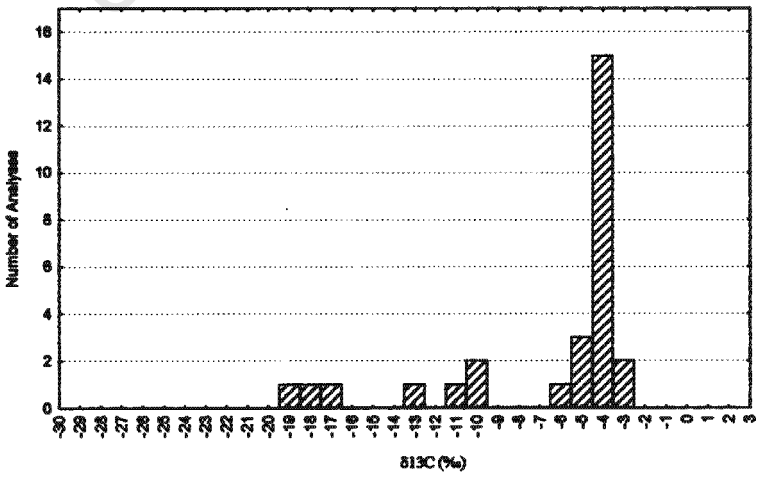

Figure 6.20c The distribution of carbon isotope ratios, $\delta^{13}C$, from the Helam diamond population (from Logan, 1999).

commonly extend to more highly fractionated $\delta^{13}C$ values. This phenomenon is used in support of the notion that eclogitic diamonds are derived from subducted crustal material (Kirkley, 1991).

Logan (1999) conducted a carbon isotopic study of the Helam diamonds in an early attempt to define the diamond source regions. The results of this study are illustrated in Figure 6.20c. It can be demonstrated that the Helam diamonds exhibit a large range of $\delta^{13}C$ values (between -19.48 ‰ and –3.79 ‰). While the majority of the Helam diamonds analysed exhibit $\delta^{13}C$ values that can be associated with either peridotitic or eclogitic diamonds, it is clear that those diamonds exhibiting highly fractionated $\delta^{13}C$ values (as low as –19.48 ‰) reflect an eclogitic source. This observation is in support of inclusion and macrocryst data which suggests that there have been significant contributions of diamond from both peridotitic and eclogitic sources.

In addition, Logan (1999) showed that the canary-yellow Helam diamonds are ubiquitously associated with the most highly fractionated $\delta^{13}C$ values (between –10.25 ‰ and –19.48 ‰). This is in agreement with the suggestion made on the basis of mineral inclusion data, that the canary-yellow diamonds are eclogitic. In addition the highly fractionated $\delta^{13}C$ values are in support of the proposal that these eclogitic diamonds have crystallised within a substrate that originated from the subduction of oceanic crustal material.

6.6.2 The Mantle Below the Bushveld Complex

As discussed previously, recent seismic data (James *et al.*, 2001) demonstrates that the mantle below the Bushveld Complex is associated with significantly lower seismic velocities than those observed below undisturbed cratonic mantle. These low mantle velocities may indicate chemical modification of the mantle during the emplacement of the complex (ca. 2.05 Ga). This hypothesis is consistent with Re-Os data from mantle xenoliths from the Bushveld region, which appear to have been reset to Proterozoic ages of approximately 2 Ga (Carlson *et al.*, 2000). Carlson *et al.* (2000) suggest that such isotopic resetting of an entire volume beneath the Kaapvaal craton requires material addition to the mantle.

While a thermal anomaly of approximately 100 °C *may* explain the seismic anomaly (Christensen, 1982), there is little evidence from xenolith studies (e.g.: Danchin, 1979; Jones, 1988) for higher geotherms in the region of the Bushveld Complex. However James *et al.* (2001) argues that 'refertilisation' (i.e.: iron enrichment) of the mantle during the Bushveld event could significantly reduce seismic velocities in the underlying mantle. Hoal (2001) reports that peridotite xenoliths from the Premier kimberlite are notably more iron rich than those of younger kimberlites, and has interpreted this to reflect such Bushveld-related enrichment. Shirey *et al.* (2001) suggest that eclogitic materials, if present in significant volumes, would also reduce mantle velocity and increase average density of the depleted peridotitic mantle.

The Premier, Klipspringer and Swartruggens kimberlites have all been successful in sampling mantle in the vicinity of the Bushveld Complex, thereby providing insight into the mantle stratigraphy below this geological feature. Analyses of the inclusions from the Helam diamonds show some striking similarities with observations made from the diamond inclusions from the Premier (e.g.: Tsai *et al.* 1979; Gurney *et al.*, 1985; Richardson, 1986; Richardson *et al.* 1993) and Klipspringer (Westerlund, 2000) kimberlites.

While all three localities provide abundant evidence for a depleted, harzburgitic and lherzolitic mantle, perhaps the most striking similarity between the kimberlites is that they have all sampled significant, if not predominant eclogitic materials. In addition all three localities preserve evidence of a websteritic paragenesis. Both Premier (Tsai *et al.*, 1979) and Helam diamonds have yielded calc-silicate clinopyroxenes, the compositions of which are indistinguishable between the localities. It is suggested therefore that these calc-silicate inclusions represent a more *regional* ingress of a calc-silicate phase.

The eclogitic inclusions from both Helam and Klipspringer diamonds (Westerlund, 2000) attest to a highly siliceous, Al-rich substrate. Excess Si appears to have resulted in the crystallisation of coesite at both localities, while excess Al has been accommodated by corundum at Helam and by kyanite and high-Al clinopyroxene at Klipspringer. The Premier diamonds, are also associated with small amounts of coesite and kyanite inclusions (Gurney *et al.*, 1985). In addition, there are some remarkable similarities between the compositions and abundance of sulphide phases from the Premier (Deines & Harris, 1995), Klipspringer (Westerlund, 2000)

and Helam diamonds. Abundant eclogitic sulphides ubiquitously characterise the diamond populations from all three localities.

The recognition of a websteritic paragenesis, and similarities between the websteritic orthopyroxene inclusions, from both the Helam and Klipspringer diamonds (Westerlund, 2000) is also noteworthy.

It appears therefore that regionally, the mantle is characterised by a heterogeneous peridotite, comprising lherzolite, garnet harzburgite, chromite-harzburgite and dunite associated with *pervasive* and volumetrically significant lenses of diamondiferous, per-aluminous eclogite and subordinate websteritric and calc-silicate veins. Perhaps the abundance of an eclogitic mantle component, together with its rather unusual mineralogy, is partly responsible for the mantle anomaly observed beneath the Bushveld Complex. This would be in accordance with predictions made by Shirey *et al.* (2001), discussed above. It is suggested here that the Bushveld anomaly may be a manifestation of both iron-enrichment of the mantle (Hoal, 2001), *and* the presence of significant volumes of eclogitic material within the mantle in the region.

It is suggested that the incorporation of this eclogitic component was the result of subduction of high-Al, pelitic material into the peridotitic mantle. This is in agreement with Shirey *et. al.* (2001), who suggest that such eclogite may have been emplaced as early as the Archean as part of the process of craton keel development. Miller (1985) showed that pelitic sediments *are* capable of producing strongly peraluminous magmas. However he argued that their generation in the upper mantle through subduction during the Archean, would be strongly influenced by lithospheric buoyancy. The consequence of such subduction therefore, would result in the formation of *pervasive* rather than restrictive peraluminous eclogite. These suggestions are thus clearly in support of the above-mentioned model accounting for the anomalous mantle in the vicinity of the Bushveld Complex.

The similarity in ages for the Klipspringer (2.5 $\pm$ 0.3 Ga; Westerlund, 2000) and some of Helam eclogitic diamonds (~ 2.9 Ga), suggest that they may be related to the same (Archean) subduction event. A Proterozoic age (~ 1.18 Ga) for one eclogitic Helam diamond compares favorably with an age of ~ 1.15 Ga for some eclogitic diamonds from Premier (Richardson, 1986). This is in support of the suggestion made

by Richardson *et al.* (1990), that eclogitic diamonds reflect episodic mantle events during the Proterozoic.

7 DISCUSSION AND CONCLUSIONS

7.1 Mantle Stratigraphy

The Swartruggens Kimberlite was successful in sampling numerous mantle minerals, of which the Helam diamonds constitute only a very small fraction. The majority of the mantle sample is represented by a diverse suite of macrocrystic minerals, which are believed to have become dissagregated from larger mantle xenoliths during the emplacement of the Swartruggens Kimberlite at approximately 150 Ma. Preserved mantle xenoliths are very rare from this locality, to the extent that none are available for study. Nevertheless, the compositions of the various macrocryst minerals have been *successful* in recording the nature and variability of the mantle rocks below the Swartruggens Kimberlite, within the vicinity of the Bushveld Complex.

Detailed chemical analysis of the macrocryst minerals suggests that the lithosphere sampled by the Swartruggens Kimberlite is characterised by garnet harzburgite, chromite harzburgite, garnet lherzolite and eclogite/grospydite lithologies. In addition, two garnet megacrystic populations have been sampled, the origins of which remain unclear. Despite the abundance of sub-calcic garnet, and lherzolitic garnet macrocrysts, the absence of similar minerals occurring as inclusions within the Helam diamonds, suggests that while the garnet harzburgites and garnet lherzolites comprise a volumetrically significant proportion of the mantle, the contribution of diamonds from these lithologies has been small.

It has become quite apparent from the abundant inclusions of olivine and chromite, in accordance with the macrocryst data, that chromite harzburgite and/or dunite lithologies have played host to the majority of the peridotitic diamonds within the Swartruggens Kimberlite. The compositions of the peridotitic mineral inclusions attest to a locally variable, highly depleted, highly magnesian chromite-harzburgite/dunite substrate. It has been demonstrated from detailed studies of sulphide inclusions, that a Ni-enriched sulphide phase (mss) was in equilibrium with these rocks at the time of diamond formation.

It is quite clear that in addition to the peridotitic mantle, there is a significant contribution of mantle material from an eclogitic source, as indicated by the abundance of eclogitic macrocryst garnets sampled by the Swartruggens Kimberlite.

These have all been classified as Group I eclogites, and are thus all associated with the conditions suitable for diamond formation. It has been shown that the presence or absence of such Group I eclogite macrocrysts among the various dykes of the Swartruggens dyke system is *strongly* correlated to diamond grade. Eclogitic garnet inclusions within the Helam diamonds are very similar in composition to these macrocrysts, suggesting that they are representative of the *same* eclogitic protolith. The abundance of both eclogitic garnet macrocrysts, together with the relative abundance of these and other eclogitic inclusions within diamond, suggest that in addition to the ultramafic rocks, there is indeed a *significant* component of grospyditic, Group I eclogite within the mantle beneath the Swartruggens Kimberlite.

Eclogitic garnet mineral inclusions provide some, limited evidence of magmatic fractionation, and thus an igneous origin for the inclusions has been inferred. Mineral inclusions within the majority of the Helam diamonds sampled, suggest that approximately equal amounts of diamond have been sourced from eclogitic and peridotitic parageneses, however it is has been demonstrated that eclogitic diamonds become more abundant among the larger crystals. The relative abundance of eclogitic sulphides, suggests an intimate relationship between a low-Ni sulphide phase and the eclogitic protolith.

A regional, lithological comparison of the mantle sample below the Swartruggens, Premier and Klipspringer kimberlites shows that in addition to harzburgitic and dunitic lithologies, the mantle in the vicinity of the Bushveld Complex is characterised by a significant high-Al, eclogitic component. Re-Os ages obtained from Helam eclogitic sulphide inclusions suggest that this protolith may have been emplaced as early as the Archean. Westerlund (2000) reports similar ages for eclogitic diamonds from Klipspringer (2500 $\pm$ 300 Ma). This is in agreement with observations made by Richardson *et al.* (2001) and Shirey *et al.* (2001) who suggest that that incorporation of such eclogite accompanied or closely followed cratonic lithosphere stabilization. Proterozoic (1150 $\pm$ 60 Ma) Sm-Nd ages for Premier eclogitic diamonds (Richardson, 1986), are possibly indicative of more recent eclogitic injection and episodic eclogitic diamond formation within the Kaapvaal Craton.

If this eclogitic component proves to be regionally pervasive, then it could well help explain the low seismic velocities that characterise the mantle in the region.

This study has shown that the eclogitic components from all three localities are broadly similar, suggesting derivation from the subduction of similar per-aluminous sediments, possibly dating back to the Archean. The presence of significant eclogitic material within the lithosphere, together with iron-enrichment of the mantle during the Bushveld magmatic event (e.g.: Hoal, 2001), may have had an additive effect, manifest by a reduction in seismic velocity and increase in the average density of mantle. It is suggested therefore that addition of eclogitic material, *and* chemical modification have resulted in the observed seismic anomaly beneath the Bushveld Complex.

Limited websteritic and calc-silicate parageneses have also been represented, suggesting that these lithologies, while also playing host to some diamond crystallisation, comprise only a small proportion of the mantle. The compositions of the websteritic mineral inclusions suggest that they are closely associated with the eclogitic paragenesis. In addition, existence of these lithologies attests to a highly heterogeneous mantle, characterised by numerous, disparate, diamondiferous lithologies.

7.2 Formation of the Helam Diamonds

7.2.1 Episodic Diamond Growth

Detailed FTIR analysis of the Helam diamonds has been instrumental in classifying the various sub-populations associated with the Helam diamonds. The sub-populations determined on the basis of the diamonds IR characteristics, correlate well with the initial empirical classification made on the basis of the diamonds' physical properties. As a consequence, the sub-populations have conveniently been named after their respective body coloration, i.e.: colourless, brown, green Cape-yellow and canary-yellow. It has been demonstrated that each of the sub-populations have prescribed to different geological histories.

It has been shown that the colourless and brown diamonds, exhibit low but significant nitrogen concentrations (200-1300 ppm) and aggregation states (10-35 %N as B). The green diamonds generally exhibit somewhat higher nitrogen concentrations (up to 2500 ppm) and aggregation states (up to 60 %N as B). The Cape-yellow

diamonds display IR characteristics that are indistinguishable from the colourless and brown diamonds, their coloration attributed to the presence of optical N3 colour centers (*EPR* P2 centers) within the diamond lattice. Consequently the colourless, brown, Cape-yellow and green diamonds can all be classified as Type IaAB diamonds (or belonging to the IaA-IaB series), suggesting geologically significant residence times within the mantle (i.e.: billions of years). The canary-yellow diamonds however, typically exhibit low nitrogen concentrations (>50-150 ppm), and are interpreted to belong to the Ib-IaA aggregation series. EPR studies have confirmed that these canary-yellow diamonds contain low concentrations of unaggregated, dispersed nitrogen. It is suggested that the single, dispersed nitrogen atoms associated with these diamonds, have imparted an intense yellow/amber coloration (canary yellow) to these diamonds.

Due to the ancient ages of most diamonds, very few naturally occurring Type Ib diamonds have been recorded in nature. The existence of diamonds containing a Type Ib diamond component within the Swartruggens Kimberlite is thus significant, particularly since these diamonds constitute as much as 5% of the Helam diamond population. These diamonds have all been interpreted to represent an eclogitic paragenesis, and it can be demonstrated that at least three significant eclogitic diamond-forming events within the mantle beneath the Swartruggens Kimberlite; Re-Os data from eclogitic sulphide inclusions from Helam diamonds suggest an Archean age for some of the eclogitic Helam diamonds. One eclogitic sulphide inclusion appears to represent a Proterozoic age. In addition, the canary-yellow diamonds have been interpreted to represent yet *another* significant eclogitic diamond-forming event that occurred subsequent to the crystallisation of the other Helam diamonds, but significantly before the emplacement of the kimberlite (as suggested by the mature aggregation states of these inherently low-nitrogen, Ib-IaA diamonds). It is clear therefore, that diamond crystallisation has occurred during numerous diamond-forming events. Certainly among the eclogitic diamonds, there is evidence for repeated, episodic diamond growth.

Observations made from the diamond plates, allow the theme of episodic growth to be extended even *further*. Diamond HB3C3 demonstrates that peridotitic diamonds are also associated with episodic diamond crystallisation. The diamond plates commonly exhibit diamond cores, displaying marked differences in impurity

characteristics and growth morphologies to the enclosing diamond. The contacts between these cores and overgrowth layers, are interpreted to represent hiatus in growth, during which significant changes in the local crystallisation environment has occurred. The inference is that such changes reflect prolonged periods of geological time, between successive periods of diamond growth. Up to three significant, *secondary* diamond growth events have been observed within single diamonds. Further, it can be argued that any observable luminescence differences between diamond growth layers, reflects subtle chemical variability, manifest by episodic growth on an even smaller time scale.

7.2.2 Significance of the Sulphide Component

Particular attention has been paid to the sulphide inclusions within the Helam diamonds. The predominance of both peridotitic (high Ni) and eclogitic (low Ni) sulphide inclusions among the Helam diamonds is not unlike observations made from other localities worldwide (Meyer, 1987). It is suggested that the predominance of a sulphide component among worldwide diamonds reflects an intimate association between the sulphide phase and diamond formation (e.g.: Gurney *et al.*, 1979b; Bulanova *et al.*, 1999). Observations made among the Helam diamonds are in agreement with this suggestion.

It has been demonstrated that a sulphide phase (mss) could have been in equilibrium with the olivine crystals of the peridotitic lithologies at the time of diamond crystallisation, and that this association need not call upon a separate sulphide paragenesis. It is suggested that the co-existence of a sulphide phase with the diamond protolith may have provided the mechanism for diamond crystallisation (see below). In addition to sulphide in the mantle, FTIR analysis has shown that nitrogen and hydrogen have also been intimately associated with the upper mantle environment, having been encapsulated within the diamond as detectable impurities during crystal growth. The Helam diamonds, therefore provide abundant evidence for the coexistence of a sulphide phase, as well as the elements of nitrogen and hydrogen with the minerals of the diamond protoliths.

Haggerty (1986) proposes that both sulphur and nitrogen could act as catalysts during diamond crystallisation. Moreover it has been suggested that the solubility of

carbon is greatly increased within a sulphide melt, as opposed to a silicate melt (Saxena, 1989). It is suggested then, that the Helam diamonds may have crystallised in association with such a sulphide melt/fluid. The complex and often mixed growth associated with the Helam diamonds suggests a variable growth rate within an environment of highly variable carbon supersaturation and nitrogen contents, possibly as a result of localised, episodic ingress of sulphide fluids of variable carbon and nitrogen concentrations. The systematic decrease in hydrogen with successive diamond growth observed in the diamond plates, suggests that mantle fluids have not added hydrogen to the system, and that this element has become systematically depleted over time.

7.2.3 The Environment of Crystallisation

In the absence of mantle xenoliths and detailed geothermobarometric analysis of diamond inclusions, inferences regarding the mantle environment must be made principally from FTIR data collected from the Helam diamonds themselves. Assuming a mantle residence time of 2.75 Ga for all Type IaAB diamonds, most Helam diamonds record mantle residence temperatures in the range of between 1090-1100 °C. No clear distinction can be made between the residence temperatures of the eclogitic, websteritic and peridotitic diamonds, which suggests that they are all associated with similar thermal environments. This is supported by the equally poor development of platelets among the various Helam diamonds. While the mantle residence temperature of the canary-yellow diamonds could not be uniquely constrained, it has been suggested, based on the low nitrogen concentrations and mature IaA aggregation of these diamonds (suggestive of an old age), that they do not necessarily represent anomalous residence temperatures.

While the thermal environment of crystallisation appears to be consistent over extended periods of geological time, IR analysis of individual diamond plates show that significant, often systematic, chemical variation has occurred during diamond growth. Within certain individual diamonds, it has been demonstrated that diamond growth has been altered from cubic to octahedral growth in nature. With a relatively constant residence temperature, it is reasonable to assume then, that *these* differences

in growth have been caused by a marked change in level of carbon supersaturation within the mantle over time.

It is suggested that the octahedral diamonds crystallised in an environment characterised by relatively low levels of carbon supersaturation, while the cubic diamonds grew in an environment characterised by exceedingly high levels of carbon supersaturation. In one diamond plate (HM01A), an initial octahedral crystal can be seen to have been overgrown by cubic growth layers, which have in turn been overgrown by octahedral growth layers. This suggests that the level of carbon supersaturation has been highly variable through time, alternating repeatedly between the levels ideal for cubic and octahedral growth. The large population of cubo-octahedral diamonds is believed to represent diamonds that crystallised during some intermediate level of carbon supersaturation.

Among the Helam diamonds therefore, the various primary morphologies of diamond are attributed to episodic crystallisation at various levels of carbon supersaturation. This is in conflict with the model proposed by Haggerty (1986) who suggests that different primary morphologies are stratigraphically controlled. These observations are also contradictory to models proposing crystallisation within a closed-system environment. It is suggested that localised changes in the levels of carbon supersaturation and nitrogen within the mantle (Chapter 5) have been caused by episodic (sulphide) fluid ingress. Based on the consistent time-averaged mantle residence temperatures derived from the diamond plates, it is proposed that while such fluids may have resulted in localised thermal fluctuations, the perturbations have been short lived and relatively small.

In addition, the analysis of the diamond plates reveal marked chemical variability with successive diamond growth. The primary observation for the majority of the Helam diamonds, is that nitrogen and hydrogen appear to become progressively depleted with successive diamond growth. This is in agreement with observations made on hundreds of other unpolished, rough Helam diamonds. These observations suggest that, in the absence of ingress of fluids containing these elements, the crystallisation environment became progressively depleted in these elements with successive growth. It follows therefore that diamonds displaying such progressive depletion of trace elements have crystallised within an apparent 'closed-system' environment.

Subtle compositional differences between similar mineral inclusions incorporated within the diamonds at different times, attest to small but significant chemical evolution of the host lithologies over time. It is clear then, that the Helam diamonds reflect a chemically dynamic, yet thermally stable, lithospheric mantle. The often imperfect crystal morphologies observed among the Helam diamonds supports the notion of crystallisation within a non-ideal, chemically dynamic mantle environment.

7.3 Significance of a Majorite Component

A probable majoritic component within the mineral inclusion suite has significant implications regarding conventional wisdom associated with the genesis of Group II kimberlites. A majoritic mantle component within a Group II kimberlite would be in support of suggestions made by le Roex (1986) and Nowell *et al.* (1999) who propose that these kimberlites may well have an asthenospheric origin. This contradicts earlier suggestions made by Smith (1983) who argues that Group II kimberlites have lithospheric origins.

7.4 Geological History of the Diamonds Subsequent to Crystallisation

The various diamond sub-populations are characterised by distinguishable physical and chemical properties, which together reflect differences in their respective geological histories. It has been demonstrated that the inherent chemical differences of the various diamond sub-populations have commonly *controlled* some of the physical characteristics of the diamonds. Not only does the composition of certain diamonds impart a particular colour-center to a crystal, but it has been shown that diamonds of particular chemical characteristics may be prone to certain secondary processes, such as deformation and irradiation, which are often manifest by colour.

Brown coloration, lamination lines, and the catastrophic degradation of platelets commonly observed among many of the Helam diamonds, suggest that a significant proportion of the crystals have been affected by plastic deformation. It has been suggested that the brown coloration of some of the Helam diamonds is a result of a deformation event that preceded the crystallisation of the other Type IaAB diamonds. In addition, the frequent occurrence of lamination lines and other strain

features in association with the 'younger' canary-yellow diamonds, suggests that a more recent deformation event may has occurred. Perhaps *this*, more recent, deformation event was related to the generation and emplacement of the Swartruggens kimberlite.

It is clear however, that individual diamonds have experienced variable degrees of deformation, and that many of the diamonds have completely escaped the effects of such deformation. It has been demonstrated that in general, diamonds with higher nitrogen concentrations and aggregation states are less susceptible to the effects of deformation. This is consistent with the observation that the canary-yellow diamonds (low nitrogen) are more frequently characterised by the effects of deformation. However, this may only in part explain the variability of deformation among the Helam diamonds, as there are some diamonds that controvert this general observation. Perhaps then, differential strain within the mantle, in addition to the predisposition of certain diamonds to the effects of such strain, more adequately explains the variability of deformation.

The relative abundance of tetrahexahedroidal diamonds attests to an extensive period of diamond dissolution within the mantle. This dissolution has been attributed to a process of mantle metasomatism. The high TiO_2 contents among many of the garnet macrocrysts are in support of such a metasomatic event. This metasomatic overprint appears better developed among the garnet macrocrysts of Changehouse Fissure, suggesting that the Main Fissure erupted at some time prior to the peak of the metasomatic event. Perhaps then, one would expect the diamonds from the Changehouse Fissure to be more resorbed than the diamonds of the Main Fissure. However due to simultaneous mining of both the Changehouse and Main fissures at the Helam Mine, this could not be verified. However, more highly resorbed chromite macrocrysts observed within the Changehouse Fissure (Klump, 1995) appear to be in agreement with this suggestion.

Oxidation processes within the kimberlite have also affected the majority of the Helam diamonds. The large variety of etch features associated with the Helam diamonds attest to a complex history of etching, and the presence of oxidation conditions over a wide range of temperatures (between 1300 °C – 900 °C) as a result of the release of CO_2, O_2 and H_2O in the hypabyssal regions of the kimberlite on cooling. The canary-yellow diamonds commonly exhibit more intense etching than

the other diamond sub-populations suggesting that their unique chemical characteristics predispose them to the effects of oxidation. Conversely, the remainder of the diamond population appears to exhibit a relative resistance to such oxidation.

A period of brittle deformation has affected a large proportion of the Helam diamonds. While the amount of breakage due to mining processes has not been determined, partial resorption/etching, and the occurrence of inclusion cavities on many of the breakage surfaces suggests that a significant amount of breakage occurred as a result of natural processes. This has been attributed to the differential expansion of the diamonds and their mineral inclusions during depressurisation, during the kimberlite ascent. Common crystal breakage may explain the relative scarcity of inclusion minerals among the Helam diamonds.

Radiation damage was perhaps the most recent natural process to have affected the Helam diamonds. This process has resulted in the green coloration of some of the diamonds at low temperatures (< 600 °C) within the oxidized portions of the kimberlite. FTIR analysis of these green diamonds reveals that they are commonly associated with very high nitrogen concentrations and aggregation states. As a result it has been suggested that perhaps nitrogen content and/or the aggregation state of a diamond, facilitates the development of the lattice disorders; that diamonds with specific IR characteristics propitiate the production of vacancies in the diamond lattice.

7.5 Implications for Industry

7.5.1 Diamond Grade Analysis and Grade Control

The Swartruggens Kimberlite, as with many other kimberlite occurrences, comprise numerous petrographically distinct intrusive phases of varying diamond grade. Detailed analyses of the macrocryst minerals from the Main and Changehouse fissures, have demonstrated that the diamond grade of the kimberlites is strongly controlled by the presence or absence of a Group I eclogitic mantle material. The high grades of the Main Fissure are attributed to the additive contributions of significant amounts of both diamondiferous peridotitic and eclogitic lithologies, and the evasion of significant metasomatism. The lower grades of the Changehouse Fissure are

ascribed to the distinct absence of significant volumes of the Group I eclogitic material. In addition, the garnet macrocrysts of the Changehouse Fissure commonly exhibit high TiO_2 contents, suggesting that a process of metasomatism occurred within the lithosphere prior to the intrusion of this kimberlitic phase. This process of metasomatism may have resulted in the complete resorption of many diamonds, and may further explain the lower grade associated with this kimberlite. By contrast the Muil dyke, which contains no diamonds whatsoever, is completely barren of all mantle minerals.

Whether the mantle sample of the respective intrusive phases is a function of random sampling within the mantle, or whether the mantle sample has become altered, by various secondary lithospheric processes, remains unclear. Nevertheless, it has been demonstrated that there exists an intimate relationship between diamond grade of a kimberlite and the composition of its constituent macrocrystic minerals. These compositional differences manifest themselves as differences in crystal colour, and as such, it becomes possible to analyse the mantle sample empirically. The empirical method employed at the Helam Diamond Mine has been given scientific credibility by this study, and it is suggested that such practices be extended to other multi-phase kimberlites as an effective and inexpensive method of grade control. This is particularly relevant for small volume deposits such as kimberlite dykes where expensive, time consuming bulk sampling of kimberlite for macro-diamonds is impractical.

7.5.2 Diamond Exploration

It is clear from studies of both the macrocryst minerals and the diamond mineral inclusions, that the Swartruggens Kimberlite has been successful in sampling a large variety of disparate, diamondiferous lithologies. Perhaps this explains the unusually high grades associated with this kimberlite occurrence. It has been emphasized that a diamondiferous eclogitic component (related to multiple diamond-forming events) has significantly contributed to the overall diamond grade of the kimberlites, suggesting that the local importance of this paragenesis should not be underestimated.

Most diamonds worldwide have been associated with the peridotitic paragenesis, and consequently most research and exploration activities have focussed

exclusively on this source. However there is growing evidence that eclogitic diamonds contribute significantly to the worldwide diamond budget. The observation that eclogitic diamonds appear more abundant among the larger crystal sizes, has significant economic implications. Consequently it is urged that exploration activities should place more emphasis on the eclogitic component, particularly within the vicinity of the so-called 'Bushveld Anomaly', which has been interpreted to, in part, reflect regionally extensive, volumetrically significant, potentially diamondiferous, Group I eclogitic mantle.

8 REFERENCES

Akaogi, M. & Akimoto, S. 1979. Pyroxene-garnet solid-solution equilibria in systems $Mg_4Si_4O_{12}$-$Mg_3Al_2Si_3O_{12}$ and $Fe_4Si_4O_{12}$-$Fe_3Al_2Si_3O_{12}$ at high pressures and temperatures. *Phys. Earth Planet. Inter.*, **15**: 90-106

Allan, P. 1990. Petrographic description of 5 samples collected at Helam Mine, Swartruggens, 21.2.1990, De Beers Consolidated Mines Ltd., Unpubl. Company Report.

Allsopp, H.L., & Barrett, D.R. 1975. Rb-Sr age determinations of South African Kimberlites. *Phys. Chem. Earth*, **9**: 605-617.

Barrett, D.R. & Allsopp, H.L. 1973. Ext. Abstr. 1st int. Kimberlite Conf. University of Cape Town: 23.

Bell, D.R., Schulze, D.J., Read, G.H., Mattioli, G.S., Shimizu, N., Moore, R.O. & Gurney, J.J. 1995. Geochemistry of Cr-poor Megacrysts from the Lace (Group II) kimberlite, South Africa. *Ext. Abstr. 6th International Kimberlite Conference, Novosibirsk, Russia*: 52-54.

Berger, S.D. & Pennycook, S.J. 1982. Detection of nitrogen at {100} platelets in diamond. *Nature*, **298**: 635-637.

Boyd, F.R. 1973. A pyroxene geotherm. *Geochim. Cosmochim. Acta*, **37**: 2533-2546.

Boyd, F.R & Finnerty, A.A. 1980. Conditions of origin of natural diamonds of peridotite affinity. *J. Geophys. Res.*, **85**: 6911-6918.

Boyd, F.R., Gurney, J.J. & Richardson, S.H. 1985. Evidence for a 150-200 km thick Archean lithosphere from diamond inclusion thermobaromatry. *Nature*, **315**: 387-389.

Boyd, F.R. & Gurney, J.J. 1986. Diamonds and the African Lithosphere. *Science*, **232**: 472-477.

Boyd, F.R. & Pillinger, C.T. 1994. A preliminary study of $^{15}N/^{14}N$ in octahedral growth form diamonds. *Chem. Geol.*, **116**: 43-59.

Bulanova, G.P., Griffin, W.L., Ryan, C.G., Shestakova, O.Y., & Barnes, S.J. 1996. Trace elements in sulphide inclusions from Yakutian diamonds. *Contrib. Mineral. Petrol.*, **124**: 111-125

Bulanova, G.P., Griffin, W.L., Kaminsky, F.V., Davies, R., Spetsius, Z.V., Ryan, C.G., Andrew, A. & Zahkarchenko, O.D. 1999. Diamonds from Zaritsna and Dalnaya Kimberlites (Yakutia), Their nature and lithospheric mantle source. In: J.J. Gurney, J.L Gurney, M.D Pascoe, S.H. Richardson (eds), *Proc. 7th Int. Kimberlite. Conf.*, **1**: 49-56. University of Cape Town.

Carlson, R.W., Boyd, F.R., Shirey, S.B., Janney, P.E., Grove, T.L., Bowring, S.A., Schmitz, M.D., Dann, J.C., Bell, D.R., Gurney, J.J., Richardson, S.H., Tredoux, M., Menzies, A.H., Pearson, D.G., Hart, R.J, Wilson, A.H., & Moser, D. 2000. Continental growth, preservation and modification in southern Africa. *GSA Today*, **10**: 1-7

Carswell, D.A. & Gibb, F.G.F. 1984. Geothermometry of garnet lherzolite nodules with special reference to those from kimberlites of Northern Lesotho. *Contrib. Mineral. Petrol.*, 74: 403-416.

Chrenko, R.N., McDonald, R.S., & Darrow, K.A. 1967. Infrared spectra of diamond coat. *Nature*, 213: 474-476.

Chinn, I.L. 1995. A study of unusual diamonds from the George Creek K1 kimberlite dyke, Colorado. Unpubl. PhD. Thesis, University of Cape Town, South Africa.

Chinn, I.L. 2001. Personal communication. De Beers Geoscience Centre, Johannesburg, South Africa.

Christensen, N.I. Seismic velocities, In: R.S. Carmichael (ed) *Handbook of Physical Properties of Rocks*. CRC Press. Florida.: 228.

Clark, C.D., Collins, A.T. & Woods, G.S. 1992. Optical spectroscopy of diamond. In: J. Field (ed) *The Properties of Natural and Synthetic Diamond*. Academic Press.: 35-69

Collins, A.T. 1980.Vacancy enhanced aggregation of nitrogen in diamond. *J. Phys. C. Solid St. Phys.*, 13: 2641-2650.

Collins, A.T. 1982. Colour centres in diamond. *J. of Gemmology*, 18: 37-35.

Craig, J.R. & Kullerud, G. 1969. Phase relations in the Cu-Fe-Ni-S system and their application to magmatic ore deposits. *Econ. Geol. Mono.*, 4: 344-358.

Craig, J.R. & Scott, S.D. 1976. Sulphide phase equilibria. In: . P.H. Ribbe (ed), *Reviews in Mineralogy*, 1, Mineral. Soc. Amer., CS1-CS110.

Danchin, R.V. 1979. Mineral and bulk chemistry of garnet lherzolite and garnet harzburgite xenoliths from Premier Mine, South Africa. In: F.R. Boyd and H.O.A Meyer (eds). *The Mantle Sample: Inclusions in Kimberlites and Other Volcanics*. Proc. 2nd Int. Kimb. Conf. Washington.: 104-126.

Daniels, L.R.M. 1991. Diamonds and related minerals from Dololwayo kimberlite, Kingdom of Swaziland. Unpublished Ph.D Thesis, University of Cape Town.

Daniels, L.R.M. & Gurney, J.J. 1999. Diamond inclusions from the Dokolwayo Kimberlite, Swaziland. In: J.J. Gurney, J.L Gurney, M.D Pascoe, S.H. Richardson (eds), *Proc. 7th Int. Kimberlite. Conf.*, 1: 134 -142. University of Cape Town.

Davidson, J.M. 1998. Summary Report for Delegates Attending the 7th International Kimberlite Conference. Unpublished.

Davidson, J.M. 2000. Personal communication. Helam Mine, Swartruggens, South Africa.

Davies, G. 1976. The A nitrogen aggregate in diamond – its symmetry and possible structure. *J. Phys C: Solid St. Phys.*, 9: L537-L542.

Davies, G. 1980. Determining the amount of nitrogen in natural diamond. *Industrial Diamond Review*: 466-469.

Davies, R.M, Griffin, W.L., Pearson, N.J., Andrew, A., Doyle, B.J., & O'Reiley, S.Y. 1999a. Diamonds from the deep: Pipe DO-27, Slave Craton. In: J.J. Gurney, J.L Gurney,

M.D Pascoe, S.H. Richardson (eds), *Proc. 7th Int. Kimberlite. Conf.*, **1**: 148-155. University of Cape Town.

Davies, R.M., O'Reilly, S.Y. & Griffin, W.L. 1999b. Growth structures and nitrogen characteristics of Group B alluvial diamonds from Bingara and Wellington, Eastern Australia. In: J.J. Gurney, J.L Gurney, M.D Pascoe, S.H. Richardson (eds), *Proc. 7th Int. Kimberlite. Conf.*, **1**: 156-163. University of Cape Town.

Dawson, J.B. 1999. Metasomatism and melting in spinel peridotite xenoliths from Labait, Tanzania. . In: J.J. Gurney, J.L Gurney, M.D Pascoe, S.H. Richardson (eds), *Proc. 7th Int. Kimberlite. Conf.*, **1**: 164-173. University of Cape Town.

Dawson, J.B. & Carswell, D.A. 1990 High temperature and ultra-high pressure eclogites. In: D.A. Carswell (ed) *Eclogite Facies Rocks*. Blackie, London.: 315-349.

Deines, P. & Harris, J.W. 1995. Sulfide inclusion chemistry and carbon isotopes of African diamonds. *Geochim. Cosmochim. Acta.*, **59**: 3173-3188.

Deines, P., Gurney, J.J. & Harris, J.W. 1984. Associated chemical and carbon isotopic composition variations in diamonds from Finsch and Premier kimberlite, South Africa. *Geochim. Cosmochim. Acta*, **48**: 325-342.

De Vries, R.C. 1975. Plastic deformation and 'work hardening' of diamond. *Mat. Res. Bull.*, **10**: 1193-1200.

de Wit, M.J., Roering, C., Hart, R.J., Armstrong, R.A., de Rhonde, C.E.J., Green, R.W.E., Tredoux, M., Peberdy, E., & Hart, R.A. 1992. Formation of an Archean continent. *Nature*, **357**: 553-562.

Erlank, A.J. & Kushiro, I. 1970. Potassium contents of synthetic pyroxenes at high temperatures and pressures. *Carneg. Inst. Wash. Yearbook*, **68**: 433-439.

Evans, T. 1976. Diamonds. *Contemp. Phys.*, **17**: 45-70

Evans, T. 1992. Aggregation of nitrogen in diamond. In: J.E. Field (ed.), *The Properties of Natural and Synthetic Diamond*. Academic Press: 259-290

Evans, T. & Phaal, C. 1962. Imperfections in Type I and Type II diamonds. *Proc. R. Soc.* A **270**: 538-552.

Evans, T. & Qi, Z. 1982. The kinetics of the aggregation of nitrogen atoms in diamond. *Proc. R. Soc.* A **381**: 159-178.

Finnerty, A.A. & Boyd, F.R. 1984. Evaluation of thermobarometers for garnet peridotites, *Geochim. Cosmochim. Acta*, **48**:15-27.

Fipke, C.E., Gurney, J.J. & Moore, R.O. 1995. Diamond exploration techniques emphasising indicator mineral geochemistry and Canadian Examples. *Geol. Serv. Canada.*, **423**: 83.

Frank, F.C. 1967. In: J Burls (ed) *Proc. Intern. Ind. Diamond Conf. Oxford, 1966. 'Science'*, **1**: Industrial Diamond Information Bureau, London: 119-135.

Frank, F.C. 1969. Diamond and deep fluids in the mantle. In: S.K. Runcorn (ed). *The Application of Modern Physics to Earth and Planetary Interiors*,. John Wiley and Sons, New York: 247-250.

Frank, F.C., Lang, A.R., Evans, D.J.F, Rooney, M.L.T., Spear, P.M. & Welbourn, C.M. 1990. Orientation-dependent nitrogen incorporation on vicinals on synthetic diamond cube growth surfaces. *J. Cryst. Growth*, **100**: 354-376.

Frank, F.C., Puttick, K.E. & Wilks, E,M. 1958. Etch pits and trigons on diamond. *Phil. Mag.*, **3**: 1262-1272.

Fritsch, E. 1998. The nature of colour in diamonds. In: Harlow, G.E. (ed). *The Nature of Diamonds*. Cambridge University Press: 23-47.

Girnis, A.V., Stachel, T., Brey, G.P., Harris, J.W. & Phillips, D. 1998. Internally consistent geothermometers for garnet harzburgites. *Ext. Abstr. 7th Int. Kimber. Conf., S. Africa*: 253-255.

Gorina, I. F. 1971. Crystal morphology of diamonds in Anabaro-Olenesky Interfluve. In: M.I. Rabkin, V.A. Milashev, & L.S. Yegorov (eds). *Kimberlite Volcanism and Prospects for Primary Diamond Content in the north-eastern part of the Siberian Platform*. Arctic Geology Research Institute of the USSR Ministry of Geology, Leningrad (in Russian).

Griffin, W.L., Gurney, J.J. & Ryan, C.G. 1992. Variations in trapping temperatures in peridotite-suite inclusions from South African diamonds: Evidence for two inclusion suites, and implications for lithosphere stratigraphy. *Contrib. Mineral. Petrol.*, **110**: 1-15.

Griffin, W.L., Jaques, A.L.S.S.H., Ryan, C.G., Cousens, D.R., & Suter, G.F. 1988. Conditions of diamond growth: A proton microprobe study of inclusions in West Australian diamonds. *Contrib. Mineral. Petrol.*, **99**: 143-158.

Griffin, W.L., Smith, D., Boyd, F.R., Cousens, D.R. Ryan, C.G., Sie, S.H., & Suter, G.F. 1989. Trace element zoning in garnets from sheared mantle xenoliths. *Geochim. Cosmochim. Acta*, **53**: 561-567.

Gurney, J.J. 1984. A correlation between garnets and diamonds in kimberlites. In: J.E. Glover & Harris, P.G. (eds). *Kimberlite Occurrence and Origin: A basis for conceptual models in exploration*. Geology Department and University Extension, University of western Australia, Publication No. **8**: 143-166.

Gurney, J.J. 1989. Diamonds. In: J. Ross (ed), *Kimberlites and Related rocks, Vol. 2. Their Mantle/Crust Setting, Diamonds and Diamond Exploration*. Geol Soc. Aust., Spec. Publ. No. 14, Blackwell: 935-965.

Gurney, J.J. 1990. The diamondiferous roots of our wondering continent. *S. Afr. J. Geol.*, **93** (3): 424-437.

Gurney, J.J., Harris, J.W. & Rickard, R.S. 1979b. Silicate and oxide inclusions in diamonds from the Finsch kimberlite pipe. In: F.R. Boyd and H.O.A. Meyer. (eds). *Kimberlite, Diatremes and Diamonds: their Geology, Petrology and Geochemistry*. A.G.U.: 1-15.

Gurney, J.J., Harris, J.W. & Rickard, R.S. 1984. Silicate and oxide inclusions in diamonds from Orapa Mine, Botswana. In: J. Kornprobst, (ed), *Kimberlites II: The Mantle and Crust Relationships*, Elsevier, Amsterdam: 3-10.

Gurney, J.J., Harris, J.W. & Rickard, R.S. 1984b. Minerals associated with diamonds from the Roberts Victor mine. In: *J. Kornprobst, (ed), Kimberlites II: The Mantle and Crust Relationships*, Elsevier, Amsterdam: 25-33.

Gurney, J.J., Harris, J.W., Rickard, R.S. & Moore, R.O. 1985. Inclusions in Premier diamonds. *Trans. Geol. Soc. S. Afr.*, **88**: 301-310.

Gurney, J.J. & Harte, B. 1980. Chemical variations in upper mantle nodules from southern African kimberlites. *R. Soc. Lond. Phil. Trans.*, **297A**: 273-293.

Gurney, J.J., Jakob, W.R.O. & Dawson, J.B. 1979. Megacrysts from the Monastery kimberlite pipe, South Africa. In: F.R. Boyd & H.O.A. Meyer, (eds), *The Mantle Sample: Inclusions in Kimberlites and Other Volcanics*. Am Geophys. Union, Washington: 227-243.

Gurney, J.J. & Kirkley, M.B. 1996. Kimberlite dyke mining in South Africa. *Afr. Geoscience. Rev.*, **3** (2): 191-201.

Gurney, JJ., Moore, R.O., Otter, M.L., Kirkley, M.B., Hops, J.J., & McCandless, T.E. 1991. Southern African kimberlites and their xenoliths. In: A.B. Kampunzu & R.T Lubala (eds.). *Magmatism in Extensional Structural Settings:The Phanerozoic African Plate*, Springer-Verlag, Berlin: 495-536.

Gurney, J.J. & Zweistra, P. 1995. The interpretation of the major element compositions of mantle minerals in diamond exploration. *J. Geochem. Exploration*, **53**: 293-309.

Haggerty, S.E. 1986. Diamond Genesis in a multiply-constrained model. Nature, **320**: 34-38.

Hall, A.E. & Smith, C.B. 1984. Deep upper mantle and transition zone xenoliths in the Jagersfontein kimberlite, Kaapvaal craton. *Eos Trans., A.G.U. Spring Meeting, Abstartcts:* 192.

Hamilton, P.J., Evenson, N.M., O'Nions, R.K., Smith, H.S. & Erlank, A.J. 1979. Sm-Nd dating of Onverwacht Group volcanics, southern Africa. Nature, 279: 289-300.

Hanley, P.L., Kiflawi, I., & Lang, A.R. 1977. On topographically identifiable sources of cathodoluminescence in natural diamonds. *Phil. Trans. Roy. Soc.*, **A284**: 329-368

Harlow, G.E. 1992. Potassium clinopyroxene at high pressure. *Geol. Soc. Amer.*, Session **48**-A129.

Harris, J.W. 1968. The recognition of diamond inclusions-Pt 2: Epigenetic mineral inclusions. *Ind. Diam. Rev.*, **28**: 458-461.

Harris, J.W. 1987. Recent physical, chemical, and isotopic research of diamond. In: P.H. Nixon (ed), *Mantle Xenoliths*. John Wiley & Sons Ltd.: 477-500.

Harris, J.W. 1992. Diamond Geology. In: J.E. Field (ed)., *The Properties of Natural and Synthetic Diamond*, Academic Press, London: 555-591.

Harris, J.W. & Gurney, J.J. 1979. Inclusions in Diamond. In: J.E. Field (ed). *The Properties of Diamond*, Academic Press, London: 555-591.

Harris, J.W., Harte, B. & Boyd, S.R. 1994. A high-chromium corundum (ruby) inclusion in diamond from the Sao Luiz alluvial mine, Brazil. *Mineral. Mag.*, **58**: 490-493.

Harris, J. W., Hawthorne, J.B & Oosterveld, M.M. 1979. Regional and local variations in the characteristics of diamonds from some southern African kimberlites. *Proc. 2nd Int. kimb. Conf*: 27-41.

Harris, J. W., Hawthorne, J.B & Oosterveld, M.M. 1983. A comparison of diamond characteristics of diamonds from some Southern African Kimberlites. In F.R. Boyd & H.O.A. Meyer *(eds), Kimberlites, diatremes and diamonds: Their geology, petrology and chemistry*, A. G. U, Washington D.C.:27-41

Harris. J.W. Hutchinson, M.T., Hursthouse, M., Light, M. & Harte, B. 1997. A new tetragonal silicate mineral occurring as inclusions in lower-mantle diamonds. *Nature*, **387**: 486-488.

Harris, J.W. & Vance, E.R. 1974. Studies of the reaction between diamond and heated kimberlite. *Contrib. Mineral. Petrol.*, **47**: 237-244

Harte, B. & Gurney, J.J. 1981. The mode of formation of chromium-poor megacryst suites from kimberlites. *J. Geol.*, **89**: 749-753.

Harte, B. & Harris, J.W. 1994. Lower Mantle mineral associations preserved in diamonds. *Mineral. Mag.*, **58A**: 384-385.

Harte, B. & Hawkesworth, C.J. 1986. Mantle domains and mantle xenoliths. In: J. Ross (ed). *Kimberlites and Related Rocks. 2. Their Mantle/Crust Setting, Diamonds and Diamond Exploration.* GSA Spec. Publ., **14**: 649-686.

Harte, B. & Harris, J.W. 1994. Lower mantle mineral associations preserved in diamonds. *Mineral. Mag.*, **58A**: 384-385.

Hatton, C.J. 1978. The geochemistry and origin of xenoliths from Roberts Victor Mine. Unpubl. PhD Thesis. University of Cape Town.

Helmstaedt, H. & Doig, R. 1975. Eclogite nodules from kimberlite pipes of the Colorado Plateau – samples of Franciscan-type oceanic lithosphere. *Phys. Chem. Earth*, **9**: 95-111.

Hervig, R.L. & Smith, J.V. 1982. Temperature dependent distribution between olivine and pyroxene in lherzolite xenoliths. *Contrib. Mineral. Petrol.*, **81**: 184-189.

Hervig, R.L., Smith, J.V., Steele, I.M., Gurney, J.J., Meyer, H.O.A. & Harris, J.W. 1980. Diamonds: Minor elements in silicate inclusions: Pressure-temperature implications. *J. Geophys. Res.*, **85**: 6919-6929.

Hill, G. 2001. Personal communication. DebTech, Johannesburg, South Africa.

Hill, S.J. 1989. A study of diamonds and xenoliths from the Star kimberlite, Orange Free State, South Africa. Unpubl. MSc Thesis. University of Cape Town.

Hoal, K.O. 2001. Samples of iron-enriched Bushveld mantle from the Premier kimberlite. *Proc. Slave-Kaapvaal Workshop*. Merrickville, Ontario. Unpaged.

Hops, J.J., Gurney, J.J., Harte, B. & Winterburn, P.A. 1989. Megacrysts and high temperature nodules from the Jagersfontein kimberlite pipe. 4th International Kimberlite Conference. *Kimberlites and Related Rocks, Vol 2*, Geol. Soc. Aust. Spec. Publ., **14**: 759-770.

Hutchinson, M.T. 1997. Constitution of the sub-lithospheric mantle shown by diamonds and their inclusions. Unpubl. PhD Thesis, University of Edinburgh.

Jacob, D.E., Jagoutz, E., Lowry, D., Mattey, D., & Kudrjavetseva, G. 1994. diamondiferous eclogites from Siberia: Remnants of Archean oceanic crust. *Geochim. Cosmochim. Acta*, **58**: 5191-5207.

James, D.E., Fouch, M.J., VanDecar, J.C. van der Lee, S. & Kaapvaal Seismic Group. 2001. Tectospheric structure beneath southern Africa. *Geophys. Res. Lett.* **28** (13): 2485-2488.

Jobes, M.Q.W. 1988. Heat flow in the Witwatersrand Basin and environs and its significance for the South African shield geotherm and lithosphere thickness. *J. Geophys. Res.*, **93**: 3243-3260.

Jones, R., Briddon., P., & Oberg, S. 1992. First principles theory of nitrogen aggregates in diamond. *Phil. Mag. Lett.*, **66**: 67-74.

Kamiya, Y. & Lang, A.R. 1965. On the structure of coated diamonds. *Phil. Mag.*, **11**: 347-357.

Kennedy, C.S. & Kennedy, G.C. 1976. The equilibrium boundary between graphite and diamond. *J. Geophys. Res.*, **81**: 2467-2470.

Kesson, S.E. & Ringwood, A.E. 1989. Slab-mantle interactions (2): The formation of diamonds. *Chem. Geol.*, **78**: 97-118.

Kiflawi, I., Meyer, A.E., Spear, P.M., van Wyk, J.A. & Woods, G.S. 1984. Infrared absorption by the single nitrogen and A defect centers in diamond. *Phil. Mag.*, **B69**: 1141-1147

Kirkley, M.B. 1998. The Origin of diamonds: Earth Processes. In: G.E. Harlow (ed), *The Nature of Diamonds*. Cambridge University Press: 48-65.

Kirkley, M.B., Gurney, J.J., & Levinson, A.A. 1991a. Age, origin and emplacement of diamonds: Scientific advances in the last decade. *Gems and Gemology*, **27**: 465-479.

Kirkley, M.B., Gurney, J.J., Otter, M.L., Hill, S.J. & Daniels, L.R. 1991b. The application of C isotope measurements to the identification of the sources of C in diamonds: a review. *Appl. Geochem.*, **6**: 477-494.

Kramers, J.D. 1977. Lead and strontium isotopes in inclusions in diamonds and in mantle-derived xenoliths from southern Africa. In: 2nd Int. Kimberlite Conf., Sante Fe, Extended Abstracts. A.G.U., Washington (unpaged).

Kramers, J.D., Roddick, J.C.M. & Dawson, J.B. 1983. Trace element and isotope studies on veined, metasomatic and 'MARID' xenoliths from Bultfontein, South Africa. *Earth and Planet. Sci. Lett.*, **65**: 90-106.

Klump, J. 1995. A pilot study of the Swartruggens kimberlite dyke swarm. Unpubl. Honours Thesis. University of Cape Town.

Kullerud, G. 1962. The Fe-Ni-S system. *Yb. Carnegie Instn. Wash.*, **61**: 144-150

Lang, A.R. 1964. A proposed structure for nitrogen impurity platelets found in diamond. *Proc. Phys. Soc. Lond.*, **84**: 871-876.

le Roex, A.P. 1986. Geochemical correlation between southern African kimberlites and southern African hotspots. *Nature*, **324**: 243-245.

Logan, F. 1999. A Mineralogical and Isotope Study of Macrodiamonds from the Helam Mine, South Africa. Unpubl. Honours Thesis. Queens University.

Loubser, J.H.N. & Van Wyk., J.A. 1981. *Diamond Conference Abstracts*, Reading: 35-40 (unpublished).

Loubser, J.H.N. & Wright, A.C.J 1973. Discussion on the Endor and ESR spectra of diamonds with the N3 optical system. *Diamond Research*, Industrial Diamond information Bureau **1973**: 16-20

MacGregor, I.D. & Carter, J.L. 1970. The chemistry of clinopyroxenes and garnets of eclogite and peridotite xenoliths from the Roberts Victor Mine, South Africa. *Phys. Earth Planet Interiors*, **3**: 391-397.

Mazzone, P. & Haggerty, S.E. 1990 Corganites and cargaspinites: Two new types of aluminous assemblages from Jagersfontein kimberlite pipe. In: D.A. Carswell (ed) *Eclogite Facies Rocks*. Blackie, London.: 795-808.

McCallum, M.E., Huntley, P.M., Falk, R.W. & Otter, M.L. 1994. Morphological, resorption and etch feature trends of diamonds from kimberlite populations within Colorada-Wyoming State Line District, USA. In: H.O.A Meyer, & O.H. Leonardos, (eds), *Diamonds: Characterisation, Genesis and Exploration*. GPRM Spec. Publ. No 1/B, CPRM, Brasilia: 32-50.

McCandless, T.E. & Gurney, JJ. 1989. Sodium in garnet and potassium in clinopyroxene: criteria for classifying mantle xenoliths. 4th International Kimberlite Conference. *Kimberlites and Related Rocks, 2,* Geol. Soc. Aust. Spec. Publ., **14**: 827-832.

McDade, P. & Harris, J.W. 1999. Syngenetic inclusion bearing diamonds from Letseng-la-Terai, Lesotho. In: J.J. Gurney, J.L Gurney, M.D Pascoe, S.H. Richardson (eds), *Proc. 7th Int. Kimberlite. Conf.*, **2**: 557-565. University of Cape Town

Mendelssohn, M.J. & Milledge, H.J. 1995. Geologically significant information from routine analysis of the mid-infrared spectra of diamonds. *International Geology Review*, **37**: 95-110.

Menzies, M.A. & Hawkesworth, C.J. 1987. *Mantle Metasomatism*. Academic Press: 472

Meyer, H.O.A. 1985. Genesis of diamond: a mantle saga. *Am Mineral.*, **60**: 413-417.

Meyer, H. O. A. 1987. Inclusions in diamond. In: P.H. Nixon, (ed). 1987. *Mantle Xenoliths*. John Wiley & Sons: 501-523.

Meyer, H.O.A. & Gubelin, E. 1981. Ruby in diamond. *Gems and Gemology*, **17**: 153-156.

Meyer, H.O.A. & McCallum, M.E. 1986. Mineral inclusions in diamond. *Carnegie Inst. Wash. Yearbook*, **67**: 130-135.

Meyer, H.O.A., Vance, E.R. & Milledge, H.J. 1965. Natural irradiation damage in Ivory Coast diamonds. *Nature*, **206**: 392

Milledge, H.J. 1961. Coesite as an inclusion in G.E.C. synthetic diamonds. *Nature*, **190**: 1181.

Miller, C.F. 1985. Are Strongly peraluminous magmas derived from pelitic sedimentary sources? *J. Geology*, **93**: 673-689.

Moore, R.O., & Gurney, J.J. 1985. Pyroxene solid-solution in garnets included in diamond. Nature, **318**: *553-555.*

Moore, R.O., & Gurney, J.J. 1989. Mineral inclusions in diamonds from Monastery kimberlite, South Africa. In: *Kimberlites and Related Rocks, Vol. 2. Their mantle/Crust Setting, Diamonds and Diamond Exploration*. Geol. Soc. Aust., Spec. Publ., **14**. Blackwell: 1029-1041.

Moore, R.O., & Gurney, J.J. 1991. Garnet megacrysts from group II kimberlites in southern Africa. Extd. Absts., 5th International Kimberlite Conference, Brazil, 289-300.

Moore, M. & Lang, A.R. 1974. On the origin of the rounded rhombic dodecahedral habit of natural diamond. *J. Crystal Growth*, **26**: 133-139.

Moore, R.O., Otter, M.L., Richardson, R.S., Harris, J.W & Gurney, J.J. 1986. The occurrence of moissanite and ferro-periclase as inclusions in diamond. In: *Ext. Abstr. 4th Int. Kimberlite Conf. Geol. Soc. Austr.*, **16**: 409-411.

Newton, M.E. & Baker, J.H. 1989. ^{14}N ENDOR of the OK1 centre in natural type Ib diamond. *J. Phys.: Condens. Matter.*, 1: 10549-10561.

Navon, O. 1999. Diamond Formation in the Earth's Mantle. In: J.J. Gurney, J.L Gurney, M.D Pascoe, S.H. Richardson (eds), *Proc. 7th Int. Kimberlite. Conf.*, **2**: 584-604. University of Cape Town

Navon, O., Hutcheon, I.D., Rossman, G.R. & Wasserburg, G.J. 1988. Mantle-derived fluids in diamond micro-inclusions. *Nature*, **335**: 784-789.

Nowell, G.M., Pearson, D.G., Kempton, P.D., Noble, S.R. & Smith, C.B. 1999. Origins of kimberlites: A Hf isotope perspective In: J.J. Gurney, J.L Gurney, M.D Pascoe, S.H. Richardson (eds), *Proc. 7th Int. Kimberlite. Conf.*, **2**: 616-624. University of Cape Town

Orlov, Yu. L. 1973. *Mineralogy of the Diamond*. Izdatel' stvo Nauka SSSR. Translated in 1977 from the Russian, John Wiley and Sons, New York: 235pp.

Otter, M. L. 1990. Diamonds and their mineral inclusions from the Sloan diatremes of the Colorado-Wyoming State Line Kimberlite District, North America. Unpubl. Ph.D Thesis, University of Cape Town, Cape Town.

Otter, M.L. & Gurney, J.J. 1986. Mineral inclusions in diamonds from the Sloan diatrenes, Colorado-Wyoming State Line district, North America. In: J. Ross (ed), Kimberlites and Related Rocks. Vol. 2. Their mantle/crust setting, diamonds and diamond exploration. *Geol. Soc. Australia Spec. Pupl.*, **14**. Blackwell, Carlton.: 1042-1053.

Phaal, C. 1965. Surface studies of diamond. *Ind. Diamond. Rev.*, **25**: 486-489

Pearson, D.G., Shirey, S.B., Harris, J.W., & Carlson, R.W. 1998. Sulphide inclusions from the Koffiefontein kimberlite, South Africa: constraints on diamond ages and mantle Re-Os systematics. *Earth. Planet. Sci. Lett.*, **160**: 311-326.

Phillips, D. & Harris, J.W. 1995. *Ext. Abstr. 6th Int. Kimberlite Conf. Russia.*

Prinz, M., Manson, D.V., Hlava, P.F. & Keil, K. 1975. Inclusions in diamond: garnet lherzolite and eclogite assemblages. In: L.H. Ahrens, J.B. Dawson, A.R Duncan, and A.J. Erlank (eds). *Phys. Chem. Earth*, **9**: 797-815.

Raman, C.V. 1944. Crystal symmetry and structure in diamond. *Proc. Ind. Acad. Sci.*, **19**: 188-199.

Richardson, S.H. 1986. Latter-day origin of diamonds of eclogitic paragenesis. *Nature*, **322**: 623-626.

Richardson, S.H., Gurney, J.J., Erlank, A.J. & Harris, J.W 1984. Origin of diamonds in old enriched mantle. *Nature*, **310**: 198-202.

Richardson, S.H., Shirey, S.B., Harris, J.W. & Carlson, R.W. 2001. Archean subduction recorded by Re-Os isotopes in eclogitic sulfide inclusions in Kimberley diamonds. *Earth & Planet. Sci. Lett.*, **52925**: 1-11.

Rickard, R.S., Gurney, J.J. & Harris, J.W. 1991. Mineral inclusions from Jagersfontein mine. In: Ext. Abst. 5th Internat. Kimb. Confr., Brazil: 336-338.

Ringwood, A.E. 1982. Phase transformations and differentiation in subducted lithosphere: Implications for mantle dynamics, basalt genesis, and crustal evolution. *J. Geol.*, **90**: 611-643.

Robertson, R., Fox, J.J. & Martin, A.E. 1934. Two types of diamond. *Phil. Trans. Roy. Soc.*, **A323**: 463

Robinson, D.N. 1979. Surface textures and other features of diamonds. Unpubl. Ph.D. Thesis, University of Cape Town, Cape Town.

Robinson, D.N., Scott, J.A., Van Niekerk, A. & Anderson, V.G. 1989. The sequence of events reflected in the diamonds of some southern African kimberlites. In: Kimberlites and Related rocks, Vol. 2. *Their Mantle/Crust Setting, Diamonds and Diamond Exploration*. Geol Soc. Aust., Spec. Publ. No. 14, Blackwell: 990-1000.

Saxena, S.K. 1989. Oxidation state of the mantle. *Geochim. Cosmochim.* Acta, **53**: 89-95

Schmidt, M.W., Poli, S., Comodi, P. & Zanazzi, P.F. 1997. High-pressure behavior of kyanite: Decomposition of kyanite into stishovite and corundum. *Am. Mineral.*, **82**: 460-466.

Schrauder, M. & Navon, O. 1993. Solid carbon dioxide in natural diamond. Nature, **365**: 42-44.

Schulze, D. J. 1986. Calcium anomalies in the mantle and a subducted metaserpentinite origin for diamonds. *Nature*, **319**: 483-485.

Scott-Smith, B. H., Danchin, R.V., Harris, J.W. & Strake, K.J. 1984. Kimberlites near Orroroo, South Australia. In: J. Kornprobst, (ed) Proc. 3rd Int. Kimberlite Conf. Kimberlites I: Kimberlites and Related rocks. Elsevier, Amsterdam.: 121-142.

Seal, M. 1965. Structure of diamonds as revealed by etching. *Am. Mineral.*, **50**, 105-123

Shirey, S.B., Richardson, S.H., Menzies, A.H., Pearson, D.G. Harris, J.W., Carlson, R.W., Wiechert, U., & Gurney, J.J. 2001. Emplacement of eclogite components into the lithospheric mantle during formation of the Kaapvaal craton. *Geophys. Res. Lett.*, **28** (13): 2509-2512

Skinner, E.M.W. & Scott, B.H. 1979. Petrography, mineralogy and geochemistry of kimberlite and associated lamprophyre dykes near Swartruggens, Western Transvaal, R.S.A.. *Extended Abstracts, Kimberlite Symposium II, Cambridge.*

Smith, C.B. 1983. Pb, Sr and Nd isotopic evidence for sources of southern African cretaceous kimberlites. *Nature*, **304**: 51-54.

Smith, C.B., Allsopp, H.L., Kramers, J.D., Hutchinson, G., & Roddick, J.C. 1985. Emplacement ages of Jurassic-Cretaceous South African kimberlites by the Rb-Sr method on phlogopite and whole rock samples. *Trans. Geol. Soc. S. Afr.*, **88**: 249-266.

Smith, D. & Boyd, F.R. 1987. Compositional heterogeneities in a high-temperature lherzolite nodule and implications for mantle processes. In: P.H. Nixon, (ed). *Mantle Xenoliths*. J. Wiley & Sons, England. 551-561.

Sobolev, N. V., Lisoivan, V. I., & Lenskaya, S.V. 1968. *Sov. Phys. Dokl.*, **12**: 665 – 668.

Sobolev, N.V. & Lavrent'yev, Yu, G. 1971. Isomorphic sodium admixture in garnets formed at high pressure. *Contrib. Miner. Petrol.*, **31**: 1-12.

Sobolev, N.V., Galimov, E.M., Ivanovskaya, I.N., & Yefimova, E.S. 1979. Isotopic composition of carbon of diamonds containing crystalline inclusions. *Sov. Phys. Dokl.*, **249**: 1217-1220.

Sobolev, N.V., Lavernt'ev, Yu.G., Pokhilenko, N.P., Usava, L.V. 1973. Chrome-rich garnets from the kimberlites of Yakutia and their paragenesis. *Contrib. Mineral. Petrol.*, **40**: 39-52.

Sobolev, N.V., Yefimova, E.S., Laverent'yev, Yu. G. & Sobolev, V.S. 1984. Dominant calc-silicate association of crystalline inclusions in placer diamonds from southeastern Australia. *Dokl. Akad. Nauk. S.S.S.R.*, **274**: 148-153.

Statchel, T., & Harris, J.W. 1997. Syngenetic inclusions in diamond from the Birim field (Ghana) – a deep peridotitic profile with a history of depletion and re-enrichment. *Contrib. Mineral. Petrol.*, **127**: 336-352.

Statchel, T., Harris, J.W. & Brey, G.P. 1998. Rare and unusual mineral inclusions in diamonds from Mwadui, Tanzania. *Contrib. Mineral. Petrol.*, **132**: 34-47.

Sunagawa, I. 1984a.Growth of crystals in nature. In: I. Sunagwa, (ed)., *Materials Science of the Earths Interior*, Terra Scientific, Tokyo: 63-105

Sunagawa, I. 1984b. Morphology of natural and synthetic diamond crystals. In: I Sunagwa, (ed)., *Materials Science of the Earths Interior*, Terra Scientific, Tokyo: 303-330.

Sutton, J.R. 1928. Kimberley diamonds: especially cleavage diamonds. Trans. Roy. Soc. S.Afr., **7**: 65–96.

Talnikova, S.B. 1995. Inclusions in natural diamonds of different habits. In*: Ext Abstr. 6th Int. Kimberlite. Conf. Russia*: 603-605.

Taylor, W.R., Canil, D. & Milledge, H.J. 1996. Kinetics of Ib to IaA nitrogen aggregation in diamond. *Geochim. Cosmochim. Acta*, **60**: 4725-4733.

Taylor, W.R., Jaques, A.L. & Ridd, M. 1990. Nitrogen-defect aggregation characteristics of some Australasian diamonds: time-temperature constraints on the source regions of pipe and alluvial diamonds. *Am. Mineral.*, **75**: 1290-1310

Tompson, J.F.H. & Barnes, S.J. 1984. The distribution of nickel and iron between olivine and magmatic sulphides in some natural assemblages. Canadian. Mineral., 22: 55-66.

Tsai, H.M., Meyer, H.O.A., Moreau, J. & Milledge, H.J. 1979. Mineral inclusions in diamond: Premier, Jaggersfontein and Finsch kimberlites, South Africa, and Williamson Mine, Tanzania. In: F.R. Boyd & H.O.A. Meyer (eds*). Kimberlites, diatremes and diamonds: Their geology, petrology and chemistry*, American Geophysical Union, Washington D.C.: 16-26.

Ulansky, C. 2001. Personal Communication. University of Cape Town, South Africa.

Urusovskaya, A.A. and Orlov, Yu. L. 1964. Nature of plastic deformation of diamond crystals. *Dokl. Akad. Nauk. S.S.S.R.*, **154**: 112-115.

Vance, E.R., Harris, J.W. and Milledge, H.J. 1973. Possible origins of α-particle damage in diamonds from kimberlites and alluvial sources. *Mineral. Mag.*, **39**: 349-360.

van Wyk, J.A., Loubser, J.H.N., Newton, M.E. & Baker, J.M. 1992. ENDOR and high-temperature EPR of the N3 centre in natural type Ib diamonds. *J. Phys.: Condens. Matter*, **4**: 2651-2662.

Viljoen, K.S. 2001. Personal communication. De Beers Geoscience Centre, Johannesburg.

Viljoen, K.S., Phillips,D., Harris, J.W. & Robinson, D.N. 1999. Mineral inclusions in diamonds from the Venetia kimberlites, Northern Province, South Africa. In J.J. Gurney, J.L Gurney, M.D Pascoe, S.H. Richardson (eds), *Proc. 7th Int. Kimberlite. Conf.*, **2**: 888-895. University of Cape Town.

Wagner, P.A. 1914. *The diamond fields of Southern Africa*. Transvaal Leader, Johannesburg.

Westerlund, K.J. 2000. A Geochemical Study of Diamonds, Diamond Inclusion Minerals and other mantle Minerals from the Klipspringer Kimberlites, South Africa. Unpubl. MSc Thesis. University of Cape Town, South Africa.

Wilding, M.C., Harte, B., & Harris, J.W. 1989. Evidence of an asthenospheric source for diamonds from Brazil. *28th International Geological Congress, Abstracts*, **3**, Washington, D.C.: 359-360.

Woodland, A.B. & O'Neill, H.St.C. 1993. Synthesis and stability of $Fe_3^{2+}Fe_2^{3+}Si_3O_{12}$ garnet and phase relations with $Fe_3Al_2Si_3O_{12} - Fe_3^{2+}Fe_2^{3+}Si_3O_{12}$ solutions. *Am. Mineral.*, **78**: 1002-1015.

Woods, G.S. 1986. Platelets and the infrared absorption of type Ia diamonds. *Proc. R. Soc.*, **A 407**: 219-238.

Woods, G.S., & Collins, A.T. 1983. Infrared absorption spectra of hydrogen complexes in Type I diamonds. *J. Phys. C: Solid St. Phys.*, **51**: 1191-1197.

Woods, G.S, & Lang, 1975. J. Cryst. Growth, 28:215-226

Woods, G.S., Purser, G.C., Mtimkulu, A.S.S. & Collins, A.T. 1990. The nitrogen content of Type Ia natural diamonds. *J. Phys. Chem. Solids*, **51**: 1191-1197.

Yefimova, E.S., Sobolev, N.V., & Pospelova, L.N. 1983. Sulphide inclusions in diamond and specific features of their paragenesis. Zap.Vses. Mineral. Obsh., **112**: 300-310 (in Russian)

Zezin, R.B., Saparin, G.V., Smirnova, E.P., Obyden, S.K. & Chukichev, M.V. 1990. Cathodoluminescence of natural diamonds from Jakutin deposits. *Scanning*, **12**: 326-333.

APPENDIX 1

ELECTRON MICROPROBE ANALYSIS OF GARNET AND CHROMITE MACROCRYSTS

Kimberlite samples from the Main and Changehouse fissures were crushed and reduced to heavy mineral concentrate at the Helam Diamond Mine. The heavy minerals were then sorted, separating garnet macrocrysts into groups of purple, red and orange crystals, with a separate group for chromite macrocrysts, for each of the kimberlite samples. The macrocrysts were mounted in Petropox epoxy, and polished mechanically to produce flat surfaces.

The individual macrocryst crystals were analysed using a wavelength-dispersive spectrometer-equipped Cameca SX-50 electron microprobe at the De Beers Geoscience Center, Johannesburg. The instrument was operated at an acceleration potential of 20 kV and at a probe current 30 nA for the silicates and oxides. Counting times of 20 seconds for all elements. Background measurements were taken for a count time of 20 seconds. K-α lines were used for all elements. Apparent concentrations were corrected for matrix effects with an on-line PAP computer program. MgO (Mg), almandine garnet (Al), Cr_2O_3 (Cr), TiO_2 (Ti), diopside (Ca,Si), Fe_3O_4 (Fe), $MnTiO_3$ (Mn), and Ni metal (Ni) were used as standards for silicate and oxide minerals.

The following table shows detection limits for component oxides of the various macrocryst minerals, calculated at 2 sigma:

Table A-1 Detection limits for component oxides of Helam macrocryst minerals.

	Garnet	Chromite
SiO_2	0.02	0.02
TiO_2	0.02	0.02
$Al2O_3$	0.02	0.03
Cr_2O_3	0.02	0.03
FeO	0.03	0.04
MnO	0.03	0.04
MgO	0.02	0.03
CaO	0.01	0.02
Na_2O	0.04	0.07
K_2O	0.02	0.02
NiO	0.03	0.04

Appendix 1.1: Chemical analyses of Main Fissure garnet macrocrysts.

	Red					Purple					
	mck2-1	mck2-2	mck2-3	mck2-4	mck2-5	mck2-6	mck2-7	mck2-8	mck2-9	mck2-10	mck2-11
Oxides											
SiO_2	41.22	41.62	41.87	41.76	41.76	41.56	42.04	41.00	41.53	42.27	41.36
TiO_2	N.D	0.03	0.09	0.12	N.D	0.02	0.29	0.77	0.16	0.16	0.33
$Al2O_3$	19.40	18.22	19.23	18.94	19.12	18.59	20.83	17.17	20.96	20.88	17.26
Cr_2O_3	5.97	6.94	5.66	5.93	6.00	5.91	2.97	7.17	3.01	3.03	7.02
FeO	6.23	6.55	6.39	6.38	6.26	6.20	7.02	6.83	8.04	6.85	6.15
MnO	0.27	0.30	0.32	0.35	0.32	0.30	0.29	0.30	0.37	0.29	0.28
MgO	21.63	20.57	21.18	20.91	21.23	21.51	21.75	20.91	20.70	21.60	20.48
CaO	5.08	5.80	4.93	5.14	4.94	5.09	4.61	4.88	4.66	4.62	5.27
Na_2O	0.04	N.D.	0.04	N.D.	N.D.	N.D.	0.04	N.D.	0.04	0.04	0.05
K_2O	N.D.	N.D.	N.D.	N.D.	N.D.	N.D.	N.D.	N.D.	N.D.	N.D.	N.D.
NiO	N.D.	N.D.	N.D.	N.D.	N.D.	N.D.	N.D.	N.D.	N.D.	N.D.	N.D.
Total	**99.84**	**100.03**	**99.71**	**99.53**	**99.64**	**99.18**	**99.84**	**99.03**	**99.47**	**99.74**	**98.20**

	mck2-12	mck2-13	mck2-14	mck2-16	mck2-17	mck2-18	mck2-19	mck2-20	mck2-21	mck2-22	mck2-23
Oxides											
SiO_2	40.64	41.95	40.95	41.92	41.49	41.53	41.82	40.53	41.59	41.27	41.8
TiO_2	0.27	0.13	0.03	0.07	0.02	N.D	0.03	0.26	0.12	0.03	N.D.
$Al2O_3$	14.79	19.83	16.75	18.82	17.13	18.97	20.72	15.09	18.82	18.09	19.3
Cr_2O_3	10.34	4.19	8.06	5.94	8.35	5.89	3.78	10.59	6.31	6.84	5.47
FeO	6.52	6.27	6.65	6.07	6.44	6.31	6.04	6.55	6.33	6.44	6.48
MnO	0.35	0.28	0.32	0.24	0.33	0.27	0.28	0.34	0.33	0.29	0.31
MgO	19.64	21.32	19.81	22.02	21.58	21.23	22.04	20.19	20.8	20.34	21.43
CaO	5.46	4.92	5.96	4.56	4.45	5.05	4.78	5.43	5.66	5.81	4.79
Na_2O	N.D.	N.D.	N.D.	N.D.	N.D.	N.D.	N.D.	0.04	N.D.	N.D.	N.D.
K_2O	N.D.	N.D.	N.D.	N.D.	N.D.	N.D.	N.D.	N.D.	N.D.	N.D.	N.D.
NiO	N.D.	N.D.	N.D.	N.D.	N.D.	N.D.	N.D.	N.D.	0.03	N.D.	N.D.
Total	**98.01**	**98.89**	**98.53**	**99.64**	**99.79**	**99.25**	**99.49**	**99.02**	**99.99**	**99.11**	**99.58**

Appendix 1.1 continued…

	mck2-24	mck2-25	mck2-26	mck2-27	mck2-28	mck2-29	mck2-30	mck2-31	mck2-32	mck2-33	mck2-34
Oxides											
SiO_2	42.04	41.58	41.10	39.71	40.61	41.82	42.41	42.02	41.60	42.04	41.19
TiO_2	0.08	0.05	0.24	0.27	0.22	0.53	N.D.	0.03	N.D.	N.D.	0.11
$Al2O_3$	21.03	19.45	23.15	22.60	22.86	22.03	21.57	20.01	18.96	19.01	18.61
Cr_2O_3	3.63	5.77	0.08	0.10	0.08	0.42	2.90	4.62	5.89	5.55	6.23
FeO	6.10	6.05	15.13	18.31	15.05	11.01	5.97	6.30	6.15	5.90	6.32
MnO	0.28	0.28	0.46	0.60	0.49	0.29	0.25	0.26	0.30	0.27	0.32
MgO	22.25	22.18	17.08	14.49	16.63	19.99	22.30	21.67	21.17	21.93	20.70
CaO	4.77	4.76	4.25	4.39	4.32	3.83	4.62	4.94	5.02	4.48	5.65
Na_2O	N.D.	N.D.	0.07	0.09	0.08	0.07	N.D.	N.D.	N.D.	N.D.	N.D.
K_2O	N.D.	N.D.	N.D.	N.D.	N.D.	N.D.	N.D.	N.D.	N.D.	N.D.	N.D.
NiO	N.D.	N.D.	N.D.	N.D.	N.D.	0.03	0.03	N.D.	0.03	N.D.	N.D.
Total	**100.18**	**100.12**	**101.56**	**100.56**	**100.34**	**100.02**	**100.05**	**99.85**	**99.12**	**99.18**	**99.13**

	mck2-35	mck2-36	mck2-37	mck2-38	mck2-39	mck2-40	Orange mck2-41	mck2-42	mck2-43	mck2-44	mck2-45
Oxides											
SiO_2	41.42	41.39	40.94	41.17	41.36	41.09	39.75	40.26	40.73	40.17	40.53
TiO_2	0.02	N.D.	N.D.	0.03	0.11	0.08	0.24	0.31	0.25	0.23	0.24
$Al2O_3$	18.86	18.88	17.10	16.64	18.30	18.74	21.58	21.89	22.27	21.81	22.27
Cr_2O_3	5.92	5.91	8.02	8.73	5.82	5.61	0.09	0.12	0.08	0.07	0.09
FeO	6.18	6.21	6.70	6.16	6.36	6.45	18.53	16.17	15.28	18.42	15.07
MnO	0.31	0.31	0.32	0.34	0.32	0.30	0.62	0.50	0.46	0.62	0.44
MgO	21.17	21.02	20.00	21.30	20.23	20.69	13.51	15.34	16.16	13.87	16.23
CaO	5.04	5.06	6.02	4.10	5.18	4.91	4.56	4.18	4.30	4.32	4.29
Na_2O	N.D.	N.D.	N.D.	N.D.	N.D.	N.D.	0.08	0.10	0.08	0.09	0.11
K_2O	N.D.	N.D.	N.D.	N.D.	N.D.	N.D.	N.D.	N.D.	N.D.	N.D.	N.D.
NiO	N.D.	N.D.	N.D.	N.D.	N.D.	N.D.	N.D.	N.D.	N.D.	N.D.	N.D.
Total	**98.95**	**98.83**	**99.14**	**98.49**	**97.71**	**97.90**	**98.99**	**98.89**	**99.60**	**99.62**	**99.28**

	mck2-46	mck2-47	mck2-48	mck2-49	mck2-50	mck2-51	mck2-52	mck2-53	mck2-54	mck2-55	mck2-57	mck2-58
Oxides												
SiO_2	40.64	39.94	40.04	40.58	40.03	39.93	40.61	39.89	40.63	40.50	40.35	40.7
TiO_2	0.22	0.26	0.27	0.29	0.23	0.27	0.24	0.28	0.23	0.23	0.23	0.23
$Al2O_3$	22.49	21.80	22.12	22.15	21.93	22.06	22.68	22.06	22.73	23.31	23.15	22.53
Cr_2O_3	0.08	0.10	0.08	0.12	0.08	0.10	0.09	0.09	0.10	0.08	0.08	0.08
FeO	15.09	18.16	18.49	16.04	18.62	18.45	15.07	18.45	15.00	15.09	14.10	15.07
MnO	0.47	0.56	0.62	0.51	0.61	0.63	0.47	0.60	0.46	0.50	0.37	0.47
MgO	16.40	13.96	13.99	15.75	13.76	13.92	16.60	14.07	16.62	17.10	17.09	16.29
CaO	4.24	4.43	4.51	4.13	4.48	4.52	4.29	4.45	4.27	4.22	5.02	4.31
Na_2O	0.10	0.08	0.10	0.09	0.07	0.09	0.09	0.09	0.07	0.10	0.07	0.09
K_2O	N.D.	N.D.	N.D.	N.D.	N.D.	N.D.	N.D.	N.D.	N.D.	N.D.	N.D.	N.D.
NiO	N.D.	N.D.	N.D.	N.D.	N.D.	N.D.	N.D.	N.D.	N.D.	N.D.	N.D.	N.D.
Total	**99.73**	**99.29**	**100.22**	**99.66**	**99.81**	**99.97**	**100.14**	**99.98**	**100.11**	**101.13**	**100.46**	**99.77**

	mck2-59	mck2-60	mck2-61	mck2-62	mck2-63	mck2-64	mck2-65	mck2-66	mck2-67	mck2-68	mck2-69	mck2-70
Oxides												
SiO_2	40.32	40.75	40.66	40.03	40.55	40.92	40.42	40.69	40.22	40.21	40.15	40.6
TiO_2	0.23	0.26	0.23	0.23	0.22	0.23	0.23	0.24	0.25	0.25	0.27	0.25
$Al2O_3$	22.79	22.81	22.55	22.47	22.44	22.76	22.33	22.50	22.69	22.28	22.10	22.43
Cr_2O_3	0.07	0.21	0.10	0.08	0.09	0.06	0.10	0.09	0.07	0.10	0.08	0.05
FeO	14.94	13.23	15.13	15.03	14.90	13.91	15.16	13.86	13.84	15.16	15.02	13.96
MnO	0.46	0.37	0.48	0.47	0.48	0.39	0.46	0.38	0.36	0.45	0.47	0.37
MgO	16.60	17.90	16.36	16.30	16.39	16.87	16.27	16.48	16.63	16.27	16.24	16.37
CaO	4.27	4.18	4.27	4.30	4.33	5.01	4.26	5.01	5.06	4.27	4.30	5.05
Na_2O	0.09	0.06	0.09	0.08	0.09	0.10	0.09	0.09	0.10	0.08	0.08	0.07
K_2O	N.D.	N.D.	N.D.	N.D.	N.D.	N.D.	N.D.	N.D.	N.D.	N.D.	N.D.	N.D.
NiO	N.D.	N.D.	N.D.	N.D.	N.D.	N.D.	N.D.	N.D.	N.D.	N.D.	N.D.	N.D.
Total	**99.77**	**99.77**	**99.87**	**98.99**	**99.49**	**100.25**	**99.32**	**99.34**	**99.22**	**99.07**	**98.71**	**99.15**

Appendix 1.2: Chemical analyses of Changehouse Fissure garnet macrocrysts.

	Purple mck1-1	mck1-3	mck1-4	mck1-5	mck1-6	mck1-7	mck1-8	mck1-9	mck1-11	mck1-13	mck1-14
Oxides											
SiO_2	42.12	41.66	41.67	41.42	41.03	42.38	41.29	41.77	41.86	41.40	42.22
TiO_2	0.04	0.13	N.D.	N.D.	N.D.	0.07	0.06	N.D.	0.02	N.D.	0.05
$Al2O_3$	20.60	19.33	20.38	21.76	19.66	21.63	18.50	21.24	19.22	20.26	21.12
Cr_2O_3	4.51	5.74	4.69	3.28	5.63	3.08	6.75	3.40	5.60	4.84	3.55
FeO	6.37	6.36	6.58	7.77	6.32	6.12	6.30	7.88	6.17	6.39	6.22
MnO	0.29	0.31	0.32	0.42	0.30	0.27	0.30	0.42	0.29	0.30	0.28
MgO	21.72	21.77	21.23	20.90	21.21	22.24	21.08	20.45	20.89	21.19	22.08
CaO	5.13	4.38	4.92	4.37	5.18	4.56	5.11	4.41	5.19	5.19	4.77
Na_2O	N.D.	0.04	N.D.	N.D.	N.D.	0.05	N.D.	N.D.	N.D.	N.D.	N.D.
K_2O	N.D.	N.D.	N.D.	N.D.	N.D.	N.D.	N.D.	N.D.	N.D.	N.D.	N.D.
NiO	N.D.	N.D.	N.D.	N.D.	N.D.	N.D.	N.D.	N.D.	N.D.	N.D.	N.D.
Total	**100.78**	**99.72**	**99.79**	**99.92**	**99.33**	**100.40**	**99.39**	**99.57**	**99.24**	**99.57**	**100.29**

	mck1-15	mck1-16	mck1-17	mck1-18	mck1-19	mck1-20	mck1-21	mck1-22	mck1-23	mck1-29	mck1-30
Oxides											
SiO_2	41.75	41.59	41.64	41.63	41.65	41.68	41.71	41.42	42.20	42.18	41.87
TiO_2	0.03	0.03	N.D.	0.02	0.02	0.23	N.D.	0.37	0.34	0.03	N.D.
$Al2O_3$	19.49	19.60	20.10	19.82	19.87	19.55	20.62	20.47	20.54	20.29	19.48
Cr_2O_3	5.77	5.57	4.85	5.67	5.56	5.75	4.66	4.24	3.44	4.85	5.59
FeO	6.16	6.27	6.33	6.13	6.20	6.49	6.37	6.63	7.00	6.49	6.22
MnO	0.34	0.30	0.31	0.29	0.32	0.32	0.29	0.28	0.33	0.32	0.34
MgO	21.18	21.16	21.10	21.49	21.52	21.90	21.68	22.01	21.47	21.32	21.10
CaO	5.25	5.19	5.16	5.19	5.19	4.33	5.14	4.72	4.63	5.15	5.20
Na_2O	N.D.	N.D.	N.D.	N.D.	N.D.	0.04	N.D.	0.05	0.05	N.D.	N.D.
K_2O	N.D.	N.D.	N.D.	N.D.	N.D.	N.D.	N.D.	N.D.	N.D.	N.D.	N.D.
NiO	0.03	N.D.	N.D.	N.D.	N.D.	N.D.	N.D.	N.D.	N.D.	N.D.	N.D.
Total	**100.00**	**99.71**	**99.49**	**100.24**	**100.33**	**100.29**	**100.47**	**100.19**	**100.00**	**100.63**	**99.80**

Appendix 1.2 continued…

	Red										
	mck1-34	**mck1-35**	**mck1-58**	**mck1-32**	**mck1-24**	**mck1-25**	**mck1-26**	**mck1-27**	**mck1-28**	**mck1-31**	**mck1-33**
Oxides											
SiO_2	42.00	42.46	41.66	41.94	41.82	42.09	42.16	42.64	42.38	42.56	42.71
TiO_2	0.03	0.04	0.52	0.02	0.15	0.30	0.32	0.04	0.03	0.03	0.04
$Al2O_3$	19.11	18.83	20.22	19.82	21.57	21.14	21.29	21.31	21.31	21.58	20.87
Cr_2O_3	5.83	5.72	3.82	4.87	3.09	2.98	2.94	3.39	3.45	3.05	3.38
FeO	6.25	6.33	7.32	6.37	6.94	7.10	7.18	6.11	6.10	6.15	6.09
MnO	0.33	0.31	0.32	0.30	0.30	0.31	0.29	0.28	0.25	0.25	0.28
MgO	20.75	20.83	21.63	21.00	22.05	21.64	21.85	22.13	22.14	22.22	21.87
CaO	5.26	5.26	4.93	5.17	4.58	4.52	4.53	4.65	4.73	4.48	4.67
Na_2O	0.08	0.07	0.08	0.03	0.04	0.02	0.05	0.03	0.05	0.03	0.02
K_2O	0.02	N.D.	N.D.	N.D.	N.D.	N.D.	N.D.	N.D.	N.D.	N.D.	N.D.
NiO	0.03	N.D.	N.D.	N.D.	N.D.	0.03	N.D.	N.D.	N.D.	N.D.	N.D.
Total	**99.69**	**99.85**	**100.50**	**99.52**	**100.54**	**100.13**	**100.61**	**100.58**	**100.44**	**100.35**	**99.93**

	mck1-36	**mck1-37**	**mck1-38**	**mck1-39**	**mck1-40**	**mck1-41**	**mck1-42**	**mck1-43**	**mck1-44**	**mck1-45**	**mck1-46**
Oxides											
SiO_2	41.88	42.08	42.40	42.32	42.15	42.30	41.96	42.19	42.21	41.80	42.31
TiO_2	0.29	0.16	0.15	0.17	0.35	0.34	0.14	0.31	0.30	0.52	0.33
$Al2O_3$	20.89	20.40	20.86	20.61	21.78	21.84	21.17	20.88	20.94	21.03	20.96
Cr_2O_3	3.05	3.10	3.08	3.14	1.74	1.71	3.12	3.39	3.02	2.99	3.06
FeO	7.08	8.01	7.05	7.13	7.40	7.26	7.91	6.81	7.13	7.13	6.96
MnO	0.29	0.37	0.30	0.27	0.34	0.31	0.37	0.29	0.30	0.28	0.28
MgO	21.53	19.96	21.31	21.24	21.45	21.37	20.39	21.81	21.44	21.52	21.85
CaO	4.61	4.75	4.58	4.66	4.61	4.58	4.72	4.57	4.56	4.56	4.61
Na_2O	0.06	0.05	N.D.	0.05	N.D.	0.05	0.04	0.05	0.05	0.06	0.06
K_2O	N.D.	N.D.	N.D.	N.D.	N.D.	N.D.	N.D.	N.D.	N.D.	N.D.	N.D.
NiO	N.D.	N.D.	N.D.	N.D.	0.03	0.04	N.D.	N.D.	N.D.	0.03	N.D.
Total	**99.68**	**98.88**	**99.73**	**99.59**	**99.85**	**99.80**	**99.82**	**100.30**	**99.95**	**99.92**	**100.42**

Appendix 1.2 continued…

	mck1-47	mck1-48	mck1-49	mck1-50	mck1-57	mck1-59	mck1-60	mck1-61	mck1-62	mck1-63	mck1-64
Oxides											
SiO_2	41.84	42.17	42.30	42.17	42.12	42.28	41.79	41.93	42.28	41.85	41.70
TiO_2	0.14	0.29	0.38	0.31	0.14	0.29	0.52	0.30	0.16	0.16	0.29
$Al2O_3$	20.92	21.21	21.39	21.15	21.04	21.11	20.03	20.67	20.89	21.51	20.16
Cr_2O_3	3.03	3.38	2.15	3.35	3.00	3.00	3.72	3.35	3.07	2.47	3.01
FeO	8.06	6.75	7.21	6.82	6.89	7.03	7.32	6.79	7.27	7.69	7.14
MnO	0.37	0.28	0.33	0.30	0.26	0.27	0.34	0.29	0.28	0.31	0.29
MgO	20.35	22.11	21.77	22.37	22.00	21.99	21.25	21.91	21.59	21.53	21.12
CaO	4.68	4.56	4.39	4.56	4.58	4.59	4.92	4.66	4.66	4.24	4.71
Na_2O	0.04	0.04	0.06	0.06	N.D.	0.05	0.09	0.04	0.04	0.05	0.06
K_2O	N.D.	N.D.	N.D.	N.D.	N.D.	N.D.	N.D.	N.D.	N.D.	N.D.	N.D.
NiO	N.D.	N.D.	N.D.	N.D.	N.D.	N.D.	N.D.	N.D.	N.D.	N.D.	N.D.
Total	**99.43**	**100.79**	**99.98**	**101.09**	**100.03**	**100.61**	**99.98**	**99.94**	**100.24**	**99.81**	**98.48**

				Orange							
	mck1-65	mck1-10	mck1-12	mck1-51	mck1-52	mck1-53	mck1-54	mck1-55	mck1-56	mck1-66	mck1-67
Oxides											
SiO_2	42.45	42.47	42.12	40.45	42.10	42.52	41.56	42.77	40.30	41.52	42.29
TiO_2	0.31	N.D.	0.03	0.66	0.41	0.40	0.69	0.41	0.41	0.68	0.41
$Al2O_3$	20.36	22.04	21.43	22.76	23.06	22.52	22.12	22.45	21.93	21.87	22.29
Cr_2O_3	3.34	2.22	3.10	0.10	0.61	0.64	0.11	0.64	0.02	0.10	0.53
FeO	6.85	5.98	6.21	13.84	7.04	7.07	14.14	6.97	18.91	14.11	7.13
MnO	0.28	0.27	0.27	0.32	0.24	0.30	0.28	0.28	0.54	0.28	0.28
MgO	21.74	22.37	22.13	18.22	22.86	22.49	17.98	22.52	14.03	17.59	22.04
CaO	4.60	4.41	4.57	4.30	4.38	4.36	4.27	4.34	4.50	4.39	4.37
Na_2O	0.06	0.02	0.01	0.15	0.06	0.05	0.16	0.06	0.14	0.14	0.05
K_2O	N.D.	N.D.	N.D.	N.D.	N.D.	N.D.	N.D.	N.D.	N.D.	N.D.	N.D.
NiO	N.D.	N.D.	N.D.	N.D.	N.D.	N.D.	N.D.	N.D.	N.D.	N.D.	0.03
Total	**99.99**	**99.78**	**99.87**	**100.80**	**100.76**	**100.35**	**101.31**	**100.44**	**100.78**	**100.68**	**99.42**

Appendix 1.2 continued…

	mck1-68	mck1-69	mck1-70	mck1-71	mck1-72	mck1-73	mck1-74	mck1-75	mck1-76	mck1-77	mck1-78
Oxides											
SiO_2	42.43	40.98	41.13	41.04	42.57	42.84	40.88	40.90	41.10	42.45	40.98
TiO_2	0.34	0.69	0.67	0.34	0.37	0.39	0.68	0.67	0.64	0.39	0.72
$Al2O_3$	22.61	21.70	22.12	22.33	22.90	22.84	21.99	22.23	22.20	22.82	22.32
Cr_2O_3	0.57	0.10	0.10	0.37	0.34	0.41	0.10	0.10	0.11	0.61	0.12
FeO	6.92	14.01	13.91	14.36	7.00	6.98	13.88	13.92	13.89	7.01	13.89
MnO	0.28	0.29	0.27	0.41	0.28	0.28	0.28	0.29	0.30	0.30	0.29
MgO	22.31	17.47	17.66	17.59	22.58	22.63	17.72	17.84	17.85	22.75	18.09
CaO	4.29	4.30	4.34	4.02	4.25	4.29	4.31	4.28	4.29	4.37	4.33
Na_2O	0.04	0.15	0.13	0.06	0.04	0.04	0.14	0.14	0.14	0.04	0.13
K_2O	N.D.	N.D.	N.D.	N.D.	N.D.	N.D.	N.D.	N.D.	N.D.	N.D.	N.D.
NiO	N.D.	N.D.	N.D.	N.D.	N.D.	N.D.	N.D.	N.D.	N.D.	N.D.	N.D.
Total	**99.79**	**99.69**	**100.33**	**100.52**	**100.33**	**100.70**	**99.98**	**100.37**	**100.52**	**100.74**	**100.87**

	mck1-79	mck1-83	mck1-84	mck1-85	mck1-86	mck1-87	mck1-88	mck1-89	mck1-90	mck1-91	mck1-92
Oxides											
SiO_2	42.46	41.70	40.27	42.24	42.20	42.25	38.58	40.83	42.38	42.05	42.22
TiO_2	0.38	0.41	0.66	0.42	0.38	0.38	0.46	0.68	0.41	0.40	0.39
$Al2O_3$	23.33	22.96	22.27	22.71	22.83	22.99	20.75	22.09	22.53	22.42	22.60
Cr_2O_3	0.47	0.48	0.10	0.68	0.41	0.33	0.02	0.08	0.42	0.67	0.50
FeO	7.02	7.01	13.79	6.98	7.04	7.00	18.55	13.91	7.01	7.10	7.05
MnO	0.29	0.26	0.27	0.31	0.31	0.29	0.53	0.27	0.27	0.28	0.28
MgO	22.91	22.72	18.04	22.77	22.82	22.81	12.86	17.83	22.38	22.48	22.40
CaO	4.29	4.32	4.31	4.46	4.30	4.26	4.57	4.36	4.33	4.39	4.30
Na_2O	0.05	0.05	0.15	0.05	0.04	0.04	0.13	0.14	0.05	0.05	0.04
K_2O	N.D.	N.D.	N.D.	N.D.	N.D.	N.D.	N.D.	N.D.	N.D.	N.D.	N.D.
NiO	N.D.	N.D.	0.03	N.D.	0.03	0.03	N.D.	N.D.	N.D.	0.03	0.03
Total	**101.20**	**99.91**	**99.89**	**100.62**	**100.36**	**100.38**	**96.45**	**100.19**	**99.78**	**99.87**	**99.81**

Appendix 1.3: Chemical analyses of Main Fissure chromite macrocrysts.

	mck2-71	mck2-72	mck2-73	mck2-74	mck2-75	mck2-76	mck2-77	mck2-78	mck2-79	mck2-80	mck2-81
Oxides											
SiO_2	0.18	0.22	0.22	0.16	0.15	0.12	0.19	0.19	0.16	0.19	0.16
TiO_2	0.20	0.31	2.18	1.08	0.06	1.79	0.23	0.51	1.09	1.16	1.05
$Al2O_3$	6.35	10.72	5.72	4.70	2.60	4.30	6.54	7.52	4.60	5.53	4.79
Cr_2O_3	61.69	53.85	56.31	62.84	68.07	60.61	61.85	61.39	63.69	60.76	63.75
FeO	16.14	20.00	21.08	15.89	14.62	18.95	16.05	15.26	15.78	18.50	15.87
MnO	0.26	0.26	0.27	0.25	0.25	0.26	0.24	0.22	0.26	0.27	0.23
MgO	13.13	12.60	12.34	13.37	13.27	13.07	13.58	14.14	13.21	12.90	13.67
CaO	N.D.	N.D.	N.D.	N.D.	N.D.	N.D.	N.D.	N.D.	N.D.	N.D.	N.D.
Na_2O	N.D.	N.D.	N.D.	N.D.	N.D.	N.D.	N.D.	N.D.	N.D.	N.D.	N.D.
K_2O	N.D.	N.D.	N.D.	N.D.	N.D.	N.D.	N.D.	N.D.	N.D.	N.D.	N.D.
NiO	0.11	0.17	0.17	0.17	0.09	0.14	0.11	0.12	0.17	0.14	0.14
Total	**98.06**	**98.13**	**98.29**	**98.46**	**99.11**	**99.24**	**98.79**	**99.35**	**98.96**	**99.45**	**99.66**

	mck2-82	mck2-83	mck2-84	mck2-85	mck2-86	mck2-87	mck2-88	mck2-89	mck2-90	mck2-91	mck2-92
Oxides											
SiO_2	0.15	0.18	0.16	0.12	0.09	0.23	0.09	0.17	0.20	0.18	0.16
TiO_2	0.03	0.59	1.11	1.89	2.52	1.71	1.20	0.08	0.50	0.17	1.19
$Al2O_3$	7.14	4.17	4.92	3.28	2.93	5.63	6.46	6.25	6.84	5.04	3.85
Cr_2O_3	61.83	64.07	63.58	63.91	57.74	57.73	56.38	63.44	59.20	64.90	62.88
FeO	16.97	16.28	15.94	17.02	24.46	20.37	23.47	14.69	18.32	14.35	16.46
MnO	0.25	0.22	0.25	0.24	0.31	0.24	0.26	0.23	0.27	0.24	0.24
MgO	13.36	14.06	14.05	13.10	10.95	12.87	10.70	12.44	13.39	13.47	13.37
CaO	N.D.	N.D.	N.D.	N.D.	N.D.	N.D.	N.D.	N.D.	N.D.	N.D.	N.D.
Na_2O	N.D.	N.D.	N.D.	N.D.	N.D.	N.D.	N.D.	N.D.	N.D.	N.D.	N.D.
K_2O	N.D.	N.D.	N.D.	N.D.	N.D.	N.D.	N.D.	N.D.	N.D.	N.D.	N.D.
NiO	0.11	0.16	0.12	0.14	0.21	0.19	0.19	0.12	0.16	0.09	0.15
Total	**99.84**	**99.73**	**100.13**	**99.70**	**99.21**	**98.97**	**98.75**	**97.42**	**98.88**	**98.44**	**98.30**

Appendix 1.3 continued...

	mck2-93	mck2-94	mck2-95	mck2-96	mck2-97	mck2-98	mck2-99	mck2-100
Oxides								
SiO_2	0.17	0.18	0.08	0.17	0.19	0.11	0.13	0.19
TiO_2	0.91	0.32	0.13	0.07	0.07	1.74	1.76	0.50
$Al2O_3$	4.79	5.31	9.18	6.68	6.68	4.89	3.57	7.01
Cr_2O_3	61.51	62.18	60.56	62.90	63.32	61.26	63.10	59.32
FeO	16.73	16.62	15.12	14.86	14.61	17.67	16.97	18.28
MnO	0.25	0.22	0.22	0.25	0.22	0.25	0.25	0.25
MgO	13.36	13.27	13.54	13.78	13.92	13.28	13.85	13.79
CaO	N.D.	N.D.	N.D.	N.D.	N.D.	N.D.	N.D.	N.D.
Na_2O	N.D.	N.D.	N.D.	N.D.	N.D.	N.D.	N.D.	N.D.
K_2O	N.D.	N.D.	N.D.	N.D.	N.D.	N.D.	N.D.	N.D.
NiO	0.15	0.14	0.08	0.12	0.14	0.12	0.14	0.16
Total	**97.87**	**98.24**	**98.91**	**98.83**	**99.15**	**99.32**	**99.77**	**99.50**

Appendix 1.4: Chemical analyses of Changehouse Fissure chromite macrocrysts.

	mck1-80	mck1-81	mck1-82	mck1-93	mck1-94	mck1-95	mck1-96	mck1-97	mck1-98	mck1-99	mck1-100
Oxides											
SiO_2	0.15	0.10	0.17	0.21	0.19	0.14	0.14	0.14	0.18	0.14	0.18
TiO_2	3.25	2.63	0.79	0.29	0.29	3.25	2.38	0.13	1.53	0.95	1.59
$Al2O_3$	4.63	3.70	7.74	6.85	6.93	4.46	4.34	6.55	8.22	5.54	5.31
Cr_2O_3	60.79	59.81	59.42	62.00	61.82	60.79	61.23	62.11	56.36	62.98	61.75
FeO	16.30	20.20	16.58	16.73	16.57	16.40	17.67	17.28	19.81	16.28	16.28
MnO	0.25	0.31	0.25	0.29	0.27	0.25	0.27	0.29	0.28	0.28	0.24
MgO	14.72	12.68	14.22	12.71	12.93	14.14	13.35	12.93	13.27	13.43	13.90
CaO	N.D.	N.D.	N.D.	N.D.	N.D.	N.D.	N.D.	N.D.	N.D.	N.D.	N.D.
Na_2O	N.D.	N.D.	N.D.	N.D.	N.D.	N.D.	N.D.	N.D.	N.D.	N.D.	N.D.
K_2O	N.D.	N.D.	N.D.	N.D.	N.D.	N.D.	N.D.	N.D.	N.D.	N.D.	N.D.
NiO	0.15	0.14	0.13	0.17	0.12	0.17	0.15	0.11	0.18	0.13	0.15
Total	**100.24**	**99.57**	**99.30**	**99.25**	**99.12**	**99.60**	**99.53**	**99.54**	**99.83**	**99.73**	**99.40**

	mck1-101	mck1-102	mck1-103	mck1-104	mck1-105	mck1-106	mck1-107	mck1-108	mck1-109	mck1-110	mck1-111
Oxides											
SiO_2	0.23	0.11	0.16	0.12	0.15	0.18	0.22	0.16	0.15	0.20	0.08
TiO_2	1.83	0.62	0.44	0.04	0.10	0.12	2.38	3.22	0.02	0.30	2.25
$Al2O_3$	4.33	7.24	4.78	4.01	6.76	6.16	5.64	4.50	5.84	7.03	1.98
Cr_2O_3	62.47	60.42	61.54	67.20	62.17	64.20	57.62	60.90	64.30	62.20	60.44
FeO	15.49	17.87	19.55	14.95	17.15	14.76	19.74	16.29	15.26	16.48	22.34
MnO	0.22	0.26	0.24	0.25	0.28	0.23	0.25	0.25	0.25	0.28	0.33
MgO	15.17	13.28	12.36	13.53	13.26	14.14	13.44	14.34	13.55	13.33	11.17
CaO	N.D.	N.D.	N.D.	N.D.	N.D.	N.D.	N.D.	N.D.	N.D.	N.D.	N.D.
Na_2O	N.D.	N.D.	N.D.	N.D.	N.D.	N.D.	N.D.	N.D.	N.D.	N.D.	N.D.
K_2O	N.D.	N.D.	N.D.	N.D.	N.D.	N.D.	N.D.	N.D.	N.D.	N.D.	N.D.
NiO	0.16	0.12	0.13	0.11	0.13	0.10	0.19	0.17	0.11	0.13	0.18
Total	**99.90**	**99.92**	**99.20**	**100.21**	**100.00**	**99.89**	**99.48**	**99.83**	**99.48**	**99.95**	**98.77**

Appendix 1.4 continued…

	mck1-112	mck1-113	mck1-114	mck1-115	mck1-116	mck1-117	mck1-118	mck1-119
Oxides								
SiO_2	0.08	0.20	0.14	0.19	0.07	0.12	0.17	0.09
TiO_2	0.48	0.44	1.28	0.41	0.17	1.75	1.81	0.03
$Al2O_3$	5.22	9.57	6.35	9.62	11.99	3.64	6.61	9.86
Cr_2O_3	60.09	55.22	59.47	54.98	56.89	61.23	58.77	59.69
FeO	21.04	20.52	19.06	20.51	17.73	19.77	17.85	16.32
MnO	0.30	0.27	0.26	0.31	0.23	0.31	0.23	0.29
MgO	11.72	12.92	12.85	12.89	12.52	12.68	13.96	12.69
CaO	N.D.	N.D.	N.D.	N.D.	N.D.	N.D.	N.D.	N.D.
Na_2O	N.D.	N.D.	N.D.	N.D.	N.D.	N.D.	N.D.	N.D.
K_2O	N.D.	N.D.	N.D.	N.D.	N.D.	N.D.	N.D.	N.D.
NiO	0.14	0.20	0.14	0.20	0.46	0.15	0.17	0.08
Total	**99.07**	**99.34**	**99.55**	**99.11**	**100.06**	**99.65**	**99.57**	**99.05**

APPENDIX 2

PHYSICAL CHARACTERISTICS OF HELAM DIAMONDS

The physical characteristics of the Helam diamonds are described principally according to the terminology applied by Robinson (1979), Otter (1990) and Chinn (1995). Abbreviations used to describe the diamonds are explained below.

COLOUR: (Col)	C = colourless	G = green	OW = off-white
	Y = canary yellow	BY = brown-yellow	LY = light yellow (Cape)
	B = brown	CG = colourless-green	
CRYSTAL STATE: (State)	W = whole C = chipped (< 10% volume loss by breakage) B = broken (10-50% volume loss by breakage) F = fragment (> 50% volume loss by breakage)		
BREAKAGE SURFACES: (Break)	C = cleavage surface	S = subconchoidal fracture	
	CS = stepped fracture		
CRYSTAL REGULARITY: (Reg)	EQ = approximately equidimensional F = 1 dimension < 1/3 other dimensions E = 2 dimensions < 1/3 other dimension		
MORPHOLOGY: (Morph)	O = octahedron	C = cube	
	THH = tetrahexahedroid	CO = cubo-octahedron	
	A = aggregate	U = unknown	
RESORPTION: (Res)	1: Category 1 = 1-55 % preservation 2: Category 2 = 56-70 % preservation 3: Category 3 = 71-80 % preservation 4: Category 4 = 81-90 % preservation 5: Category 5 = 91-99 % preservation 6: Category 6 = 99-100% preservation		
	U = uncertain	Dr = differential resorption	
SURFACE FEATURES:			
GROWTH FEATURES (Xeno)	SF = smooth faces	TP = triangular plates	
	SL = serrate laminae	KA = knob-like asperities	
DEFORMATION FEATURES (Defm)	WLL = wide lamination lines (> 100 μm separation between individual lamination lines) FLL = fine lamination lines (< 100 μm separation between individual lamination lines)		

	SPT = scotch-plaid texture / intersecting wide or fine lamination lines.
OCTAHEDRAL SURFACES (Octa)	TP = trigonal etch pits, either negative (-) or positive (+) orientation. HP = hexagonal etch pits HPT = hexagonal etch pits containing trigonal pits
CUBIC SURFACES (Cube)	TTP = tetgragonal etch pits, either negative (-) or positive (+) orientation OT = other
TETRAHEXAHEDROIDAL SURFACES (TTH)	EH = elongate hillocks T = terraces CS = corrosion sculpture MH = micro-hillocks OT = other CP = circular micro-disks HH = hexagonal etch pits on elongate hillocks
OTHER SURFACE FEATURES	R = rut FE = degree of etching on crystal surfaces, either absent (0), moderate (-), or intense (+). BE = degree of etching on breakage surfaces, either absent (0), moderate (-), or intense (+). IC = inclusion cavity

PRIMARY INCLUSION ASSESMENT

TRANSPARENT INCLUSIONS (Transparent)	OR = orange (eclogitic garnet) CL = colourless (e.g.: olivine, SiO_2, clinopyroxene, orthopyroxene, diamond, corundum) GR = green(clinopyroxene)
OPAQUE INCLUSIONS (Opaque)	Bre = black sulphide rosette with crystalline 'eye' BR = black sulphide rosette, no 'eye' visible B = red-brown inclusion (e.g.: chromite)

Appendix 2.1 Physical characteristics of Helam diamonds and recovered primary inclusions.

Sample	Col	State	Break	Reg	Morph	Res	Dr	Xeno	Defm	Octa				Cube		TTH					R	FE	BE	IC	Primary Inclusions		
										TP	HP	HPT	OT	TTP	OT	EH	T	HH	CS	MH	CP	OT					Transparent OR	CL GR	Opaque
HB01A	C	W		EQ	O	6		SF															0	0		X		
HB03B	Y	W		EQ	O	4		SFTP		-													-	0				
HB1A10	C	W		EQ	THH	1										X				X	X	X	0	0		X		
HB1B6	C	W		EQ	O	5		SF SL TP		-													0	0		X		
HB2A2	LY	W		EQ	THH	1										X				X			0	0		X		
HB3A4	C	W		EQ	THH	1										X	X			X	X	X	0	0		X		
HB3B8	C	W		F	THH	1										X				X		X	0	0		3X		
HB3C1	C	W		EQ	THH	1										X				X			-	0				3Bre
HB3C3	C	W		EQ	THH	1										X				X			0	0		X		3Bre
HB2D3	C	W		EQ	THH	1																						
HM01-01	C	W		EQ	O	5		SF SL		-													-	0				
HM01-02	C	C		EQ	O	4		SF SL TP															0	0				
HM01-03	C	C	CS	EQ	THH		X		WLL							X	X			X			-	-	X			
HM01-04	C	C	CS	EQ	O	6		SF SL TP															0	0				
HM01-05	C	C	CS	EQ	O	5		SF SL															0	0				
HM01-06	C	C	CS	EQ	CO	4		SF SL TP														X	0	0				
HM01-07	C	C	CS	EQ	O	5		SF SL TP															0	0				
HM01-08	C	C	CS	EQ	O	5		SF SL TP															0	0				
HM01-09	C	C		E	CO	4		SF SL												X			0	-	X			
HM01-10	C	B	CS	E	CO		X	SF SL TP				+				X			X				0	0	X			
HM01-11	C	C	CS	EQ	O		X	SF TP								X							0	0	X			
HM01-12	C	B	C	EQ	A	5		SF TP															0	0				
HM02-01	C	B	C	E	A		X	SF SL TP								X	X			X			0	0	X			
HM02-02	C	C	C	EQ	CO	4		SF SL TP															0	-				
HM02-03	C	W		EQ	O		X	SF SL TP															0	0				
HM02-04	C	B	C	E	O	5		SF TP		+													-	0				
HM02-05	C	B	CS	D	O	4		SF SL TP		+													-	0				
HM02-06	C	W		EQ	O	6		SF SL TP								X				X			0	0				
HM02-07	C	C	CS	EQ	O	4		SF SL TP															0	0				
HM02-08	C	W		EQ	O	4		SF SL TP								X	X			X			0	0				
HM02-09	C	C	CS	EQ	CO	5		SF SL TP								X	X			X			0	0				
HM02-10	C	W		EQ	O	4		SF TP															0	0				
HM02-11	C	W		EQ	O	5		SF TP															0	0				
HM02-12	C	W		D	O	4		SF TP															0	0				
HM03-01	C	W		E	TTH	1										X				X			0	0				
HM03-02	C	W		EQ	TTH	1										X			X	X	X		0	0				
HM03-03	C	W		EQ	TTH	1										X				X			0	0				
HM03-04	C	W		E	TTH	1			FLL							X				X			0	0				
HM03-05	C	W		E	TTH	1										X				X			0	0				
HM03-06	C	W		D	TTH	1			FLL							X			X	X	X		0	0				
HM03-07	C	W		D	TTH	1			FLL							X							0	0				
HM03-08	C	W		E	TTH	1			WLL							X			X	X	X		0	0				
HM03-09	C	W		F	TTH	1			FLL							X			X		X		0	0				
HM03-10	C	W		EQ	TTH	1			WLL							X			X		X		0	0				

Appendix 2.1 continued...

Sample	Col	State	Break	Reg	Morph	Res	Dr	Xeno	Defm	Octa				Cube		TTH					R	FE	BE	IC	Primary Inclusions		
										TP	HP	HPT	OT	TTP	OT	EH	T	HH	CS	MH	CP	OT					Transparent OR CL GR	Opaque
HM03-11	C	W		EQ	TTH	1										X	X			X				0	0			
HM03-12	C	W		D	TTH	1										X	X							0	0			
HM05-01	B	W		D	O	5		SL TP		-														-	0			
HM05-02	B	W		EQ	O	5		SF SL TP		-														0	0			
HM05-03	B	W		EQ	O	5		SF SL TP																0	0			
HM05-04	B	W		EQ	O	5		SF SL TP																0	0			
HM05-05	B	W		EQ	O	5		SL TP																0	0			BR
HM05-06	B	W		EQ	O	5		SL TP																0	0			
HM05-07	B	B		EQ	O	4		SF SL TP																0	0	X		
HM05-08	B	C		EQ	O	5		SF SL TP																0	0			
HM05-09	B	W		EQ	O	5		SL TP		-													X	0	0			
HM05-10	B	W		EQ	O	5		SL TP		-	X	-												0	0			
HM05-11	B	W		EQ	O	5		SL TP																0	0			
HM05-12	B	W		EQ	O	5		SL TP																0	0			
HM06-01	B	W		EQ	O	4		SF SL TP		-														-	0			
HM06-02	B	W	CS	EQ	O	5		SF SL TP		-														-	0			
HM06-03	B	W	CS	EQ	O	5		SF SL TP																0	0			
HM06-04	B	C	C	EQ	O		X	SF SL TP																0	0			
HM06-05	B	W	S	EQ	O	5		SF SL TP								X				X				0	0			
HM06-06	B	W	CS	EQ	O	4		SF SL TP																0	0			BR
HM06-07	B	C	C	D	O	5		SF SL TP		-														0	0			
HM06-08	B	B		EQ	O	5		SF SL TP		-														0	0			
HM06-09	B	W	C	D	A		X	SF SL TP								X				X				0	0			
HM06-10	B	W		EQ	O	5		SF SL TP																0	0			
HM06-11	B	W	CS	EQ	O	5		SF SL TP																0	0			
HM06-12	B	W	C	E	O	5		SF SL TP								X				X				0	0			
HM07-01	B	W		E	THH	1			WLL							X	X			X				0	0			BR
HM07-02	B	W		F	THH	1			SPT							X	X			X	X			0	0			
HM07-03	B	W		EQ	THH	1			FLL							X	X			X		X		0	0			
HM07-04	B	C	CS	D	THH	1			FLL							X	X							0	0			
HM07-05	B	W		F	THH	1			FLL							X	X			X				0	0			
HM07-06	B	W		EQ	THH	1			FLL							X	X			X				0	0			
HM07-07	B	C	CS	E	THH	1			FLL							X	X			X		X		0	0			
HM07-08	B	B	S	E	THH	1										X				X		X		0	-			
HM07-09	B	W		F	THH	1										X				X		X		0	0			
HM07-10	B	W		EQ	THH	1			SPT							X	X			X				0	0			
HM07-11	Y	W		D	THH	1			FLL							X				X				0	0			
HM07-12	B	W		EQ	THH	1										X								0	0			
HM08-01	G	C	CS	EQ	O	5		SF SL TP		-	X													0	0			B
HM08-02	G	W		EQ	CO	4		SF SL TP						U										0	0			
HM08-03	G	W		EQ	O	5		SF SL TP																0	0			
HM08-04	G	W		D	O	5		SF SL TP		-														0	0			
HM09-01	G	W		F	THH	1			WLL							X	X							0	0			
HM09-02	G	C	CS	E	THH	1										X				X			X	0	-			

Appendix 2.1 continued...

Sample	Col	State	Break	Reg	Morph	Res	Dr	Xeno	Defm	Octa				Cube		TTH					R	FE	BE	IC	Primary Inclusions			
										TP	HP	HPT	OT	TTP	OT	EH	T	HH	CS	MH	CP	OT					Transparent OR	CL	GR	Opaque
HM09-03	G	W		EQ	THH	1			SPT							X				X				0	0					
HM09-04	G	W		E	THH	1										X				X	X			0	0					
HM09-05	G	W		F	THH	1										X			X	X				-	0					
HM09-06	G	W		EQ	THH	1			FLL							X				X				0	0					
HM09-07	G	B	CS	D	THH	1			FLL					U		X				X	X			0	-	X				
HM09-08	G	W		F	THH	1			SPT							X								0	0					
HM09-09	G	C	S	E	THH	1										X	X							0	0					
HM09-10	G	W		F	THH	1										X	X			X	X		X	0	0					
HM09-11	G	C	S	F	THH	1			WLL							X							X	0	0					
HM09-12	G	C	S	D	THH	1										X								0	0					
HM10-01	Y	W		F	THH	1			WLL					U		X				X	X			+	0	X				
HM10-02	Y	B	C	E	THH	1			FLL							X				X				0	0		X			BR
HM10-03	Y	W		E	THH	1										X					X		X	0	0					BR
HM10-04	Y	B	C	F	THH	1													X	X	X			0	0					BR
HM10-05	Y	W		D	THH	1										X				X	X			0	0					
HM10-06	Y	C	C	D	THH	1										X				X			X	0	0					
HM10-07	Y	B	C	F	THH	1			FLL							X				X			X	+	0					
HM10-08	Y	B	S	E	THH	1			SPT							X				X			X	-	0					
HM10-09	Y	W		F	THH	1			FLL							X				X			X	0	0					
HM10-10	Y	W		E	THH	1			WLL							X				X			X	-	0					
HM10-11	Y	W		D	THH	1			SPT							X				X	X			0	0					
HM11-01	Y	B	C	EQ	O	U		SF		-													X	-	○	0				
HM11-02	Y	B	C	EQ	O	4		SF		-													X	-		0				
HM11-03	Y	B	C	E	U	U				-														-		0				
HM11-04	Y	B	C	EQ	O	5		SF SL		-													X	+		0	X			Br
HM11-05	Y	B	C	EQ	O	4		SL																0		0				
HM11-06	Y	B	C	E	THH	1										X				X	X			-		0				
HM11-07	Y	B	C	F	U	U			WLL	-						X				X				-		0				
HM11-08	Y	C	C	F	THH	1										X				X				0		0				
HM11-09	Y	W		F	THH	1			WLL							X				X				0		0				Br
HM11-10	Y	W		EQ	THH	1			WLL							X				X				0		0				
HM11-11	Y	W		F	THH	1										X				X				0		0				
HM001	C	W		D	THH	1			SPT							X				X				0		-				
HM002	BY	F	C	E	THH	1			WLL											X				0		-	X			Bre
HM003	Y	B	CS	E	THH	1			FLL							X				X				0		0				Bre
HM004	C	B	C	EQ	O		X	SF/SL		-							X		X	X			X	X		-	X			
HM005	C	W		EQ	O	3		KA											X	X			X	-		0				Bre
HM006	Y	F	C	E	THH	1		TP/SC	FLL											X				0		0		3X		
HM007	C	F	C/S	E	THH	1										X							X	0		-			X	
HM008	C	F	C	EQ	O	3										X				X			X	-		0			5X	Bre
HM009	C	W		D	THH	1			FLL							X			X	X				0		-			2X	
HM010	C	W		EQ	THH	1			FLL							X				X			X	0		0				
HM011	C	W		E	THH	2													X		X		X	0		0			X	
HM012	C	W		E	THH	1										X			X	X	X			0		0				

Appendix 2.1 continued...

Sample	Col	State	Break	Reg	Morph	Res	Dr	Xeno	Defm	Octa				Cube		TTH					R	FE	BE	IC	Primary Inclusions		
										TP	HP	HPT	OT	TTP	OT	EH	T	HH	CS	MH	CP	OT					Transparent OR	CL	GR	Opaque
HM013	Y	F	C	EQ	O	4		KA		-				XU						X			X	+	0		8X		
HM014	CG	F	C	E	THH	2			SPT							X				X			X	+	+				
HM015	Y	F	C	E	THH	1			FLL							X				X			X	0	-	X			
HM016	C	W		EQ	THH	1														X				0	0				
HM017	Y	W		E	THH		X		FLL							X	X			X				0	-				
HM018	YW	C	S	E	THH		X		FLL							X				X			X	-	0	X	X		
HM019	BY	W		E/F	THH	1			FLL							X			X	X	X		X	-	0		X		
HM020	G	W		EQ	THH	2			SPT							X				X				0	0				
HM021	OW	F	CS	EQ	O	4		TPSL								X			X	X			X	-	-	X	X		
HM022	G	F	CS	E	THH	1			SPT							X		X		X			X	-	-	X			Bre
HM023	Y	F	C	E	THH	1			FLL							X				X				0	0				Bre
HM024	G	F	C	E	O	4										X			X				X	-	-	X			Bre
HM025	Y	F	CS	EQ	O	6		TPSL		-													X	-	-				
HM026	C	B	CS	E	A	1				-						X				X			X	+	-				
HM027	C	F	CS	EQ	O	6		TPSL		-						X				X			X	-	0				
HM028	LY	B	CS	F	O	5		TPSL		-	+	+											X	0	-				
HM029	C	F	CS	E	THH		X		FLL							X	X			X			X	-	-				
HM030	C	F	CS	F	O	1										X							X	0	-				
HM031	C	F	CS	EQ	O	5		TPSL											X	X				0	-				4B
HM032	C	W		F	THH		X									X				X				0	0				2B
HM033	Y	F	C	EQ	O	U										X				X			X	0	-				Bre
HM034	C	F	C/S	E	THH	2			FLL							X				X			X	0	-	X		X	
HM035	Y	W		D	THH	1			FLL								X			X			X	0	0				
HM036	C	F	CS	E	THH	U			FLL							X				X			X	0	-				
HM037	C	F	C/S	E	THH		X		FLL							X				X			X	0	0				B
HM038	C	B	C	E	A		X	TPSL															X	0	-				
HM039	C	B	C	EQ	CO	5		TPSL																0	+				
HM040	Y	F	CS	EQ	O	6		TPSL																0	0			X	
HM041	C	W		F	THH	1			FLL							X				X			X	-	0	X			
HM042	Y	B	CS	E	THH	1			SPT											X				0	0			X	
HM043	C	F	CS	F	O	4		TPSL									X							-	-			X	
HM044	Y	F	C	E	THH	1										X	X		X	X			X	+	+	X		X	
HM045	C	C	C	EQ	O	6		TPSLKA																0	0				
HM046	Y	F	CS	E	THH	U											X			X				-	-				
HM047	BY	W		EQ	THH	1			FLL							X				X				-	-				
HM048	Y	F	CS/S	F	THH	U			FLL							X				X				-	-	X			
HM049	C	F	CS	E	THH	2			WLL							X	X			X			X	-	-	X			
HM050	C	F	C	EQ	O	6		TPSL															X	-	-				
HM051	C	B	C	EQ	THH	1											X						X	-	-				
HM052	C	W		EQ	THH	1			FLL							X	X			X			X	0	0				
HM053	C	B	CS	EQ	O	6		TPSL															X	-	0		X		
HM054	C	W		EQ	THH	1			FLL										X	X				-	-				
HM055	Y	F	C	F	THH	1			FLL											X			X	-	-				2B
HM056	B	B	C/S	E	THH	1										X	X			X				-	+				

Appendix 2.1 continued...

Sample	Col	State	Break	Reg	Morph	Res	Dr	Xeno	Defm	Octa				Cube		TTH					R	FE	BE	IC	Primary Inclusions	
										TP	HP	HPT	OT	TTP	OT	EH	T	HH	CS	MH	CP	OT					Transparent OR CL GR	Opaque
HM057	Y	F	C	E	THH	U			WLL							X	X			X			X	-	-			
HM058	C	F	C/S	E	THH	U			FLL							X	X			X			X	0	-			
HM059	B	F	C	E	THH	U			FLL							X	X			X			X	-	-			Bre
HM060	Y	W		E	O		X	SF TP		-						X								+	0			
HM061	Y	B	S CS	EQ	O	4		SF TP		-							X						X	-	0			
HM062	C	B	CS	F	THH	1			WLL							X				X			X	0	-	X		
HM063	Y	B	S	E	THH	1			WLL							X				X				0	0	X		
HM064	C	C	CS	D	THH	1										X					X		X	0	0			
HM065	Y	B	CS	EQ	O	4		SF TP		-													X	-	0			
HM066	C	W		EQ	O	6		SF SL TP		-														+	0			
HM067	C	W		EQ	O	6		SF SL TP		-														-	0			B
HM068	C	W		EQ	THH	1		SF SL TP								X				X	X			-	0			
HM069	LY	W		EQ	O	6				+														-	0			
HM070	Y	B	CS	F	THH	1		SF TP		-						X				X			X	-	0			
HM071	B	C	CS	EQ	O	6				-														+	0			
HM072	C	B	CS	EQ	O	U		SF SL TP		U														-	0			
HM073	B	C	CS S	F	THH	1			SPT							X	X						X	-	-			
HM074	C	W		EQ	C		X			-	X			U										+	0			
HM075	B	W		F	THH		X	SL TP								X				X			X	+	0			
HM076	Y	W		EQ	THH	1		SL TP	FLL							X	X			X				-	0			
HM077	Y	B	CS	EQ	THH	1			SPT							X				X			X	-	0			
HM078	C	B	CS S	EQ	O	4																		0	0			
HM079	B	W		EQ	THH	1		SL TP	SPT							X				X				-	0			
HM080	C	W		EQ	THH	1										X				X	X		X	-	0			
HM081	C	W		EQ	C		X							U		X				X				+	0			
HM082	G	B	CS	E	THH	1		TP								X					X			-	0			
HM083	C	W		EQ	O	U		SF																-	0			
HM084	C	B	C	EQ	THH	1										X				X	X		X	-	0			
HM085	Y	W		E	THH	1										X				X			X	0	0	X		
HM086	C	C	C	EQ	O	5		SF SL TP		-														+	0			Bre
HM087	C	B	C	EQ	O	6		SF TP		-														-	0			
HM088	G	C	C	EQ	O	5		SF SL TP																0	0			
HM089	Y	B	C	E	THH	1										X				X	X		X	0	0			
HM090	C	W		EQ	THH	1										X				X	X			0	0			
HM091	C	W	C	EQ	THH	1										X				X				0	0			
HM092	C	W		EQ	THH	1										X								0	0			
HM093	C	W		EQ	THH	1										X				X	X			0	0			
HM094	Y	B	C	EQ	O	4		SF SL TP		-														+	0			
HM095	C	W		EQ	O	5		SF																0	0			
HM096	C	W		EQ	O	6		SF TP		-														-	0			
HM097	Y	B	C	EQ	THH	1					FLL					X				X				0	0			
HM098	Y	W		F	THH	1					FLL					X	X			X				0	0			
HM099	C	B	C	F	O	5		SF TP		-														+	0			
HM100	C	W		EQ	THH	1										X				X				0	0			

Appendix 2.1 continued…

Sample	Col	State	Break	Reg	Morph	Res	Dr	Xeno	Defm	Octa				Cube		TTH					R	FE	BE	IC	Primary Inclusions		
										TP	HP	HPT	OT	TTP	OT	EH	T	HH	CS	MH	CP	OT					Transparent OR CL GR	Opaque
HM101	Y	B	C	E	U	U																	0	0			
HM102	C	B	C	EQ	O	6		SF TP		-													-	0			
HM103	C	B	CS	EQ	O	5		SF SL TP															0	0			
HM104	Y	W		EQ	O	5		SF TP		-													-	0			
HM105	C	W		EQ	CO	5		SF TP						-									+	0			
HM106	C	W		F	THH	1										X				X		X	0	0			
HM107	B	C	C	EQ	O	6		SF SL TP															0	0			
HM108	Y	B	CS	E	U																		-	0		2X	
HM109	C	W		EQ	THH	1										X			X				-	0			3B
HM110	C	B	CS	E	THH	1										X				X			-	0			
HM111	LY/C	B	CS	E	THH	1			FLL							X		X					-	0			Bre
HM112	LY/C	W		EQ	THH	1										X		X		X			-	0		X	
HM113	C	W		E	THH	1			FLL							X				X			-	0		X	2Bre
HM114	G	W		EQ	THH	1										X							0	0		4X	
HM115	C	F	CS	F	U	U																	0	0		X	Bre
HM116	C	W		EQ	THH	1										X							-	0			Bre
HM117	Y	B	CS	E	THH	1										X				X			-	0			
HM118	C	B	CS	E	THH	1										X				X			-	0			
HM119	C	W		EQ	CO	6		SF SL TP					X										+	0		X	
HM120	C	W		EQ	THH	1										X				X			-	0			
HM123	C	W		E	THH	1										X				X			0	0			2Bre
HM124	C	W		E	THH	1										X				X			0	0			Bre
HM126	C	W		EQ	THH	1										X				X			0	0			Bre
HM127	C	W		EQ	THH	1										X				X			0	0			Bre
HM129	Y	W		E	THH	1			FLL							X							0	0			Bre
HM201	Y	W		E	THH	1		SF SL TP								X				X		X	-	0			
HM202	Y	W		E	THH	1		SF SL TP								X				X			-	0			
HM203	Y	B	CS	E	THH	1			FLL							X				X		X	0	0			2Bre
HM204	C	B	CS	E	THH	1			FLL							X			X	X		X	0	0			
HM205	C	B	C	EQ	THH	1			FLL							X				X		X	0	-	X		
HM206	C	B	CS	E	O	4		TP		-												X	+	-			
HM207	C	C	CS	EQ	THH	1										X					X		-	0			
HM208	Y	F	C	F	THH	1			FLL							X						X	0	0		3X	
HM209	LY/C	F	CS	E	THH	1		TP	FLL				-			X				X		X	+	-	X	X	
HM210	C	F	CS	EQ	O	6		SF SL TP		-						X						X	+	0	X	X	
HM211	Y	F	CS	F	O	4		SF TP		-						X						X	+	0	X	X	
HM212	C	F	C	F	THH	1										X			X	X		X	-	-			
HM213	C	W		EQ	O	5		SF TP		-													-	0			
HM214	C	W		EQ	THH	1										X				X	X	X	-	0	X		
HM215	C	B	CS	EQ	O	5		SF TP		-												X	-	0	X		
HM216	C	W		F	O	4		SF TP														X	0	0	X		
HM217	B	W		EQ	THH	1										X	X			X		X	-	0	X		Bre
HM218	C	B	C	EQ	O	6		SF TP		-													-	0			
HM219	LY	B	C	F	THH	1										X				X		X	-	0	X		

Appendix 2.1 continued...

Sample	Col	State	Break	Reg	Morph	Res	Dr	Xeno	Defm	Octa				Cube		TTH					R	FE	BE	IC	Primary Inclusions			
										TP	HP	HPT	OT	TTP	OT	EH	T	HH	CS	MH	CP	OT					Transparent OR	CL	GR	Opaque
HM220	C	B	CS	EQ	THH	1										X				X			X	-	0					Bre
HM221	C	W		EQ	THH	1										X								0	0					Bre
HM222	C	B	CS	E	THH	1										X	X			X			X	0	0	X				
HM223	Y	F	CS	F	O	4		SF TP		-													X	-	0					
HM224	C	W		EQ	O	5		SF SL TP																0	0					
HM225	C	B	CS	EQ	O	6		SF SL TP		-						X								-	0	X				
HM226	Y	B	U	E	THH	1							U			X				X			X	-	0	X				
HM227	Y	W		EQ	THH	1										X				X				0	0					
HM228	Y	W	U	E	U	U										X				X				0	0					
HM229	C	W		E	THH	1										X			X	X				0	0					
HM230	Y	B	O	E	THH	1										X				X			X	0	0					
HM231	Y	W	U	F	THH	1			WLL							X			X	X			X	0	0	X				
HM232	C	W		EQ	O	5		SF TP																0	0					
HM234	C	F	U	E	U	U																		0	0					
HM235	C	W		E	THH	1							-			X			X	X			X	0	0					2Bre
HM236	Y	W		F	THH	1			FLL							X				X				0	0			X		
HM237	Y,B	W		E	THH	1			FLL							X				X				0	0					
HM238	C	W		EQ	O	6		SF SL TP																0	0					
HM239	C	W		EQ	O	6		SF TP		-														0	0					
HM240	C	W		E	U	U																						3X		
HM1A1	C	W		EQ	THH	1								-		X				X	X		X	-	0	X				
HM1A2	C	W		E	THH	1										X				X				-	0					4Bre
HM1A3	B	B	CS	EQ	O		X	SF TP		-				-										0	0	X				
HM1A4	Y	W		EQ	THH	1										X				X	X			0	0					
HM1A6	C	B	C	E	THH	1										X				X			X	0	0	X				
HM1A7	C	E	CS	E	U	U																		0	0					Bre
HM1A8	C	B	C	E	U	U																		0	0					
HM1A9	C	B	C	E	U	U																	X	0	0	X				10B
HM1A12	C	B	C	E	THH	1										X				X			X	0	0	X		X		
HM1B2	C	W		E	THH	1										X							X	0	0		X	X		
HM1B3	C	W		EQ	THH	1															X		X	0	0					
HM1B5	C	W		E	THH	1										X					X		X	0	0					
HM1B7	C	W		E	U	U																		0	0					
HM2A1	C	B	C	EQ	O	5		SF SL TP		-														0	0					
HM2A4	C	B	C	EQ	O	6		SF TP		-														-	-	X				Bre
HM2A5	C	B	C	EQ	O	5		SF TP		-													X	+	0					
HM2A6	C	W		EQ	THH	1										X				X			X	0	0					
HM2A8	B	W		F	THH	1										X				X				-	0					
HM2A9	B	W		EQ	THH	1										X	X							0	0					
HM2A10	B	W		EQ	THH	1								-		X				X				-	0					
HM2B2	B	B	C	EQ	O	4		TP																0	0			17X		
HM2B3	C	B	C	EQ	THH	1										X				X				0	0			X		
HM2B7	C	W		E	THH	1										X				X			X	0	0					Bre
HM2C1	C	W		EQ	THH	1			FLL							X				X				0	0					

Appendix 2.1 continued…

Sample	Col	State	Break	Reg	Morph	Res	Dr	Xeno	Defm	Octa				Cube		TTH					R	FE	BE	IC	Primary Inclusions			
										TP	HP	HPT	OT	TTP	OT	EH	T	HH	CS	MH	CP	OT					Transparent OR	CL	GR	Opaque
HM2C2	C	W		E	THH	1										X			X	X				0	0					
HM2C3	C	W		EQ	O	5																		0	0					
HM2C4	C	B	C	EQ	O	6		TP SL																0	0					
HM2C5	C	W		EQ	O	5		TP SL		-														-	0					
HM2C6	C	B	CS	E	THH	1										X				X			X	0	0					
HM2C7	C	F	C	E	U	U										X														
HM2C9	Y	W		F	THH	1										X				X			X	0	0					
HM2C10	B	F	CS	F	THH	1										X								0	0					
HM2C12	C	W		F	THH	1										X				X				0	0					
HM2D6	C	W		EQ	O	5		TP SL																0	0					B
HM2D8	C	W		EQ	O	5		TP SL												X				0	0					
HM2D9	Y	B	CS	E	O	5		TP	-															-	0					
HM2D11	C	W		EQ	C		X							-										0	0					
HM2D5	C	W		EQ	C		X																	-	0					
HM3A1	B	W		EQ	O	5		TP		-													X	-	0					
HM3A2	B	F	CS	E	THH	1										X				X			X	0	0					
HM3A5	C	B	C	EQ	O	1		SF SL TP		-														-	0			X		
HM3A9	C	W		E	THH	6				-						X				X			X	-	0					
HM3A11	Y	B	C	F	O	5		TP	-															-	0					2Bre
HM3A12	Y	W		F	THH	1										X		X					X	0	0					
HM3B2	B	W		E	THH	1										X			X					0	0					
HM3B4	C	W		EQ	THH	1										X				X				0	0			4x		Bre
HM3B6	C	W		E	THH	1										X				X			X	0	0					
HM3B7	C	W		E	THH	1										X				X			X	0	0					3Bre
HM3B9	C	W		F	THH	1										X				X			X	0	0					3Bre
HM3B10	C	W		EQ	O	6		SF SL TP						-										-	0		x	x		Bre
HM3B11	C	W		EQ	O	5		TP																0	0					
HM3D1	B	F	C	F	THH	1										X								0	0					Bre
HM3D2	Y	W		F	THH	1			FLL							X				X				0	0					
HM3D5	C	W		F	THH	1																								
HM3D6	C	W		EQ	THH	1										X				X				0	0					Bre

Appendix 2.2 Resorption classification scheme used to describe the Helam diamonds. Resorption category numbers decrease with increasing degree of resorption, from a perfect octahedron (6) to a perfect tetrahexahedroid (1). Modified from Otter (1990) and McCallum (1994).

RESORPTION CATEGORY

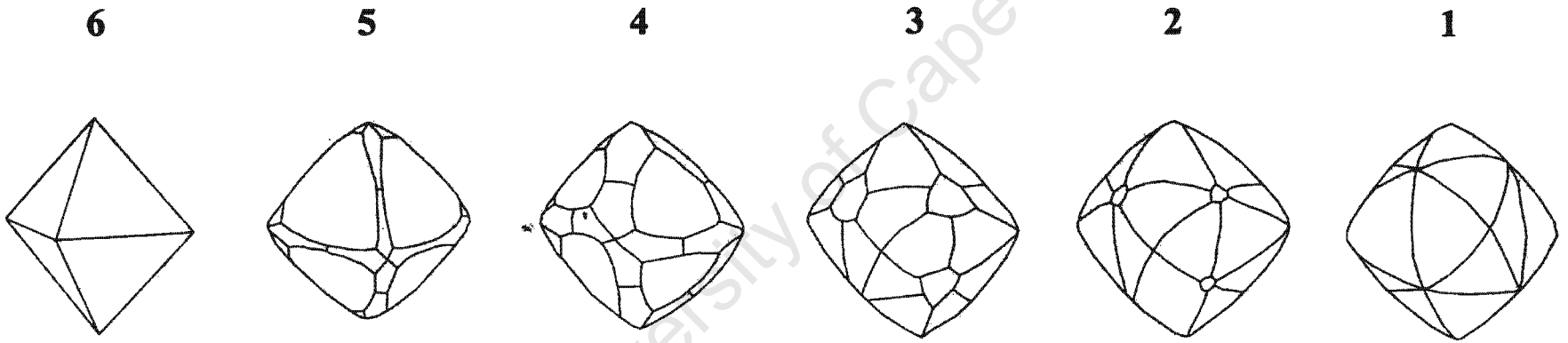

Estimated Preservation Values

APPENDIX 3

FOURIER TRANSFORM INFRA-RED (FTIR) AND CATHODOLUMINESCENCE (CL) ANALYSIS OF HELAM DIAMONDS

FTIR ANALYSIS

All diamonds were cleaned repeatedly with water, dichloromethane and ethanol in an ultrasonic bath, to remove all surface grime. The diamonds were then mounted side by side on double-sided tape along the length of a glass slide. This is a useful method of analysing a large sample of diamonds conveniently. FTIR spectra were measured at the University of Cape Town using a Nicolette Magna-IR 560 spectrometer, with an attached KBr beam splitter and a MCT/A detector that was cooled with liquid nitrogen. In addition nitrogen gas was purged over the sample during analyses to create a localised nitrogen atmosphere around the sample, thereby preventing the build up of CO_2. Spectra were recorded over the range 4000 – 650 cm^{-1}, at a resolution of 8 cm^{-1}. Background spectra were recorded after each diamond analysis over the same range and resolution, and subtracted from the diamond spectra so as to illuminate non-sample, atmospheric contributions. These analyses were performed on-line using Nicolette OMNIC 5.0 software.

Deconvolution, and peak extraction from the spectra of the Type IaAB diamonds was performed using Bruker OPUS/3D software. Peak information was transferred electronically into the Mendelssohn and Milledge (1995) Quattro-Pro spreadsheet for quantitative analysis of the diamond defect contents. Quantitative estimations of the amount of nitrogen aggregation was assessed in the spreadsheet based on various peak ratios (see Chapter 5). The various absorption peak ratios result in different estimations of nitrogen aggregation, and it becomes necessary to assess the validity of the computed results interactively, by comparison of the sample spectra with reference 'thumb-nail' spectra (Mendelssohn and Milledge, 1995) of synthetic mixtures of different proportions of A and B defects (Appendix 3.1). This procedure ensures the correct estimate of nitrogen aggregation.

Deconvolution and quantitative analysis of the spectra from natural Type Ib diamonds (canary-yellow) was performed using a deconvolution programme at the De Beers Geoscience Centre, Johannesburg. However, because the method represents in-house intellectual property the details of the programme can not be discussed or published.

CATHODOLUMINESCENCE ANALYSIS

Polished diamond plates were cleaned repeatedly with water, dichloromethane and ethanol in an ultrasonic bath, and mounted on strips of carbon conductive tape placed on aluminium plates. CL imaging of the plates was performed at the Electron Microscopy Unit, University of Cape Town using a Cambridge S200 scanning electron microscope at 15 kV and an electron beam current of between 1.5 – 2.0 nA. In addition colour CL images were captured of all the plates using an optical microscope attached to a Technosyn luminescence generator with an accelerating voltage of 15 kV and an electron beam current set at 0.8 mA. Colour images have the advantage of indicating the position of mineral inclusions within the diamond plates, while the SEM images provide images of better resolution .

The diamond plates were cleaned again and mounted on glass slides as for the unpolished diamonds. FTIR analysis was conducted (as above) in transects across the diamond plates so as to record subtle chemical variability across the plates. The approximate positions of the individual analyses have been indicated in the CL images in Chapter 5.

Appendix 3.2 IR absorption characteristics of the rough (IaAB) diamonds from Helam. Mantle residence temperatures have been calculated for a mantle residence time of 2.75 Ga. The suffix 'e' and 'c' on sample number indicates analysis made at the 'edge' and 'center' of the crystal.

Analysis	T(cm^{-1})	H(3107)	H(3237)	mu(1430)	mu(1365)	N (ppm)	%N as B	A (ppm)	B (ppm)	T(°C)calc
Colourless										
HM01-01e1	1372.1	0.006	0.000	0.009	0.224	805	6.7	750.8	54.2	1062
HM01-02e2	1374.6	0.038	0.003	0.046	0.478	1467	34.3	964.0	503	1093
HM01-04c1	1373.1	0.025	0.000	-0.001	0.033	641	13.2	556.6	84.4	1084
HM01-05c1	1375.3	0.079	0.002	0.003	0.035	699	13.9	601.2	97.8	1083
HM01-05e1	1374.6	0.005	0.002	-0.006	0.108	841	8.0	774.0	67.0	1065
HM01-06e1	1373.1	0.011	0.004	0.012	0.213	1148	24.8	863.2	284.8	1088
HM01-06e2	1373.9	0.014	0.000	0.035	0.318	1551	26.6	1138.0	413.0	1083
HM01-07e1	1372.7	0.000	0.000	0.007	0.037	596	16.5	497.2	98.8	1091
HM01-07e2	1376.4	0.053	0.003	-0.003	0.041	736	13.6	636.2	99.8	1081
HM01-08c1	1375.1	0.060	0.000	-0.003	0.061	575	16.5	480.3	94.7	1092
HM01-08e1	1370.6	0.016	0.000	0.025	0.044	326	11.7	288.3	37.7	1096
HM01-09e1	1373.1	0.017	0.000	0.025	0.330	1147	22.6	887.6	259.4	1085
HM01-10e1	1373.2	0.013	0.000	-0.002	0.044	671	16.2	562.6	108.4	1088
HM01-11e1	1373.1	0.009	0.003	0.024	0.255	999	26.9	729.6	269.4	1094
HM02-01e2	1375.2	0.023	0.000	0.001	-0.003	154	12.0	135.1	18.9	1115
HM02-03e1	1376.9	0.000	0.000	-0.002	0.006	575	14.7	490.4	84.6	1089
HM02-04e2	1374.3	0.015	0.000	0.037	0.250	934	23.9	710.5	223.5	1092
HM02-05c2	1375.1	0.092	0.005	-0.002	0.030	728	13.6	629.4	98.6	1081
HM02-07c1	1371.8	0.027	0.003	0.034	0.090	609	21.3	479.2	129.8	1098
HM02-09c2	1374.5	0.017	0.000	0.053	0.416	1946	35.1	1264.2	681.8	1087
HM02-12e1	1370.5	0.037	0.000	0.000	0.098	673	14.3	576.5	96.5	1085
HM03-05e1	1371.2	0.017	0.002	-0.005	0.147	673	20.0	538.5	134.5	1094
HM04-01c1	1373.5	0.028	0.004	0.029	0.351	1416	33.8	937.5	478.5	1093
HM04-01e1	1373.0	0.012	0.004	0.021	0.279	1182	32.5	798.2	383.8	1096
HM04-03c1	1376.4	0.072	0.004	0.040	0.326	1527	26.6	1120.2	406.8	1084
HM04-03e1	1375.8	0.054	0.000	-0.004	0.239	1183	17.9	970.8	212.2	1078
HM04-04e1	1373.5	0.020	0.003	0.028	0.341	982	20.0	785.4	196.6	1085
HM04-05c2	1373.1	0.028	0.000	0.003	0.258	845	6.3	791.5	53.5	1059
HM04-06e1	1376.6	0.009	0.000	0.025	0.053	617	12.0	542.8	74.2	1082
HM04-07c1	1372.9	0.000	0.000	0.006	0.263	1210	31.2	832.9	377.1	1094
HM04-07e1	1374.9	0.036	0.000	0.022	0.283	1212	10.1	1090.2	121.8	1062
HM001c1	1375.8	0.083	0.007	0.133	0.162	657	34.6	430.1	226.9	1112

Appendix 3.2 continued…

Analysis	T(cm^{-1})	H(3107)	H(3237)	mu(1430)	mu(1365)	N (ppm)	%N as B	A (ppm)	B (ppm)	T(°C)calc
HM007e1	1374.7	0.000	0.004	-0.004	0.018	276	6.7	257.2	18.8	1086
HM008c	1380.5	0.056	0.000	0.083	0.100	467	14.7	398.5	68.5	1094
HM010e2	1369.2	0.000	0.000	0.009	0.177	787	29.2	557.2	229.8	1102
HM012e3	1370.3	0.199	0.012	0.047	1.035	1179	34.5	771.4	407.6	1098
HM012e4	1373.1	0.138	0.000	-0.008	1.571	1666	22.0	1299.7	366.3	1076
HM021e2	1381.1	0.017	0.000	0.004	0.011	631	29.8	442.7	188.3	1108
HM021e3	1380.8	0.022	0.000	0.083	0.089	371	20.0	296.9	74.1	1108
HM022e4	1384.7	0.005	0.000	0.035	0.040	194	12.8	168.9	25.1	1111
HM025e1	1390.5	0.005	0.000	0.008	0.006	131	5.9	123.7	7.3	1098
HM026c1	1383.9	0.204	0.010	0.039	0.071	431	26.4	317.7	113.3	1113
HM026e2	1365.4	0.174	0.016	0.028	0.027	454	28.9	322.4	131.6	1114
HM027e4	1366.3	0.000	0.000	0.013	0.015	229	8.8	208.7	20.3	1097
HM028c3	1372.2	0.380	0.021	0.062	0.765	893	30.3	621.7	271.3	1100
HM028c4	1371.3	0.501	0.028	0.069	0.608	689	27.8	497.1	191.9	1103
HM029c3	1385.6	0.005	0.005	0.037	0.046	431	27.5	312.5	118.5	1114
HM030c1	1376.7	0.070	0.005	0.021	0.106	1012	31.4	693.8	318.2	1098
HM031c1	1375.7	0.027	0.000	0.016	0.045	510	10.1	458.6	51.4	1082
HM034c2	1368.5	0.065	0.002	0.075	0.049	371	13.2	322.0	49.0	1096
HM037e2	1374.4	0.020	0.003	0.018	0.064	664	24.8	499.1	164.9	1101
HM037e3	1375.5	0.051	0.000	-0.016	0.106	711	11.7	628.6	82.4	1078
HM039e1	1380.4	0.019	0.000	0.011	0.015	515	6.3	482.7	32.3	1070
HM054c2	1373.1	0.073	0.003	0.004	0.117	714	15.8	601.1	112.9	1086
HM055c	1381.3	0.017	0.006	-0.021	0.032	138	34.3	90.7	47.3	1149
HM058c3	1382.2	0.061	0.000	0.014	-0.005	462	24.2	349.9	112.1	1108
HM064c3	1372.4	0.069	0.002	0.007	0.009	669	29.8	469.9	199.1	1106
HM066c2	1376.2	0.090	0.006	0.032	0.224	859	27.8	620.3	238.7	1098
HM066e2	1376.9	0.014	0.000	0.020	0.089	657	17.9	538.7	118.3	1091
HM067c3	1373.5	0.007	0.000	0.023	0.292	1331	23.9	1013	318.0	1083
HM068e1	1376.9	0.084	0.003	0.017	0.173	1012	19.3	816.3	195.7	1084
HM072e2	1373.7	0.049	0.000	0.030	0.314	988	14.3	846.8	141.2	1076
HM076e2	1373.6	0.000	0.000	0.015	0.015	105	16.5	87.6	17.4	1132
HM078c2	1371.9	0.014	0.000	0.099	0.060	234	12.4	205.1	28.9	1105
HM083c2	1376.2	0.059	0.000	-0.003	0.074	734	16.2	615.5	118.5	1086
HM083e1	1380.8	0.068	0.000	0.008	0.015	399	5.0	379.1	19.9	1070
HM086e3	1380.8	0.026	0.006	-0.008	0.018	330	4.6	314.6	15.4	1073

Appendix 3.2 continued…

Analysis	T(cm^{-1})	H(3107)	H(3237)	mu(1430)	mu(1365)	N (ppm)	%N as B	A (ppm)	B (ppm)	T(°C)calc
HM087c1	1376.8	0.034	0.000	0.063	0.168	680	13.6	587.6	92.4	1083
HM088e1	1369.4	0.003	0.003	0.087	0.086	240	6.3	224.5	15.5	1088
HM091e2	1374.1	0.035	0.005	0.075	0.447	1471	31.2	1012.9	458.1	1090
HM093c1	1376.0	0.020	0.003	0.044	0.079	532	17.9	436.5	95.5	1096
HM096e1	1374.3	0.021	0.003	0.039	0.333	1680	38.6	1031.3	648.7	1094
HM099c2	1357.7	0.026	0.000	0.040	-0.005	167	13.9	143.6	23.4	1116
HM100e2	1376.6	0.086	0.007	0.008	0.035	702	12.0	617.4	84.6	1079
HM102c1	1373.1	0.007	0.000	0.023	0.008	116	5.9	109.1	6.9	1103
HM103e1	1373.6	0.007	0.000	0.029	0.268	1134	26.0	838.8	295.2	1090
HM106e2	1373.1	0.045	0.003	0.029	0.310	1118	29.2	791.1	326.9	1094
HM109c	1383.3	0.109	0.010	0.018	0.028	591	24.2	448.0	143.0	1103
HM113c	1373.6	0.046	0.009	0.207	0.211	400	5.9	376.8	23.2	1074
HM116c	1377.4	0.047	0.031	0.117	0.319	1340	37.5	838.1	501.9	1098
HM210c	1378.2	0.142	0.005	0.064	0.338	1533	19.3	1237.0	296.0	1074
HM220c	1365.4	0.000	0.000	0.022	0.022	108	6.3	101.6	6.4	1104
HM235c	1364.9	0.033	0.025	0.126	0.125	358	23.2	274.3	83.7	1113
HM240c	1372.9	0.006	0.019	-0.089	0.409	875	34.6	572.8	302.2	1105
HM1A10c	1372.8	0.000	0.000	-0.006	0.027	459	16.5	383.2	75.8	1097
HM1A10e	1373.1	0.005	0.000	-0.006	0.043	449	12.4	393.4	55.6	1090
HM1A2c	1374.6	0.046	0.004	0.091	0.083	252	6.8	235.3	16.7	1088
HM1A7c	1370.8	0.007	0.003	0.011	0.045	558	15.8	469.9	88.1	1092
HM1A9c	1379.0	0.008	0.000	0.004	0.002	195	7.6	179.9	15.1	1097
HM1B2e	1377.4	0.012	0.000	0.107	0.106	252	11.6	222.3	29.7	1102
HM2A4	1361.2	0.046	0.000	0.001	0.001	297	10.5	265.8	31.2	1095
HM2a4c	1377.2	0.051	0.000	0.009	0.002	318	17.9	260.9	57.1	1108
HM2B11c	1384.7	0.029	0.000	0.039	0.041	233	4.6	222.4	10.6	1080
HM2D3	1380.8	0.072	0.030	0.242	0.221	283	20.0	226.3	56.7	1114
HM2D6c	1373.9	0.049	0.000	0.030	0.371	1187	22.0	926.2	260.8	1084
HM2D6e	1372.4	0.037	0.000	0.100	0.259	714	15.8	601.2	112.8	1086
HM2D6c	1373.1	0.045	0.000	0.034	0.246	849	20.7	673.8	175.2	1089
HM2d6e	1373.8	0.058	0.000	0.035	0.361	1252	29.8	879.4	372.6	1092
HM3A5c	1385.2	0.009	0.003	0.025	0.021	199	20.0	159.0	40.0	1123
HM3A11e	1378.8	0.023	0.000	-0.010	0.032	230	9.3	209.1	20.9	1097
HM3B10e	1368.4	0.000	0.009	-0.023	0.003	223	8.0	204.7	18.3	1096
HM3B11c	1371.1	0.007	0.002	-0.023	0.076	271	7.6	250.5	20.5	1089

Appendix 3.2 continued…

Analysis	T(cm^{-1})	H(3107)	H(3237)	mu(1430)	mu(1365)	N (ppm)	%N as B	A (ppm)	B (ppm)	T(°C)calc
HM3B4c	1371.8	0.025	0.000	0.093	0.092	216	11.2	191.4	24.6	1105
HM3B4e	1373.0	0.023	0.003	0.026	0.207	1149	24.8	863.6	285.4	1088
HM3B9c	1365.1	0.000	0.000	-0.004	0.259	379	22.0	296.0	83.0	1110
HM3B10c	1361.5	0.039	0.000	0.125	0.101	380	4.6	362.3	17.7	1070
HM3B11c	1381.1	0.021	0.000	0.104	0.103	325	12.4	284.3	40.7	1098
HM3D6	1365.4	0.015	0.025	0.054	0.060	150	17.9	122.8	27.2	1126
Brown										
HM05-01c1	1371.9	0.020	0.000	-0.007	0.122	647	23.9	492.7	154.3	1100
HM05-01c3	1372.6	0.016	0.004	0.073	0.250	722	13.2	626.7	95.3	1081
HM05-02c1	1372.4	0.000	0.003	-0.004	0.062	800	19.0	648.2	151.8	1088
HM05-02e1	1371.8	0.004	0.000	0.034	0.033	840	28.4	601.9	238.1	1099
HM05-03e2	1374.8	0.018	0.000	0.014	0.001	204	2.8	198.2	5.8	1072
HM05-05c2	1379.0	0.059	0.002	-0.004	0.012	490	7.2	454.8	35.2	1074
HM05-06e1	1368.9	0.000	0.000	0.004	0.116	579	15.4	490.0	89.0	1090
HM05-06e2	1368.0	0.003	0.000	0.051	0.108	498	27.8	359.5	138.5	1111
HM05-07c2	1368.2	0.006	0.000	-0.005	0.068	354	16.5	295.5	58.5	1103
HM05-07c3	1373.1	0.026	0.000	0.010	0.211	1006	34.3	661.0	345.0	1102
HM05-08c1	1370.5	0.034	0.000	-0.005	0.041	572	15.4	483.7	88.3	1090
HM05-09e1	1374.2	0.025	0.000	0.009	0.042	639	8.4	585.0	54.0	1072
HM05-12c2	1368.6	0.007	0.000	0.034	0.022	143	5.5	135.6	7.4	1094
HM06-01e3	1372.9	0.014	0.000	0.027	0.377	970	15.8	817.2	152.8	1079
HM06-02e3	1370.1	0.000	0.000	-0.002	0.056	575	15.4	486.6	88.4	1090
HM06-03e2	1370.6	0.016	0.000	-0.005	0.006	398	15.8	335.1	62.9	1099
HM06-06e1	1367.8	0.000	0.004	0.011	0.042	514	23.9	391.4	122.6	1105
HM06-07e1	1374.0	0.016	0.002	0.030	0.196	835	22.3	648.6	186.4	1092
HM06-10e1	1374.2	0.012	0.000	0.001	0.018	490	20.3	390.4	99.6	1102
HM07-01e2	1381.8	0.042	0.000	0.019	0.004	334	21.0	263.8	70.2	1112
HM07-02e1	1384.1	0.030	0.000	0.010	-0.006	169	8.9	154.4	14.6	1103
HM07-02e2	1370.1	0.039	0.000	0.007	0.013	308	10.9	274.9	33.1	1095
HM07-04c1	1384.2	0.019	0.003	0.007	0.001	188	17.2	155.3	32.7	1120
HM07-05c2	1377.0	0.037	0.000	-0.004	0.015	497	26.6	364.3	132.7	1110
HM07-06e1	1374.5	0.048	0.004	0.012	0.207	1170	32.5	789.7	380.3	1096
HM07-10e1	1370.2	0.020	0.000	-0.003	0.030	494	17.9	405.0	89	1098
HM07-11c1	1384.7	0.000	0.000	0.008	-0.006	111	5.9	104.4	6.6	1104
HM001e3	1378.1	0.105	0.005	0.032	0.032	573	21.7	448.9	124.1	1100

Appendix 3.2 continued…

Analysis	T(cm^{-1})	H(3107)	H(3237)	mu(1430)	mu(1365)	N (ppm)	%N as B	A (ppm)	B (ppm)	T(°C)calc
HM047c3	1376.9	0.089	0.005	-0.008	0.014	511	11.2	453.2	57.8	1085
HM050e1	1375.7	0.061	0.007	0.058	0.291	987	20.0	789.9	197.1	1085
HM071e2	1376.6	0.007	0.000	0.004	0.001	172	10.9	153.3	18.7	1109
HM073e3	1381.9	0.175	0.013	0.080	0.032	949	14.3	813.4	135.6	1077
HM107e1	1370.6	0.007	0.000	-0.011	0.048	685	21.7	536.8	148.2	1096
HM117e	1369.2	0.006	0.006	0.019	0.019	148	19.0	120.2	27.8	1128
HM217c	1377.0	0.006	0.000	0.006	0.000	132	15.4	111.7	20.3	1125
HM217c2	1373.1	0.000	0.000	0.097	0.070	117	7.2	108.8	8.2	1107
HM221c	1378.7	0.026	0.000	0.031	0.042	276	10.1	248.1	27.9	1096
HM2B2C	1368.9	0.007	0.013	0.158	0.167	104	15.4	87.8	16.2	1131
HM3C10c	1376.9	0.004	0.004	0.012	0.008	106	8.0	97.9	8.1	1111
Green										
HM08-01c2	1375.5	0.157	0.017	0.444	2.339	2139	65.8	732.0	1407.0	1114
HM08-01e2	1375.2	0.173	0.019	0.405	2.386	2498	60.6	982.8	1515.2	1106
HM08-03e2	1373.1	0.012	0.006	0.000	0.297	1130	44.0	632.7	497.3	1108
HM09-01e1	1376.0	0.056	0.004	0.068	0.414	972	44.0	544.3	427.7	1112
HM09-02e2	1373.2	0.006	0.002	0.000	0.045	838	15.1	711.5	126.5	1081
HM09-03c3	1375.8	0.015	0.003	0.102	0.573	1433	51.9	689.6	743.4	1110
HM09-03e1	1375.5	0.035	0.003	0.071	0.503	1368	46.2	736.4	631.6	1106
HM09-04c1	1376.7	0.037	0.003	0.076	0.435	2181	63.2	801.3	1379.7	1111
HM09-05e3	1373.9	0.018	0.006	0.006	0.161	1019	28.7	726.7	292.3	1095
HM09-06e1	1373.2	0.020	0.003	0.001	0.376	1342	43.4	759.6	582.4	1104
HM09-06e2	1373.1	0.045	0.000	0.070	0.517	1352	39.5	817.7	534.3	1100
HM09-07e1	1373.4	0.070	0.000	0.018	0.161	1090	34.5	713.4	376.6	1100
HM09-08c1	1375.0	0.029	0.000	0.035	0.417	1914	49.1	973.7	940.3	1101
HM09-09c1	1374.2	0.028	0.000	0.048	0.331	1252	36.5	795.1	456.9	1099
HM09-09e1	1373.7	0.012	0.003	0.050	0.514	1279	50.9	628.2	650.8	1112
HM09-10e1	1376.9	0.021	0.007	-0.003	0.052	795	15.8	669.6	125.4	1083
HM09-10e2	1378.1	0.036	0.004	0.041	0.084	683	22.0	532.7	150.3	1096
HM020E1	1373.6	0.059	0.003	-0.003	0.229	1141	27.5	826.7	314.3	1091
HM024c2	1378.7	0.047	0.000	0.103	0.167	1042	28.9	740.0	302.0	1095
HM024e1	1380.6	0.051	0.003	0.027	0.100	866	22.0	675.3	190.7	1091
HM082c2	1374.5	0.023	0.000	0.008	0.082	546	17.6	449.9	96.1	1095
HM114c	1374.3	0.022	0.044	0.379	0.634	1159	34.5	758.4	400.6	1099

Appendix 3.4 IR absorption characteristics across the Helam diamond plates. Mantle residence temperatures have been calculated for a mantle residence time of 2.75 Ga.

Analysis	T(cm^{-1})	H(3107)	H(3237)	mu(1430)	mu(1365)	N (ppm)	%N as B	A (ppm)	B (ppm)	T(°C)calc
HB01A_1	1369.2	0.006	0.000	-0.003	0.187	796	14.3	682.1	113.9	1081
HB01A_2	1369.5	0.000	0.000	-0.002	0.181	802	12.4	702.4	99.6	1077
HB01A_3	1369.5	0.000	0.003	0.004	0.181	909	28.4	651.1	257.9	1098
HB01A_4	1369.4	0.000	0.000	0.003	0.188	802	12.0	705.7	96.3	1076
HB01A_5	1369.3	0.003	0.003	0.003	0.165	744	11.2	660.0	84.0	1076
HB01A_6	1369.8	0.006	0.000	-0.003	0.182	843	15.8	709.9	133.1	1082
HB01A_7	1369.8	0.009	0.006	-0.003	0.166	805	19.7	647.0	158.0	1089
HB01A_8	1369.4	0.016	0.003	-0.003	0.162	730	22.0	569.6	160.4	1095
HB01A_9	1369.3	0.015	0.003	0.009	0.155	739	14.7	630.1	108.9	1083
HB01A_10	1369.2	0.003	0.003	0.003	0.145	755	19.7	606.4	148.6	1091
HB01A_11	1369.0	0.003	0.006	0.015	0.153	667	7.2	619.4	47.6	1067
HB01A_12	1369.2	0.009	0.003	0.003	0.145	744	16.5	620.7	123.3	1086
HB01A_13	1369.2	0.006	0.000	-0.006	0.152	799	20.7	634.0	165.0	1091
HB3C1_1	1375.5	0.003	0.003	0.008	0.018	361	8.8	329.3	31.7	1086
HB3C1_2	1373.1	0.010	0.000	0.008	0.002	307	14.0	264.4	42.6	1102
HB3C1_3	1377.0	0.007	0.000	-0.003	0.000	338	9.3	307.2	30.8	1089
HB3C1_4	1377.1	0.037	0.000	0.001	0.004	570	18.3	466.0	104.0	1095
HB3C1_5	1382.0	0.054	0.003	0.001	0.004	522	12.4	456.9	65.1	1087
HB3C1_6	1376.9	0.070	0.003	0.001	0.001	528	13.6	456.1	71.9	1089
HB3C1_7	1375.8	0.040	0.000	-0.006	0.014	580	14.7	494.7	85.3	1089
HB3C1_8	1378.4	0.033	0.000	-0.003	0.007	464	11.2	411.6	52.4	1087
HB3C1_9	1376.9	0.017	0.000	0.001	0.007	487	11.2	431.8	55.2	1086
HB3C1_10	1373.6	0.007	0.000	0.001	0.014	506	17.6	416.8	89.2	1097
HB1A10_1	0.0	0.010	0.003	0.009	0.000	355	11.7	313.9	41.1	1094
HB1A10_2	1384.4	0.015	0.003	0.000	0.000	360	9.2	326.4	33.6	1088
HB1A10_3	1380.7	0.029	0.000	0.032	0.031	416	16.5	347.3	68.7	1100
HB1A10_4	1380.2	0.063	0.005	0.000	0.000	432	12.4	378.0	54.0	1091
HB1A10_5	0.0	0.077	0.005	-0.002	0.000	477	16.5	398.1	78.9	1096
HB1A10_6	0.0	0.096	0.008	0.016	0.000	504	12.0	443.4	60.6	1087
HB1A10_7	1380.8	0.089	0.007	-0.002	0.000	522	11.3	463.2	58.8	1084
HB1A10_8	0.0	0.083	0.005	0.001	0.000	452	13.6	390.6	61.4	1092
HB1A10_9	1371.2	0.014	0.000	-0.006	0.000	330	12.1	290.7	39.3	1096
HB1A10_10	1376.9	0.007	0.000	0.008	0.008	352	9.2	319.2	32.8	1088

Appendix 3.4 continued…

Analysis	T(cm^{-1})	H(3107)	H(3237)	mu(1430)	mu(1365)	N (ppm)	%N as B	A (ppm)	B (ppm)	T(°C)calc
HB1A10_11	1367.0	0.000	0.002	0.010	0.013	323	10.5	289.5	33.5	1093
HB1A10_12	1373.1	0.000	0.002	0.058	0.060	284	10.9	253.5	30.5	1097
HB3C3_1	0.0	0.000	0.000	0.006	0.000	149	15.8	125.1	23.9	1123
HB3C3_2	1378.0	0.012	0.000	0.040	0.033	175	13.6	151.3	23.7	1114
HB3C3_3	1384.7	0.016	0.000	0.033	0.030	184	12.1	162.2	21.8	1110
HB3C3_4	0.0	0.017	0.000	0.016	0.000	170	9.3	154.4	15.6	1105
HB3C3_5	1381.9	0.019	0.000	-0.010	0.016	155	11.6	136.8	18.2	1113
HB3C3_6	1382.0	0.021	0.000	0.036	0.021	183	13.6	158.0	25.0	1114
HB3C3_7	0.0	0.021	0.000	0.068	0.000	168	9.2	152.3	15.7	1105
HB3C3_8	0.0	0.023	0.000	0.049	0.000	210	13.2	182.2	27.8	1109
HB3C3_9	1382.4	0.023	0.000	0.052	0.042	197	5.9	185.6	11.4	1090
HB3C3_10	0.0	0.024	0.000	0.033	0.000	147	9.3	133.6	13.4	1108
HB3C3_11	1385.2	0.020	0.000	0.076	0.064	127	8.9	116.2	10.8	1110
HB3C3_12	1380.1	0.021	0.002	0.039	0.007	128	18.3	104.7	23.3	1130
HB3B8_1	1377.1	0.078	0.003	-0.002	0.058	870	21.7	681.5	188.5	1090
HB3B8_2	1376.6	0.107	0.008	0.003	0.039	723	8.8	659.5	63.5	1071
HB3B8_3	1376.0	0.134	0.008	0.003	0.029	760	13.6	657.0	103.0	1080
HB3B8_4	1380.0	0.159	0.005	0.000	0.022	757	12.0	665.9	91.1	1077
HB3B8_5	1381.0	0.136	0.003	0.003	0.017	715	15.4	604.9	110.1	1085
HB3B8_6	1378.3	0.138	0.003	0.009	0.067	897	12.0	789.0	108.0	1074
HB3B8_7	1378.3	0.132	0.006	-0.002	0.068	1010	22.0	788.1	221.9	1087
HB3B8_8	1378.1	0.119	0.006	-0.003	0.063	991	22.9	763.6	227.4	1089
HB3B8_9	1377.7	0.098	0.003	0.006	0.081	1035	21.0	817.6	217.4	1085
HB3B8_10	1379.2	0.092	0.000	-0.011	0.069	890	10.5	797.2	92.8	1070
HB3A4_1	1374.1	0.005	0.000	0.003	0.104	491	17.2	406.2	84.8	1097
HB3A4_2	1373.6	0.008	0.000	-0.003	0.103	479	17.3	396.8	82.2	1097
HB3A4_3	1374.3	0.016	0.000	0.016	0.162	759	27.5	550.3	208.7	1101
HB3A4_4	1375.7	0.013	0.000	0.029	0.165	850	28.7	606.5	243.5	1099
HB3A4_5	1376.1	0.008	0.000	-0.006	0.183	824	27.8	595.1	228.9	1099
HB3A4_6	1374.7	0.010	0.000	0.013	0.102	532	17.9	436.7	95.3	1096
HB3A4_7	1375.7	0.000	0.000	-0.003	0.074	452	14.7	385.5	66.5	1094
HB3A4_8	1376.4	0.013	0.000	0.034	0.220	978	27.5	708.8	269.2	1095
HB3A4_9	1373.6	0.013	0.000	0.019	0.209	798	23.9	607.4	190.6	1095

Appendix 3.4 continued…

Analysis	T(cm^{-1})	H(3107)	H(3237)	mu(1430)	mu(1365)	N (ppm)	%N as B	A (ppm)	B (ppm)	T(°C)calc
HB3A4_10	1373.7	0.016	0.000	0.029	0.297	1010	16.5	843.0	167.0	1079
HB3A4_11	1374.4	0.013	0.003	0.034	0.331	1403	30.1	981.4	421.6	1089
HB3A4_12	1373.1	0.016	0.000	0.016	0.248	1142	28.7	814.5	327.5	1093
HB3A4_13	1372.0	0.000	0.000	0.003	0.160	751	12.0	660.3	90.7	1078
HB1B6_1	1370.4	0.002	0.000	0.012	0.073	571	15.4	482.6	88.4	1090
HB1B6_2	1371.5	0.000	0.000	0.003	0.044	565	22.6	437.2	127.8	1102
HB1B6_3	1367.1	0.000	0.000	0.000	0.005	251	16.5	209.4	41.6	1111
HB1B6_4	1376.9	0.000	0.000	0.007	-0.002	168	13.2	146.2	21.8	1114
HB1B6_5	1371.2	0.000	0.000	0.185	0.192	185	10.4	165.2	19.8	1107
HB1B6_6	1382.6	0.004	0.002	0.059	0.058	178	10.5	174.0	20.0	1105
HB1B6_7	1370.0	0.000	0.002	0.012	0.017	266	17.6	219.1	46.9	1112
HB1B6_8	1371.0	0.000	0.000	0.003	0.005	270	10.0	242.5	27.5	1097
HB1B6_9	1370.1	0.000	0.002	0.003	0.01	303	11.6	267.3	35.7	1098
HB1B6_10	1369.9	0.000	0.002	0.000	0.014	295	6.8	275.3	19.7	1084
HB1B6_11	1369.2	0.010	0.005	0.028	0.057	470	8.4	430.2	39.8	1079
HB2A2_1	1372.0	0.000	0.003	0.007	0.000	123	14.0	106.1	16.9	1123
HB2A2_2	1369.3	0.000	0.000	0.004	0.000	162	10.4	144.8	17.2	1110
HB2A2_3	1380.1	0.084	0.000	0.001	0.003	337	11.2	298.7	38.3	1094
HB2A2_4	1375.8	0.188	0.009	0.003	0.015	530	14.7	452.1	77.9	1091
HB2A2_5	1378.3	0.209	0.009	-0.002	0.023	572	14.3	490.1	81.9	1088
HB2A2_6	1375.0	0.253	0.011	-0.002	0.055	714	18.3	583.7	130.3	1090
HB2A2_7	1375.1	0.210	0.009	0.003	0.040	642	15.4	543.3	98.7	1088
HB2A2_8	1373.1	0.148	0.006	0.001	0.069	704	18.3	575.1	128.9	1090
HB2A2_9	1373.1	0.104	0.003	0.001	0.071	626	13.6	540.7	85.3	1085
HB2A2_10	1375.1	0.134	0.006	-0.003	0.006	429	13.6	370.6	58.4	1094
HB2A2_11	1377.8	0.011	0.000	-0.002	0.000	213	9.2	193.1	19.9	1100
HB2A2_12	1381.0	0.000	0.000	-0.005	0.000	124	10.0	111.3	12.7	1115
HB2A2_13	1381.3	0.000	0.000	0.056	0.061	100	7.2	92.9	7.1	1111
HB2A2_14	1371.9	0.021	0.000	0.003	0.033	437	17.2	361.9	75.1	1100
HB2A2_15	1373.1	0.093	0.003	0.001	0.030	508	18.3	415.5	92.5	1098
HB2A2_16	1372.4	0.054	0.000	0.000	0.027	469	16.5	391.5	77.5	1097
HB2A2_17	1373.1	0.155	0.006	-0.003	0.044	586	14.7	500.3	85.7	1088
HB03B_1	1373.1	0.016	0.003	0.004	-0.002	328	16.1	274.8	53.2	1105
HB03B_2	1377.6	0.029	0.000	-0.002	0.000	106	5.9	99.3	6.7	1106

Appendix 3.4 continued…

Analysis	T(cm^{-1})	H(3107)	H(3237)	mu(1430)	mu(1365)	N (ppm)	%N as B	A (ppm)	B (ppm)	T(°C)calc
HB03B_3	1373.1	0.032	0.003	-0.005	0.000	80	5.4	75.6	4.4	1109
HB03B_4	1369.6	0.039	0.000	-0.007	0.015	90	5.0	85.8	4.2	1103
HB03B_5	1376.9	0.038	0.003	-0.009	0.01	76	5.0	72.3	3.7	1108
HB03B_6	1361.5	0.044	0.003	-0.005	0.001	73	4.6	69.4	3.6	1109
HB03B_7	1365.4	0.059	0.003	0.007	-0.005	74	4.1	70.6	3.4	1107
HB03B_8	1369.2	0.044	0.003	-0.005	0.004	73	4.6	69.4	3.6	1109
HB03B_9	1361.4	0.066	0.000	0.004	-0.006	72	5.0	68.2	3.8	1111
HB03B_10	1376.0	0.067	0.000	0.016	0.004	70	5.0	66.8	3.2	1108
HB03B_11	1365.4	0.064	0.003	0.01	-0.003	73	5.9	68.7	4.3	1113
HB03B_12	1381.2	0.055	0.000	0.007	0.004	121	8.0	110.9	10.1	1110
HB03B_13	1369.4	0.025	0.013	0.044	0.029	356	12.8	310.2	45.8	1096
HB03B_14	1376.9	0.030	0.005	0.005	0.010	470	19	380.7	89.3	1101

Appendix 4.1a Chemical analyses for olivine inclusions from Helam diamonds. Sample notations a, b, c...etc. indicates multiple inclusions from an individual diamond. Cations were recalculated according to the formula unit of olivine; ie: containing 4 oxygen atoms.

	HM008d	HM008c	HM008f	HM208a	HM208c	HM208g	HM209a	HM210a	HM240a	HM240c	HM240d
Oxides											
SiO_2	40.89	41.66	40.84	40.48	40.37	41.43	40.91	41.52	41.47	40.71	41.25
TiO_2	N.D	0.03	0.02	N.D	0.02	N.D	N.D	N.D	N.D	N.D	N.D
Al_2O_3	N.D	N.D	0.02	N.D	N.D	N.D	N.D	N.D	N.D	0.03	N.D
Cr_2O_3	0.04	0.05	0.05	0.06	0.04	0.04	0.07	0.03	0.04	0.04	0.04
FeO	7.85	8.03	7.99	7.24	7.36	7.42	7.35	7.30	7.15	6.94	7.15
MnO	0.12	0.11	0.12	0.07	0.08	0.08	0.08	0.09	0.10	0.08	0.08
MgO	51.24	50.21	51.19	51.71	50.64	51.33	51.99	50.90	51.35	51.72	51.19
CaO	0.07	0.08	0.08	0.05	0.05	0.05	0.07	0.06	0.04	0.06	0.06
Na_2O	N.D	N.D	N.D	N.D	0.04	N.D	N.D	N.D	N.D	0.05	0.05
K_2O	N.D	N.D	N.D	N.D	N.D	N.D	N.D	N.D	N.D	N.D	N.D
NiO	0.32	0.32	0.32	0.40	0.42	0.38	0.39	0.37	0.40	0.40	0.38
Total	**100.54**	**100.51**	**100.63**	**100.02**	**99.03**	**100.74**	**100.86**	**100.28**	**100.56**	**100.03**	**100.21**
Cations											
Si	0.991	1.009	0.990	0.985	0.993	1.000	0.987	1.005	1.001	0.989	1.000
Ti	0.000	0.001	0.000	0.000	0.000	0.000	0.000	0.000	0.000	0.000	0.000
Al	0.000	0.001	0.001	0.000	0.000	0.000	0.000	0.000	0.000	0.001	0.000
Cr	0.001	0.001	0.001	0.001	0.001	0.001	0.001	0.001	0.001	0.001	0.001
Fe	0.159	0.163	0.162	0.147	0.151	0.150	0.148	0.148	0.144	0.141	0.145
Mn	0.002	0.002	0.002	0.001	0.002	0.002	0.002	0.002	0.002	0.002	0.002
Mg	1.852	1.812	1.850	1.876	1.857	1.846	1.870	1.837	1.848	1.874	1.849
Ca	0.002	0.002	0.002	0.001	0.001	0.001	0.002	0.002	0.001	0.002	0.002
Na	0.001	0.001	0.000	0.000	0.002	0.001	0.001	0.001	0.001	0.002	0.002
K	0.000	0.000	0.000	0.000	0.000	0.000	0.000	0.000	0.000	0.000	0.000
Ni	0.006	0.006	0.006	0.008	0.008	0.007	0.008	0.007	0.008	0.008	0.007
Total	3.009	2.991	3.009	3.014	3.007	3.000	3.013	2.995	2.999	3.011	3.001
Mg#	**92.09**	**91.77**	**91.95**	**92.72**	**92.46**	**92.50**	**92.65**	**92.55**	**92.76**	**93.00**	**92.73**

Appendix 4.1a: continued.....

	HM113a	HM3B4d	HM3B4e	HM3B4f	HM3B4b	HM3B4a
Oxides						
SiO_2	40.85	41.20	40.23	41.03	42.15	40.42
TiO_2	N.D.	N.D.	N.D.	N.D.	N.D.	N.D.
Al_2O_3	N.D.	N.D.	N.D.	N.D.	N.D.	N.D.
Cr_2O_3	0.05	0.06	0.05	0.05	0.05	0.02
FeO	7.56	6.06	6.11	6.14	5.97	5.96
MnO	0.10	0.08	0.08	0.10	0.10	0.09
MgO	51.54	53.11	53.18	53.36	53.19	54.80
CaO	0.07	0.01	0.03	0.02	0.04	0.03
Na_2O	0.03	0.04	N.D.	N.D.	0.04	N.D.
K_2O	N.D.	N.D.	N.D.	N.D.	N.D.	N.D.
NiO	0.41	0.39	0.40	0.39	0.38	0.37
Total	**100.61**	**100.95**	**100.08**	**101.09**	**101.92**	**101.69**
Cations						
Si	0.989	0.988	0.975	0.983	0.999	0.964
Ti	0.000	0.000	0.000	0.000	0.000	0.000
Al	0.000	0.000	0.000	0.000	0.000	0.000
Cr	0.001	0.001	0.001	0.001	0.001	0.000
Fe	0.153	0.122	0.124	0.123	0.118	0.119
Mn	0.002	0.002	0.002	0.002	0.002	0.002
Mg	1.861	1.898	1.922	1.906	1.879	1.949
Ca	0.002	0.000	0.001	0.000	0.001	0.001
Na	0.002	0.002	0.000	0.000	0.002	0.001
K	0.000	0.000	0.000	0.000	0.000	0.000
Ni	0.008	0.007	0.008	0.007	0.007	0.007
Total	3.011	3.013	3.024	3.016	3.002	3.036
Mg#	**92.39**	**93.98**	**93.95**	**93.93**	**94.07**	**94.25**

Appendix 4.1c Chemical analyses for pyroxene inclusions from Helam diamonds. Sample notations a, b, c....etc. indicates multiple inclusions from an individual diamond. Cations were recalculated according to the formula unit of pyroxene; ei: 6 oxygen atoms.

	cpx HM007a	cpx HM008a	cpx HM008b	cpx HM018a	cpx HM3B11c	opx HM108a
Oxides						
SiO2	54.36	54.54	55.64	54.53	52.99	57.60
TiO2	N.D.	0.18	0.74	0.21	0.52	N.D.
Al2O3	2.11	0.26	0.23	7.81	5.35	0.06
Cr2O3	3.02	0.15	0.08	0.05	0.06	0.40
FeO	2.13	2.62	2.57	5.97	6.82	8.04
MnO	0.06	0.06	0.28	0.10	0.06	0.05
MgO	15.50	17.50	17.55	11.37	11.87	34.13
CaO	19.23	24.16	22.02	14.23	20.33	0.22
Na2O	2.74	0.33	1.53	5.10	2.19	0.12
K2O	N.D.	N.D.	0.64	0.08	N.D.	N.D.
NiO	0.05	N.D.	N.D.	N.D.	N.D.	N.D.
Total	**99.20**	**99.85**	**101.31**	**99.45**	**100.19**	**100.62**
Cations						
Si	1.985	1.989	2.000	1.977	1.943	1.989
Ti	0.000	0.005	0.020	0.006	0.014	0.000
Al	0.091	0.011	0.010	0.334	0.231	0.002
Cr	0.087	0.004	0.002	0.001	0.002	0.011
Fe	0.065	0.080	0.077	0.181	0.209	0.232
Mn	0.002	0.002	0.009	0.003	0.002	0.001
Mg	0.844	0.951	0.940	0.614	0.649	1.756
Ca	0.752	0.944	0.848	0.553	0.799	0.008
Na	0.194	0.023	0.107	0.358	0.156	0.008
K	0.000	0.001	0.029	0.004	0.000	0.000
Ni	0.001	0.001	0.001	0.000	0.000	0.001
Total	4.023	4.011	4.042	4.031	4.005	4.009
Mg#	**92.84**	**92.25**	**92.41**	**77.25**	**75.63**	**88.33**

Appendix 4.2a: continued.....

	HB3C3b	HB3C3c	HM086a	HM109b	HM1A9a	HM1A9b	HM1A9c	HM1A9d	HM1A9e	HM1A9f	HM1A9g	HM1A9h
Oxides												
SiO_2	0.14	0.15	0.09	0.08	0.13	0.11	0.12	0.10	0.11	0.10	0.10	0.13
TiO_2	0.07	0.05	0.16	0.17	0.59	0.54	0.47	0.47	0.48	0.46	0.47	0.45
Al_2O_3	5.28	5.24	4.60	2.47	4.26	4.25	4.58	4.66	4.66	4.55	4.68	4.59
Cr_2O_3	65.73	66.45	66.23	67.65	65.67	66.15	65.84	65.82	65.55	66.11	65.38	65.79
FeO	14.20	14.35	15.22	15.09	14.42	14.52	14.71	15.10	15.00	15.35	15.14	15.29
MnO	0.24	0.25	0.24	0.30	0.22	0.22	0.24	0.28	0.28	0.28	0.28	0.26
MgO	13.69	13.43	13.29	12.69	13.33	13.46	13.36	13.23	13.35	12.96	13.36	12.85
CaO	0.06	0.11	0.10	0.10	N.D.	N.D.	N.D.	0.02	N.D.	N.D.	N.D.	N.D.
Na_2O	N.D.	N.D.	N.D.	N.D.	N.D.	N.D.	N.D.	N.D.	N.D.	N.D.	N.D.	N.D.
K_2O	N.D.	N.D.	N.D.	N.D.	0.02	N.D.	N.D.	N.D.	N.D.	N.D.	N.D.	N.D.
NiO	N.D.	N.D.	0.04	0.06	0.13	0.10	0.11	0.12	0.08	0.11	0.09	0.07
Total	**99.41**	**100.03**	**99.97**	**98.61**	**98.77**	**99.35**	**99.43**	**99.80**	**99.51**	**99.92**	**99.50**	**99.43**

	HM1A9i	HM1A9j	HM1A10b
Oxides			
SiO_2	0.15	0.11	0.15
TiO_2	0.52	0.46	0.59
Al_2O_3	4.27	4.78	4.71
Cr_2O_3	66.18	65.95	65.35
FeO	14.58	14.93	17.61
MnO	0.21	0.28	0.36
MgO	13.51	13.42	11.22
CaO	N.D.	N.D.	0.04
Na_2O	N.D.	N.D.	N.D.
K_2O	N.D.	N.D.	N.D.
NiO	0.12	0.09	0.09
Total	**99.54**	**100.02**	**100.12**

Appendix 4.3a: Chemical analyses for mss inclusions from Helam diamonds. Sample notations a, b, c....etc. indicates multiple inclusions from an individual diamond. Sample notations (2), (3)....etc indicate multiple analyses of different phases within an individual sulphide inclusion.

	HM1A2c (2)	HM1A2e	HM2B3a (2)	HM2B3b (2)	HM3A11a (2)	HM3C10b	HM3C10a (2)	HM008c	HM221a (5)	HM2B7a	HM2B7a (2)	HB3B4d
S	37.80	38.63	39.08	38.72	38.92	37.21	38.13	37.31	38.13	39.24	38.93	36.38
Cr	N.D.	N.D.	N.D.	N.D.	N.D.	N.D.	N.D.	0.07	0.06	0.10	0.10	0.00
Mn	N.D.	N.D.	N.D.	N.D.	N.D.	N.D.	N.D.	N.D.	N.D.	N.D.	N.D.	N.D.
Fe	50.63	54.31	53.18	54.06	53.06	49.37	54.75	43.55	44.77	39.88	45.53	41.61
Co	0.93	1.05	0.62	0.37	0.77	1.32	0.77	0.36	0.24	0.62	0.31	2.55
Ni	8.42	4.04	4.89	4.40	5.08	9.71	5.31	17.31	16.09	18.46	13.04	19.25
Cu	N.D.	N.D.	0.89	0.37	0.72	1.16	0.31	0.47	N.D.	N.D.	N.D.	0.07
Zn	N.D.	N.D.	N.D.	N.D.	N.D.	N.D.	N.D.	N.D.	N.D.	N.D.	N.D.	N.D.
Total	**97.78**	**98.03**	**98.66**	**97.92**	**98.55**	**98.77**	**99.27**	**99.07**	**99.29**	**98.30**	**97.91**	**99.86**

Appendix 4.3b: Chemical analyses for pyrrhotite inclusions from Helam diamonds. Sample notations a, b, c....etc. indicates multiple inclusions from an individual diamond. Sample notations (2), (3)....etc indicate multiple analyses of different phases within an individual sulphide inclusion.

	HM059a	HM115a	HM124a	HM126a	HM235f	HM1A2a	HM1A2b	HM1A2c	HM1A2d	HM1A2e (2)	HM1A7a	HM2A4a	HM2B3c
S	39.24	38.72	38.64	38.60	37.80	39.32	39.22	39.33	39.30	39.19	40.22	39.15	39.18
Cr	N.D.	N.D.	N.D.	N.D.	N.D.	N.D.	N.D.	N.D.	N.D.	N.D.	N.D.	N.D.	N.D.
Mn	N.D.	N.D.	N.D.	N.D.	N.D.	N.D.	N.D.	N.D.	N.D.	N.D.	N.D.	N.D.	N.D.
Fe	58.09	58.76	58.06	59.56	57.48	57.95	58.18	58.06	58.42	58.20	57.41	59.39	57.14
Co	0.29	0.02	0.20	0.01	0.19	0.09	0.07	0.06	0.07	0.09	0.52	N.D.	0.06
Ni	1.13	0.54	2.21	0.27	2.43	0.46	0.44	0.36	0.34	0.64	2.27	0.42	1.33
Cu	N.D.	N.D.	0.11	0.05	0.15	N.D.	N.D.	N.D.	N.D.	N.D.	N.D.	N.D.	N.D.
Zn	N.D.	N.D.	N.D.	N.D.	N.D.	N.D.	N.D.	N.D.	N.D.	N.D.	N.D.	N.D.	N.D.
Total	**98.76**	**98.03**	**99.22**	**98.50**	**98.05**	**97.81**	**97.90**	**97.80**	**98.13**	**98.11**	**100.42**	**98.96**	**97.72**

	HM2B3a	HM2B3b	HM3A11 a	HM3A11 b	HB3B4d (2)	HM3C10a	HM3D6a
S	40.69	39.44	38.99	39.01	39.19	38.17	38.73
Cr	N.D.	N.D.	N.D.	N.D.	N.D.	N.D.	N.D.
Mn	N.D.	N.D.	N.D.	N.D.	N.D.	N.D.	N.D.
Fe	59.34	57.66	56.28	57.32	58.81	56.84	59.22
Co	0.06	0.10	0.23	0.13	0.08	0.35	0.01
Ni	1.16	1.31	2.43	1.63	0.36	2.47	0.40
Cu	N.D.	N.D.	N.D.	N.D.	0.06	0.37	N.D.
Zn	0.07	N.D.	N.D.	N.D.	N.D.	N.D.	N.D.
Total	**101.31**	**98.51**	**97.93**	**98.08**	**98.50**	**98.20**	**98.35**